Synthesis and Reactivity of [3.1.1]Propellane

Nils Frank

St Hilda's College

University of Oxford



A thesis submitted to the Board of the Faculty of Physical Sciences in partial fulfilment of the requirements for the degree of

MSc by Research in Organic Chemistry

Trinity Term 2022

University of Oxford

Abstract: Synthesis and Reactivity of [3.1.1]Propellane

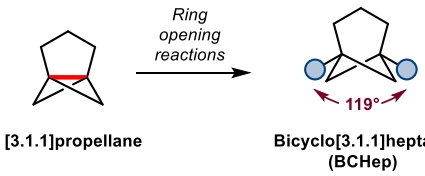
Nils Frank | St Hilda's College, University of Oxford

MSc by Research in Organic Chemistry | Trinity 2022

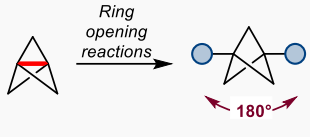
[1.1.1]Propellane (TCP) has gained attention in physical organic chemistry because of its unusual geometry and bonding properties as well as in medicinal chemistry, as a precursor towards the bicyclo[1.1.1]pentane (BCP) unit being used as bioisosteres for *para*-substituted benzene rings in drug design.

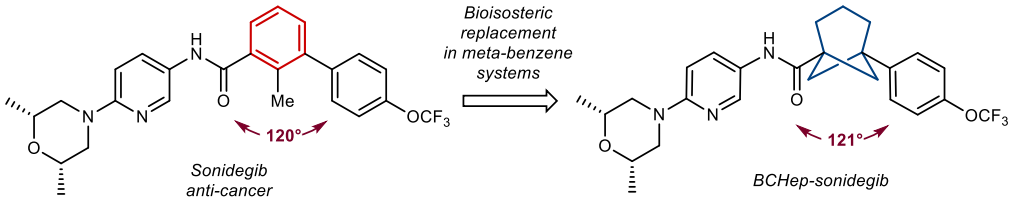
In this thesis, the question about reactivity and character of a higher propellane, [3.1.1]Propellane (TCHep), is posed which was so far only synthesised on milligram scale. In Chapter 2 a novel multigram scale synthesis of TCHep is developed. This made exploration of the chemistry of TCHep possible for which a scope on a variety of reliable reaction is prepared yielding bridgeheaded substituted bicyclo[3.1.1]heptanes (BCHep). Chapter 2 continues with computational and mechanistic approaches to decipher characteristic differences between TCP and TCHep.

Chapter 3 recognises that the BCHep substitution pattern map precisely onto the geometry of *meta*-substituted benzenes. Functionalisation reactions of BCHep iodides were explored. The BCHep-pharmaceutical analogues of Sonidegib and URB597 was prepared. These drugs revealed enhanced ADME properties to their parent drugs, validating the potential of this *meta*-arene analogue as a sp^3-rich motif in drug design.



Established concept: BCP as bioiosostere for para-substituted benzene ring





mouse liver microsomal stability $T_{1/2}$ = 53 min
CYP2C9 inhibition IC_{50} = 4.2 μM

mouse liver microsomal stability $T_{1/2}$ = 75 min
CYP2C9 inhibition IC_{50} = 18.5 μM

Declaration

The work presented in this thesis was conducted at the Department of Chemistry, University of Oxford. The thesis is a product of my own work and includes no results through collaboration, except where specifically indicated in the text. The work presented has not been submitted, either partially or in full, for any qualification at this or any other institution.

Nils Frank,

August 2022

Data availability

The data presented in this Thesis, including cartesian coordinates, output files, density and NBO files used for data processing are publicly-available on the Oxford University Research Archive (ORA) under the title *"Computational supplementary material to the thesis 'Synthesis and Reactivity of [3.1.1]Propellane'"*.

Acknowledgements

First, I would like to thank Prof. Edward Anderson for the opportunity of doing my Master by Research in his research group. Your guidance, advice and critical feedback are about to make me not only a better synthetic chemist but also a more astute human being.

Second, I would also like to thank Prof. Duarte for giving me the opportunity to work and get integrated into her computational chemistry group. Working so close at the intersection between synthetic and computational chemistry feels like paradise and is a great honour. Thanks for all the support throughout the time!

Thirdly, I am indebted to Dr Jeremy Nugent, who supervised and taught me preparative skills and good scientific practice starting with efficient project planning and ending with proper compound characterisation. Thank you for always having an open ear, even remotely during shift work, and being willing to go down even the most useless discussion with me!

Special thanks to Dr Alistair Sterling for raising me into the computational community and being my lone companion when it comes to the interest in ‘whatever holds the world together in its inmost folds’. Another computational thanks to Dr Tom Young for helping me with technical questions.

Thank you, Beth, for joining me in the BCHep-quest, bringing it into a real application, nice places in the North (which I will never visit), and so much more!

Thank you, Ana, for having countless discussions about doomed human relationships, sometimes in German! Thanks, Philip, for being an early-morning workmate. And thank you, Ryan, for selecting me as your computational partner and having you as a knowledgeable lab member. Sorry Hannah, for all the photobook moans. Thanks, Yasmin, for all the coffee and food for the nerves! Ayan, see you in Basel or Mannheim!

Kenny, it was a pleasure to support you with computational power in your total synthesis project. What a rewarding project it was! My apologies to Jieyan. You must endure a lot with me; I think the negative force field is broken! Dear Zixuan, it is always a pleasure to discuss the computational results with you. Thanks to you, Guoduan, for always having a laugh. Ben, we have not buried [3.1.1]propellane, but maybe someone will do some day. Pavle, it is a pleasure to discuss with you the disgusting European undergraduate lab courses. Priyansh, you have a lot of video material against me in your hands, please use it wisely! I never thought I would discuss Nietzsche in the Atrium Café — thanks Tackie.

I would also like to thank Andrew Maitland for UV-lamp support and Roman Kučera for his support in conducting high-pressure hydrogenations. Special thanks to Dr Patrick Rabe for being willed to perform bioconjugation experiments with me and Prof. Schofield for support in this regard. I am beyond grateful to Dr Tryfon Zarganis-Tzitzikas and Prof. Brennan for making ADME-testing of the BCHep-drugs possible! Thanks, Matthew, for connecting us. Thanks to all Duarte group member in general. Special thanks to Ren.

Thank you, Helena, for shining high-energy photons on my molecules and harming me in many ways. Thanks for being a fan of Rieke-metals — ‘nothing better since sliced butter’.

I am indebted to my father and my mother, you brought me here. Thank you, Oma Ute, you formed my character in lonely East Germany, I would not be pursuing the path of trying to be a scientist without you.

Thanks to all pawed and hoofed friends here and in Germany, you always remind me of peace, gratitude, and humility.

Publications

This thesis is based on the following publications:

1. N. Frank, J. Nugent, B. Shire, H. Pickford, P. Rabe, A. Sterling, T. Zarganes-Tzitzikas, T. Grimes, A.Thompson, R. Smith, C. Schofield, P. Brennan, F. Duarte, E. Anderson, "Synthesis of *meta*-substituted arene bioisosteres from [3.1.1]propellane" *Nature* **2022**, doi: 10.1038/s41586-022-05290-z

2. A. J. Sterling[†], N. Frank[†], E. A. Anderson, F. Duarte, "Strain and reactivity in organic chemistry", invited Perspective in *Chemical Science*, manuscript in preparation. *[†]Equal author contribution*

Contributions were made to the following work published, submitted or prepared for submission that do not form part of this Thesis:

1. J. Nugent, A. Sterling, N. Frank, J. Mousseau, E. Anderson, "Synthesis of α-quaternary bicyclo[1.1.1]pentanes through synergistic organophotoredox and hydrogen atom transfer catalysis", *Org. Lett*. **2021**, 23, 21, 8628–8633.

2. K. H. K. Park[†], N. Frank[†], F. Duarte, E. A. Anderson, "Collective Synthesis of Illudalane Sesquiterpenes via Cascade Inverse Electron Demand (4 + 2) Cycloadditions of Thiophene *S,S*-Dioxides" *J. Am. Chem. Soc.* **2022**, 144, 22, 10017–10024. *[†]Equal author contribution*

3. Y. Wu, N. Frank, E. A. Anderson, X. Bi "Silver catalysis in organic synthesis: a computational view", manuscript in preparation.

4. R. E. McNamee, N. Frank, K. E. Christensen, F. Duarte, E. A. Anderson, "Bicyclobutonium Ions and Selective Ring Formation", manuscript in preparation.

Abbreviations

$\|\Psi\|^2$	Electron density
2-mphen	2-Methylphenanthroline
3D	Three-Dimensional
A^-	Nucleophilic counteranion
Ac	Acyl
acac	Acetylacetonate
ACV	L-δ-(α-aminoadipoyl)-L-cysteinyl-D-valine
ADME	Absorption, distribution, metabolism, and excretion
AIBN	Azobisisobutyronitrile
App.	Apparent
Aq.	Aqueous
Ar	Aryl
ARC	Aromatic ring count
ATRA	Atom Transfer Radical Addition
BACE1	Beta-Secretase 1
BCB	Bicyclo[1.1.0]butane
BCHep	Bicyclo[3.1.1]heptane
BCHex	Bicyclo[2.1.1]hexane
BCP	Bicyclo[1.1.1]pentane
BHT	Butylated hydroxytoluene
Bn	Benzyl
Bpin	(Pinacolato)boron

Br.	Broad
BTMG	2-*tert*-Butyl-1,1,3,3-tetramethylguanidine
Bu	Butyl
Cat.	Catalyst
$C_{int,app}$	Apparent intrinsic clearance
clog(P)	Partition coefficient
C_{max}	Maximum (or peak) serum concentration
COD	Cyclooctadiene
Cy	Cyclohexyl-
d	Doublet
DBPO	Dibenzoyl peroxide
DCE	1,2-Dichloroethane
DCM	Dichloromethane
DEAD	Diethyl azodicarboxylate
DIBAL	Di-*iso*-butyl Aluminium Hydride
Diglyme	Bis(2-methoxyethyl) ether
DIPEA	*N*,*N*-Diisopropylethylamine
DMAP	4-Dimethylaminopyridine
DMF	Dimethylformamide
DMPU	*N,N′*-Dimethylpropyleneurea
DMSO	Dimethyl sulfoxide
dppe	1,2-Bis(diphenylphosphino)ethane
dppf	1,1'-Bis(diphenylphosphino)ferrocene

dtbbpy	4,4′-Di-*tert*-butyl-2,2′-dipyridyl
DTBP	Di-*tert*-butylperoxide
EDA	Electron-donor-acceptor
EDC	*N*-(3-Dimethylaminopropyl)-*N*′-ethylcarbodiimide hydrochloride
EI	Electron Ionisation
EnT	Triplet energy transfer
EPR	Electron paramagnetic resonance
Equiv.	Equivalents
ESI	Electrospray Ionisation
Et	Ethyl
EWG	Electron withdrawing group
fac-	Facial
Fe(Pc)	Iron(II) phthalocyanine
Fsp^3	fraction of sp^3 hybridised carbon atoms
glyme	1,2-Dimethoxyethane
GSH	Gluthathione
h	Hour
HAT	Hydrogen Atom Transfer
Het.	Hetero-
HOBt	1-Hydroxybenzotriazole hydrate
HPLC	High-performance liquid chromatography
HRMS	High Resolution Mass Spectrometry

i-	*iso*-
IC_{50}	half maximal inhibitory concentration
IPNS	Isopenicillin *N* synthase
^{i}PrOBpin	2-*iso*propoxy-4,4,5,5-tetramethyl-1,3,2-dioxaborolane
IR	Infra-Red Spectrometry
LC-MS	Liquid chromatography–mass spectrometry
LDA	Lithium diisopropylamide
LED	Light Emitting Diode
LiHDMS	Lithium bis(trimethylsilyl)amide
logD	Water:octanol partition coefficient
m	Multiplet
M	Transition metal
Me	Methyl
MeCN	Acetonitrile
Mes	Mesitylene
Min	Minutes
MLM	Mouse liver microsomal
mp.	Melting Point
Ms	Mesyl
MTBE	Methyl *tert*-butyl ether
n-	*normal*-
Naphth	Naphthalene
NBS	*N*-Bromosuccinamide

NHPI	*N*-hydroxyphthalimidyl
NIS	*N*-Iodsuccinimide
NMR	Nuclear Magnetic Resonance
NMM	*N*-Methylmorpholine
NPhth	*N*-Phthalimide
NSAID	Nonsteroidal Anti-Inflammatory Drug
o-	*Ortho*-
OBO	4-methyl-2,6,7-trioxa-bicyclo[2.2.2]octan-1-yl
p-	*Para*-
Pent	Pentyl
PG	Protecting Group
Ph	Phenyl
PIDA	(Diacetoxyiodo)benzene
PIFA	Bis(trifluoroacetoxy)iodobenzene
Piv	Pivalate
ppy	2-Phenylpyridyl
Propellane	Tricyclo[x.y.z.$0^{1,(x+2)}$]alkane
PTSA	*Para*-toluenesulfonic acid
Py	Pyridine
q	Quartet
quin.	Quintet
R	Generic group/Substituent
Ref.	Reference

rt	Room Temperature
s	Singlet
s	Seconds
Sat.	Saturated
SDS	Sodium dodecyl sulfate
SET	Single Electron Transfer
SIMes	1,3-Dimesityl-imidazole-4,5-dihydro-2-ylidene
SOMO	Singularly Occupied Molecular Orbital
t	Triplet
t-	*Tert*-
TBAC	Tetra-*n*-butylammonium chloride
TBDMS	tert-butyldimethylsilyl
TBHP	*t*-Butyl Hydroperoxide Solution
TCHep	Tricyclo[3.1.1.$0^{1,3}$]heptane, [3.1.1]Propellane
TCHex	Tricyclo[2.1.1.$0^{1,3}$]heptane, [2.1.1]Propellane
TCP	Tricyclo[1.1.1.$0^{1,3}$]pentane, [1.1.1]Propellane
TEMPO	(2,2,6,6-Tetramethylpiperidin-1-yl)oxyl
Tf	Triflate
THF	Tetrahydrofuran
TLC	Thin Layer Chromatography
TMEDA	Tetramethylethylenediamine
TMG	Tetramethylguanidine
TMS	Trimethylsilyl

TPSA	Topological Surface Area
Ts	Tosyl
TTMSS	Tris(trimethylsilyl)silane
UV	Ultra Violet
XAT	Halogen atom transfer
Ψ	Wavefunction
ψ	Dihedral angle

Table of Contents

Abstract: Synthesis and Reactivity of [3.1.1]Propellane 2

Declaration 4

Data availability 5

Acknowledgements 6

Publications 8

Abbreviations 10

Table of Contents 17

1. Introduction 21

1.1. Propellanes — A Family of Strained Tricyclic Hydrocarbons 21

1.1.1. The Origin of the Concept of Strain in Organic Chemistry 21

1.1.2. Strain as a Boundary Condition of Structural Space? 22

1.2. Bicyclo[1.1.1]pentanes (BCPs) and [1.1.1]Propellane 25

1.2.1. BCP units as a challenging target 25

1.2.2. Reactivity modes of TCP 27

1.2.3. Recent methodology of TCP 28

1.3. Non-classical bioisosteres 34

1.3.1. Isosteres 34

1.3.2. Bioisosteres 34

1.3.3. Non-classical bioisosteres 36

1.4. Contribution of this thesis 39

2. Synthesis and Reactivity of [3.1.1]Propellane 41

2.1. Introduction 41
2.1.1. Investigations into Higher Propellanes 41
2.1.2. Synthesis and Characterisation of TCHep 43
2.2. Synthesis of TCHep 48
2.2.1. Dibromo bicyclo[3.1.1]hexane-Precursor Approach 48
2.2.2. Tetrahalo-Precursor Approach 49
2.3. Radical-based Reactivity 54
2.3.1. ATRA Addition of Organic Iodides 54
2.3.2. Addition of Perhalides Without any Initiator/Catalyst 58
2.3.3. Addition of Chalcogen Reagents 58
2.3.4. Exploration of UV-Induced Reactivity 60
2.3.5. *N*-centred Radicals 63
2.3.6. Summary 66
2.4. Exploring Anion-based Reactivity 66
2.5. Mechanistic Comparison with TCP 68
2.5.1. Benchmarking Computational Methods 68
2.5.2. Static Properties of TCHep: The Propellanic Bond 73
2.5.3. Strain and Strain-Release 79
2.5.4. Dynamic Properties of TCHep: Reactions 80
2.5.5. Polymerisation 85
2.5.6. Unproductive side reactions 87
2.5.7. Radical clock experiments and competition experiments 89

2.5.8. Summary 94

2.6. Reactivity under Physiological Conditions 95

2.7. Conclusion 100

3. Applications in the context of bioisosterism 102

3.1. Introduction 102

3.1.1. The Underexplored BCHep Motif 102

3.1.2. Bioisosteres for *meta*-substituted Benzene Systems 103

3.2. Crystallographic and *in silico* evidence for isosterism 108

3.3. Functionalisation of *C,I*–Bicyclo[3.1.1]heptanes 112

3.3.1. Target Drug Selection 112

3.3.2. Lithiation strategy 114

3.3.3. Alternative metalation strategies 122

3.3.4. Miscellaneous reactions 126

3.3.5. Kumada cross-example strategy 127

3.4. Physicochemical and metabolic evidence for bioisosterism 130

3.5. Conclusion 136

4. Conclusion and further work 138

5. Supporting information 144

5.1. General Experimental Considerations 144

5.2. General Procedures 148

5.3. Synthesis of [3.1.1]Propellane (Section 2.2) 152

5.4. Characterisation of the BCHep compounds (Section 2.3) 166

5.5. Reactivity under Physiological Conditions (Section 2.6) 208

5.6. Lithiation strategy (Section 3.3.2) 212

5.7. Kumada-cross coupling products (Section 3.3.5) 230

5.8. Preparation of starting material 246

5.9. Evaluation of ADME properties (Section 3.4) 252

5.10. Computational details (Section 2.5, 2.6 and Chapter 3) 267

5.11. Methods (Associated with Section 2.5.2) 269

5.12. Crystallographic data (Associated with Section 3.2) 272

5.13. Geometrical data (Associated with Section 3.2) 277

5.14. Data for Reactivity under Physiological Conditions (Section 2.6) 278

5.15. Computational Benchmarking Data (Section 2.5.1) 279

5.16. Computational Thermodynamic Data (Section 2.5, 2.6 and 3.3.2) 283

References 288

1.

Introduction

Propellanes showcase how fundamental a theoretical interest in chemical bonding and curiosity-driven synthesis of at the first sign ‘useless’ molecules can open the floodgates into new chemical and structural spaces that were not anticipated before — being suddenly highly relevant for medicinal chemistry. This chapter highlights these theoretical and synthetic achievements during recent decades on a class of highly strained, geometrically abnormal compounds: Propellanes.

1.1. Propellanes — A Family of Strained Tricyclic Hydrocarbons

1.1.1. The Origin of the Concept of Strain in Organic Chemistry

It was Adolf von Baeyer in 1885 who proposed the intuitive concept of ‘strain’ (‘*Spannung’*) as the deviation from the ideal tetrahedral angle of 109.5° in an sp^3-bonded carbon atom (Figure 1A).[1] Following Brown’s B-strain hypothesis in 1946,[2] connecting reactivity with ‘strain relief’ during a specific reaction (Figure 1B), strain as a concept became increasingly ingrained as an intuitive tool in chemists minds. Nowadays, the simplistic picture of strained molecular systems as distorted ‘balls-and-springs’ is used unquestioningly as a popular rationale to explain the chemical phenomena of enhancing reactions by ‘strain-release’.[3]

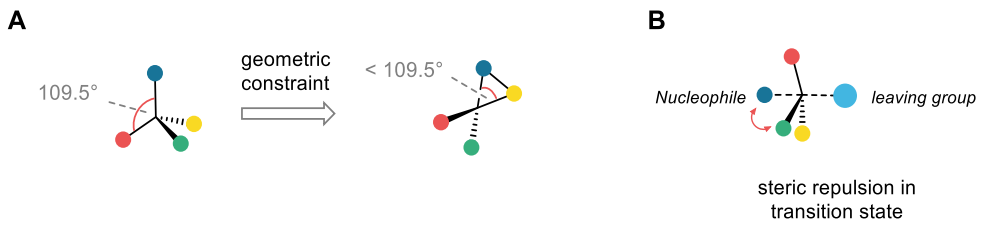


*Figure 1. (**A**) Baeyer's ring strain hypothesis, (**B**) Brown's B-strain rationale.*

The lack of a direct connection between 'strain' and a quantum chemical origin did not prevent physical chemists from putting the idea of 'strain' on firmer, more quantifiable ground. In 1949, Franklin[4] and Benson[5] developed the so-called 'group equivalents' tabulating heat of formations for molecular fragments. Under the general assumption of additivity, these fragments can be summed up by serving as an unstrained enthalpy reference making a comparison to separately measured heat of formations of strained molecules possible. After the rise of computational chemistry, computed group equivalents made estimating strain easier and more accessible.[6]

1.1.2. Strain as a Boundary Condition of Structural Space?

As soon as chemists accepted the general belief that saturated hydrocarbons should ideally adhere to bonding angles of 109.5°,[7] they also started to challenge this dogma in trying to find more exotic examples that deviate further and further from the tetrahedral ideal (Figure 2).

Besides the early examples of the monocyclic oxirane **1** (1859),[8] oxetane **2** (1878),[9] cyclopropane **3** (1882)[10] and cyclobutane **4** (1907),[11] synthetic chemists in the 1950s and 1960s were successful in synthesising bicyclic systems, including bicyclo[1.1.0]butanes (BCBs, 1965)[12] **5** and bicyclo[1.1.1]pentanes (BCPs, 1966)[13] **6**. Platonic solids, like cubane **7**[14] or tetra(*tert*-butyl)tetrahedrane **8**,[15] and the synthesis of

fenestranes **9**[16] challenged more and more the intuitive picture that strain limits structural space. Between the 1970s and 1980s, the synthesis and characterisation of tricyclic, caged compounds of the type tricyclo[x.y.z.$0^{1,(x+2)}$]alkane **10**-**14** — usually called propellanes — culminated this movement. All these examples show the limits of a 'ball-and-spring' model and demand further development.[17]

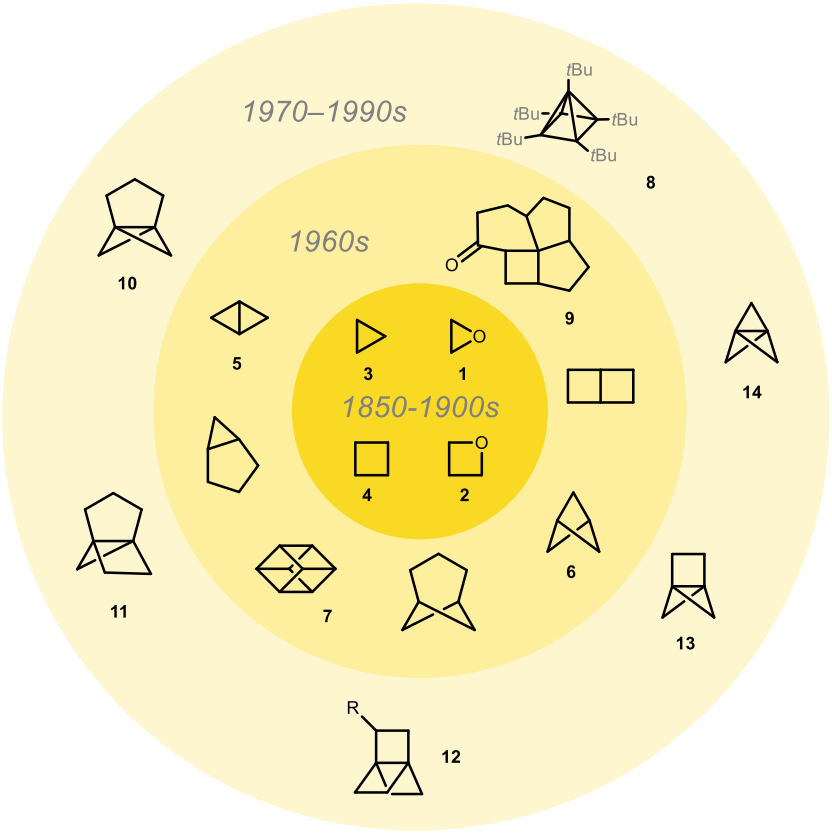


Figure 2. Eras of strained-carbocycle synthesis exemplified by characteristic examples.

Extensive work was done on physical-organic chemistry frontiers describing the bonding of cyclopropane by Coulson-Moffitt,[18] Walsh[19] or Dewar.[20] Coulson proposed bent bonds between sp^3-carbon atoms,[18] whereas Walsh's model consists of p-carbon atoms with 'turnstile' inwards-pointed sp^2-orbitals forming the crucial bond.[19] Dewar invokes similarity to benzene and assumes cyclopropane involves σ-delocalisation (Figure 3A).[20] Recently, DPhil student Alistair Sterling (from the Duarte and Anderson groups)

developed models for explaining reactions involving three-membered ring openings incorporated in bicyclic or tricyclic cores.[21-22] This work revealed that fused cyclopropyl-systems inherently delocalise electronic density onto their bridge, thus lowering the activation barrier in reactions where the inter-bridgehead bond is broken. A relationship (I) was found between strain-release energy difference ΔSRE, the difference in numbers of three-membered ring Δn_3 and the difference in activation energy between two comparable reactions.

$$\Delta\Delta H^{\ddagger} \approx 0.5\,\Delta SRE - 10\Delta n_3 \qquad \text{(I)}$$

This equation demonstrates that strain-release enthalpy ΔSRE still has to be seen as a driving force, lowering the activation barrier in line with the Bell-Evans-Polanyi principle.[23-24] At the same time (I) shows that other influences besides strain, such as delocalisation, can play an essential role in determining the reactivity of compounds (Figure 3B).

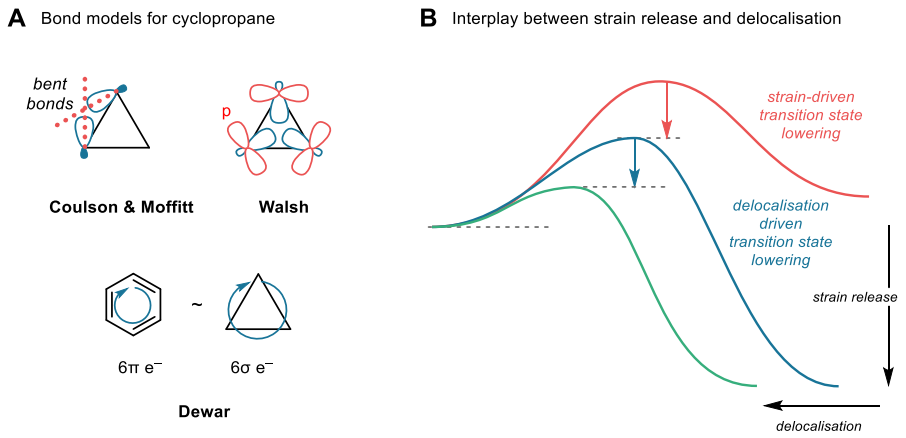


*Figure 3. (**A**) Different models for explaining the bonding situation in cyclopropane, (**B**) Sterling's et al. model dissecting strain-release driven enhancement of reaction rate from delocalisation effects, see also equation (I) and Figure 6.*

Secondly, it is vital to notice that stability must be seen from a *thermodynamic* and *kinetic* perspective. All the molecules mentioned above are highly strained compared to their

unstrained ‘group equivalents’ counterparts, indicating they all should decompose to *thermodynamically* more stable fragments. Nonetheless, energetically achievable reaction pathways have to exist to connect to those unstrained products. If these pathways have a Gibbs free energy activation energy barrier which is too high, decomposition or rearrangement is kinetically too slow to be relevant (Figure 4).

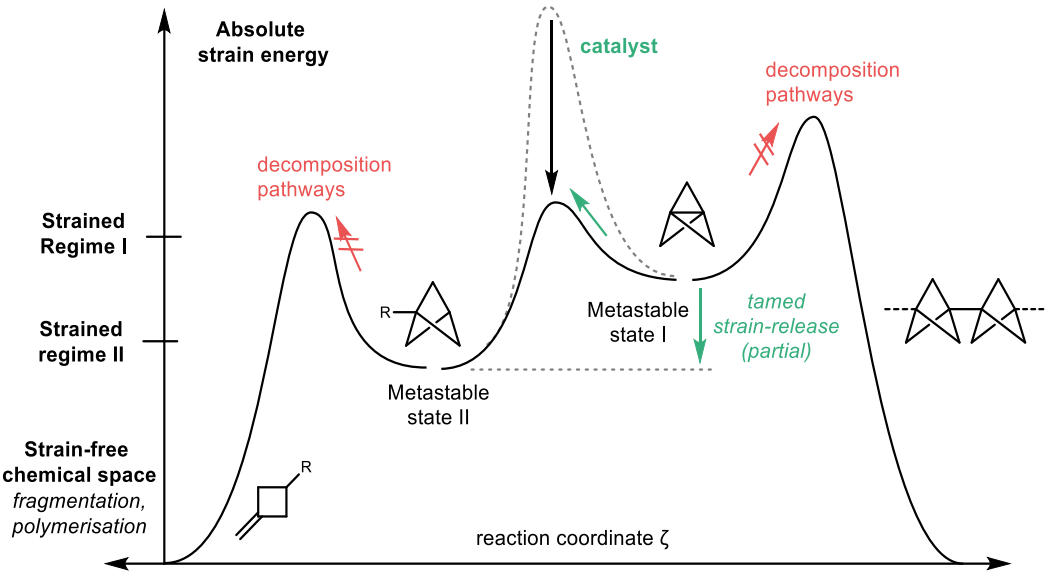


Figure 4. Design principle of strain-release reagents showing energetic requirements.

A kinetically stable reagent whose strain-release can be catalytically tamed and exploited might be of high interest. Significantly, synthesising somehow still strained compounds, like bicyclic systems, from tricyclic systems through controlled *strain release*, might solve the quest for efficient and high-yielding syntheses of otherwise hard-to-obtain structural moieties.

1.2. Bicyclo[1.1.1]pentanes (BCPs) and [1.1.1]Propellane

1.2.1. BCP units as a challenging target

One of those success stories of bringing exotic molecules into a practical synthetic context is the use of [1.1.1]propellane **14** (also known as TCP, tricyclo[1.1.1.$0^{1,3}$]pentane) as a

'spring-loaded' precursor for obtaining bicyclo[1.1.1]pentanes **6** (BCPs) *via* radical or anionic opening of their inter-bridgehead bond. To date, entry *via* TCP to **6** is the most practical way to gain access to BCP units.

Alternatively, BCP cores can be synthesised by increasing the strain instead of releasing it. These strategies usually require harsher reaction conditions and thus suffer from limited substrate tolerance, smaller yields and less applicability. Early examples include Wurtz-coupling (Figure 5a), Hg-sensitised bicyclo[2.1.1]pentanone ring contractions (Figure 5b)[25] or cycloadditions of 1,4-pentadiene (Figure 5c).[26]

More recently, carbene insertion (Figure 5d) into bicyclo[1.1.0]butanes[27] — another strain-release approach — or the intramolecular Barluenga-Valdés coupling[28] (Figure 5e, proceeding through 1,2-alkyl shift from an intermediate boronate onto a diazonium center derived by a hydrazone) have gained momentum, slowly reducing the prevalence of TCP in accessing BCPs *via* a strain-release strategy. Nonetheless, TCP remains the primary entry vector into BCP structural space.

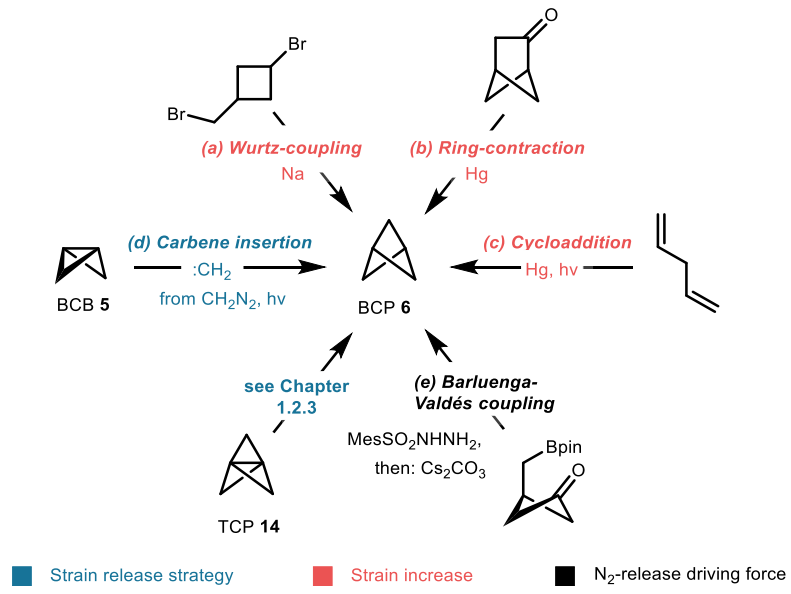


Figure 5. Strategies for the synthesis of BCPs.

1.2.2. Reactivity modes of TCP

The reactivity of TCP can be divided into three main reaction modes: Radical, anionic, and cationic. Only reactions *via* anionic and radical pathways retain the BCP system, whereas cationic reactions usually lead to ring fragmentation (Figure 6A).

Sterling et al. rationalised this unusual 'omniphilic' reactivity by constructing a symmetry-adapted linear combination of the atomic orbital set of TCP containing the inter-bridgehead σ-bond and the three p-orbitals of the bridge carbon atoms, forming a rotationally invariant π* molecular orbital (Figure 6B). Even though TCP suffers from already high electron density within the inter-bridgehead region and corresponding Pauli repulsion with the other inward-oriented C–C bonds, donations from the inter-bridgehead σ orbital into these π* orbitals (σ → π*) can delocalise excess electron density if nucleophiles (R^-) or SOMOphiles ($R^\bullet$) approach. Moreover, the TCP core exerts a counter-intuitive compression motion on approach of R^-, enabling increased σ → π* delocalisation. In fact, σ → π* delocalisation seems to be an electronic necessity for sustaining the TCP core, since fragmentation of the core occurs when electron density is withdrawn by an approaching electrophile R^+ (Figure 6B).[22]

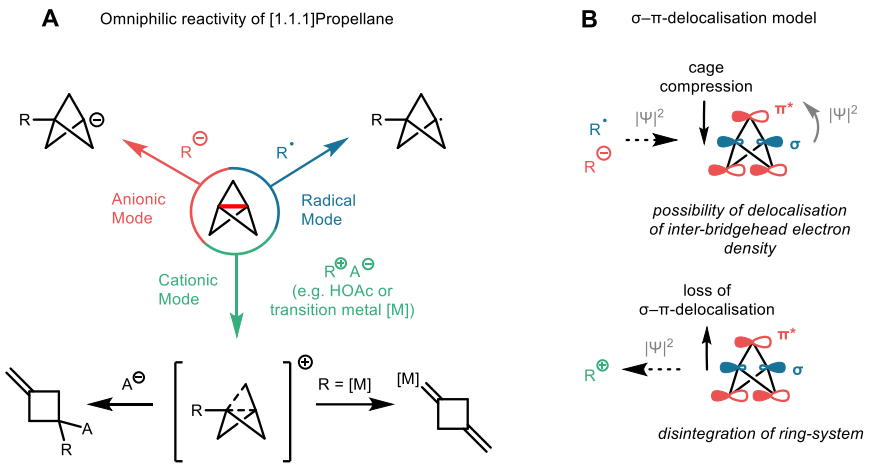


*Figure 6. (**A**) Omniphilic reactivity of TCP, (**B**) Molecular orbital model explaining omniphilic character of TCP by Sterling et al.*

Wiberg and co-workers performed a seminal exploration of TCP's reactivity, trying to characterise reactivity patterns of TCP towards various functional group/compound classes. Without any catalyst or initiator, they found PhSH, PhSeH, $BrCCl_3$, CCl_4, CF_3I and *t*-BuOCl could be added into the inter-bridgehead bond of TCP.[29] Bentrude and co-workers further investigated the insertion into P–H bonds, such as phosphinic acid or dimethyl phosphonate, employing DTBP as a radical initiator (Figure 7).[30] Thus, it is believed that all these reactions proceed through a radical chain propagation process; as initiator-free reactions, they appear to have a highly efficient radical chain. The UV-induced addition of diacetyl and subsequent oxidation with sodium hypobromite afforded the first widely applied BCP dicarboxylate building block **15**, which has been incorporated in drug design.[31]

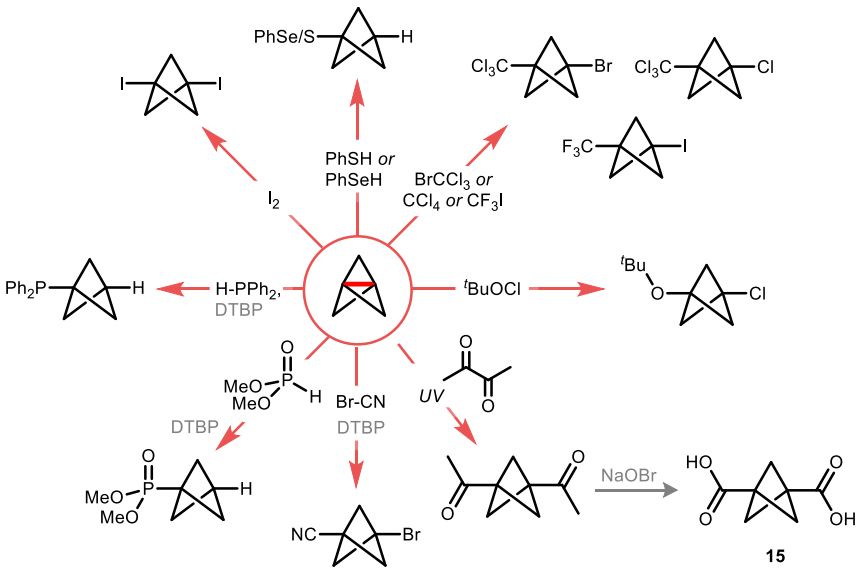


Figure 7. Reactivity of TCP towards small molecules proceeding without any catalyst.

1.2.3. Recent methodology of TCP

The recent renaissance of TCP as a source of BCPs has resulted in the development of milder and more applicable reaction methodologies to access many different substitution patterns. Seminal work by de Meijere and co-workers in 2000[32] showed anionic addition

of Grignard reagents to TCP is possible (Figure 8). A refined protocol by Knochel and co-workers in 2007[33] resulted in higher yields and shorter reaction times (Figure 8). De Meijere and Knochel presented various ways to trap the resulting BCP, either *via* cross-coupling (Figure 8b, 8d) or electrophilic quench (Figure 8c). It was found that transmetalation of the BCP-organomagnesium to an organozinc species, or the direct addition of allylic zinc reagents/zinc enolates to TCP, resulted in higher tolerance towards substrates containing more sensitive functional groups.[34] Due to the higher stability of organozinc compounds, a subsequent transmetalation to organocopper species using CuCN·LiCl was often necessary to achieve efficient trapping with various electrophilic species E-Y.[35] Recently, Aggarwal described a method to employ the initially-obtained BCP-Grignard intermediates in a Zweifel olefination that directly installs olefins on BCPs (Figure 8a).[36]

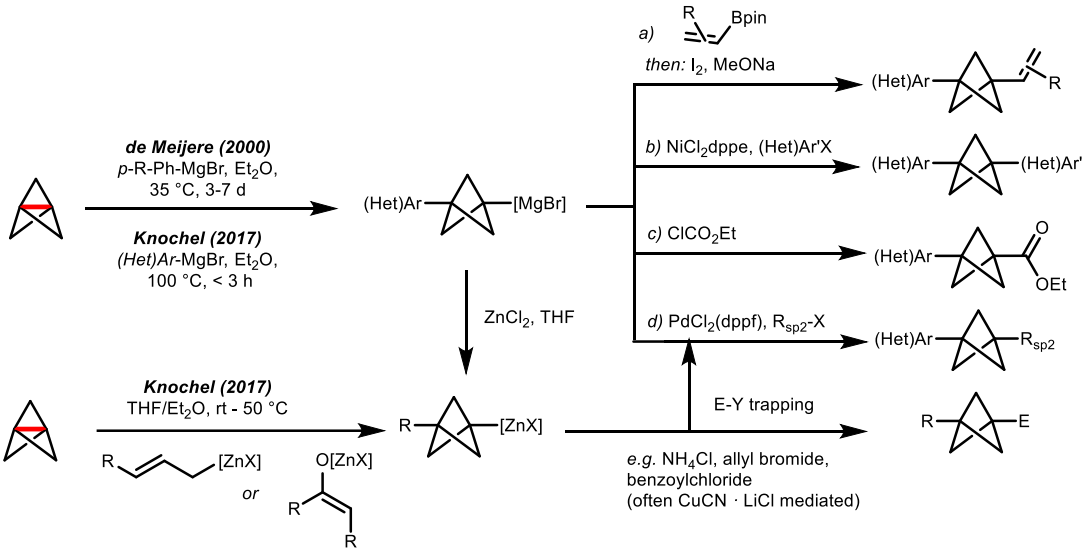


Figure 8. Addition of Grignard and organozinc reagents to TCP.

Other anionic reactions involve the addition of 'turbo amides' RR'NMgCl·LiCl, reported by Baran and co-workers in 2016 (Figure 9A).[37-38] In 2019, Gleason and co-workers showed that the anionic nitrogen-substituted BCP intermediates can be transmetalated

with CuI and trapped with various aliphatic electrophiles (Figure 9A).[39] Recently, Walsh and co-workers explored the addition of 2-azaallyl anions, and reported the interception of the intermediate with *i*PrOBpin (Figure 9B).[40-41] The resulting BCP-Bpins offer versatile handles for further functionalisation, as recently explored by Hartwig and co-workers.[42] Walsh also reported the addition of deprotonated 2-aryl-1,3-dithianes to TCP and successive deprotection (Figure 9C).[43]

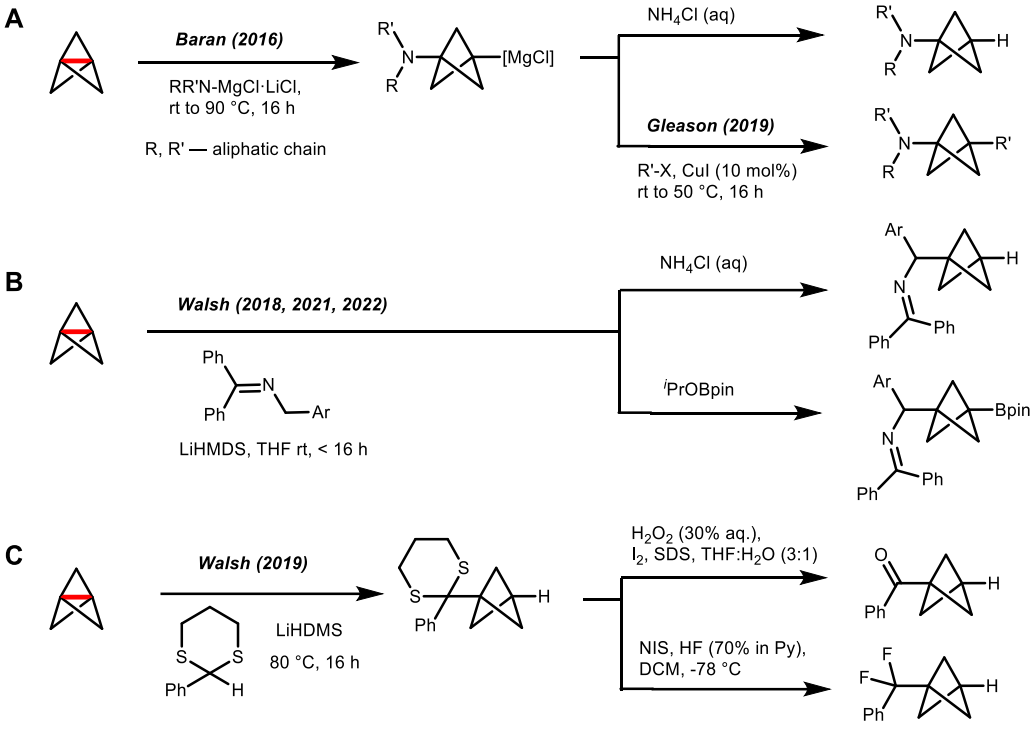


Figure 9. Miscellaneous anionic additions.

A wider variety of radical-based transformations of TCP are known (Figure 10). Our group developed an efficient and versatile way to insert carbon-iodide bonds into TCP *via* BEt_3 initiation[44] or a photoredox-protocol[45] (Figure 10A). The obtained BCP iodides could be either further functionalised *via* lithiation strategies[32] or through Kumada-cross coupling methodology.[46] A large variety of *N*-centred radical additions to TCP is known: our group employed radical fragmentation of α-iodoaziridines which will form allyl sulfonamide-substituted BCP iodides (Figure 10B). The BCP iodide

handle can be conveniently functionalised *via* photo-catalysed Giese-addition to Michael acceptors.[47] Leonori and co-workers reported a three-component reaction *via* a photoredox-catalysed decarboxylation of amidyl precursor adding to TCP, which is consequently trapped with a final SOMOphile component X-Y (Figure 10C).[48] Similarly, Hong and co-workers showed that an EDA (Electron-Donor-Acceptor) complex of **16** can generate sulfonamidyl radicals. These radicals can add into TCP, which is trapped by the remaining pyridyl-fragment of **16** in a Minisci-type manner (Figure 10D).[49] Uchiyama reported the generation of *C*-centred radicals, through oxidative denitrogenation of an aryl hydrazine, which add into TCP and are subsequently trapped by diethyl azodicarboxylate DEAD (Figure 10E). The obtained BCP-hydrazine can be reduced to afford a free BCP amine.[50] Further, Uchiyama reported a silaboration of TCP with Me_2PhSi-Bpin under UV-irradiation affording a silaboro-BCPs which can be functionalised (Figure 10F).[51]

MacMillan and co-workers reported a versatile three-component coupling platform in 2020, coupling *N*-azarenes, amides, anilines, imines, or sulfonamides with *C*-centred radicals generated photoredox-catalytically from iodonium dicarboxylate (Figure 10G). They suggest the addition of the *C*-centred radical to TCP and a subsequent Cu-catalysed cycle in which the BCP-radical is bound to a catalytically generated Cu(II)-species possessing an *N*-azarene ligand. In the next step, a reductive elimination couples the BCP ligand and the *N*-azarene. The Cu-species is oxidatively regenerated through reduction of the photoredox-catalyst, closing the photoredox cycle.[52]

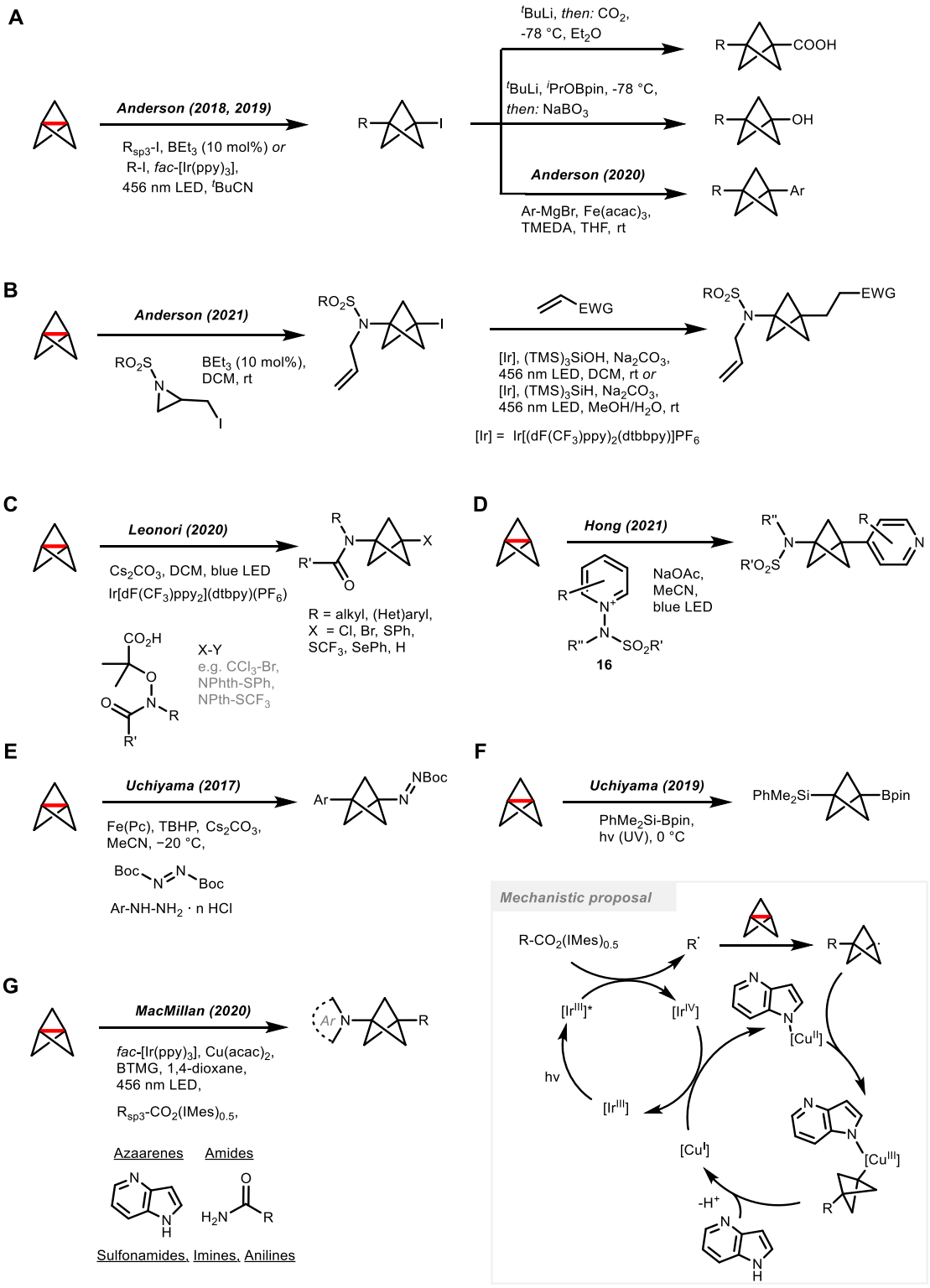


Figure 10. Panoply of radical methodology involving TCP.

Although cationic reactivity dismantles the BCP core, as already found by Wiberg and coworkers (Figure 10A), several transformations have been reported yielding interesting structural motifs.[29, 53] In 2019 Aggarwal reported the Ni-catalysed decomposition of the TCP cage towards methylenespiro[2.3]hexanes comprising an alkenyl unit (Figure 11C).[54] Tolnai reported the Cu(I)-catalysed formation of **17** and **18** (Figure 11B) incorporating an alkynyl- and TMS-protected alkynyl unit, which is directly cross-coupled to aryl halides.[55] A notable exception to the carbocationic decomposition is the electrophilic activation of the TCP with NIS and subsequent nucleophilic trapping of anilines reported by Aïssa and co-workers (Figure 11D). A control experiment in presence of TEMPO as a radical scavenger showed no reaction suppressing ruling out a radical mechanism.[56]

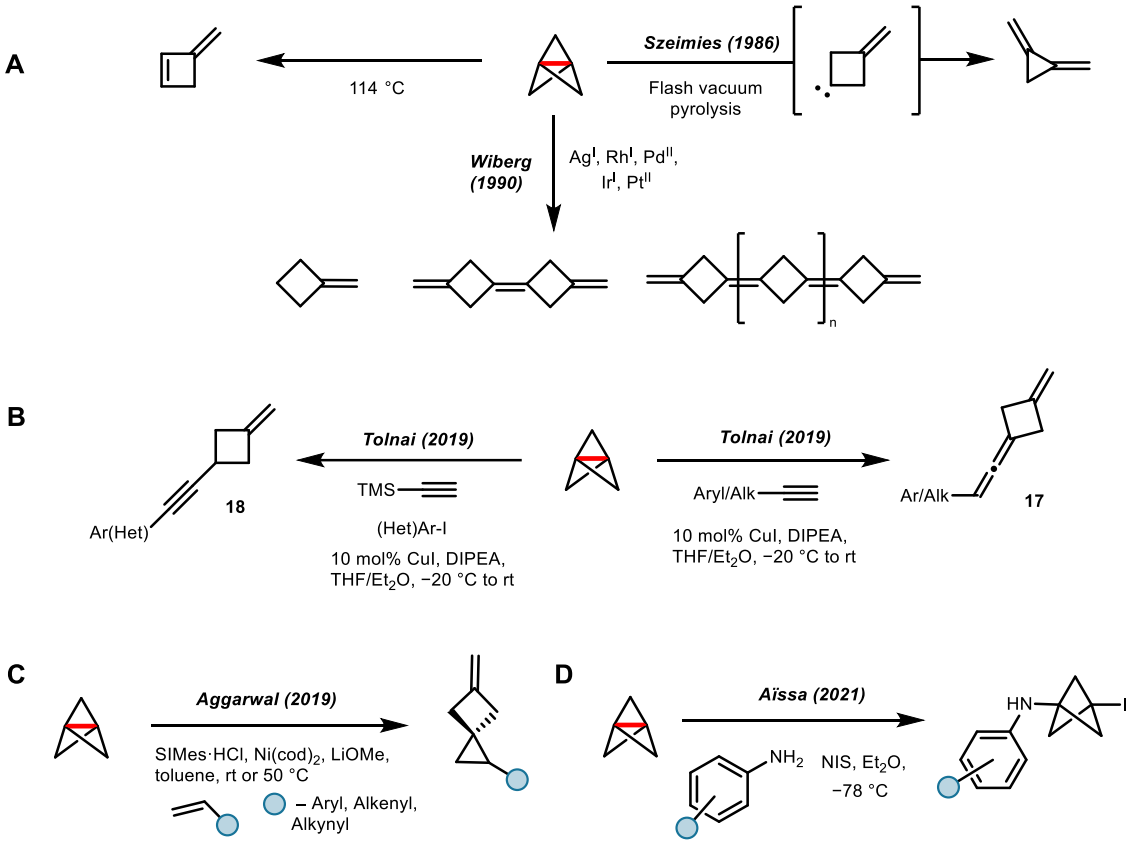


Figure 11. Cationic reactivity of TCP.

1.3. Non-classical bioisosteres

In 1996 Pellicciari et al. recognised that the bridgehead-substituted BCP unit can be used as a surrogate for *para*-substituted benzene rings in the mGluR1 antagonist (*S*)-4CPG.[57] The idea of BCP units being non-classical bioisosteres was born.

1.3.1. Isosteres

In 1919, Langmuir recognised that the similar physical properties in the two pairs of (co)molecules CO and N_2, and N_2O and CO_2, can be traced back to a similar electronic structure.[58] He defines them as isosteric:

> *"Comolecules are thus isosteric if they contain the same number and arrangement of electrons. The comolecules of isosteres must, therefore, contain the same number of atoms." (Langmuir, 1919)*[58]

Isosterism is exemplified by Grimm's Hydride Displacement law (1925) which states that an atom bonded to additional hydrogen will possess the properties of the next-heavier atom, e.g. [CH] to [N], [NH] to [O] or [CH_4] to [NH_4^+].[59] Erlenmeyer was the first to broaden this definition by focussing only on the valence electron and not limited to the same geometric arrangement. Under less harsh criteria, he identified benzene and thiophene as two isosteres replacing the [HC=CH] unit with the [S] atom.[60]

1.3.2. Bioisosteres

Friedman, in 1951, first mentioned the term 'bio-isosteric':

> *"We shall term compounds 'bio-isosteric' if they fit the broadest definition for isosteres and have the same type of biological activity." (Fridman, p. 298)*[61]

Thornber describes the properties to consider when making a bioisosteric replacement: size, shape, electronic distribution (polarisability, inductive effects, dipoles, charges),

lipophilicity and hydrophilicity, acidity, chemical reactivity and H-bonding abilities. He further classifies bioisosteres in different roles:[62]

- **Structural:** The isostere only acts as a geometric spacer unit – retaining bond lengths and vector angles which are of utmost importance.
- **Receptor interactions:** The bioisosteric group directly interacts with the biological system. Therefore, all the parameters mentioned above are critical.
- **Pharmacokinetics:** The bioisosteres replace a group crucial for absorption, transport and excretion. In particular, hydro- and lipophilicity as well as acidity and hydrogen bonding abilities are essential.
- **Metabolism:** If the replaced group is involved in metabolism, it is especially important to consider the bioisostere's chemical reactivity.[62]

The currently most-widely accepted definition of bioisosterism stems from Burger:

> *"Bioisosteres are compounds or groups that possess near-equal molecular shapes and volumes, approximately the same distribution of electrons, and which exhibit similar physical properties such as hydrophobicity. Bioisosteric compounds affect the same biochemical systems as agonists or antagonists and thereby produce biological properties that are related to each other" (Burger, 1991)*[63]

Figure 12 shows examples of such kinds, highlighting two specific examples. One of those is Procaine and Procainamide, in which an ester group is replaced by an amide which circumvents metabolism pathways through ester hydrolysis (pseudocholinesterase).[64] Another example is Celecoxib, an NSAID developed by Pfizer, in which a methyl substituent was replaced by a $-CF_3$ group aiming to inhibit benzylic metabolism. ADME (Absorption, Distribution, Metabolism, and Excretion)

profiling revealed challenges in the form of deterioration of the pharmacokinetic profile. This highlights that each bioisosteric replacement can result in other undesired side effects, even though they are each intended to solve one specific problem. This brief examination of the use of bioisosteres in pharmaceutical applications reveals that there is no bioisostere that solves all issues holistically.

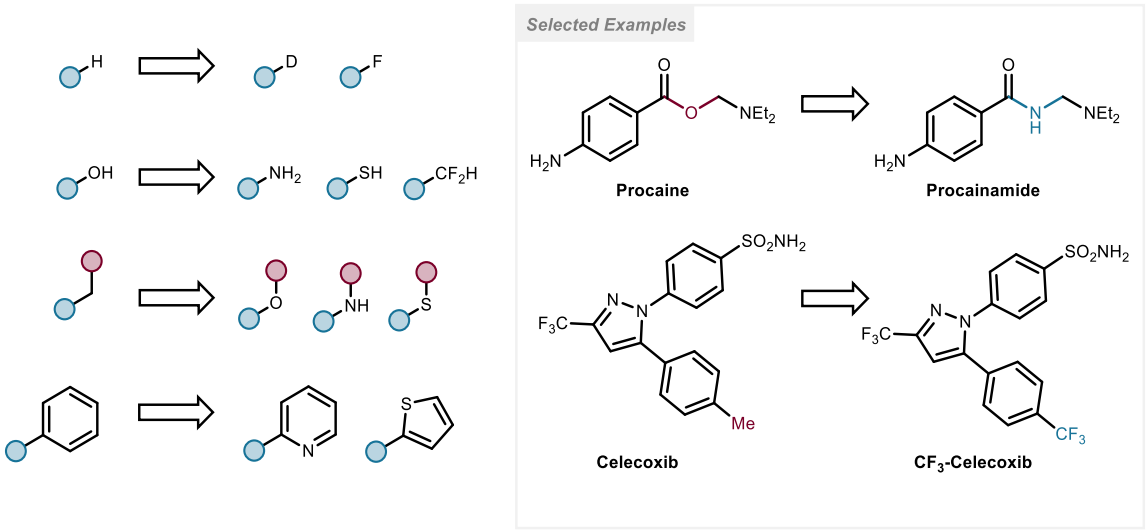


Figure 12. Generic and specific examples of classical bioisosteres.

1.3.3. Non-classical bioisosteres

Non-classical bioisosteres are not required to possess *"near-equal molecular shapes and volumes"*,[63] and *"approximately the same distribution of electrons"*[63] is not necessarily needed. Therefore, every structural moiety can be classified as a non-classical bioisostere as long as the biological activity is retained and the disposition of substitutents.

Studies have shown that a drug molecule's aromatic ring count (ARC) correlates negatively with aqueous solubility, whereas the fraction of sp^3 hybridised carbon atoms in a molecule (Fsp^3) correlates positively with solubility.[65] Moreover, evaluation of GSK drug candidates at different stages has shown an overall reduction in mean ARC from

preclinical candidates (ARC = 3.3) to final proof of concept (ARC = 2.3).[66] Further, aromatic systems are susceptible to metabolic oxidation through cytochrome P450 enzymes, whereas saturated carbocycles exhibit a greater metabolic inertness.[67]

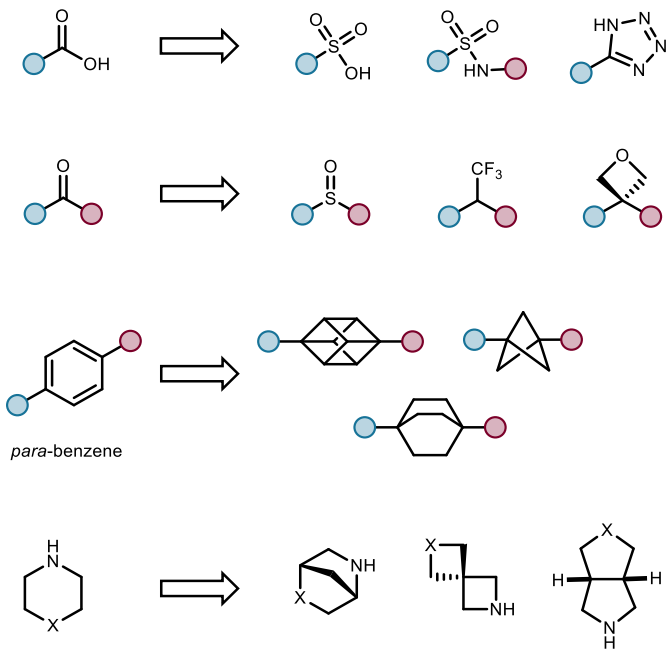


Figure 13. Examples of non-classical bioiososteres.

These findings motivated the development of the theme *'escaping flatland'* and, in the context of this thesis, encouraging the construction of sp^3-caged hydrocarbons as non-classical bioisosteres with a higher degree of three-dimensionality to replace sp^2-planar arene systems in the search for better ADME profiles.[68] Figure 13 highlights selected, popular non-classical bioisosteres, most showing higher three-dimensionality than their parent structure.[69-72]

One specific example is the drug Avagacestat in which Stepan et al. replaced the central *para*-substituted fluorophenyl ring with a BCP unit. As a result, γ-secretase inhibition remained equipotent but pharmacokinetic properties dramatically improved. For

example, solubility and cell permeability values improved, and oral C_{max} increased fourfold in a mouse model.[73] Another example is Resveratrol for which its poor pharmacokinetics limit its potential use. Similarly to Avagacestat, better metabolic stability in hepatocytes was observed as well as higher C_{max} for the non-classical counterpart.[74]

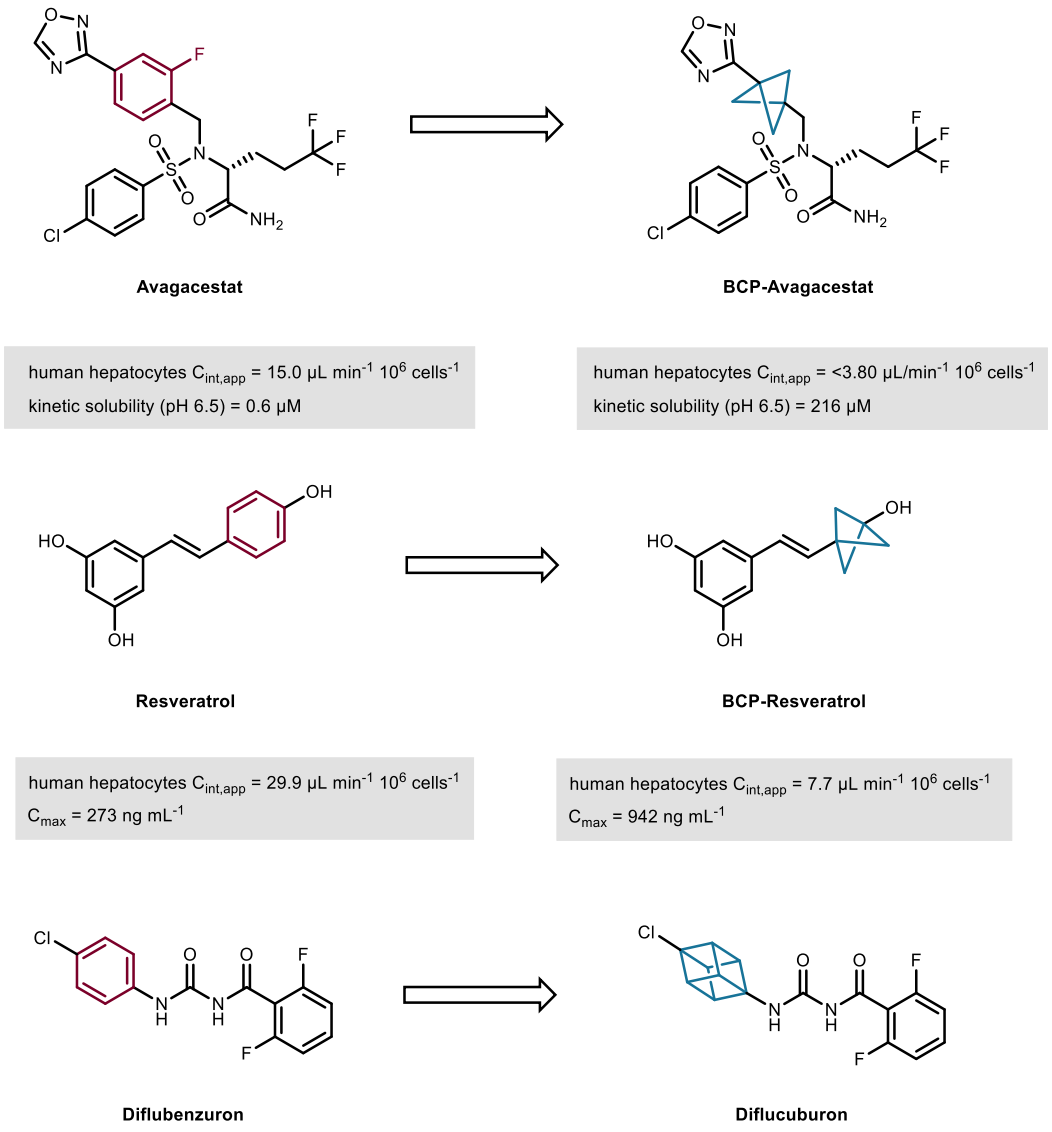


Figure 14. Selected examples of non-classical bioisosteric replacement in current drug examples.

Finally, the replacement of the *para*-chloro substituted benzene ring in Diflubenzuron with a chlorocubane unit enhanced structural extension into the third dimension and, similar to BCP units, led to increased bioactivity.[75]

1.4. Contribution of this thesis

This chapter outlined how TCP grew from 'just another' strained carbocycle to a rising star in the medicinal chemistry landscape, being the synthetic precursor of choice to BCP bioisosteres for *para*-substituted benzene rings. This motivated the development of reams of new methodology using TCP, which might now be described as a mature field (at least from the perspective of bridgehead substitution) in accessing nearly all main substitution patterns of BCP through TCP.

Chapter 2 will focus on 'yet another' tricyclic strained molecule, and indeed another propellane: [3.1.1]propellane (TCHep). It describes how a new synthesis of TCHep was found and performed on a practical, multi-gram scale for the first time. Further, this chapter will describe the exploration of reactivity of TCHep in a way Wiberg embarked on for TCP. It will be shown that some of the recently reported methodologies can be translated onto TCHep, whereas others pose challenges. In this part of the thesis, beginnings will be made in trying to characterise and differentiate the reactivity of TCHep and TCP experimentally as well as computationally — allowing connections to be made with the models developed by Sterling et al. Additionally, the potential of TCHep as a bioconjugation agent was explored under physiological conditions, shedding light on the behaviour of TCHep (and propellanes in general) in protic environments (in collaboration with the Schofield group in Oxford).

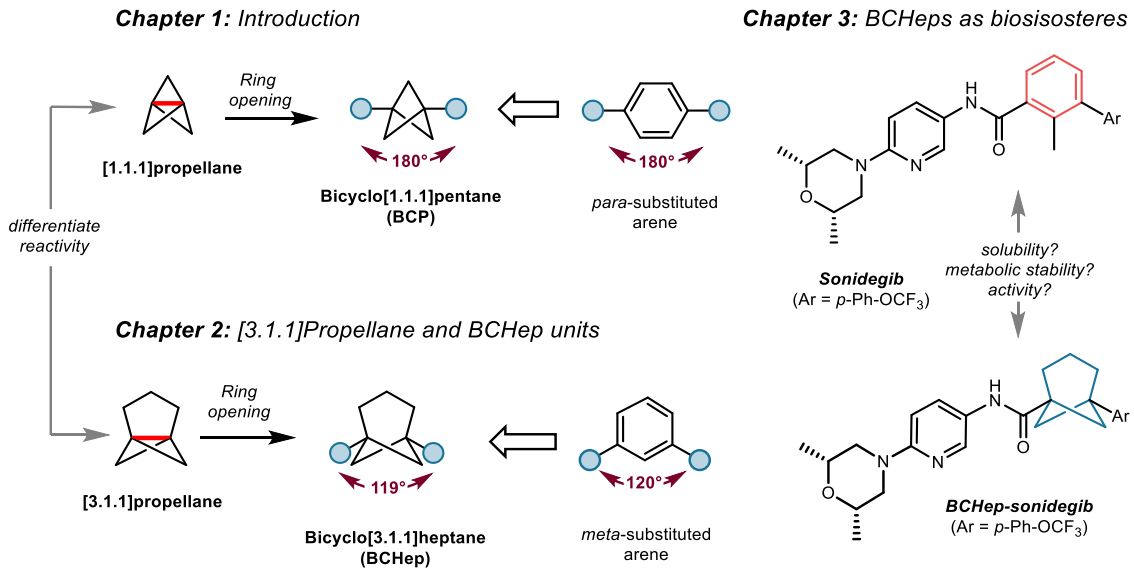


Figure 15. Summary of the content presented in each Chapter.

Chapter 3 shows that the obtained bicyclo[3.1.1]hexanes units (BCHep) possess exit vector angles replicating the ones of *meta*-substituted benzene *via* computational as well as crystallographic analysis. In line with their BCP cousins, ways of functionalising obtained BCHep iodides were explored, culminating in the successfully synthesis of two drug analogues: BCHep-Sonidegib and BCHep-URB597. Besides this, problems in the attempted drug synthesis of BCHep-Ketoprofen and BCHep-Olaparib are discussed. Finally, the successfully obtained drug analogues, BCHep-Sonidegib and BCHep-URB597, were compared in their ADME and metabolic profile (in collaboration with the group of Prof. Paul Brennan in Oxford), showing for the first time the bioisosteric potential of the BCHep unit.

Finally, Chapter 4 will conclude the work presented in this thesis, and consider future questions and project directions which could be worthwhile to follow.

In summary, this thesis describes how TCHep transitioned from one example in the myriad of strained molecules into real-world applications as a precursor for accessing the bioisosteric unit BCHep for *meta*-substituted benzene system.

2.

Synthesis and Reactivity of [3.1.1]Propellane

2.1. Introduction

2.1.1. Investigations into Higher Propellanes

Besides TCPs, other higher propellanes have been synthesised and characterised. They were defined by Ginsberg as being tricyclic molecules having non-zero bridges (with a carbon atom count *x*, *y* and *z*) and one zero bridge *"being common to all three rings […] we should have an object very reminiscent of a propeller"*.[76]

This definition includes a wide span of compounds ranging from inorganic tetrelic propellanes **20** synthesised by Breher and co-workers[77-78] to unsaturated propellanes[79] **19** to propellic structures in natural products, for example, in modhephene **21** and canataxpropellane[80] **22** (Figure 16A). Here we will to limit our discussion to the 'true carbocyclic propellanes', tricyclo[$x.y.z.0^{1,(x+2)}$]alkanes, of which numerous examples were characterised and isolated (Figure 16B). Notable is the first-ever synthesised propellane, [3.2.1]propellane, by Wiberg et al. (1969)[81] and Gassman et al. (1968)[82] – a propellane which is metastable in solution at ambient temperature. Subsequently, [2.2.2]propellane was isolated by Eaton and co-workers in 1973, possessing a half-life of 28 min at 25 °C in $CDCl_3$ solution.[83]

In between the homologous series of [1.1.1]propellane (TCP) and [3.1.1]propellane (TCHep) lies [2.1.1]propellane (TCHex), synthesised in 1982 by Wiberg, which is surprisingly less stable than its 'neighbours',[84] It is only stable in a cold CsI matrix (29 K) and readily polymerises above 50 K,[85] similar to [2.2.1]propellane.[84] This is in stark contrast to TCP and TCHep which were isolated by Wiberg in 1982,[86-87] and [4.1.1]propellane (prepared in 1981 by Trennery and co-workers), which could be isolated as a solution in benzene and stored at ambient temperature. The homologous series [n.3.3]propellane (n = 3, 4, 6, 10) were synthesised and proved to all be bench stable compounds at room temperature.[88]

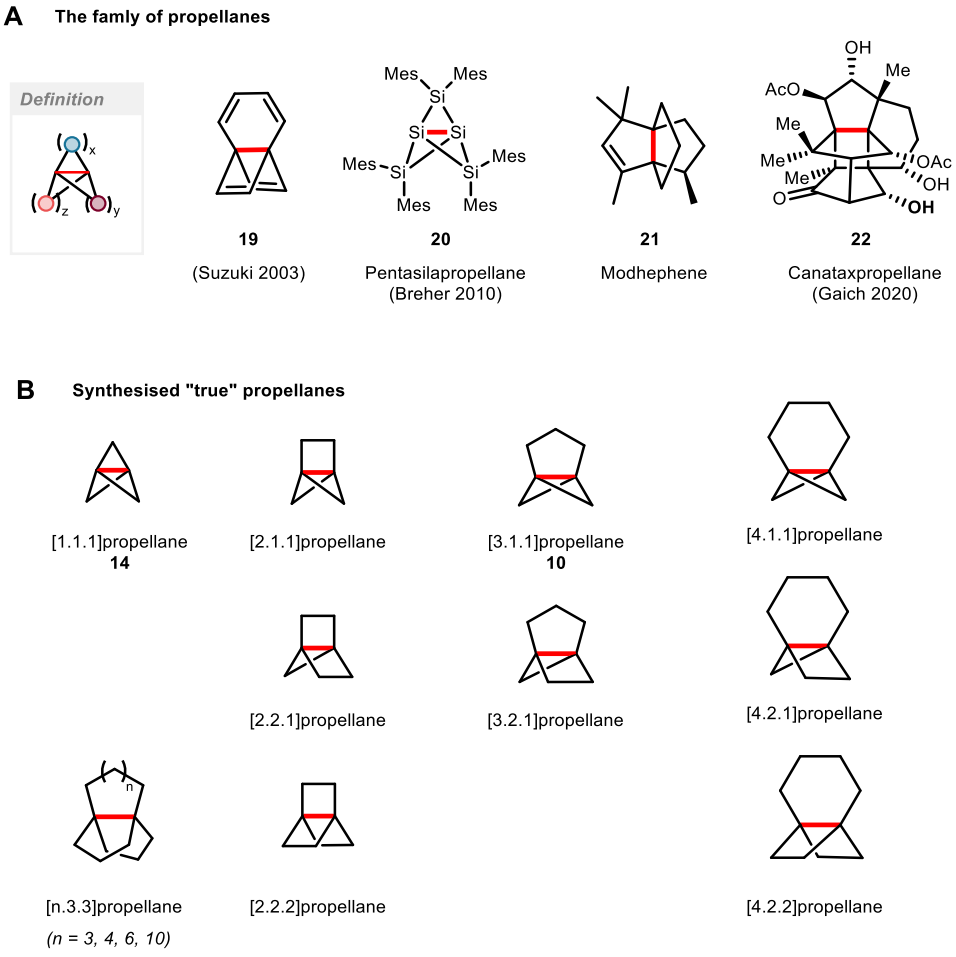


*Figure 16. (**A**) The definition of a propellane covers a broad range of compounds, (**B**) To date synthesised 'true' propellanes.*

Based on the computational and experimental mechanistic work on TCP by DPhil student Alistair Sterling, the next logical implication would be to aim to synthesise higher [n.1.1]propellane homologues, of which TCHep seemed practically the most feasible.

2.1.2. Synthesis and Characterisation of TCHep

In 1980, Gassman and Proehl reported a synthesis of TCHep, shown in Figure 17. Diester **24** was obtained from isophthalic acid **23** through esterification and hydrogenation. Alkylation of **24** with diiodomethane and subsequent ring closure afforded **25**, which could be hydrolysed and converted into propellane precursor **26** *via* the Cristol-Firth modification[89] of the Hunsdiecker reaction. TCHep was prepared by dropwise addition of a solution of **26** into a refluxing slurry of sodium in diglyme, followed by distillation of TCHep directly out of the reaction flask and trapping in a −78 °C cold trap. TCHep was isolated neat as a colourless liquid, or as a solution in d_8-toluene; polymerisation of the neat TCHep into a white solid was observed while warming it to room temperature. Gassman and Proehl achieved in this route TCHep in 4.2% overall yield over seven steps, but involved a number of undesirable reagents (e.g. KH, HgO, Na).[87]

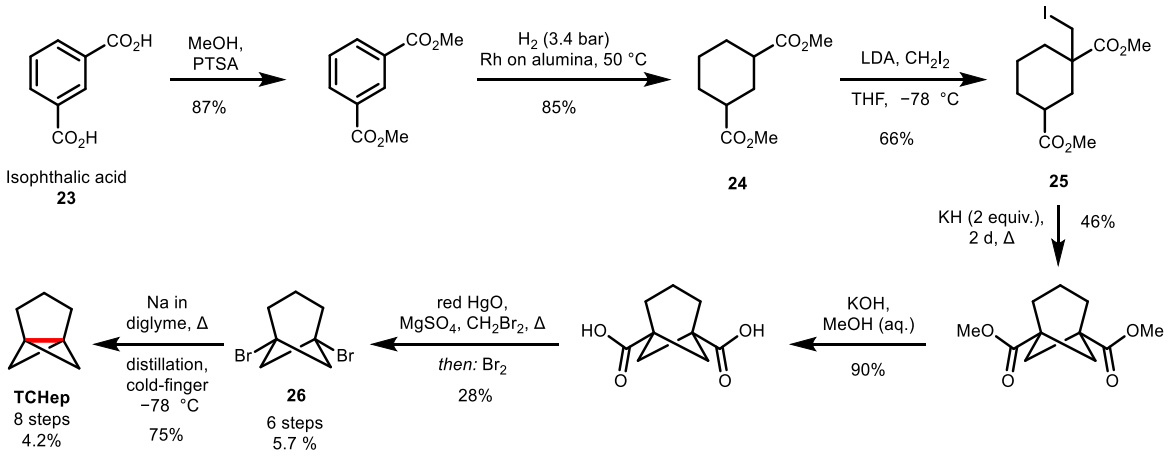


Figure 17. Synthesis of TCHep by Gassman and Proehl.

In 1992, Szeimies and co-workers reported a unified synthetic procedure towards [n.1.1]propellanes, of which the synthesis of TCHep (n = 3) is shown in Figure 18. The strategy employed tetrahalo-precursor **27** to prepare [n.1.1]propellane *via* bromine-lithiation exchange, and subsequent double ring closure, which notably has proved to be the most practical way to date to prepare TCP. For n = 1, this tetrahalo-precursor is commercially available and is used to prepare TCP on large scale in ethereal solution.[90] The Szeimies route affords TCHep in 2.5% yield over five steps, but involves multiple cumbersome distillations in the last two steps to afford neat TCHep. Furthermore, their ring-closure towards the final TCHep suffers from the formation of byproduct **29**, which arises from methylation of the lithiated intermediate **28** with the *in-situ* generated byproduct MeBr. This side-reaction inherently lowers the yield and makes purification more challenging.[85]

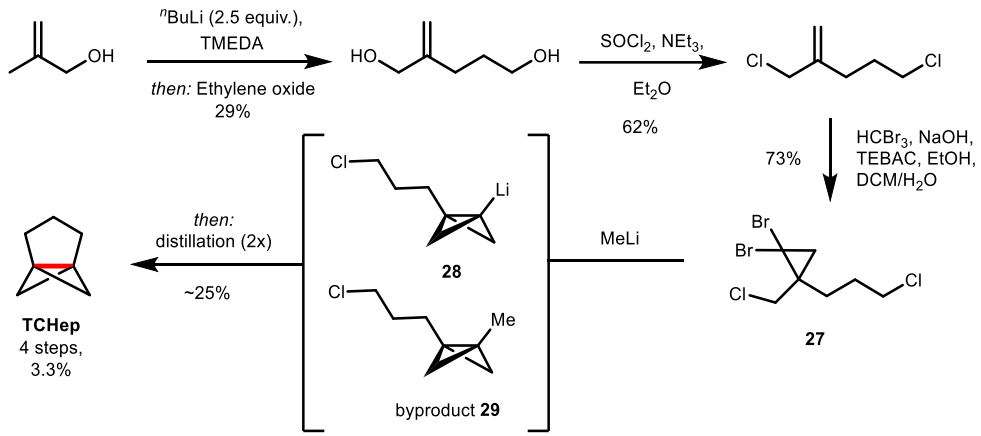


Figure 18. Synthesis of TCHep by Szeimies and Fuchs.

Szeimies and Fuchs reported a single addition reaction of TCHep: the reaction with thiophenol ethereal solution, affording **30** (Figure 19A). They also performed a vacuum flash photolysis (380 °C, $6 \cdot 10^{-6}$ Torr) on TCHep, which afforded the rearranged products **31** and **32**, presumably through retro-carbene cleavage of TCHep (Figure 19B).[85] In

addition, Gassman and co-workers reported the decomposition of TCHep in MeOH at −78 °C to various ring-opened products (Figure 19C).

It is worth mentioning that a related adamantyl-caged TCHep derivative, 2,4-methano-2,4-dehydroadamantane **33**,[91] was reported in 1980 by Majerski, along with a norbornyl-caged system **34**.[92] Majerski investigated the reactivity of **33**, finding three different product types: the opening of the inter-bridgehead bond, the opening of a 1-carbon bridge bond and the isomerisation towards an *exo*-methylene (Figure 20).

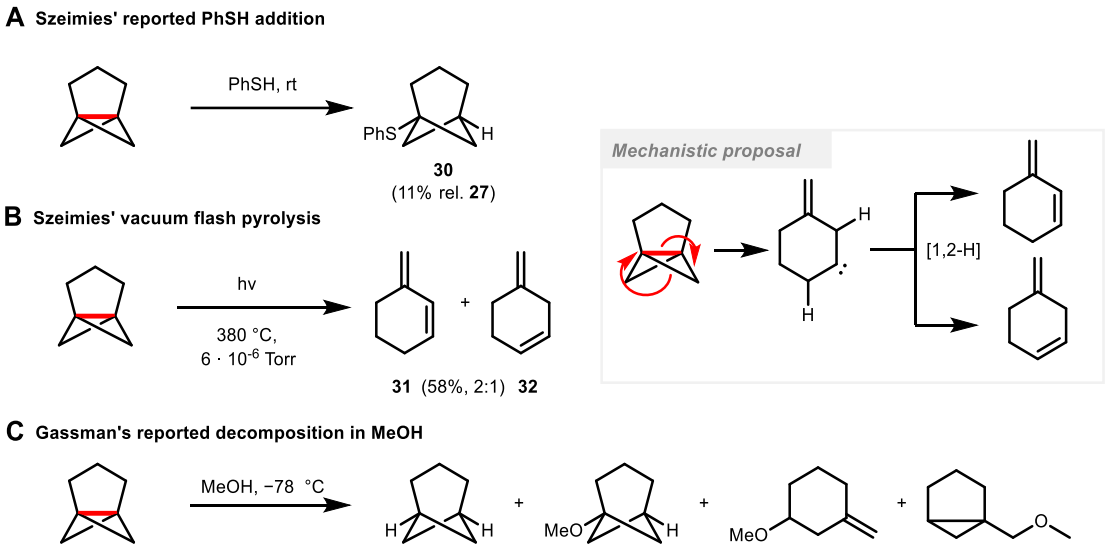


Figure 19. To-date reported reactivity of TCHep.

Under Benkeser-reducing conditions, the inter-bridgehead bond is opened, whereas the one-carbon bridge bond is reduced under hydrogenation conditions. Reagents bearing acidic hydrogens result in mixtures of all three product types. On the other hand, radical additions of PhSH, TsCl or CCl_4 afford only the inter-bridgehead ring-opened product,[91] where evidence for a radical pathway was given by EPR spectroscopy.[93] They also report the dimerisation with $AgBF_4$.[94] However, no reaction was observed with nucleophilic amines and polymerisation was observed under an O_2 atmosphere. A half-life for **33** of

approximately ten hours was measured in dry d_6-benzene solution under a nitrogen atmosphere at 65 °C.[91]

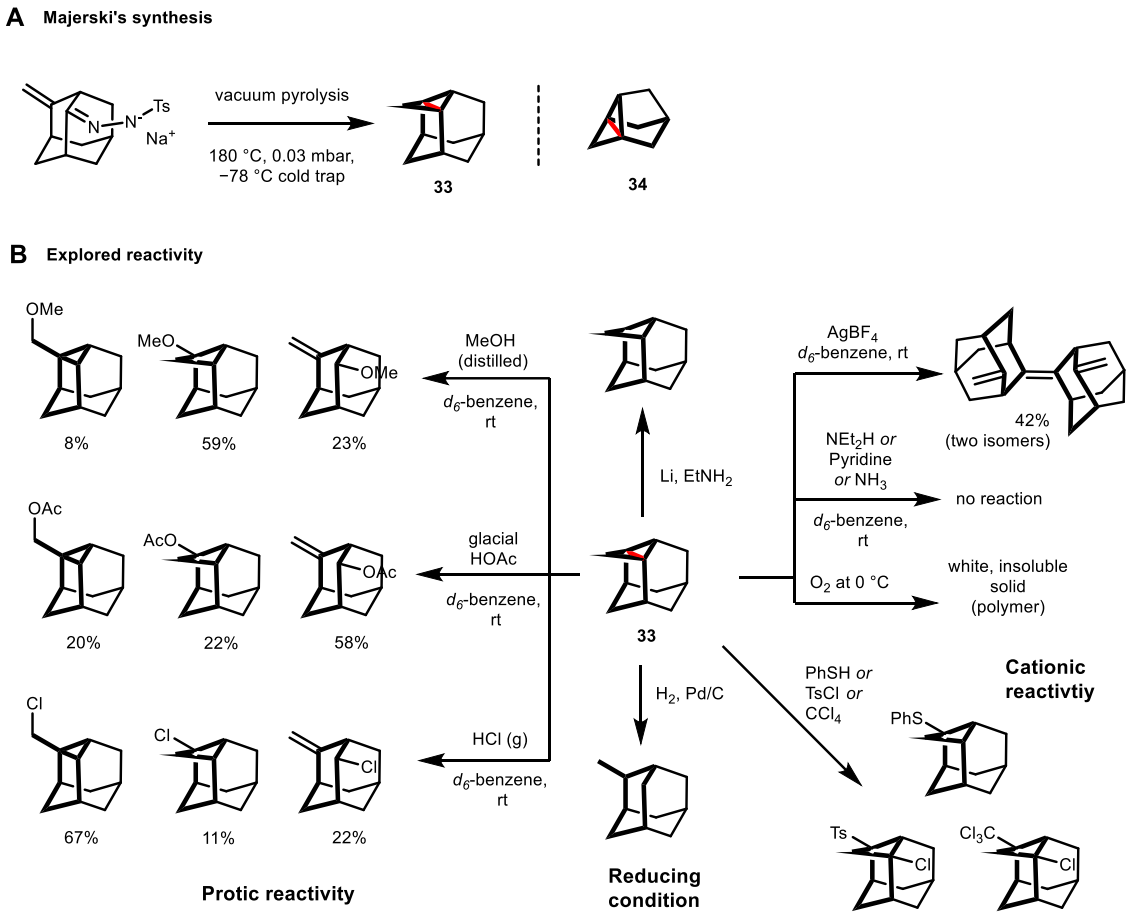


*Figure 20. (**A**) Synthesis of a caged TCHep, (**B**) Reactivity of the caged TCHep.*

Since then, interest in higher 'true' propellanes has been lost, aside from the recent flourishing research on TCP and its use in a bioisosteric context to derive BCPs. As noted, this is a topic of high interest,[65] as shown in the *Web of Science* citation rates (Figure 21). In contrast, TCHep remained 'in the dark'. Not least out of mechanistic interest, to compare higher [n.1.1]propellanes with TCP, we embarked on the synthesis of TCHep.

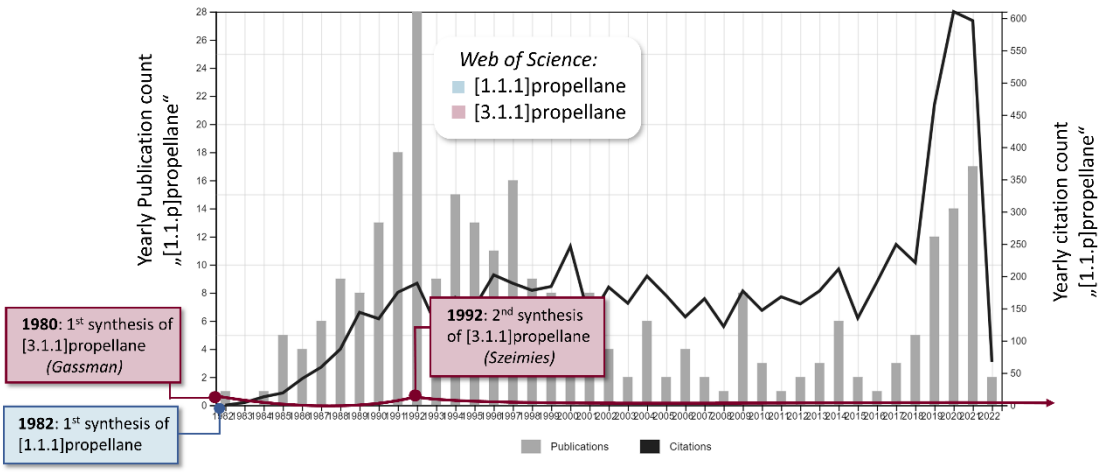


Figure 21. Citation count of the keyword "[1.1.1]Propellane" in Web of Science (accessed on 17th of February 2022).

2.2. Synthesis of TCHep

2.2.1. Dibromo bicyclo[3.1.1]hexane-Precursor Approach

First, a synthesis of TCHep similar to Gassman was attempted. The acid **35** is commercially available, making the synthesis of **24** straightforward through simple esterification. **36** was prepared in a stepwise manner using LDA with DMPU, and replacing the use of KH as base in the second alkylation step with LDA. Finally, saponification gave the BCHep-dicarboxylic acid **37** in 9.7% yield over 4 steps.

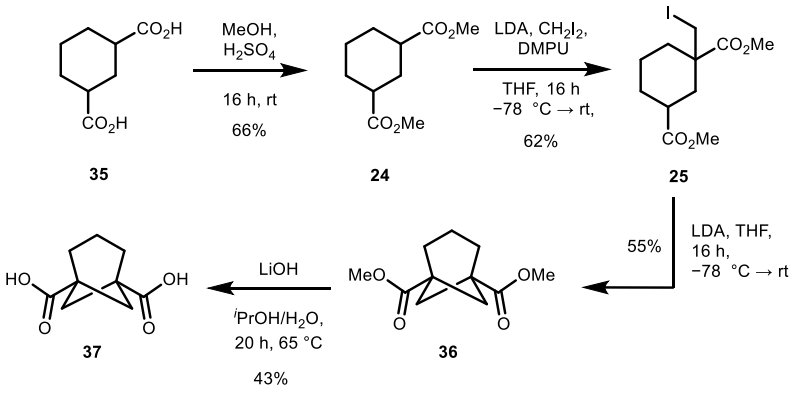


*Figure 22. Synthesis of BCHep dicarboxylic acid **37**.*

The next challenge was to find alternative conditions for the decarboxylative bromination, previously conducted using the hazardous and environmentally harmful red HgO (Figure 17). The accompanying low yield would likely make the scalability of the route problematic; therefore, alternative approaches were investigated. Gassman and co-workers already highlighted extensive screening and failure of different Hunsdiecker conditions, leaving only room for improvement through novel methodology.[87]

Recently, Uchiyama and co-workers reported a decarboxylative bromination of sterically hindered aliphatic carboxylic acids using (diacetoxyiodo)benzene (PIDA) and potassium bromide under fume hood illumination (Figure 23B).[95] The successful synthesis of tertiary bicyclic bromides in their scope encouraged us to try this reaction on the BCHep

diacid, however, poor NMR yields were observed and only 8% of **38** could be isolated after 48 h of reaction time. Similarly, a variation employing bis(trifluoroacetoxy)iodobenzene (PIFA) did not improve the yield (Figure 23B).

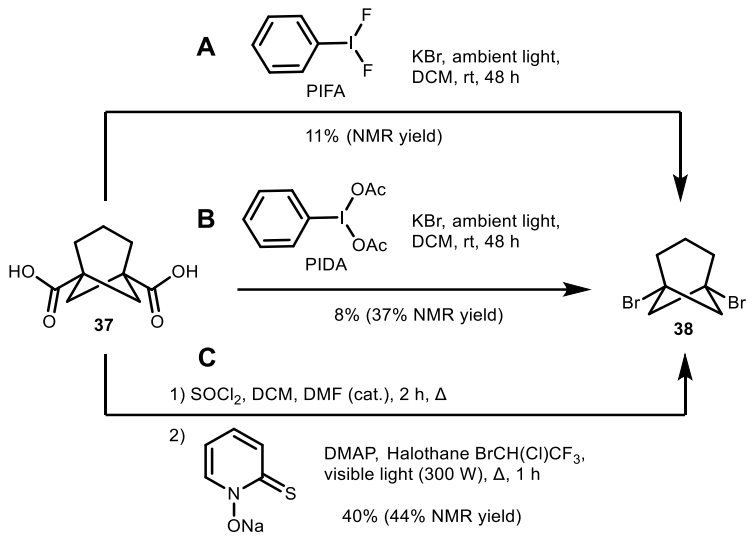


Figure 23. Alternative decarboxylative bromination.

A variation of the Barton decarboxylation exploiting a XAT from $HCBrClCF_3$ (Halothane) using visible light irradiation[96] resulted in higher yields (Figure 23C) of 44% of **38**. However, the reaction proved inconsistent on scale-up (0.27 mmol → 1.36 mmol) with a drop in yield to 14%. Therefore, at this point, the decision was made to switch synthetic strategies to employ the Szeimies 'tetrahalo' precursor, instead of relying on an inherently hard-to-access BCHep dibromide **38**, which in any case would require treatment with sodium (or equivalent metal) to effect cyclisation.

2.2.2. Tetrahalo-Precursor Approach

A novel route was developed to yield the tetrahalo precursor employing a Kulinkovich cyclopropanation[97] of commercially available γ-chloroester **39** (88%), then mesylation of the resulting cyclopropanol (96%), followed by $TiCl_4$-mediated cyclopropyl–allyl

chlorinative rearrangement (86%) to afford the intermediate **42**, intercepting with the Szeimies route. Notably, all three of these steps do not involve any purification aside from a workup step, with the resulting products obtained with purities higher than 90%.

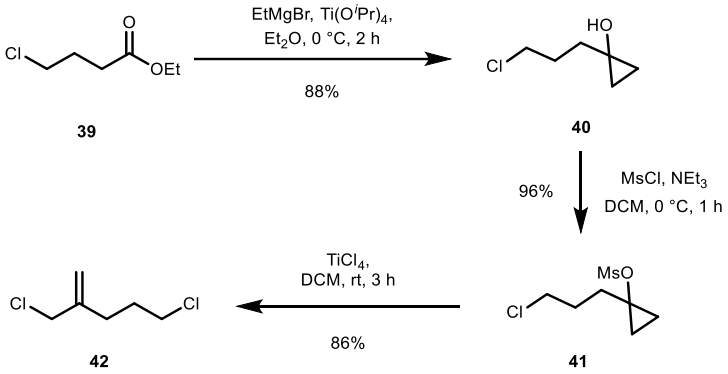


*Figure 24. Alternative synthesis towards intermediate **42**.*

The next step, a phase transfer-catalysed addition of dibromocarbene to afford the tetrahalo propellane precursor **27**, can be low yielding, accompanied by complex workups involving a slowly-separating emulsion.[98-99] Using Szeimies initially phase transfer procedure yielded **27** in 51%, which is slightly lower than the reported 73% yield. The work-up involved multiple DCM and water extractions to break up the emulsion, which was problematic, especially during scale-up.

Therefore, this step was optimised building on existing protocols developed for synthesising the tetrahalo precursor of TCP.[98-101] Monitoring the reaction progress *via* NMR (aliquots) showed the reaction reached completion after five hours at 50 °C, reducing the initially-used reaction times of 3 days at room temperature. During workup, dilution with *n*-pentane and water and a subsequent filtration through Celite turned out to be favourable compared to the recommended pentane/acetone wash. A final purification by column chromatography afforded the tetrahalo precursor **27** in 79% yield. The sequence shown in Figure 24 and 25 was successfully performed on scales up to 30 mmol.

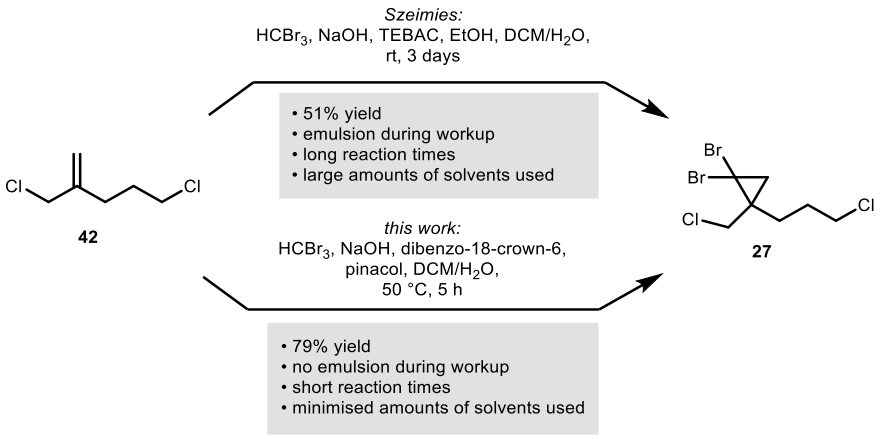


Figure 25. Improved protocol for dibromocarbene addition.

This modified dibromocarbene addition protocol makes scale-up to 30 mmol quite feasible — with higher scales, in principle, possible. However, due to safety concerns, a larger scale than 30 mmol was not performed because of the exothermic quenching of the Kulinkovich reaction and the $TiCl_4$ rearrangement. Proper mechanical stirring and internal temperature monitoring would allow better control over quenching conditions.

With this convenient procedure in hand, the synthesis of TCHep itself was undertaken. In a first proof-of-concept reaction, **27** was stirred with two equivalents of MeLi and quenched after 20 h with PhSH. The crude reaction spectrum revealed the characteristic heptet of the bridgehead proton of **30**, as reported by Szeimies and Fuchs.[85] Encouraged by this result, we gained confidence combining of the two ring closures in one single step in contrast to Szeimies and Fuchs who conducted the cyclisation stepwise *via* the bicyclobutane intermediate **28**.

Further, circumventing side-product **29** would be favourable. Baran and co-workers showed that PhLi could replace MeLi as a lithiating reagent in the synthesis of TCP, which could eliminate the issue of production of **29** *via* S_N2 (see Figure 18).

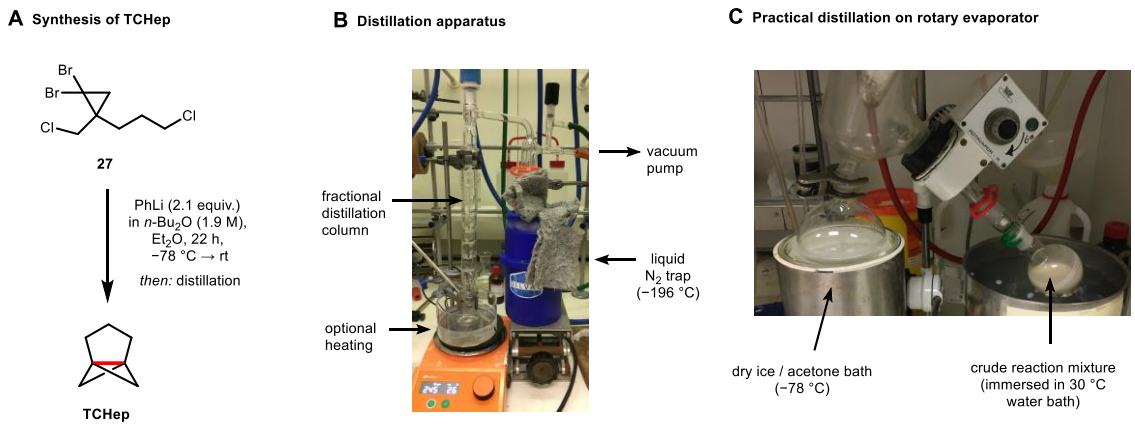


*Figure 26. (**A**) Synthesising TCHep, (**B**) First fractional distillation of TCHep reaction mixture, (**C**) Simplified distillation setup using a rotary evaporator.*

Szeimies reports distillation of TCHep at 40 mbar at 30 °C after a reaction time of 22 h at room temperature. A fractional distillation, using an apparatus constructed by DPhil student Alistair Sterling, was pursued after stirring **27** in a solution of Et_2O with 2.1 equivalents of PhLi over 22 h at room temperature (Figure 26B). TCHep was isolated as the last fraction as a solution in *n*-Bu_2O. This fractional distillation was later simplified using a rotary evaporator under inert gas (Figure 26C), distilling off first an Et_2O fraction (1013 mbar → 150 mbar, 30 °C). A second fraction (150 mbar → < 10 mbar, 30 °C) was then collected containing *n*-Bu_2O (and residual Et_2O), bromobenzene and TCHep. No evidence for the formation of byproduct **29** demonstrating the advantage of using PhLi instead of MeLi solution.

Monitoring the evolution of the TCHep NMR-peak showed a maximum concentration of TCHep after seven hours, with significant or even predominant decomposition observed afterwards (Figure 27A). Therefore, the usual reaction time was reduced to 7 h. This procedure was adapted as a general procedure, regularly affording TCHep on a scale of 30 mmol in concentrations from 0.25 – 0.50 M (~ 30 mL). This solution of TCHep can be stored in a sealed bottle at −20 °C over several months.

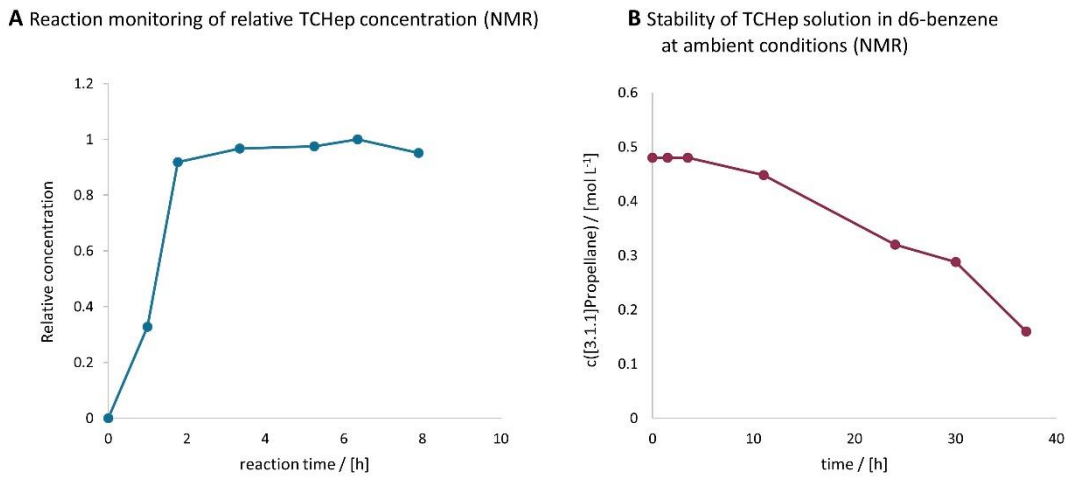


*Figure 27. (**A**) Monitoring of TCHep synthesis over time (relative to consistent n-Bu_2O peak), (**B**) decomposition of TCHep in d_6-benzene under ambient conditions (relative to internal standard 1,2-dichloroethane).*

The stability of TCHep in a solution of d_6-benzene under ambient conditions showed similar stability to TCP as determined by DPhil student Bethany Shire.[102] Both propellanes degrade slowly in d_6-benzene solution under ambient conditions (NMR tube), reaching half of their initial concentration after ca. a day (Figure 27B). This shows that TCHep is stable enough to participate in reaction profiles over several hours.

2.3. Radical-based Reactivity

Having large quantities of TCHep in hand, which was conveniently stored in a sure-sealed bottle in the freezer, the array of radical-based reactivity shown in Sections 1.2.2 and 1.2.3 was then tested on TCHep.

2.3.1. ATRA Addition of Organic Iodides

Investigations started with chemistry developed in the Anderson group, namely the BEt_3 initiated atom transfer radical addition of alkyl iodides to TCP was investigated.[44] This reaction system translated well onto TCHep for electron-deficient radicals, like **43** or **44**. As a third successful substrate, we found the Boc-protected iodoaziridine **45** added in moderate yield to TCHep, perhaps being somewhat electrophilic through higher s-orbital contribution (Figure 28A).

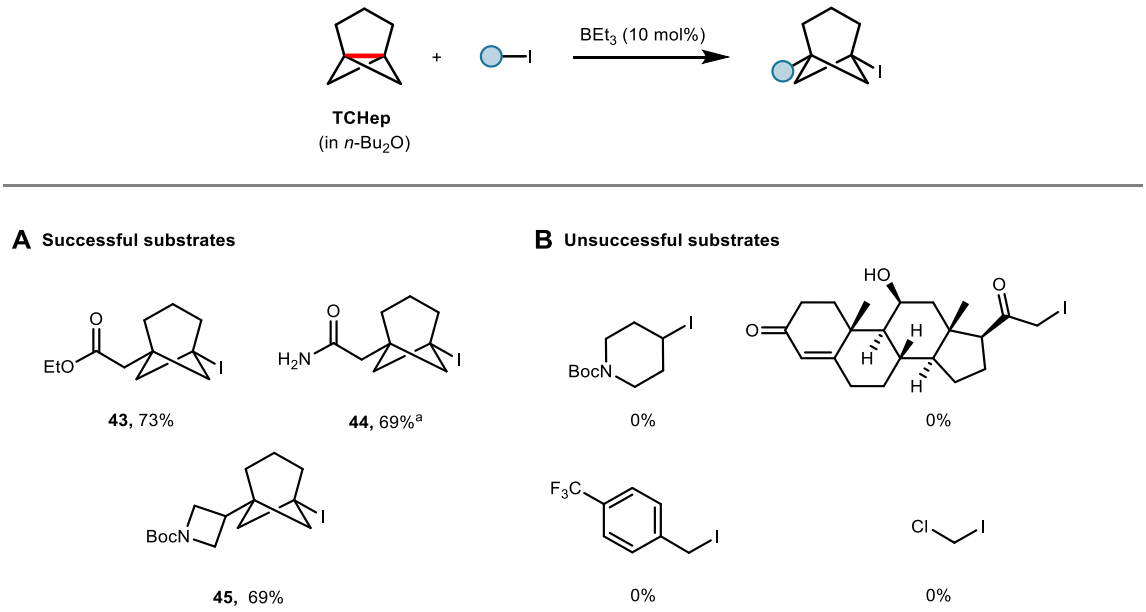


*Figure 28. BEt_3 initiated reaction of R-I with TCHep (**A**) Successful reactions, (**B**) Unsuccessful reactions. [a] MeOH was added as a co-solvent to facilitate the solubility of acetamide.*

More electron-rich substrates not bearing a carbonyl moiety in the α-position to the iodo-substituent resulted in complex reaction profiles, leading to unsuccessful reaction. Even

complex α-iodo carbonyls, like a corticosterone derivative, failed to undergo ATRA chemistry with BEt_3 and TCHep (Figure 28B).

The use of photoredox-catalysed conditions, using *fac*-[$Ir(ppy)_3$] (456 nm blue LED irradiation) was next investigated – chemistry which also developed by the Anderson group for TCP.[45] This method turned out to be more versatile and higher-yielding, successfully converting benzyl iodides (**48** – **49**) and alkyl iodides (**50**, **45**) into their BCHep iodide counterparts. Even nucleophilic radicals, derived from **51** and **52**, inserted into TCHep in good yield under these conditions, and heteroaryl iodides also reacted well in good yields (**55**, 71%). Probing the reactivity of electron-deficient aryl iodides, like 4-iodobenzonitrile or methyl 4-iodobenzoate, showed no product formation for TCHep, although they were known to react with TCP.[45] Already at this point, the central schizophrenia between TCP and TCHep becomes clear: Why does some TCP methodology translate seamlessly onto TCHep, whereas others fail or pose strict limitations to the substrate scope? These questions will be explored in Section 2.5.

Nonetheless, complex drug examples can be late-stage decorated with a BCHep-unit, like a brequinar analogue **56**, a nicotinic acid **58** or an indomethacin derivative **59**. In contrast to employing BEt_3, the reaction with an iodide derivative of corticosterone **57** proceeded successfully in 70% yield. Particular important for potential applications in protein modification, α-iodo amino acids **54** can be functionalised in good yields retaining their stereocenter. Several of the substrates in Figure 29 were performed on scales greater than 1.0 mmol, demonstrating that scalability is possible with TCHep. Finally, the addition of bromomalonates (**60**) proceeded similarly to TCP.

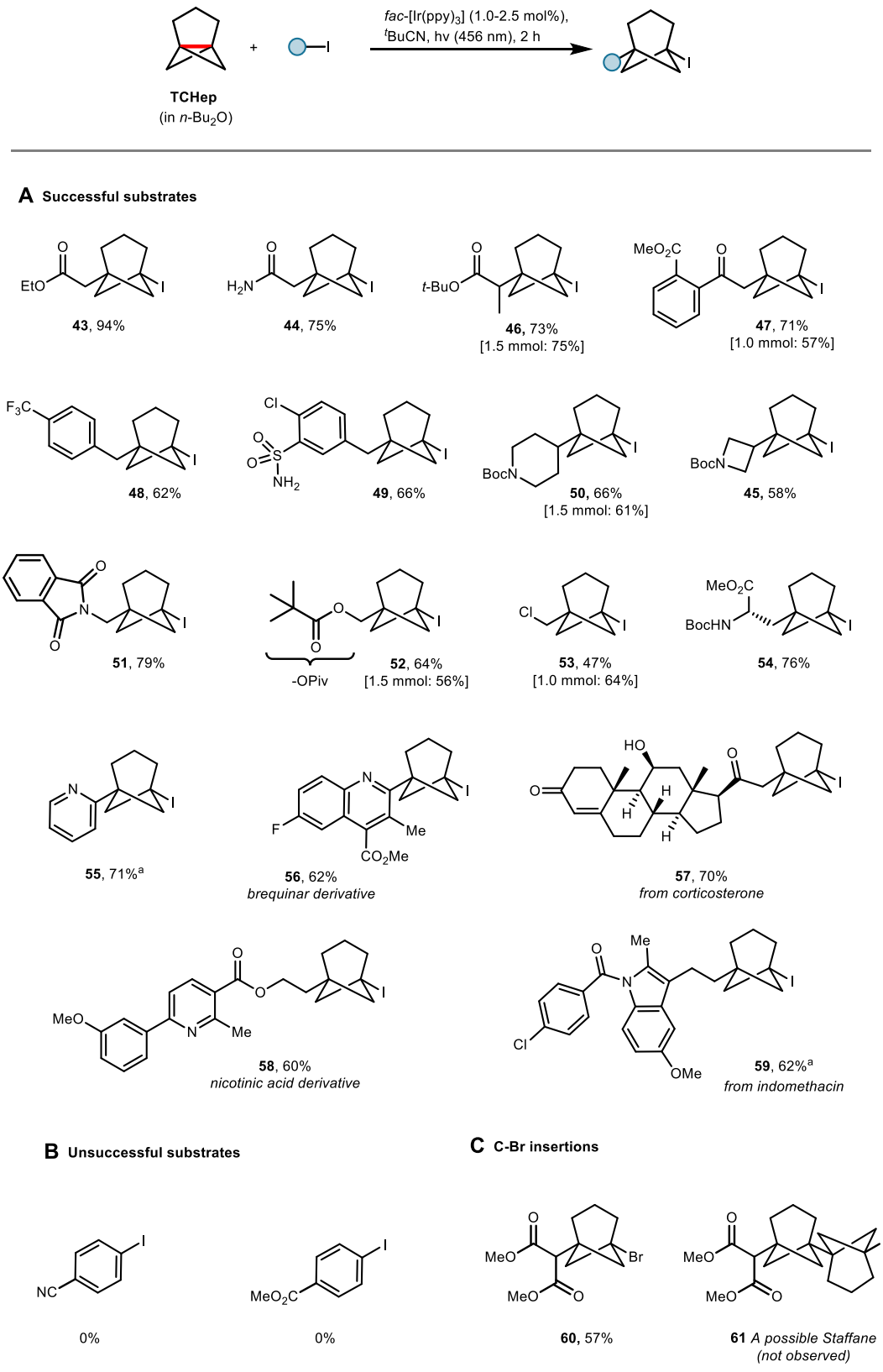


*Figure 29. (**A**) Successful scoped organic iodides inserted into TCHep, (**B**) Unsuccessful reactions. [a] Reaction was performed and characterised by Dr Jeremy Nugent. Reactions were performed on a 0.1-0.2 mmol scale unless stated otherwise. (**C**) Carbon-bromide scope.*

At this point, one further aspect of the reactivity of TCHep is of note: In contrast to TCP, no ‘staffane’ byproducts (i.e. **61**, dimerised or oligomerised BCHep-units), were observed or could be isolated besides **60**, which is in marked contrast to TCP (see Section 2.5.5).

Our group reported successful cascade cyclisation / bicyclopentylation for various substrates (Figure 30). Surprisingly, when TCHep was employed in these cascade substrates **62** and **63**, only an unidentifiable reaction profile was observed. Purification of these mixtures *via* column chromatography did not reveal a specific ratio of the possible products shown in Figure 30, indicating that other unproductive side reactions were dominant.

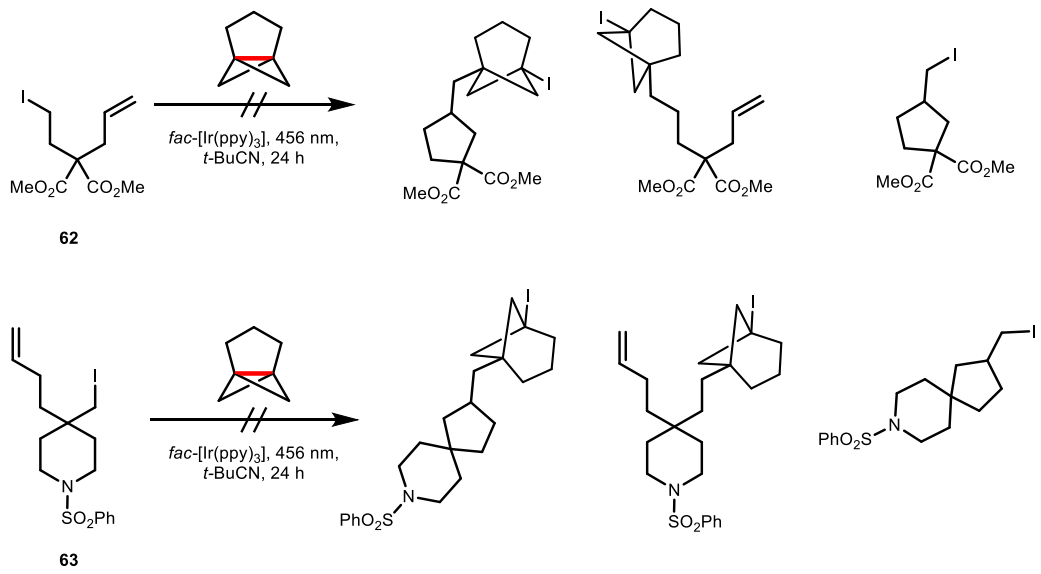


Figure 30. Failed cascade BCHep-ylations with shown possible products.

In summary, for the first-time versatile carbon bridgehead-substituted BCHep iodides can be prepared using ATRA chemistry of organic iodides.

2.3.2. Addition of Perhalides Without any Initiator/Catalyst

Some organic halides add into propellanes without any apparent external initiation, as reported by Wiberg and co-workers. The same appears to be true for TCHep, which afforded adducts **64**, **65** and **66** in moderate to good yield (Figure 31). The investigation of other fluoroperhalides would be worthwhile, and could give further interesting BCHep-units. Similarly, a reaction between TCHep and *tert*-BuOCl was conducted at −78 °C, and afforded crude product **67** with unidentified byproducts. This reaction was reported (for TCP) to be highly sensitive to control of the reaction conditions, especially ambient light, and similar results were found for TCHep. Interestingly, the addition of I_2 (added as a solution in THF) does not proceed in a quantitive fashion as it does for TCP; inspection of the crude ^{1}H NMR spectrum showed several unidentifiable byproducts despite the setup being handled under the exclusion of light.

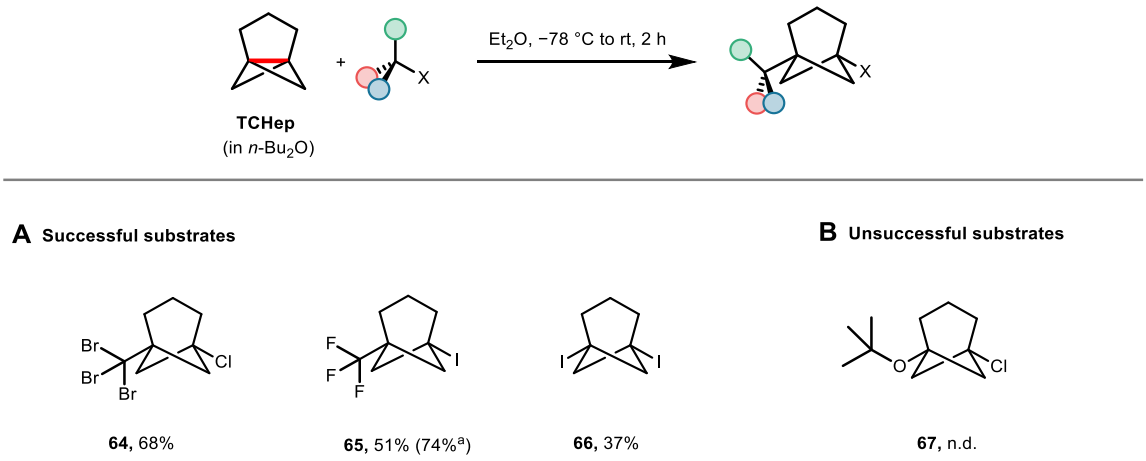


Figure 31. Addition of halides to TCHep without external initiator. [a]NMR yield.

2.3.3. Addition of Chalcogen Reagents

It was next verified whether thiophenol can also add without external initiator, this being the only known reaction of TCHep already reported (by Szeimies and co-workers).[85]

This result was reproduced with quantitative yield (**68**), and was further demonstrated on a more complex, aliphatic thiol using *N*-Boc-L-cysteine methyl ester **69**. Unprotected peptides, like glutathione **70**, yielded no apparent BCHep product and were later investigated in further detail (Section 2.6). Interestingly, *tert*-butyl thiol showed no reactivity towards **71**, presumably because of the high steric hindrance of two sulfur-adjoined tertiary carbon centres or because of different initiation abilities. Higher chalcogens, like selenophenol PhSeH, added smoothly into TCHep as well (**70**, Figure 32). It should be noted that no *in-situ* reduction with $NaBH_4$ of the selenophenol batch (fresh bottle) was performed. This reagent is known to form phenyl diselenide readily under ambient conditions. Therefore, whether the reaction proceeds *via* PhSeH, *via* homoloytic cleavage of PhSe-SePh or through both pathways is unclear.

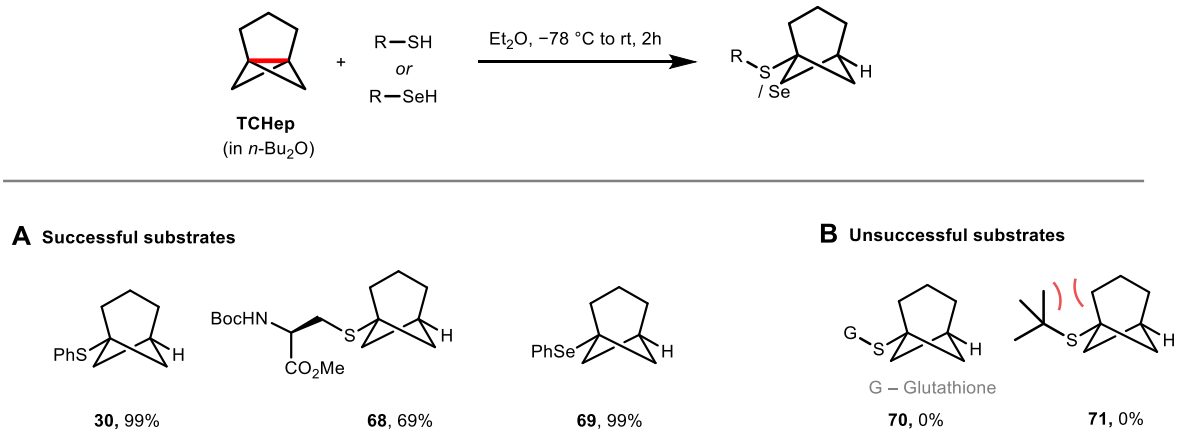


Figure 32. Addition of chalcogenides to TCHep without any external initiator.

The thiophilicity of TCHep was further demonstrated by Dr Jeremy Nugent, who showed the 'thermal' addition of thiosulfonates **72** and **73** proceeds for TCHep in excellent yields of 90% and 95% (Figure 33A). Further, UV-induced addition of disulfides to form **74** was investigated using a 365 nm LED lamp (UV-A), mimicking a medium-pressure UV

lamp used in earlier reports on UV-induced reactivity of TCP.[29, 90] Admittedly, the single-line emission spectra of the used LED does not fully reproduce the broad spectrum of a medium-pressure Hg lamp with a range from 200 to 600 nm. Interestingly, no reaction for **75** and **76** was observed, the former potentially due to solubility issues (Figure 33C).

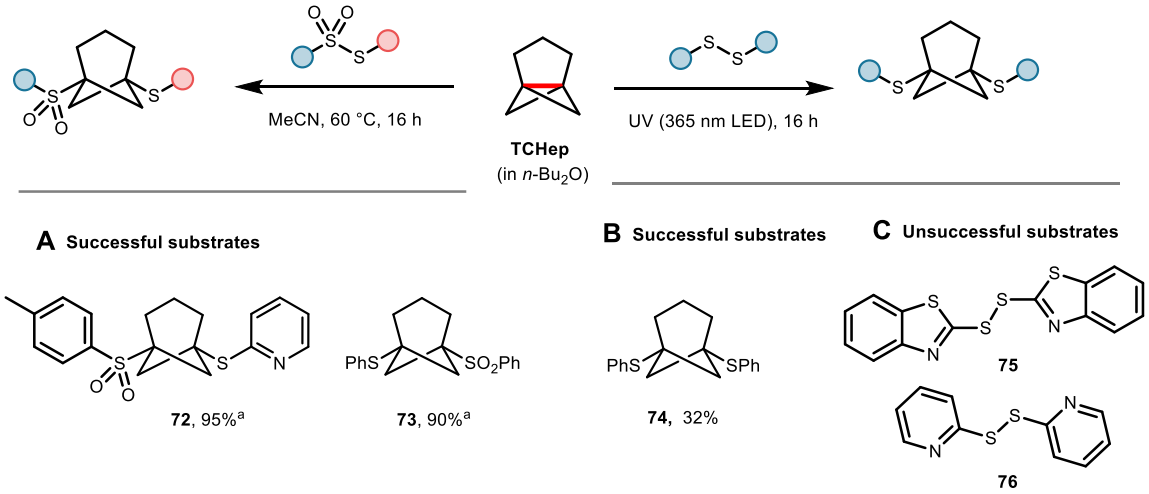


*Figure 33. Sulfur radical reactivity of TCHep for (**A**) thiosulfonates and (**B**) disulfides. [a]Synthesised and characterised by Dr Jeremy Nugent.*

2.3.4. Exploration of UV-Induced Reactivity

Motivated by this initial success, other UV-induced reactions known for TCP[31] (compare to Figure 7) were probed, shown in Figure 34. The general mechanism likely features the UV-initiated cleavage of the reagent dimer, which adds into TCHep followed by a standard propagation pathway.

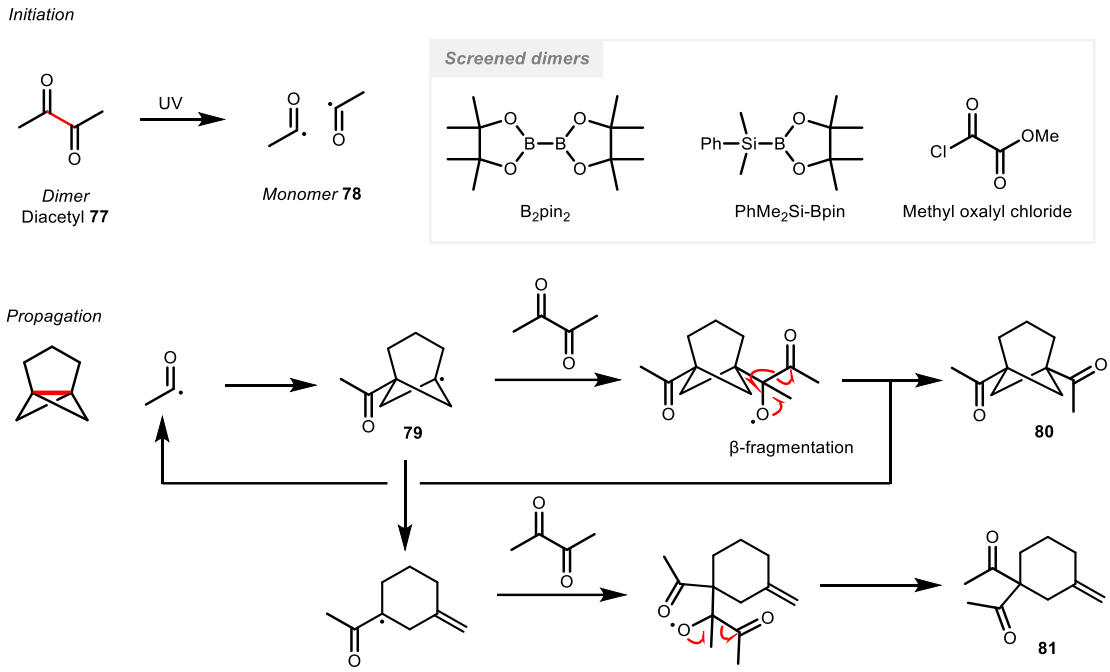


Figure 34. Mechanistic proposal of the UV-induced radical chain.

For example, in the case of diacetyl **77** (Figure 34), the resulting BCHep radical **79** turns over the chain by adding into another diacetyl molecule, with subsequent β-fragmentation releasing another acyl-radical **78** and delivering product **80**. A similar propagation mechanism can be imagined for the dimers methyl oxalyl chloride,[103] B_2pin_2[104] or $PhMe_2Si$-Bpin[51] (α-fragmentation). Table 1 summarises the screen of reaction conditions, and Figure 35 shows the set-up used involving the above-mentioned 365 nm UV LED, transmitted through a boron-free fibre into the reaction mixture immersed in a cryogenic cooling bath or heating oil bath.

Unfortunately, methyl oxalyl chloride, B_2pin_2 and $PhMe_2Si$-Bpin showed no trace of the characteristic splitting pattern of BCHep products, with a complex reaction profile. For diacetyl, two products **80** and **81** were observed, resulting either from inter-bridgehead bond cleavage or cleavage of the one-carbon bridge bond. This unique example of TCHep reactivity in which a bridge C–C bond is cleaved is examined further mechanistically in Section 2.5.6. The ratio between **80** and **81** can be marginally influenced by temperature

control, but no linear trend was observed (see Table 1). All reactions (including those that failed for TCHep) were verified to be reproducible on TCP.

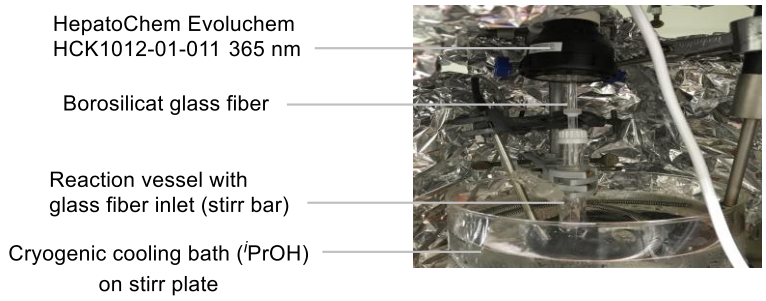


Figure 35. Set-up for UV-induced reactions.

Table 1 Attempted reaction of dimers and reaction conditions. All reactions were performed under N_2-atmosphere unless stated otherwise.

Reagent	**Temperature**	**Time**	**Conditions**	**Result**
B_2pin_2	20 °C	24 h	365 nm (UV)	No productive reaction
		24 h	none	
		2 h	none	
$PhMe_2Si$-Bpin	20 °C	24 h	365 nm (UV)	No productive reaction
		24 h	none	
		2 h	none	
		24 h	non-inert (air)	
	0 °C	5 h	non-inert (air)	
Methyl oxalyl chloride	20 °C	24 h	365 nm (UV), Morpholine	No productive reaction
Diacetyl	20 °C	24 h	365 nm (UV)	**81** : **80** = 1 : 1.5
	0 °C		365 nm (UV)	**81** : **80** = 1 : 2.3
	−20 °C		365 nm (UV)	**81** : **80** = 1 : 2.3

2.3.5. *N*-centred Radicals

Next, the established chemistry of *N*-centred radicals (on TCP) was studied. Pleasingly, the fragmentation of α-iodoaziridines to generate sulfonamidyl radicals, as developed in our group by DPhil student Helena Pickford,[47] was found to translate successfully to TCHep furnishes **82** (Figure 36). However, a drop-in yield of approximately 20% was observed compared to the BCP analogue, similar to the photoredox-transformations reported in Section 2.3.1. A full substrate scope was not probed and leaves room for further analysis.

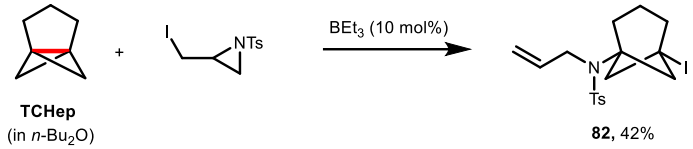


Figure 36. Addition of α-iodoaziridines to TCHep.

The addition of *N*-iodopyrazole to TCHep, as reported by Zarate et al.[105] on TCP using I_2, 3-iodopyrazole and Cs_2CO_3, afforded **83** for TCHep (Figure 37). The authors do not comment on a detailed mechanism.

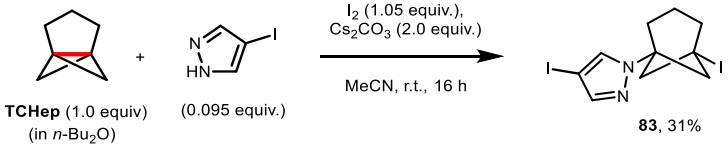


Figure 37. Addition of iodopyrazole to TCHep.

MacMillan and co-workers report a versatile photoredox platform for addition of *N,C* substituents to TCP employing iodonium dicarboxylates such the one shown in Figure 38, and metallaphotoredox catalysed conditions (Cu salt and *fac*-[$Ir(ppy)_3$] catalysts). With a slight modification, those conditions were successfully employed on TCHep for azarenes (**84**–**88**) and sulfonamides (**89**). In contrast to MacMillan's conditions, an

increase in reaction time from 2 h to 16 h was required to give product. Other *N*-nucleophiles, like oxazaindoles **91**, pyrroles **92** or imines **93**, were not successful. In contrast, no limitations were observed for the iodonium dicarboxylates compared to the published scope for TCP. As such, tetrahydrofuran **84**–**87** or *tert*-butyl units **88** can be installed as well as complicated drug moieties (e.g. **90** derived from gemfibrozil). This demonstrates how TCHep can be used to functionalise pharmaceuticals to easily derive modified scaffolds at a late stage (Figure 39). The corresponding iodonium dicarboxylates can be easily derived by stirring iodomesitylene and 2.0 equivalents of the carboxylic acid under air in toluene, with the solvent subsequently distilled off at 50 °C (Figure 38).

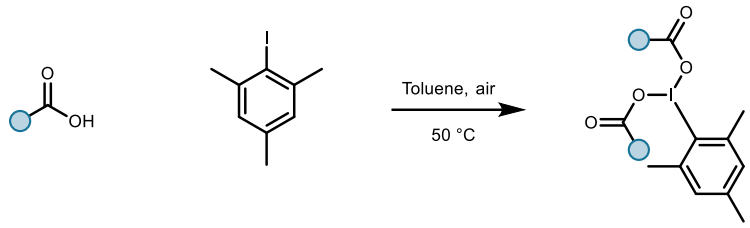


Figure 38. Synthesis of iodonium dicarboxylate precursors according to a procedure of MacMillan and co-workers.[106]

The reaction profile (as judged by the ^{1}H NMR spectrum of the crude reaction mixture) appeared to be less clean compared to that using TCP. This may be rationalised by the longer reaction times needed, and the accompanying susceptibility of TCHep to undergo various (unidentifiable) side reactions, to be discussed in Section 2.5.6. Again, a reduction of 20% in yield compared to TCP was observed, also because of the burdensome purifications needed that involved multiple column chromatographies, recrystallisation, and acid-base washes (see individual procedures in Supporting Information). Figure 39 presents the full scope, along with examples such as the Togni reagent II as a *C*-centred radical source being unsuccessful on TCHep.

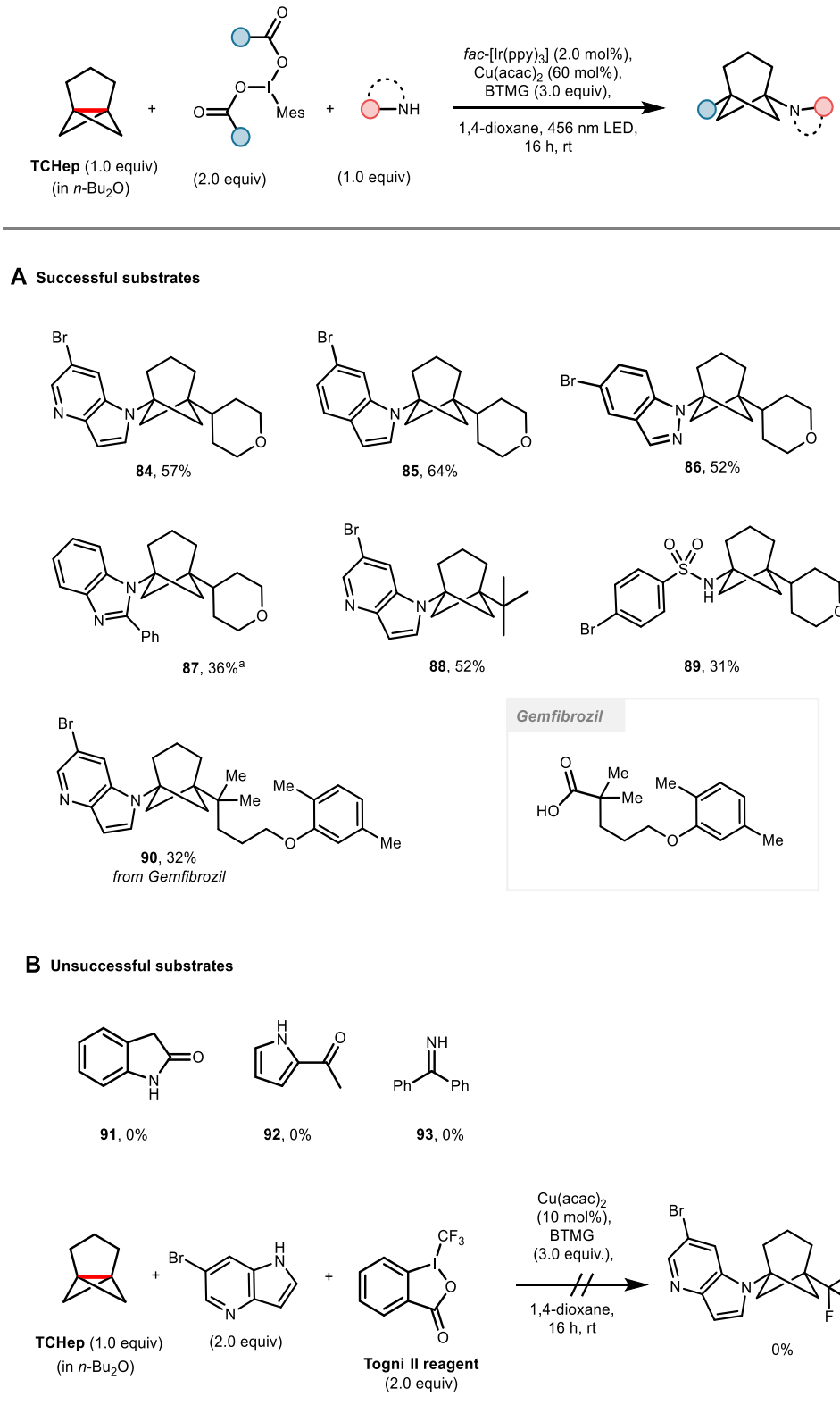


Figure 39. MacMillan and co-workers metallaphotoredox system of N-nucleophiles and iodonium carboxylic acids employed on TCHep. [a]Cu(TMHG)$_2$ (60 mol%) was used instead of Cu(acac)$_2$.

2.3.6. Summary

In summary, several productive reactivity channels known for TCP have been identified to be successful on TCHep. For each, a substrate scope was prepared, showing the tolerance range. Some reactions, like MacMillan and co-workers' three-component coupling, showed some limitations relative to the scope reported for TCP. Others proved equally successful, especially the insertion of C–I bonds into TCHep under photoredox conditions which was similarly versatile and high-yielding as for TCP, giving access to bridgehead-substituted BCHep units, which were near-impossible to access previously.

2.4. Exploring Anion-based Reactivity

The anionic addition methodologies developed for TCP (as described in Section 1.2.3) offer the possibility to be probed on TCHep too. However, the addition of turbo-amides, e.g. $Bn_2NMgCl{\cdot}LiCl$,[37-38] was not successful on TCHep neither at the reported 60 °C nor at room temperature (Figure 40A). The $Bn_2NMgCl{\cdot}LiCl$ solution used in this experiment was prepared fresh, and the reaction was reproducible on TCP. An explanation for the failing reactivity will be sought in Section 2.5.4.

Similarly, the addition of Grignard reagents following the protocol of Knochel and co-workers[33] (see Section 1.2.3) did not yield any product (Figure 40B). Knochel's addition of Zn-enolates[34] was reproduced on TCP, ensuring successful preparation of the cyclopentanone enolate **94**, although it did not deliver any identifiable product for TCHep (Figure 40C). Walsh's addition of 2-azaallyl-anions **95** was also tested without success on TCHep (Figure 40D).[40] Despite multiple trials to translate the abovementioned reactions to TCHep, it was concluded that apparently, TCHep does not undergo productive addition of anions – in stark contrast to TCP. Section 2.5 will try to elucidate this noticeable difference in reactivity between TCHep and TCP.

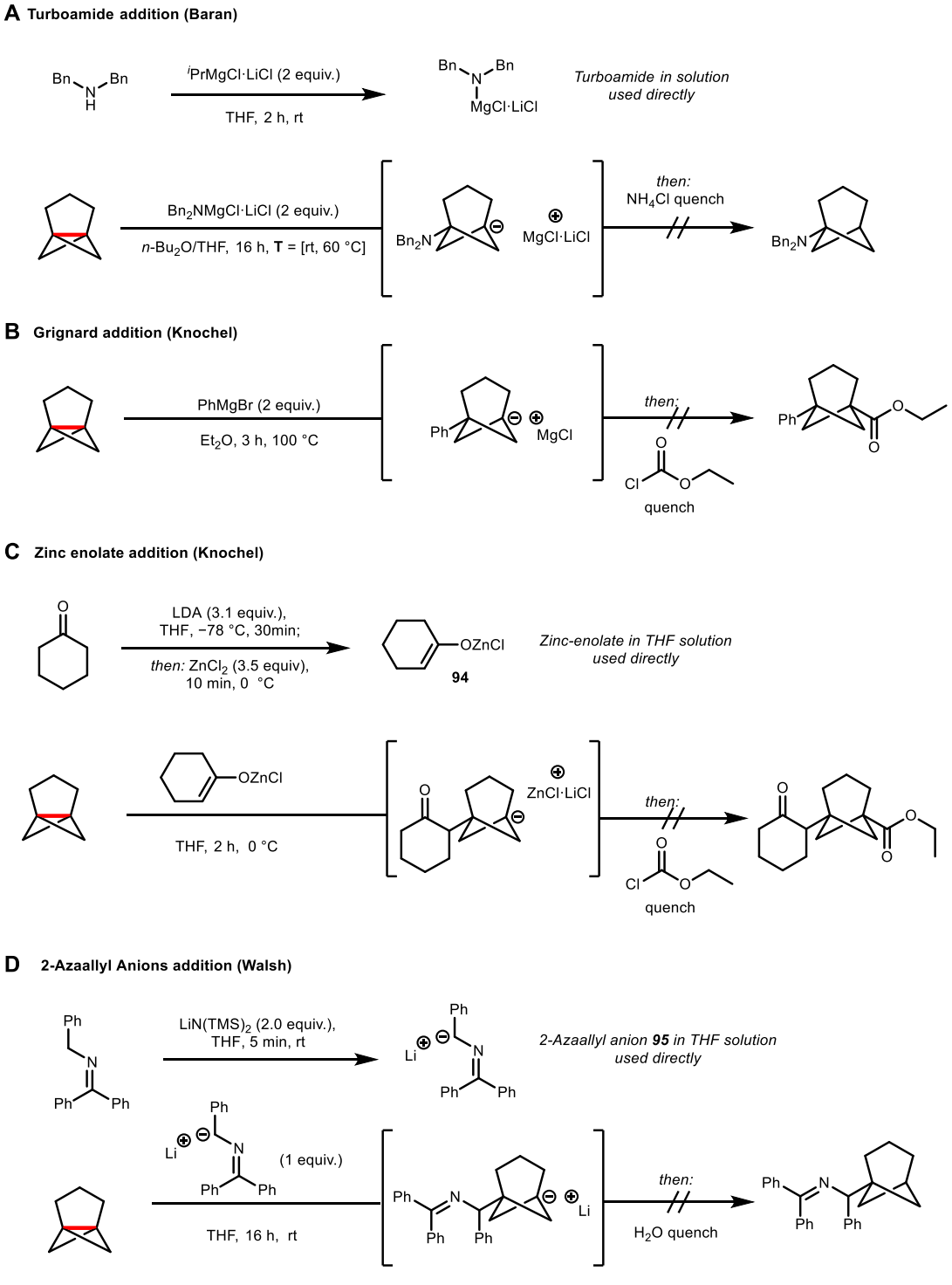


Figure 40. Unsuccessful attempted anionic additions to TCHep.

2.5. Mechanistic Comparison with TCP

Several key differences in reactivity between TCP and TCHep can be identified when comparing their reaction profile and the scope of the tested reactions in Section 2.3 and 2.4. They can be summarised as follow:

1. No anionic methodology was successfully translated onto TCHep,
2. No staffane formation was found for TCHep in contrast to TCP,
3. In general, a more complex reaction profile was obtained, accompanied by a yield reduction of approximately 20% compared to TCP in many reactions.

This section attempts to develop hypotheses for this behaviour, aided by competition experiments and computational analysis. To begin, a short benchmark of the chosen computational level is given to ensure robust computational results, showing how benchmarking geometric features alone is insufficient. For further technical details, see the Supporting Information. The second half aims to characterise bonding properties of the TCHep inter-bridgeheaded bond as well as its reactivity compared to TCP.

2.5.1. Benchmarking Computational Methods

To understand the difference between TCHep and TCP, the first step is to characterise their geometry and electronic properties. Toward this aim, a series of DFT functionals and basis sets where evaluated and compared to the results obtained at the RI-SCS-MP2/def2-QZVPP level of theory.[107] The DFT functionals BLYP, B3LYP, and the double-hybrid functional B2GB-PLYP and B2PLYP was evalulated.

Geometric parameters evaluated in TCHep include the bridgehead bond length r(1-5) and the dihedral angle between C1, C7, C5 and C6. Evaluation of different basis sets demonstrated that a double-zeta basis set underestimates r(1-5) and that a triple-zeta basis

set (def2-TZVP or def2-QZVPP) is required to achieve converged results (Figure 41). Regarding the tested DFT functionals, BLYP reproduces the bridgehead bond distance best compared to SCS-MP2/def2-QZVPP, followed by B2PLYP. Incorporation of the dispersion correction D3BJ was found to have little effect on geometries (Figure 42).

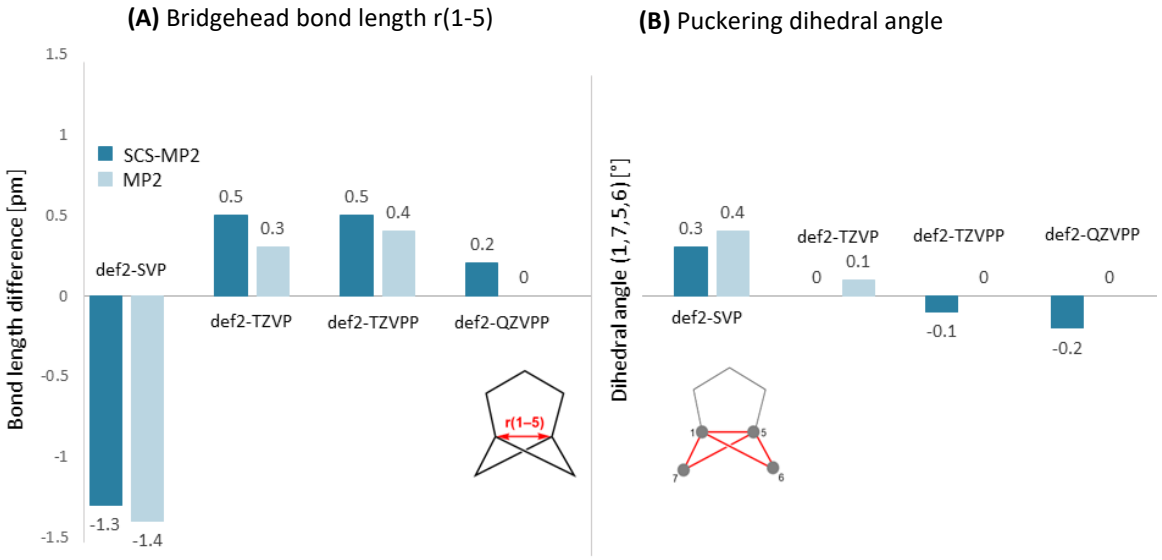


*Figure 41. Effect of basis set on (**A**) bridgehead bond length r(1-5) and (**B**) dihedral angle (1,7,5,6) relative to SCS-MP2/def2-QZVPP.*

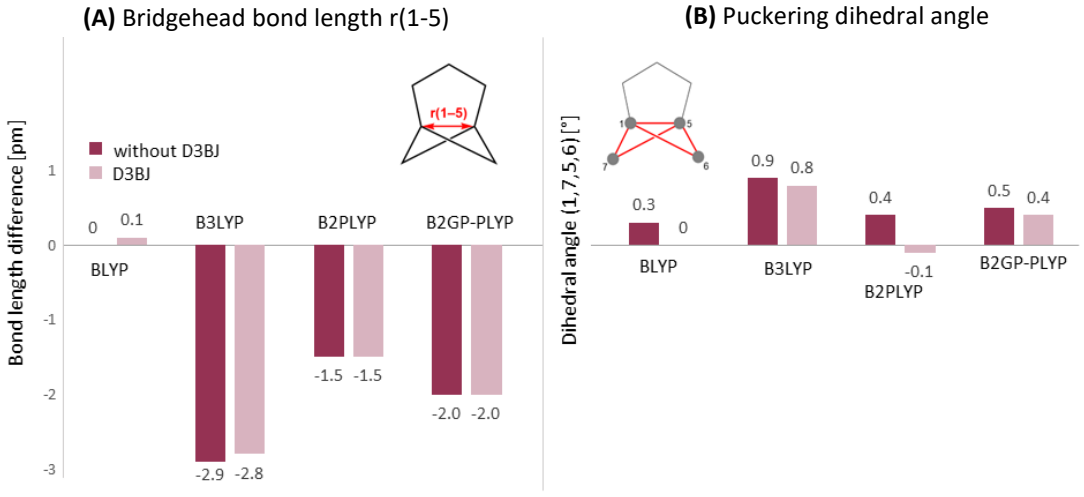
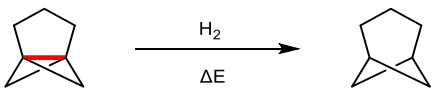


*Figure 42. Effect of DFT functional choice and inclusion of dispersion corrections on (**A**) inter-bridgehead bond length r(1-5) and (**B**) puckering dihedral angle (1,7,5,6) relative to RI-SCS-MP2/def2-QZVPP.*

Following these studies, we sought to further investigate the performance of these methodologies on electronic properties, such hydrogenation energy, electron densities and singlet-triplet gaps. Evaluation of these properties has been previously found to provide a good guideline to identify robust methodologies for exploring reactivity in TCP.[22]

The hydrogenation energy of TCHep was obtained with different functionals and basis sets and compared to results obtained at DLPNO-CCSD(T)/def2-QZVPP//SCS-MP2/def2-QZVPP level of theory (57.8 kcal mol^{-1}, Table 2). In summary, consistent results were obtained for all methods tested, with ΔE ranged from 54.1 kcal mol^{-1} to 56.4 kcal mol^{-1}. This demonstrates the reliability of the herewith used method.

Table 2. Electronic hydrogenation energies comparison.



	Absolute ΔE [kcal mol^{-1}]	$\Delta E - \Delta E_{DLPNO\text{-}CCSD(T)}$ [kcal mol^{-1}]
DLPNO-CCSD(T)/def2-QZVPP//SCS-MP2/def2-QZVPP	-57.8	0.0
SCS-MP2/def2-TZVP	-54.1	3.7
SCS-MP2/def2-QZVPP	-54.7	3.1
SCS-MP2/def2-QZVPP//SCS-MP2/def2-TZVP	-54.7	3.1
B3LYP/def2-QZVPP	-54.7	3.1
B2PLYP-D3BJ/def2-TZVP	-56.2	1.6
B2PLYP-D3BJ/def2-QZVPP	-56.4	1.4

Density differences (ρ) obtained by SCS-MP2 and DFT-functionals were compared to the density obtained using the (linearised) DLPNO-CCSD/def2-QZVPP density (Figure 43). SCS-MP2 densities proved to be similar to DLPNO values, while densities from DFT functionals provide mixed results. For example, BLYP and B3LYP were found to provided significantly different densities, even though both of them performed well in the geometry benchmark. In contrast, the double hybrid functionals, B2PLYP and B2GP-PLYP, were found to reproduce the DLPNO-CCSD/def2-QZVPP electronic density. This is in line with previous studies by DPhil student Alistair Sterling recognised that benchmarking electron densities and singlet-triplet gaps were critical to identifying robust methodologies.

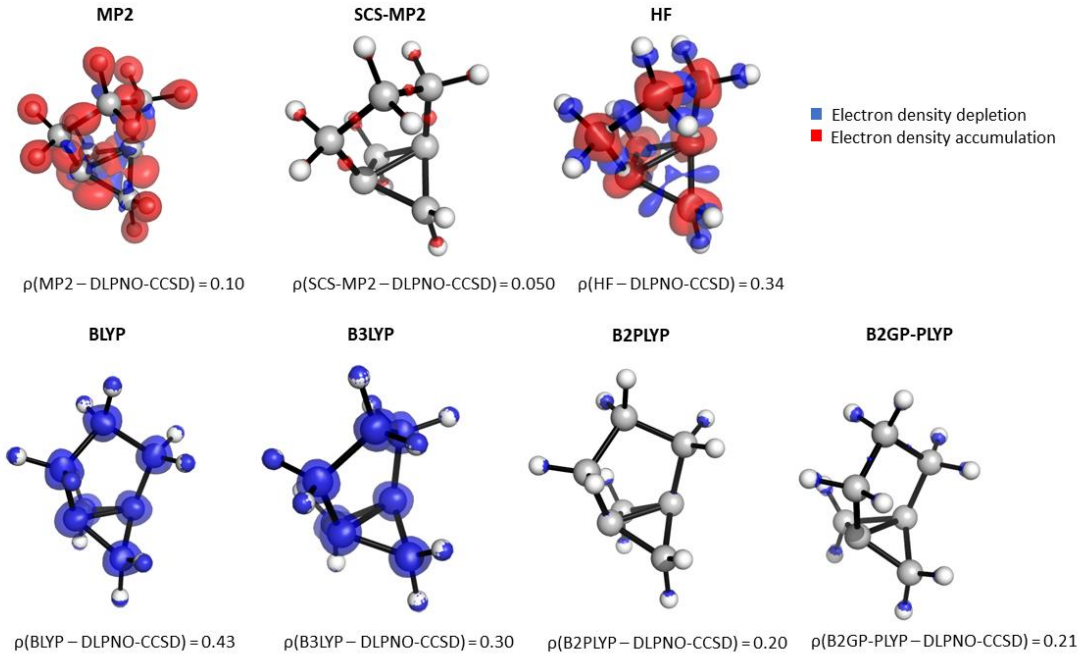


Figure 43. Visualised electronic density difference between (linearised) DLPNO-CCSD/def2-QZVPP densities (NormalPNO as the threshold condition) and the respective post-HF-method or DFT functional using the geometry of the SCS-MP2/def2-QZVPP calculation. In each case, an isovalue of ±0.005 eÅ^{-3} was chosen. Red lobes correspond to an accumulation of electron density, blue to depletion of electron density. (Integration grid = 120).

Finally, the singlet-triplet gap is an indicator of electron pairing in the bridgeheaded bond and has been previously being used as a description of σ-π delocalisation in TCP. The computed absolute and vertical singlet-triplet gaps were compared to the values obtained at the DLPNO-CCSD(T)/def2-QZVPP//SCS-MP2/def2-QZVPP level of theory (Figure 44). Once again, BLYP fails to reproduce the DLPNO-CCSD(T) values whereas the double-hybrid functionals B2PLYP and B2GP-PLYP perform well. A DLPNO-CCSD(T)/def2-QZVPP (NormalPNO) or B2PLYP-D3BJ/def2-QZVPP was chosen for a final electronic energy evaluation.

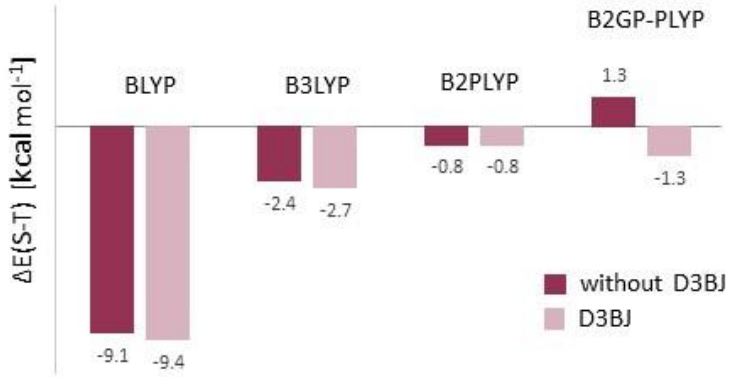


Figure 44. Deviation of the (vertical) singlet-triplet gap from the DLPNO-CCSD(T)/def2-QZVPP//SCS-MP2/def2-QZVPP singlet-triplet gap of the tested methods.

For TCP, a relaxed singlet-triplet gap of 99 kcal mol^{-1} was obtained, whereas the relaxed singlet-triplet gap of TCHep is smaller with 59 kcal mol^{-1}, indicating less paired inter-bridgehead electrons. This may be rationalised through the enhanced Pauli repulsion TCHep suffers from compared to TCP, where another cyclopropane bridge is available for σ-π delocalisation.

2.5.2. Static Properties of TCHep: The Propellanic Bond

Before turning the attention to reactivity, it is worth comparing the ground state electronic structure of TCHep and TCP, in particular the nature of the propellanic bond. Several concepts of bonding have been proposed for the inter-bridgehead bond of TCP, like the recent delocalisation model from our and the Duarte group (see Section 1.1.2), or the charge-shifted bond concept proposed by Shaik et al.[108] Each of them highlights the unusual bonding situation of TCP.

The quantum theory of atoms in molecules (QTAIM) by Bader [109] is employed to derive bond-critical points which characterise a bond defined by bearing a maximum of electron density $\rho(\mathbf{r})$ in two dimensions (see Section 5.11 for further technical details). Bond critical points lie on bond paths which connect the atom centers.

Figure 45 visualises the results of a QTAIM analysis of the ρ of TCHep calculated with SCS-MP2/def2-QZVPP. The bond paths do not resemble the direct connection between the nuclei but instead follows the gradient towards the (bond) critical point. Therefore, its distortion from the direct connecting path is a measure of ring strain.

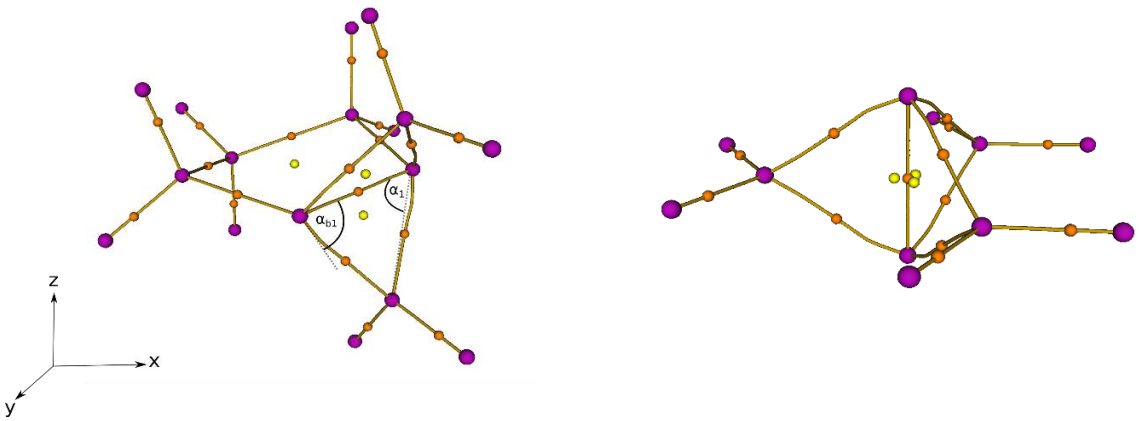


Figure 45. Visualised atomic position (violet), bond critical points (3,-1) in orange and ring critical points (3,+1) in yellow for TCHep, left, and TCP, right. Atoms and bond critical points are connected through bond paths. The underlying (relaxed MP2-)density was obtained with SCS-MP2/def2-QZVPP for TCHep and CASSCF(2,2)/def2-QZVPP//SCS-MP2/def2-QZVPP for TCP and analysed with the MultiWfn-package.[110]

The critical points can be undertaken further quantitative analysis, e.g. determination of the Laplacian or the measurement of the ellipticity. The ellipticity $\epsilon(r)$ describes the deviation of a bond from a centrosymmetric σ-bond. Therefore, it shows how a cylindrical bond is stretched preferentially in one plane containing the bond axis. Sometimes, it is used as a measure of π-bond character. Generally, it is assumed that the higher the ellipticity, the less stable the bond. Unsymmetrical propellanes typically exhibit high ellipticities[1] on the bond critical point of the bridgehead bond, e.g. TCHep an ellipticity of 2.59. Wiberg et al.[111] report an ellipticity of 7.10 for the inter-bridgeheaded bond of [2.1.1]propellane. These unusual high ellipticities could be interpreted as an indication of high delocalisation of the electron density within a specific plane. The bond critical point of the bridgehead bond of TCP does not possess ellipticity due to the symmetry of the molecule (delocalisation of the bridgehead electron density in every direction).

The Laplacian $\nabla^2\rho(\mathbf{r})$ of a point shows local charge depletion ($\nabla^2\rho(\mathbf{r}) > 0$) or accumulation ($\nabla^2\rho(\mathbf{r}) < 0$) around that point. The bridgehead bond critical point of TCP possesses an unusual positive Laplacian with +0.17. Usually, covalent bonds possess a negative Laplacian (e.g. bond critical point of a C-C bond of ethane with a Laplacian of −0.74). The Laplacian of TCHep is with −0.080 more balanced between a 'normal' covalent bond and the unique inverted propellanic bond, but still rather on the side of an inverted propellanic bond (Table 3). Therefore, it would be expected to see experimentally reactivity more similar to TCP than classical olefins or carbocycles.

[1] The bond critical point of the double bond of ethene possesses only an ellipticity of around 0.3.

Table 3. Quantitative analysis of bond critical point in the inter-bridgehead bond of TCHep and TCP performed with MultiWfn.

Bond critical point in inter-bridgehead bond	**TCHep**	**TCP**
Level of Theory	SCS-MP2	CASSCF(2,2)
Density ρ	0.196	0.178
Laplacian (norm)	– 0.0804	+ 0.167
x	– 0.279	– 0.0442
y	0.276	– 0.0442
z	– 0.0776	0.256
Ellipticity	2.59	0.00293
Geometric angle α_1	58.2°	58.4°
Bond path angle α_{b1}	74.4°	60.7°
$\Delta\alpha$	16.2°	2.3°

Further, the difference $\Delta\alpha = \alpha_1 - \alpha_{b1}$ between the geometry angle and bond path angle is a measurement of ring strain (see Figure 45). The geometric angle α_1 is the angle between 3 atoms connected by straight lines. The bond path angle α_{b1} is the angle between two bond paths. According to this measure, TCP is surprisingly less strained at the inter-bridgehead axis than TCHep, which again can be rationalised with Sterling's model of delocalisation, which mitigates angle-strain (see Section 1.1 and 1.2).

Figure 46 shows the plotted Laplacian $\nabla^2\rho(\mathbf{r})$ and ellipticity along the inter-bridgehead bond path of TCHep and TCP. The curve of the Laplacian $\nabla^2\rho(\mathbf{r})$ of TCP is qualitatively similar to TCHep but significantly shifted to lower, negatives values of $\nabla^2\rho(\mathbf{r})$ whereas the $\nabla^2\rho(\mathbf{r})$ curve of TCHep resides in the positive $\nabla^2\rho(\mathbf{r})$ section. This means that in

TCP electron density is depleted along the bond path of the inter-bridgehead bond. In contrast, in TCHep, electron density is rather accumulated along the bond path compared to the local vicinity around the inter-bridgehead bond. These plots are qualitatively like the ones of the bond path of the C-C bond of ethane, whose Laplacian curve looks similar W-shaped.

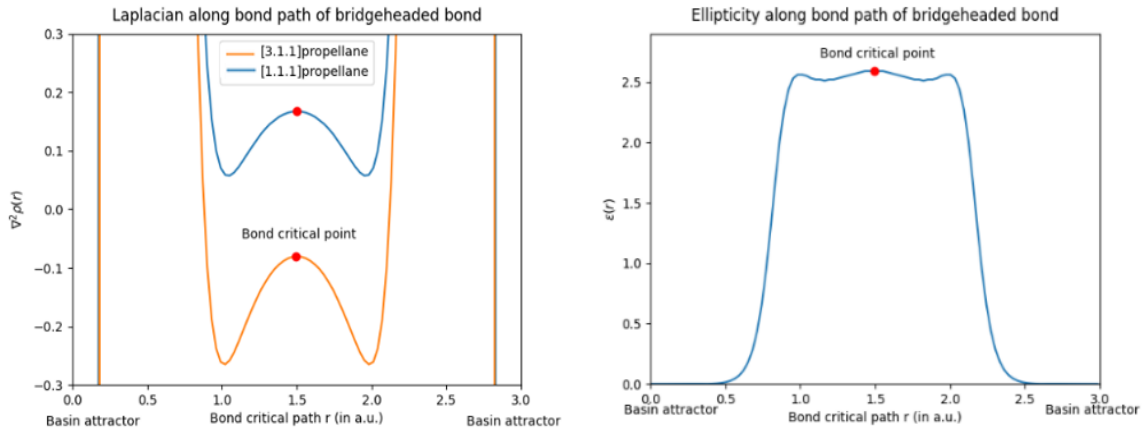


Figure 46. Plotted Laplacian and ellipticity along the bridgehead bond path of TCHep and TCP derived by the QTAIM theory with MultiWfn. The ellipticity of the bridgehead bond path of TCP is negligible.

More insight can be gained if the real spatial function is displayed on a plane bisecting the inter-bridgehead bond. Figure 47 shows these for a plane parallel to the xy, xz and yz-plane bisecting the bond critical point of the inter-bridgehead bond.

The density-plot in the xz-plane shows significant density distribution from the bond critical point of the inter-bridgehead bond towards the bridge-bonded CH_2 groups of both three-membered rings, but no density 'ridge' towards the five-membered ring (a 'valley' floor is visible). This follows Sterling's model of a delocalisation-enabled bonding in TCP (see Section 1.1.2) in which each cyclopropyl bridge, but no higher membered bridge, accepts electron density to reduce Pauli repulsion.

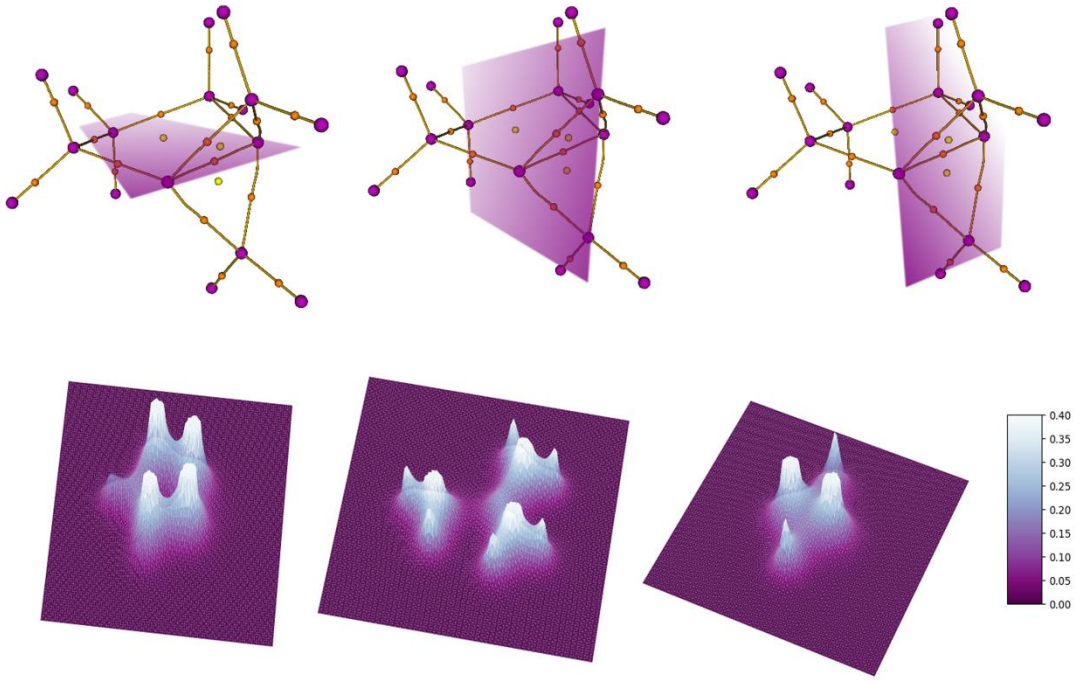


Figure 47. Plotted electron density in a plane parallel to the xy, xz and yz plane, respectively, bisecting the bond critical point of the bridgehead bond. Electron density (spikes) at atom position is cut off at 0.400.

Non-covalent interactions are usually not discovered by the QTAIM analysis. NCI- (non-covalent interaction) or DORI- (Density Overlap Region Indicator analysis) plots are used to visualise those (see Section 5.11 for technical details) and are shown in Figure 48. Red surfaces indicate steric clash, and blue surfaces dispersion interaction, which is energetically favoured. Both analyses reveal similar findings that the congested tricyclic core suffers from steric clash, caused by enhanced Pauli-repulsion between the carbocycles bridges. Interestingly, this repulsion can only be found in the five-membered bridge and not in the cyclopropyl-core hinting towards relieving delocalisation effects described before.

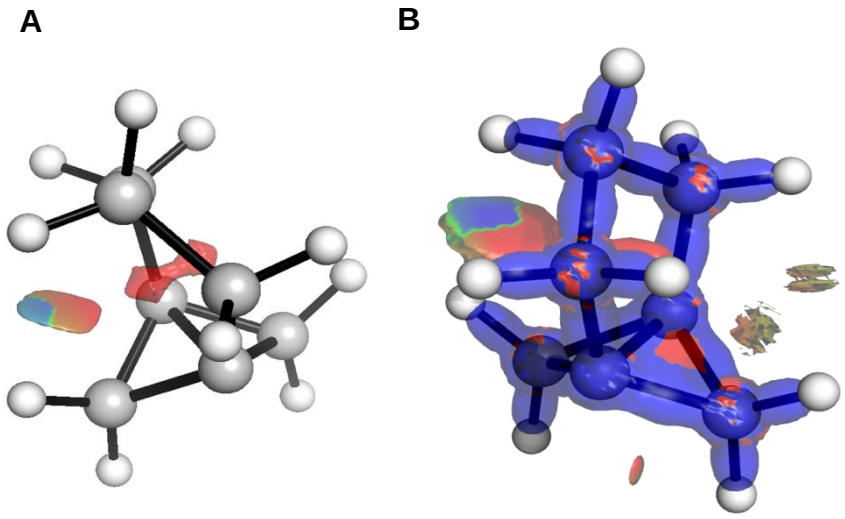


*Figure 48. Plotted NCI isosurface (**A**, isovalue = 0.60) and DORI-isosurface (**B**, isovalue = 0.89). Red surfaces indicate steric clash, and blue surfaces dispersion interaction, which is energetically favoured.*

Lastly, conceptual DFT offers the possibility to define an electrophilicity index ω. The higher the value of ω, the higher the global electrophilicity of the molecule of interest.[112] For TCHep, a ω = 1.7 eV was found, and for TCP, ω = 2.5 eV, indicating that TCHep is less susceptible to nucleophilic attack which is in line with failing anionic methodology (Section 2.4) and intrinsically higher activation barriers of anionic attack (see Section 2.5.4).

In summary, the QTAIM delivers an indication of an exceptional bonding situation of the bridgehead bond in TCHep, e.g. with unusual positive Laplacians and high ellipticities. The obtained values are similar to the ones from TCP, although not as outstanding. The less positive Laplacian and ellipticities at the bond critical point of TCHep compared to TCP can be interpreted as the transition towards a common covalent bond leaving significant special propellanic-character. These results support the finding of similar reactivity between TCHep and TCP as presented in Section 2.3.

2.5.3. Strain and Strain-Release

An obvious starting point to compare the reactivity of TCHep relative to TCP, is to consider the absolute strain energy and the strain-energy being release in a reaction. Absolute strain energies for TCP have been reported by Wiberg[113] and Rablen[114]. Here we use the values reported by DPhil student Alistair Sterling[115] using computational group increments at W1BD level of Rablen and co-workers.[114] As expected because of a higher cyclopropane count, TCP is more strained than TCHep, with strain energies of 99.2 kcal mol^{-1} and 76.4 kcal mol^{-1} respectively. The values for their bicyclic counterparts' follow a similar trend, with strain energies of 66.9 kcal mol^{-1} BCP and 33.1 kcal mol^{-1} for BCHep. The difference between the tricyclic and the bicyclic counterparts' strain-energy is −32.3 kcal mol^{-1} (TCP to BCP) and −43.3 kcal mol^{-1} (TCHep to BCHep), which is a first approximation towards the strain-release energy of their reactions. Similar values can be obtained considering an isodesmotic[116] hydrogen transfer reaction onto the inter-bridgehead bonds of TCP and TCHep, Sterling calculated a strain release energy of −28 kcal mol^{-1} (TCP to BCP) and −39 kcal mol^{-1} (TCHep to BCHep).

Counter-intuitively, these results suggest that approximately 10 kcal mol^{-1} more strain is released during the cleavage of TCHep than it is for TCP. To explain this, firstly, greater σ-π delocalisation of the inter-bridgehead bond means that TCP is actually less strained per cyclopropane ring than TCHep (99 kcal mol^{-1} / 3 = 33 kcal mol^{-1} vs. 76 kcal mol^{-1} / 2 = 38 kcal mol^{-1}). Secondly, BCP can be seen as a cyclobutyl-bridged cyclobutane (which is still relatively strained) whereas BCHep can be considered as a less-strained cyclobutyl-bridged cyclohexane. This shows how absolute strain values can misguide chemical judgement about reactivity: Only the *relative* strain release is important, rather than the *absolute* strain of a starting material or product.

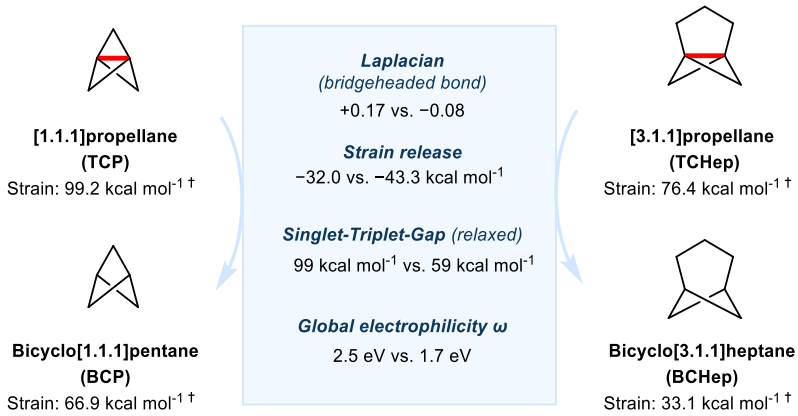


Figure 49. Summary of the most important static properties of TCP and TCHep. Calculations were performed on SCS-MP2/def2-QZVPP and B2PLYP-D3BJ/def2-QZVPP level of theory. †These calculations were performed by DPhil student Alistair Sterling.[115]

2.5.4. Dynamic Properties of TCHep: Reactions

All the above-mentioned properties were calculated before TCHep was even synthesised in our group. Additionally, Gibbs free activation energies and Gibbs free energies of reaction were determined for a set of nucleophiles (NH_2^-, Ph^-) and SOMOphiles (PhS•, I•, CH_3•) *a priori* (Figure 50). It was hoped to anticipate certain reactivity of TCHep, however retrospectively it has to be admitted that the predictive power of the obtained values was limited.

Nonetheless, the free activation and reaction energies shown in Figure 50 help to rationalise the observed behaviour of TCHep in comparison to TCP *a posteriori*. Several interesting trends can be observed:

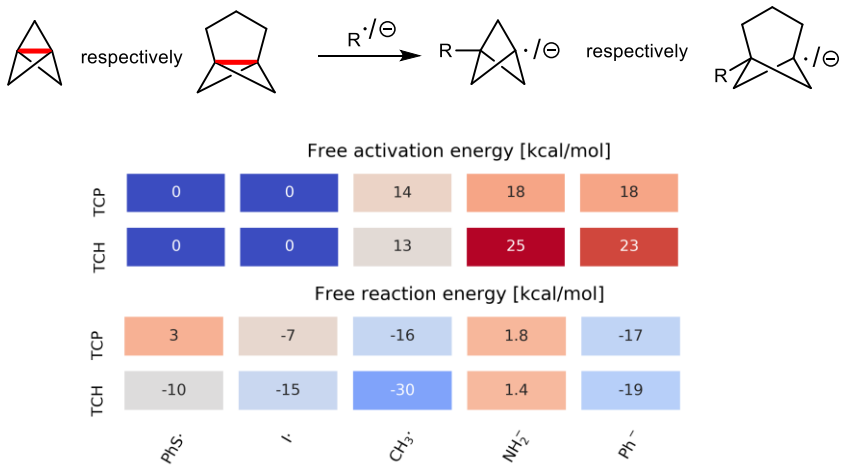


Figure 50. Gibbs free activation energies and Gibbs free energies of reaction for addition of prototypical radicals and nucleophiles with TCHep and TCP at CPCM(THF)-B2PLYP-D3BJ/def2-QZVPP//CPCM(THF)-B2PLYP-D3BJ/def2-TZVP level of theory.

- For certain radicals, like PhS• or I•, no transition state could be located (for TCHep). It is therefore assumed that the addition of those radicals proceeds under diffusion-controlled conditions.
- Other radicals, e.g., CH_3•, involve considerable activation energies. The activation energy is similar for TCP and TCHep with 14 and 13 kcal mol^{-1}, respectively.
- On the one hand, the free activation energy for the anions NH_2^- and Ph^- is considerably higher for TCHep than it is for TCP, $\Delta\Delta G^{\ddagger}$ = 7 kcal mol^{-1} for NH_2^- and $\Delta\Delta G^{\ddagger}$ = 5 kcal mol^{-1} for Ph^-.
- On the other hand, Gibbs free reaction energies for anions are similar for TCP and TCHep. It is important to note that addition of NH_2^- is nearly ergoneutral, whereas addition of Ph^- is exergonic.
- The Gibbs free reaction energy of the addition of radicals is more exergonic for TCHep than for TCP, $\Delta\Delta G$ = 13 kcal mol^{-1} for PhS•, $\Delta\Delta G$ = 8 kcal mol^{-1} for I·, and $\Delta\Delta G$ = 14 kcal mol^{-1} for CH_3•.

To summarise, TCHep appears to have a schizophrenic character. Transition states involving anions are less stabilised for TCHep than TCP, whereas the anionic BCHep anion **94** do not suffer from destabilisation compared to TCP. The opposite is true for radicals: TCP and TCHep stabilise radicals equally well in the transition state but BCHep radicals are more stabilised than BCP radicals. Figure 51 again shows these relative differences for the NH_2^- and $CH_3^{\bullet}$.

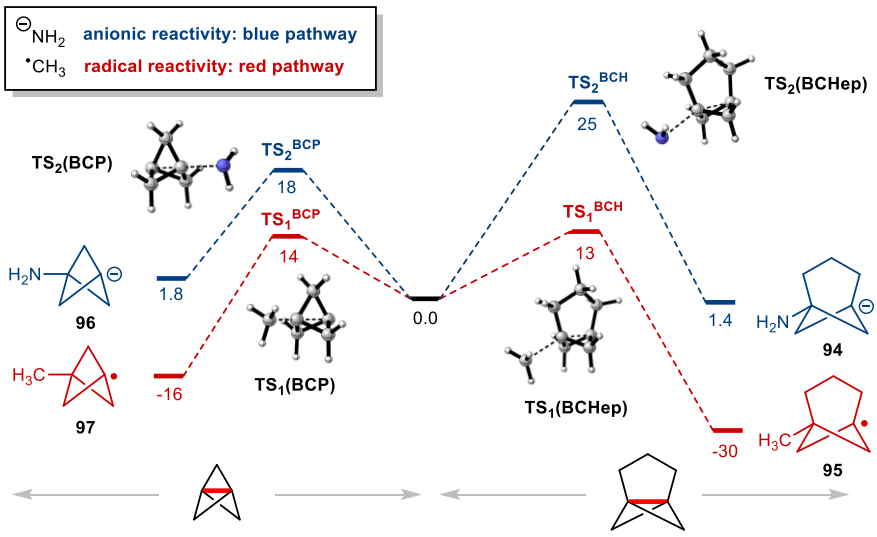


Figure 51. Free energy diagram comparing the values of NH_2^- and $CH_3\cdot$ addition at CPCM(THF)-B2PLYP-D3BJ/def2-QZVPP//CPCM(THF)-B2PLYP-D3BJ/def2-TZVP level of theory (298 K / 1 M).

The relative stability difference between radical intermediates **95** and **97** and respective anionic intermediates **94** and **96** has to be clarified in order to resolve these paradoxical characteristics. Figure 52 shows the in-depth analysis of the electronic structure of all four intermediates. NBO analysis was performed to capture deviations from a classical Lewis picture by second-order perturbation analysis, thus identifying crucial stereoelectronic stabilisation effects.

The bridgehead carbanion of BCHep **94** is stabilised through donation into the antibonding σ* orbital of the indicated three-membered bridge C–C bond by approximately 9 kcal mol^{-1}. The BCP carbanion **96** is stabilised *via* through-space donation into the C–N σ* bond, similarly as effects were observed by Leonori and co-workers, although to a lesser extent than the BCHep carbanion **94** is stabilised.[48]

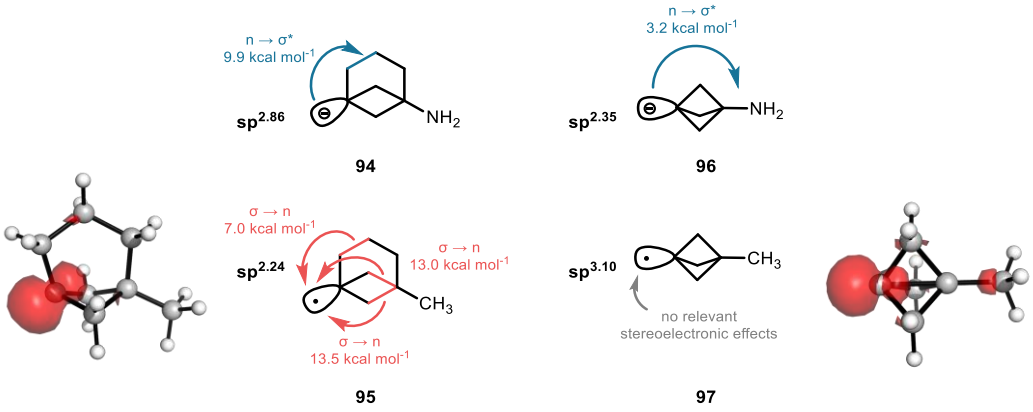


*Figure 52. NBO analysis of obtained intermediates at CPCM(THF)-B2PLYP-D3BJ/def2-QZVPP//CPCM(THF)-B2PLYP-D3BJ/def2-TZVP level of theory. Only donations associated with the bridgehead radical/anion with a threshold > 2.5 kcal mol^{-1} are displayed. For the radicals **95** and **97**, the isosurface of the spin density is shown at an isovalue of 0.01.*

Considerably larger disparities in the stabilisation behaviour were found between the bridgehead radicals **95** and **97**. In contrast, the NBO package did not find a relevant stereoelectronic effect for the bridgehead BCP radical **97**. Several donations of flanked sigma-bonds into the bridgehead SOMO, ranging from 7 to 13 kcal mol^{-1}, were found for BCHep. This indicates higher stabilisation of **95** compared to **97**, which is directly connected to the observed more negative Gibbs free reaction enthalpy for TCHep radical additions. The beneficial stereoelectronic stabilisation effects can be further rationalised by acknowledging the geometric difference between the BCHep and the BCP hydrocarbon core: Only BCHep has the correct periplanar alignment between the spin-density (SOMO, see Figure 52) and the σ orbital. In BCP, the σ bridges are nearly

perpendicular to the SOMO, making donations impossible. Interestingly, anionic systems **94** and **96** possess completely different stereoelectronic profiles compared to the radicals **95** and **97**. An explanation is found in the highly electronically congested cores in BCHep or BCP, which make donations from the bridgehead carbanion into the cyclopropyl-unit unfavourable.

Equation (I) readily explains the activation energies by combining the σ-π delocalisation model and Bell-Evans-Polanyi principle, showing the influence of the Gibbs free reaction enthalpy on the activation barrier.[23] In each case, the additional cyclopropane ring stabilises the transition state of the TCP by approximately 10 kcal mol^{-1}. Since there is a negligible difference in Gibbs free energy Δ(ΔG) for the anionic additions, this σ-π delocalisation term of equation (I) directly explains the lower anionic free activation barrier of TCP.

The same is true for the radical addition, but since there is a striking difference in Gibbs free energy ΔΔG of around 14 kcal mol^{-1} in favour of the BCHep product **94**, this counteracts — although only with half-fold influence (factor ½ in equation (I)) — the beneficial effect of the σ-π delocalisation. This brings the two activation barriers back to an approximately equal level again.

The higher activation barriers for anionic additions give a first hypothesis as to why the anionic methodology was not successfully probed on TCHep (Section 2.4). It is also apparent now why radical-based methodology was translated so successfully: The resulting BCHep bridgehead radical is favourably stabilised, offsetting a 'missing' σ-π delocalisation in the transition state.

2.5.5. Polymerisation

One common problem in TCP reactions is the observed byproduct ‘staffane’, which results from the dimerisation and eventual oligomerisation of BCP radicals with remaining TCP molecules. Similar behaviour can be imagined for TCHep (see Figure 53).

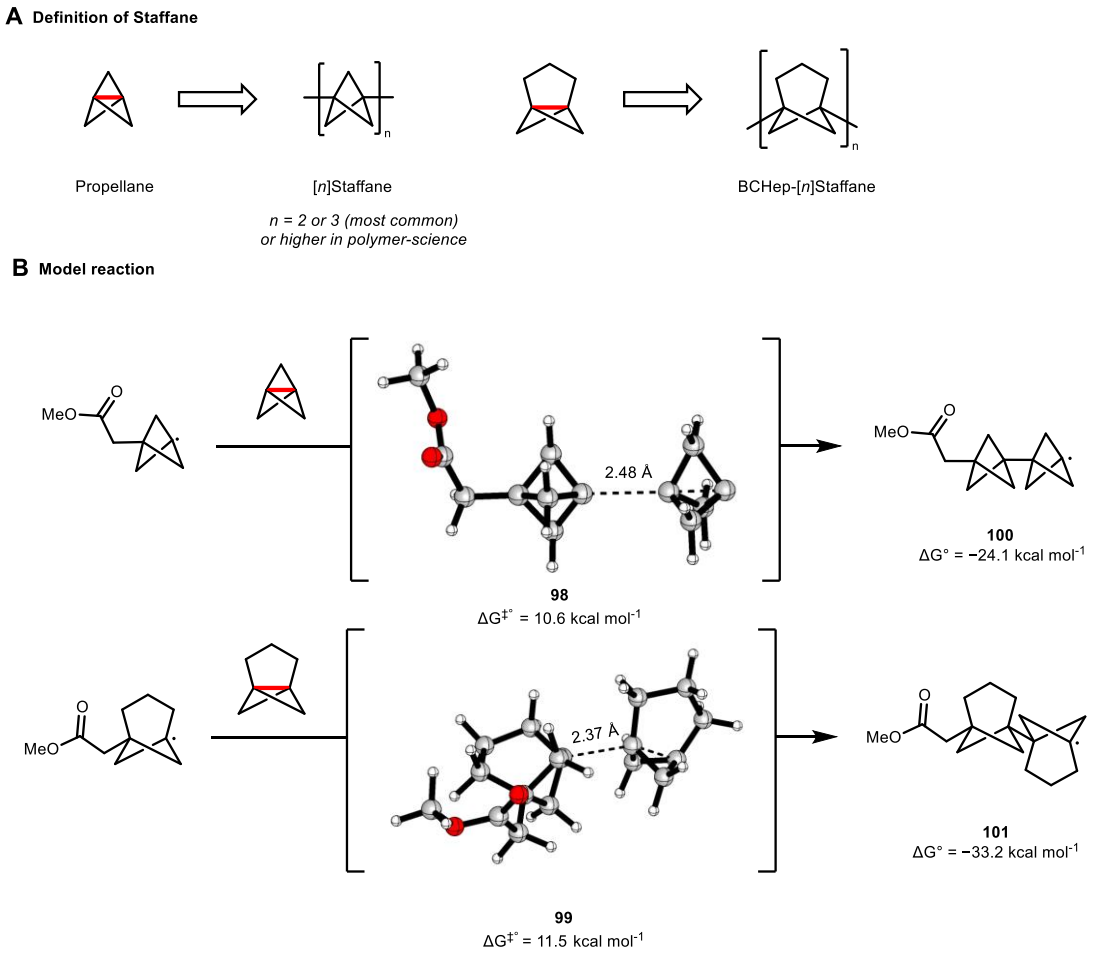


*Figure 53. (**A**) Definition of [n]Staffane, (**B**) Model reaction of [n]Staffane formation for TCP and TCHep at CPCM(THF)-B2PLYP-D3BJ/def2-QZVPP//CPCM(THF)-B2PLYP-D3BJ/def2-TZVP level of theory (298 K / 1 M).*

Computational analysis of these two reactions revealed no intrinsic difference between TCP and TCHep in forming a staffane dimer, since they possess the same activation

barrier overcoming **98** and **99** (Figure 53). In addition, as Section 2.5.4 explains, **101** is more stabilised than the BCP radical **100**.

Experimentally, however, no BCHep-Staffane was observed in any reaction explored in Chapter 2. This indicates that consecutive reactions, like chain propagation steps, are probably more favoured for BCHep radicals than for BCP radicals, for which staffane formation can come in competition. It has to be assumed that the XAT-step is the selectivity determining step in these rival reactions, but so far, no transition states for the XAT step have been located computationally which would support this hypothesis.

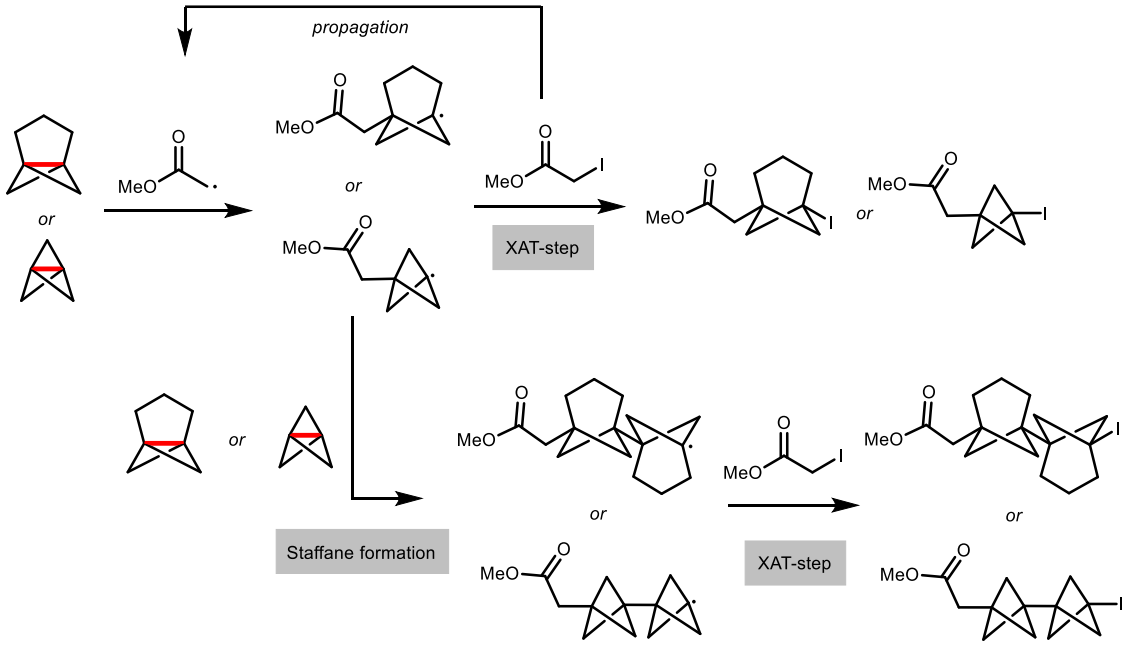


Figure 54. Consecutive reaction and their competition in staffane formation.

Interestingly, the bond length between the two bicyclic systems in transition state **98** and **99** for the [3.1.1]-system is shorter than for the [1.1.1]-system. However, the [3.1.1]system is sterically more congested, i.e. less 'tied back' than BCP, so steric effects may play a more important role in this polymerisation. Unexpectedly, a conformational scan revealed that the most favoured conformation of a [2]-staffane system of BCHep is not the antiperiplanar arrangement of the three-membered bridge, but rather a gauche

conformation (Figure 55). Consequently, a pseudo-helical secondary structure can be expected for a [3.1.1]-staffane polymer.

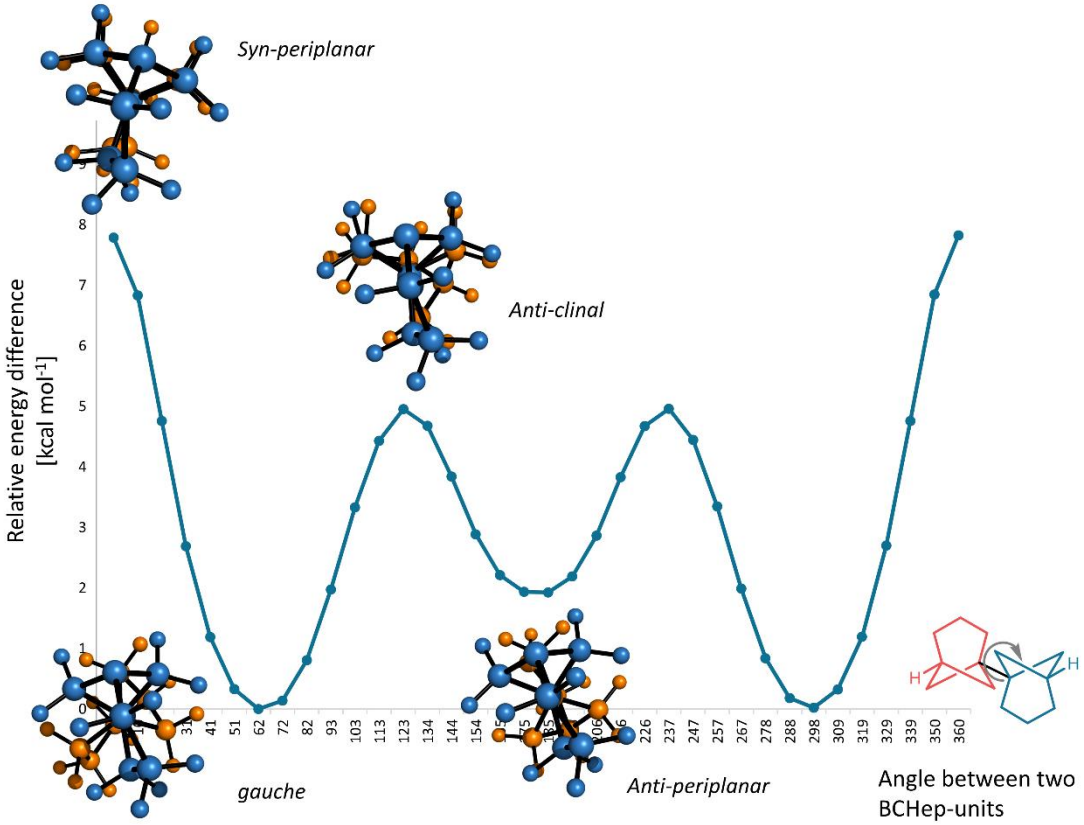


Figure 55. Conformational analysis of rotamers of H-BCHep-BCHep-H with crucial local minima depicted in a Newman projection. Scan performed at B2PLYP-D3BJ/def2-SVP level of theory.

2.5.6. Unproductive side reactions

So far, only an explanation for the failure of anionic methodology has been found. But why do reactions known for TCP (e.g. UV-induced reactions) not translate to TCHep? Calculating the activation barrier for the prototypical $CH_3^{\bullet}$ radical revealed no difference in activation barrier; therefore, the reason likely lies in competing side reactions.

For the BCHep system, opening of the bridgehead–bridge bonds could occur, and various side reactions are subsequently initiated. For the methyl-substituted BCHep substrate,

Gibbs free energies for the opening of the 3-membered and 1-membered bridges were calculated relative to the inter-bridgehead opened BCHep unit (Figure 56).

The relative stability is in line with the system's ring strain; therefore, the bicyclobutane BCB **103** anion or radical and is less stable than the BCHep anion (25 kcal mol^{-1}) or radical (24 kcal mol^{-1}) **102**. An *exo*-methylene cyclohexyl-system **104**, derived by one-carbon bridge opening, is 23 and 19 kcal mol^{-1} more stable than the BCHep radical or anion, respectively. Interestingly, a thujone-like intermediate **105** — which could be proposed as a resonance structure of **104** in a fashion of the non-classical intermediate — is not a stable local minimum and converges into structure **104**. From a thermodynamic control perspective, only **104** should be obtained in TCHep chemistry.

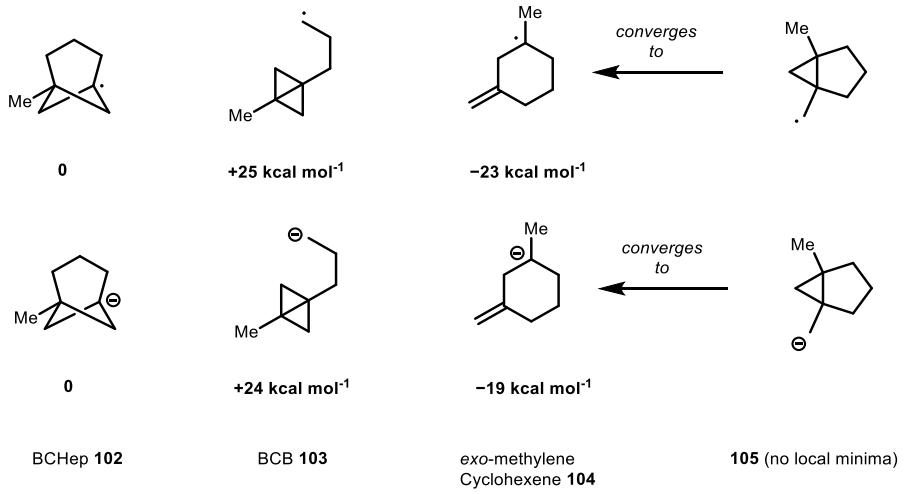


Figure 56. Relative Gibbs free energies for different ring-opened intermediates at CPCM(THF)-B2PLYP-D3BJ/def2-TZVP level of theory (298 K / 1 M).

Instead, BCHep **102** is observed experimentally, except for the diacetyl addition **81**, which has to be explained *via* kinetic arguments. Computationally, a fragmentation pathway from BCHep **102** to **104** was found to possess a considerable, although not energetically unfeasible, activation barrier (**106**) of approximately 25 kcal mol^{-1}. The Gibbs free activation barrier is considerably lower for a stabilised system, like the diacetyl

addition **81** whose transition states **108** and product are stabilised through an enolate contribution (Figure 57).

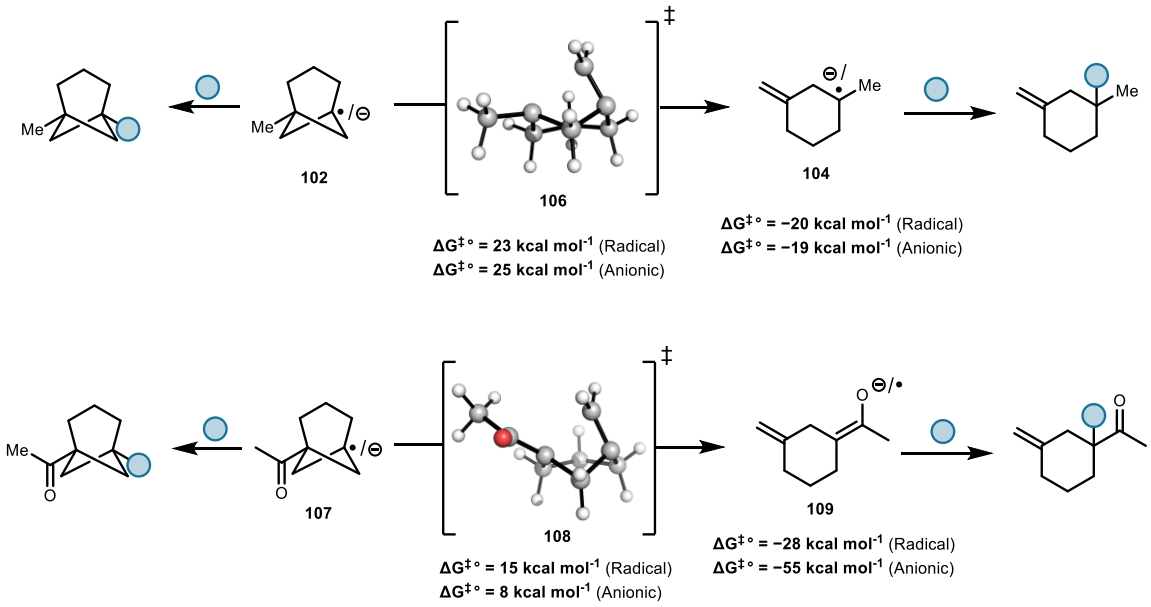


Figure 57. Gibbs free activation energies for the competition between direct trapping (left) and wing-bond opening (right) for unstabilised (Me) and stabilised (acetyl) systems. Calculations were conducted at CPCM(THF)-B2PLYP-D3BJ/def2-TZVP level of theory (298 K / 1M).

Selectivity between trapping towards a BCHep structure and the competing rearrangement is determined by the relative difference in Gibbs free activation energies. A low Gibbs free activation barrier of only 8 kcal mol^{-1} rationalises that the formation of **81** as the major product in the diacetyl addition. It can be imagined that for the other failed radical reactions, similar competition reactions might take place, resulting in complex reaction profiles which we were unable to easily elucidate.

2.5.7. Radical clock experiments and competition experiments

To determine the relative rate of TCHep and TCP in ATRA chemistry, radical clock experiments were conducted to narrow down the rate windows in which the chemistry of

TCP and TCHep is believed to take place. Three radical clocks were selected (**110**–**112**), which would be applied by assuming that the relative radical reactivity of TCHep and TCP can be judged by the disappearance of signals in the double bond regions, or by accumulation of isolated products **113** and **114**. The rate constants of the calibrated clocks were used to delimit the k-scale at which the herein used photoredox-mediated reaction takes place.[117-118] Alkyl radicals generated from **111** undergo direct addition to TCHep whereas the ones generated from **110** undergo beforehand cyclisation. Therefore, it can be concluded that TCHep with $10^3 < k_{TCHep} < 10^5$. Similarly, TCP was inclosed by the two radical clocks **110** and **112** reacting at least one magnitude (and up to 4 magnitudes) slower than TCP with $10^5 < k_{TCP} < 10^7$ (Figure 58).

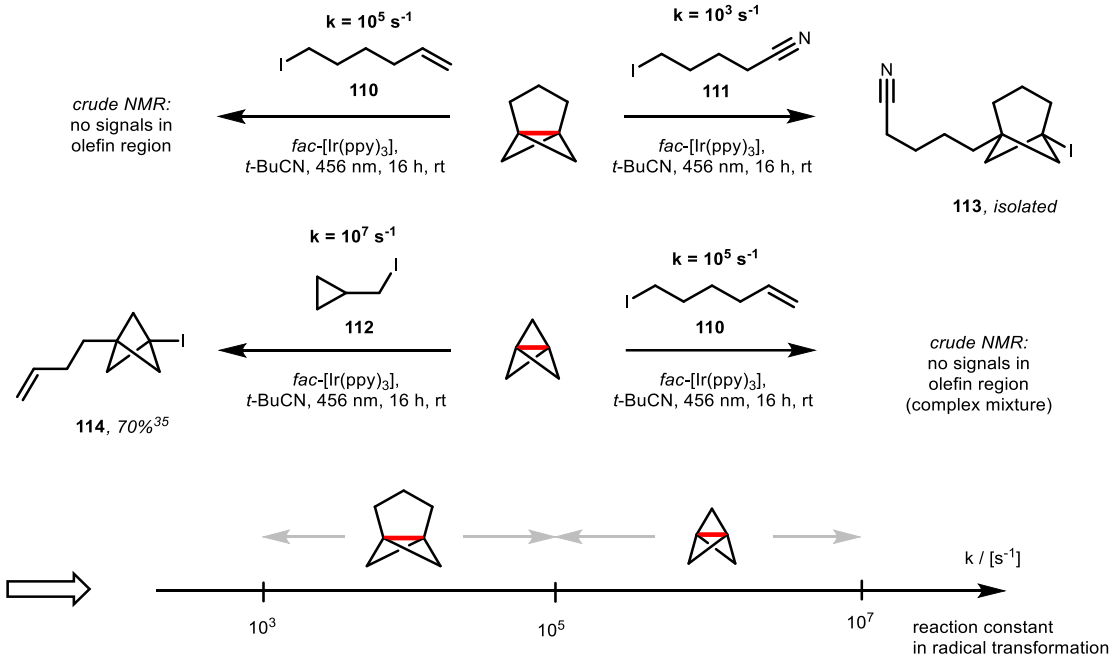


Figure 58. Radical clock experiments using calibrated radical clocks.[117-118]

The small difference in Gibbs activation energies with *C*-centred radicals ($Me^{\cdot}$: $\Delta\Delta G^{\ddagger} = -0.9$ kcal mol^{-1}) suggests that the difference in k_{TCHep} and k_{TCP} might be indeed just one or two orders of magnitude, estimating k_{TCHep} / k_{TCP} with the Eyring equation (II), assuming the same preexponential factor ($\kappa \cdot k_B T \cdot h^{-1}$) and including an estimation of the

computational error of ± 2 kcal mol^{-1} using temperature T = 298 K and R = 1.9859 · 10^{-3} kcal mol^{-1} K^{-1}:

$$k = \kappa \frac{k_B T}{h} e^{-\frac{\Delta G^{\ddagger}}{RT}} \quad \text{(II)}$$

$$\frac{k_{TCP}}{k_{TCHep}} = e^{-\frac{\Delta\Delta G^{\ddagger}}{RT}} \xrightarrow{\Delta\Delta G^{\ddagger} = 2.9 \; to \; -1.1 \; kcal \; mol^{-1}} 0.16 < \frac{k_{TCP}}{k_{TCHep}} < 134$$

To further probe the differences between TCHep and TCP, competition experiments were conducted by mixing TCP and TCHep solutions in an equimolar ratio. The mixture was stirred at −78 °C, then a limiting amount of the requisite radical precursor was added, with the mixture warmed to room temperature and stirred for a further one hour. The ratio between BCP and BCHep products were then determined by NMR spectroscopy of the crude reaction mixture, revealing perplexing ratios as shown in Figure 59.

In line with the radical clock and the computational results (see above), TCP outcompetes TCHep in photoredox-mediated reactions; BCHep peaks could not be identified in the crude ^{1}H NMR spectrum. This ratio does not change when the philicity of the substrate radical is changed from electrophilic (ethyl iodoacetate **113**) to nucleophilic (iodopivalate **115**) or when an sp^{2}-centred radical is employed (2-iodopyridine **114**).

Remarkably, when switching the initiation method to BEt_3 and employing iodoacetamide as a substrate, a balanced ratio of 2.5:1 between BCHep and BCP product was observed, *in favour of BCHep*. This challenges the assumption that only the addition to TCHep or TCP influences the determined ratio. Thus, estimating ratios *via* transition state theory and the associated Eyring-equation appears too simplistic, and for reasons that are not clear, it seems that the initiation process for photoredox catalysis or BEt_3 plays an important role in determining the reaction outcome.

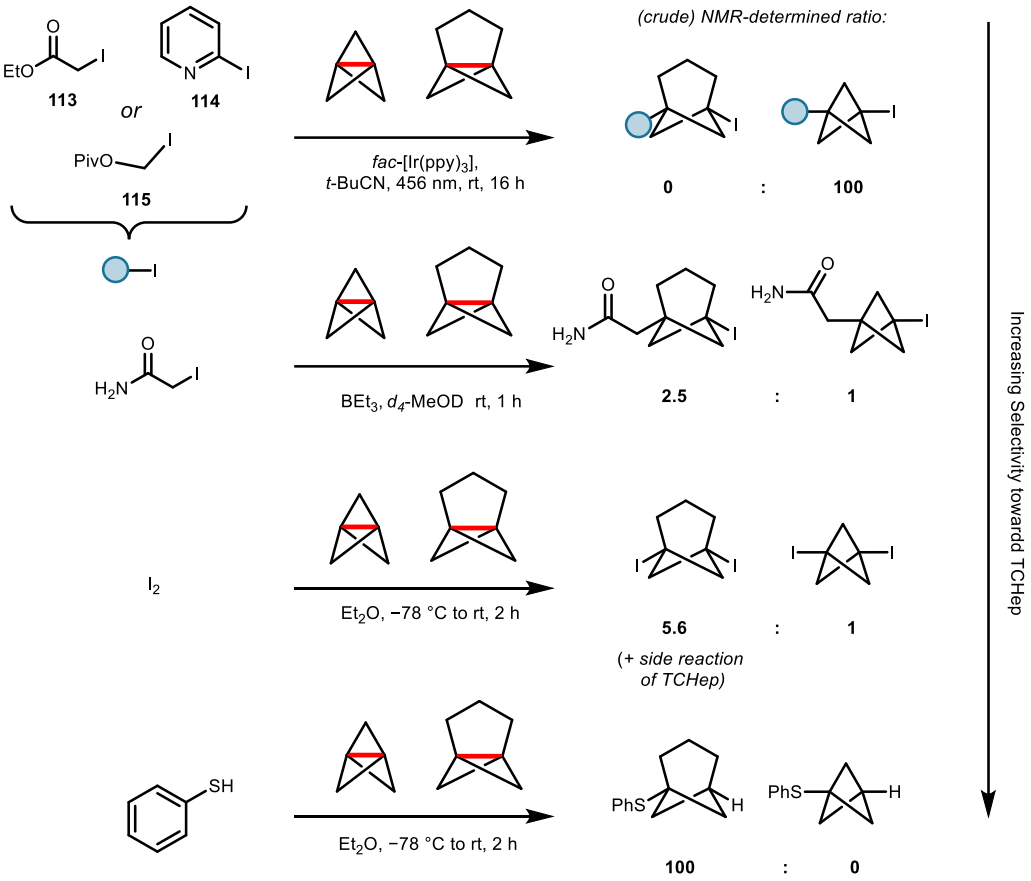


Figure 59. Competition experiment between TCHep and TCP.

Similarly, the addition of an I_2 solution to TCHep and TCP delivers a moderate ratio between BCHep and BCP in favour of the former, although decomposition products arising from the iodination of TCHep were also visible. Here, no quantitative conclusion could be made from the obtained ratio.

Even more surprising was the finding that the addition of thiophenol *is completely selective towards TCHep*, with no TCP addition product visible — in stark contrast to other radical additions. The corresponding mechanism is assumed[119] to proceed *via* a thiyl radical adding into the propellane and subsequent HAT from thiophenol, regenerating the thionyl chain carrier and producing product **30** and **118** (Figure 60). It is

not understood how the initiation of the process happens without any external initiator. A hypothesis of a diradicaloid propellane initiation was discarded due to a high singlet-triplet gap of both propellanes (see Figure 49). Table 4 summarises approaches to elucidate ambient initiation sources, such as the fumehood illumination.

Table 4. Investigating the change of reaction conditions on competition of TCHep and TCP adding (conditions see Figure 32).

Change in reaction conditions	**Result**
Dark 456 nm (*hv)* irradiation BEt_3 TEMPO BHT	BCHep-product **68** is still observed as the only product (No BCP peak visible)
Change solvent to MeCN	No reaction

The reaction was not inhibited by addition of TEMPO or BHT. The addition of BEt_3, or irradiation with a 456 nm LED, or running (and quenching) the reaction entirely in the dark did not alter the results, with BCHep still obtained as the sole product. Paradoxically, switching the solvent to MeCN supressed thiol reactivity completely. Further work is needed to identify the crucial initiation mechanism and its effect on the reaction outcome.

As reported in Section 2.5.4, the addition of thiophenol to both propellanes is thought to proceed under diffusion control. Likewise, no transition state was found computationally for the following HAT step. A diffusion-controlled situation would predict a 1:1 product ratio. Computations suggests that the addition of PhS• to TCP is slightly endergonic (forming **117**), whereas the addition to TCHep is exergonic (forming **116**). Given the

observed product ratio, a hypothesis can therefore be made that **117** can revert to starting material (Figure 60). In contrast, for TCHep, the equilibration constant K is too large. If a further assumption is made that the subsequent HAT step is slower than re-equilibration (thought to be of diffusion control, too), pseudo-Curtin Hammett control can be invoked, explaining why BCHep production is favoured.

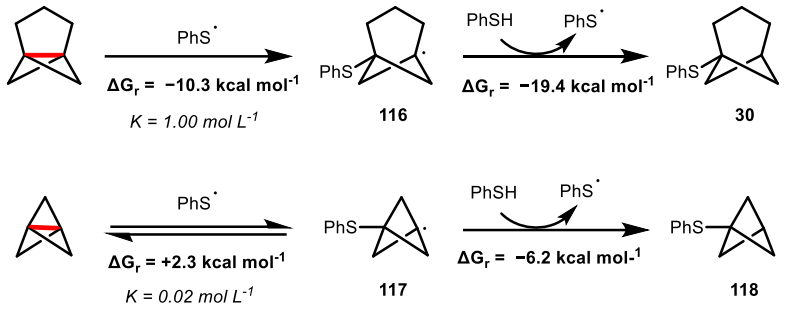


Figure 60. Gibbs free energies of addition of PhS· to TCHep and TCP showing how TCP can be under equilibration control. Computation at CPCM(THF)-B2PLYP-D3BJ/def2-QZVPP//CPCM(THF)-B2PLYP-D3BJ/def2-TZVP level of theory (298 K / 1M). Shown equilibration constant was calculated at 298 K via ΔG° = −RT ln(K).

2.5.8. Summary

In this chapter, the challenge of mechanistic investigation was experienced: in the end, a vague *'you know that you know nothing'* remains. A reasonable explanation was found why anionic additions towards TCHep are challenging and unachieved so far. However, it poses the question of why the enhanced activation barrier of ca. 10 kcal mol^{-1} compared to TCP cannot be overcome by harsher reaction conditions?

The failure of radical methodology can be explained by alternatively characterised reactivity channels, such as polymerisation or bridge bond-opening. Nevertheless, the associated byproducts have only been identified for the reaction of diacetyl with TCHep; more work is required in this area to understand the outcome of other radical reactions of TCHep.

Radical clock experiments and competition experiments fit the computationally obtained data within the exponential error, helping to narrow down the kinetic window. On the other hand, complete reversed selectivity was observed for thiophenol. Although an explanation was attempted, questions remain – namely why is it different for the I_2 addition, which should possess similar thermodynamic properties, and how are the thiol additions initiated? Over and above that, a surprising new mechanistic mode of TCHep reactivity will be discovered in the next chapter. Finding the 'character' of TCHep and differentiating it from TCP remains a topic of current research in our group.

2.6. Reactivity under Physiological Conditions

The success of the catalyst- and initiator-free addition of thiols (Section 2.3.3) stimulated a collaboration with Dr Patrick Rabe from the Prof. Christopher Schofield group. Strained systems, such as monosubstituted bicyclo[1.1.0]butane carboxylic amides[120] and bicyclo[1.1.0]butane sulfones,[38] have recently received increased attention as thiol-reactive electrophiles for the selective and irreversible binding of proteins under physiologically relevant conditions (Figure 61A). Similarly, it was envisioned that TCHep could covalently bind to cysteines in proteins (Figure 61B).

Different conditions were screened employing the ACV tripeptide **119** as a model system which is a cysteine-containing peptide on the surface of the isopenicillin N synthase enzyme.[121] The ACV tripeptide **119** and TCHep (0.30 M in *n*-Bu_2O, 50 equiv.) were added to various aqueous tris- or phosphate buffers (varied pH 5.0-9.0, final concentration of ACV 50 mM) at room temperature (22 °C) or 4 °C (Figure 62).

No difference in the reaction profile was observed between 4 °C and 22 °C. While the reaction in phosphate buffer did not yield any side products, the reaction in tris buffer

showed single (*) and double (#) labelled tris adducts (Figure 62). Only at pH 8.0 and 9.0 of the phosphate-buffered systems were significant peaks associated with the product mass, a mono-BCHep labelled ACV tripeptide, observed. Therefore, it was decided to use aqueous phosphate buffer at pH 8.0 as the optimal physiological reaction conditions.

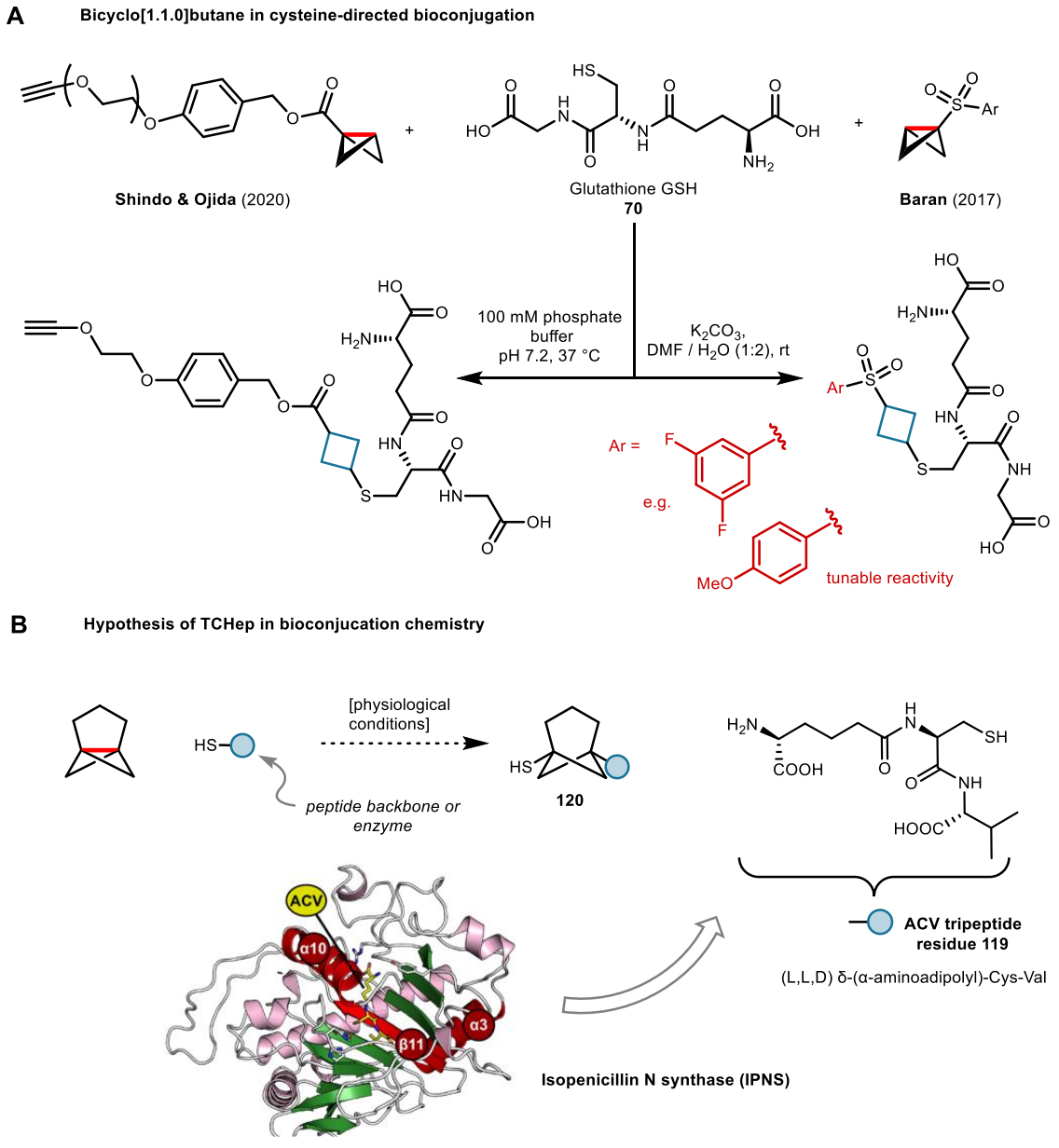


*Figure 61. **(A)** Bioconjugate systems published by Ojida and co-workers[120] and Baran and co-workers[38]. **(B)** Envisioned reactivity of TCHep under physiological conditions using the ACV tripeptide (L,L,D) δ-(α-aminoadipolyl)-Cys-Val from the Isopenicilline N synthase as a model peptide. Picture of IPNS taken from [121].*

Since two peaks with the same molecular mass (blue and purple in Figure 62) eluted at similar retention times, it was decided to perform a large-scale reaction using 4 mg ACV tripeptide. The crude reaction mixture was purified *via* reverse-phase HPLC, and NMR analysis (conducted together with Dr Patrick Rabe) revealed **121** and **122** as the two co-eluting products. None of the intended BCHep-product **120** was found or isolated (see Section 5.5 for further details).

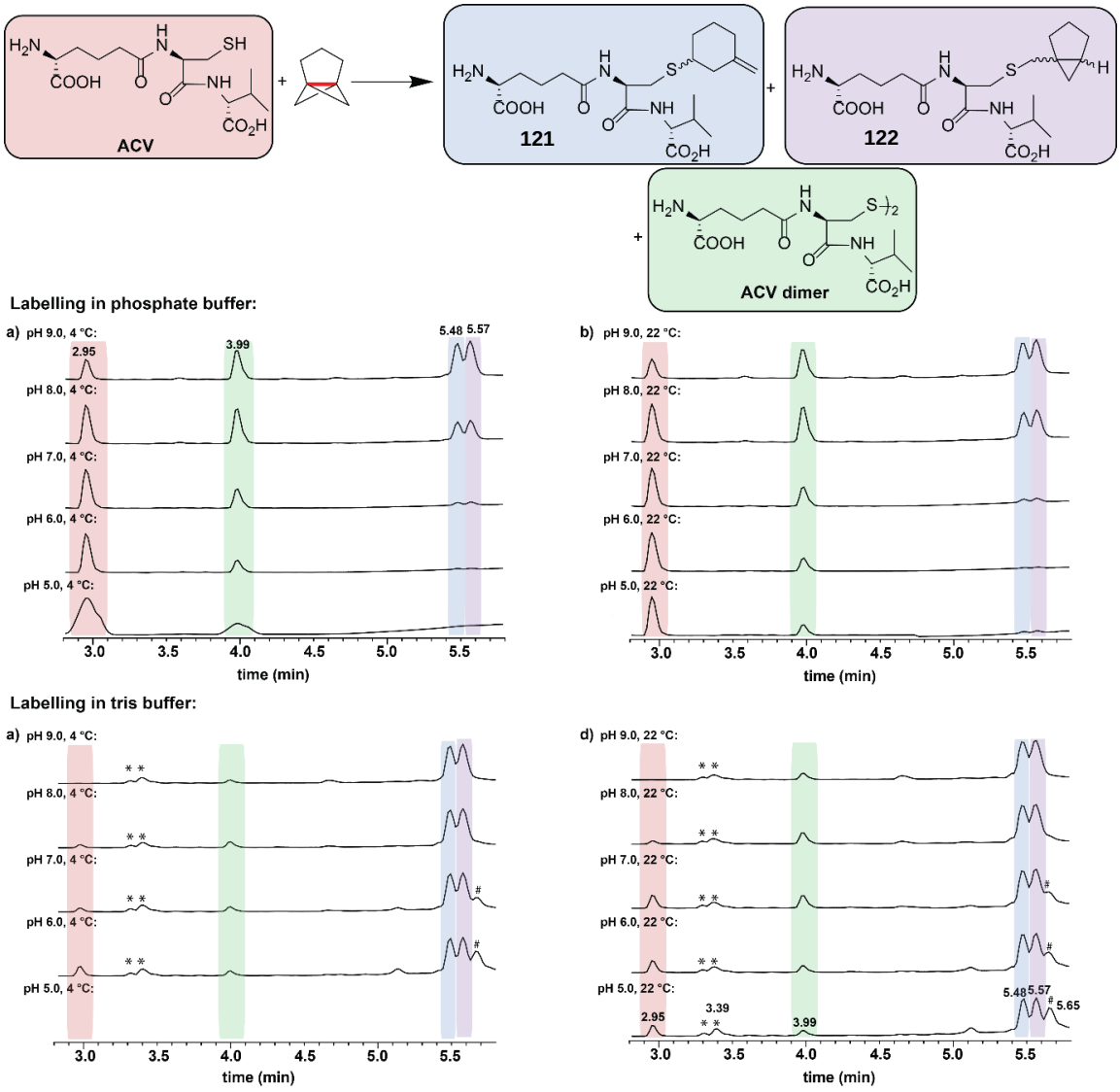


*Figure 62. Reaction of ACV with TCHep. LC-MS analysis of the reaction of ACV (1 mM, 1 eq., red) with TCHep (50 mM, 50 eq.) yielding **121** (blue), **122** (purple, as a mixture of both diastereoisomers) and dimeric ACV (green) performed in phosphate or tris buffer (50 mM in water) with altering the pH from pH 5.0 to pH 9.0 after a reaction time of 1 hour. LC-MS traces*

of the reaction performed in phosphate buffer at a) 4 °C and b) 22 °C and of the reaction performed in tris buffer at c) 4 °C and d) 22 °C. Spectral data was compiled and visualised by Dr Patrick Rabe.

This appearance of these products, including the thujone-like structure **122** (see in contrast Chapter 2.5.6), can be explained by proposing a cationic reaction pathway of the TCHep core *via* initial protonation (Figure 63) as is known for TCP.[22] Compared to the reported BCHep-thiols which are reacted under typically dry, ethereal conditions, the aqueous protic environment appears to enable protonation of TCHep to form the two isomers **123** and **125**. These exist in an equilibrium connected through a low-lying transition state **124**. Trapping of these intermediates by the ACV sulfide anion affords the observed products **122** and **121,** respectively.

Further experiments are underway to re-investigate the behaviour of TCHep in a cationic environment. This includes 'blind' experiments of TCHep in a buffer solution (without peptide), where capture by water may be expected.

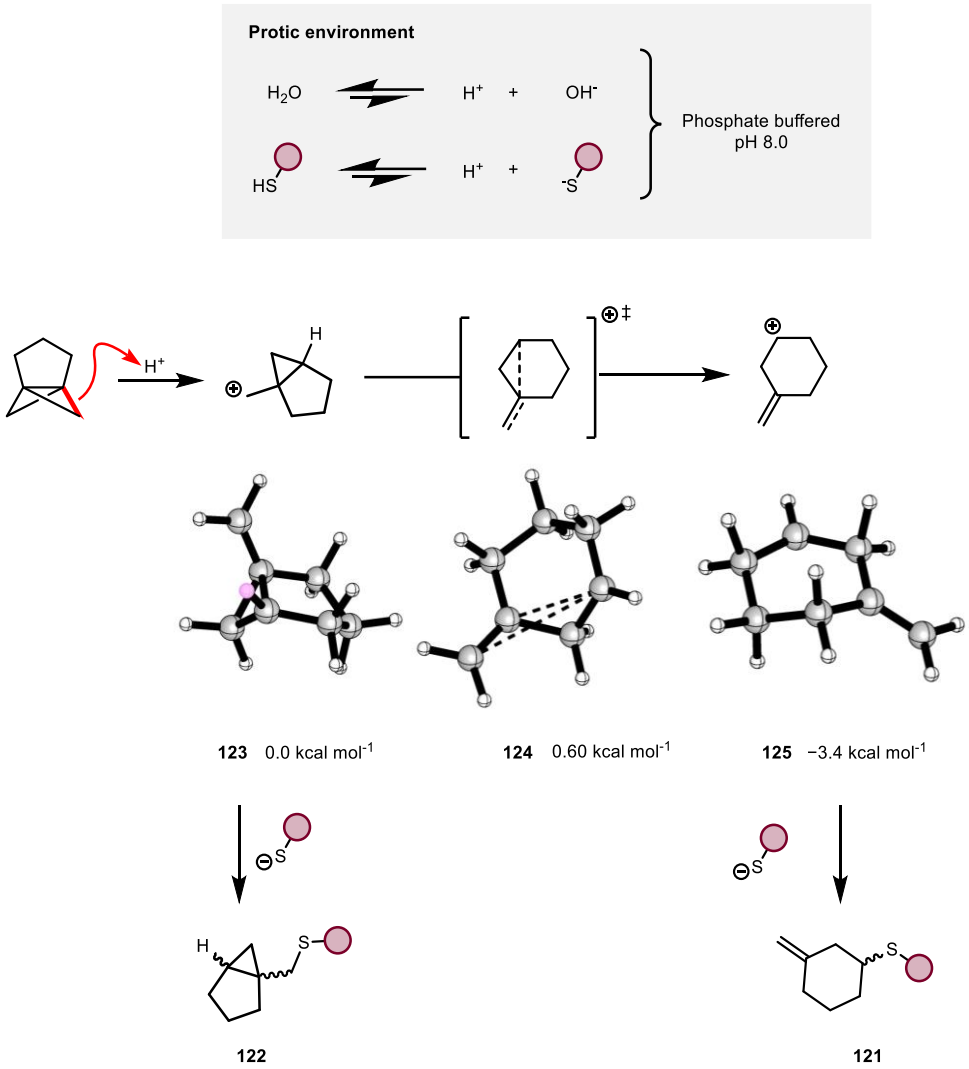


Figure 63. Rationale for observed products ***121*** *and* ***122*** *with calculated Gibbs free activation* $\Delta G^{\circ,\ddagger}$ *and reaction energies* ΔG°*. Computations were performed at CPCM(water)-DLPNO-CCSD(T)/def2-QZVPP//CPCM(water)-B2PLYP-D3BJ/def2-TZVP 298 K / 1 M level of theory.*

2.7. Conclusion

This chapter described a practical and scalable synthesis of TCHep in only five steps from commercial starting materials, involving just one column purification, building from strategies developed by Szeimies in the 1990s.

Further, this Chapter established and explored the chemistry of TCHep for the first time — as well as contrasting it from TCP. Many similarities were found for photoredox mediated or catalysed methodologies, which translated conveniently onto TCHep. The transfer of anionic chemistry of TCP onto TCHep was unsuccessful, and this issue was rationalised *via* computational analysis. Further, multiple challenges were identified computationally, which may pose a problem for side reactions of TCHep that are not an issue for TCP.

Interesting new cationic mechanistic modes were discovered during bioconjugation experiments, not delivering the structures hoped for, but showing a more complex cationic isomerism, which is impossible for TCP.

Relevant reactivity, especially photoredox-mediated insertion of carbon-iodine bonds and MacMillan and co-workers' three-component coupling, was scoped and the limits tested. The afforded bridgehead-substituted BCHep units were impossible to access before this work, and structures similar to those shown in Figure 20 or 39 are unprecedented. This opens up the floodgates into new structural and chemical space.

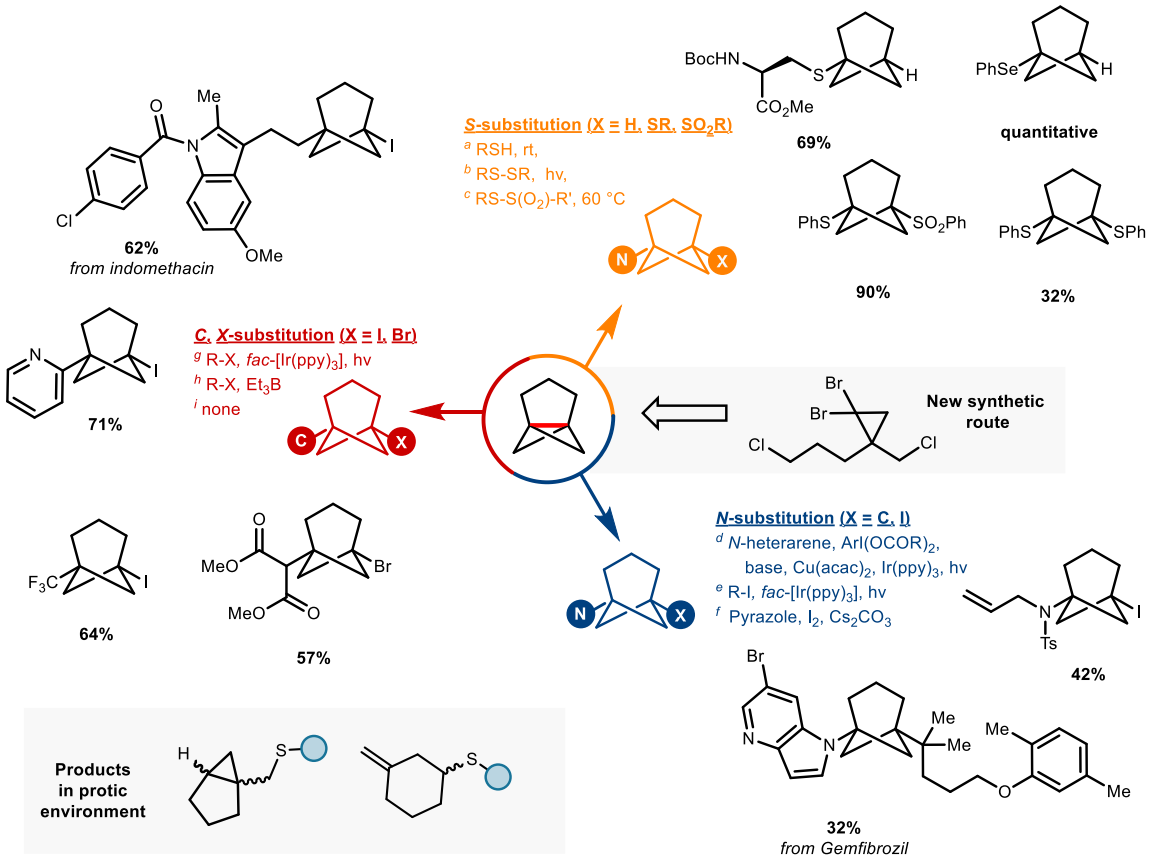


Figure 64. Summary of the work presented in Chapter 2.

3.

Applications in the context of bioisosterism

3.1. Introduction

3.1.1. The Underexplored BCHep Motif

A search for structures containing an exclusively bridgehead-substituted, ‘naked’ BCHep unit (all carbon, saturated, no additional bridge substitution) reveals that only 53 structures are known (results collected by a *SciFinder* query in March 2022). They are structurally closely related to the parent BCHep-dicarboxylic acid **37**, from which they originated synthetically (Figure 65). However, this source comes with significant limitations in structural diversity. Moreover, the cost of BCHep diacid **37** and similar derivatives ranges from 280 to 1000 $ / g (depending on the supplier), putting financial strain on research endeavours.

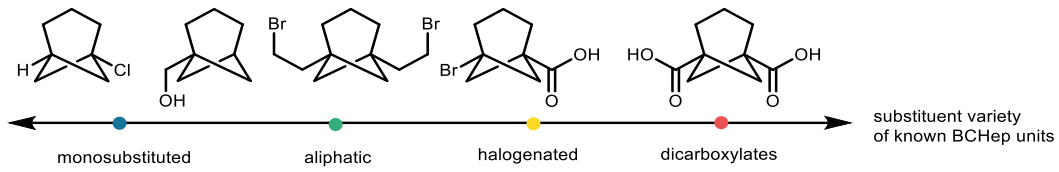


Figure 65. Structural space known for BCHep to date.

Chapter 2 presented novel transformations that advance the structural space of BCHep units into unexplored areas, including sp^2-substituted BCHeps and more complex, directly installable handles, which are likely to be of use in 'scaffold hopping'.[122] Even more encouraging is the development of new building blocks that fit the requirements of bioisosteric replacement, as defined in Section 1.3. It does not take long to see, and indeed

was already theoretically proposed by Mykhailiuk,[71] that the bridgehead vectors of BCHep units superimpose remarkably well onto a *meta*-benzene ring, accurately replicating the 120° *meta*-benzene substitution angle (Figure 66). Further, BCHep units fit into the notions of 'escaping flatland' as already described in Section 1.3.3. Given the success of using TCP to attain BCPs, well-established bioisosteres for *para*-substituted arenes, BCHeps appear to offer much promise in this regard.

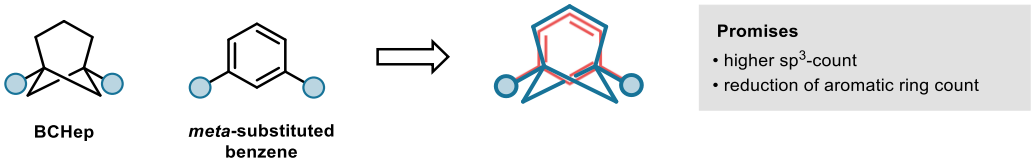


Figure 66. General hypothesis of using BCHep units as bioisostere for meta-substituted arene systems.

This reasearch coincides with a period in which many other research groups are proposing *meta*-arene bioisosteres with novel building blocks. The quest for finding the 'perfect' one has already started, as will be discussed in the next section.

3.1.2. Bioisosteres for *meta*-substituted Benzene Systems

An early example of a *meta*-substituted arene bioisostere was reported by Kuhn et al. in 2016, which employs a *trans*-cyclopropyl ketone as the replacer unit in the BACE1 inhibitor family to decrease IC_{50} and logD of **127** compared to **126**. This *trans*-cyclopropyl ketone still possesses a rotatable bond and thus does not exhibit ideal rigidity.[123] A similar *trans*-cyclopropyl amide **129** was tested by Winneroski et al. in 2019 but was found to show similar IC_{50} values as the parent drug **128** (Figure 67).[124]

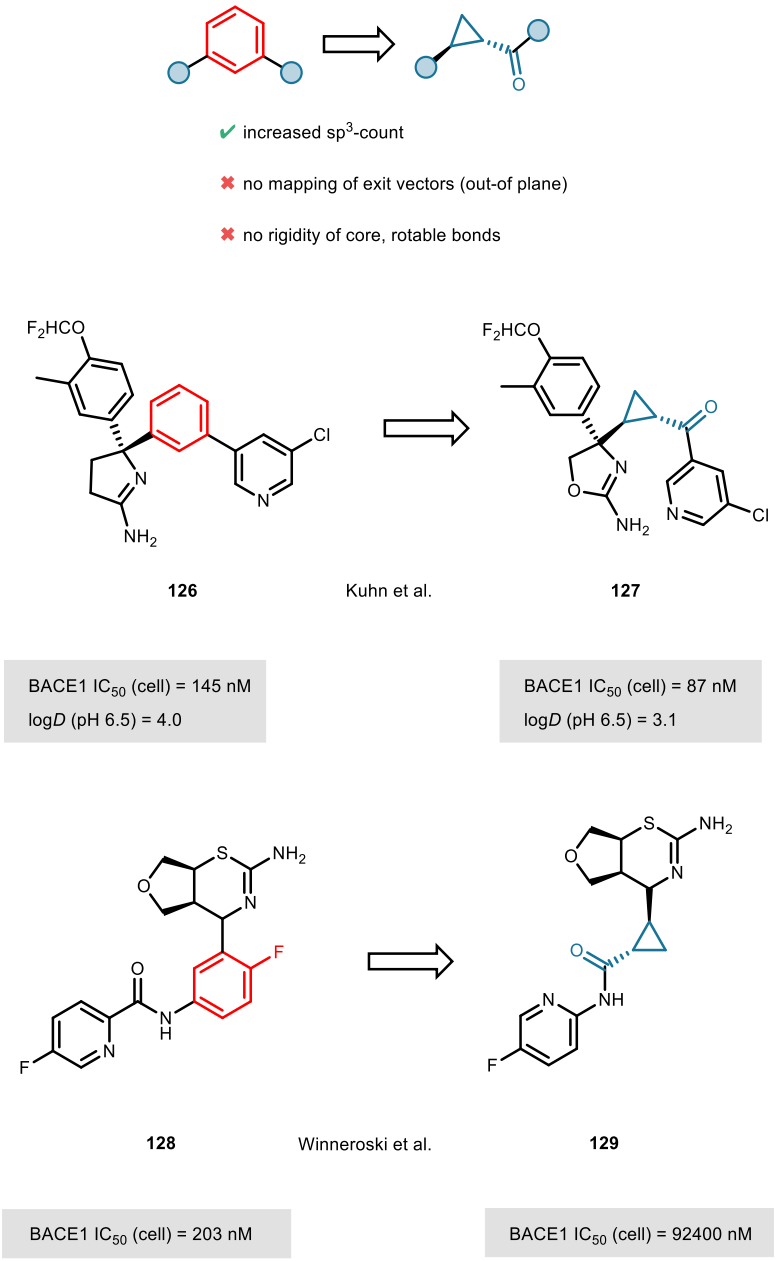


Figure 67. Trans-cyclopropyl ketone as one approach to replace meta-benzene rings.

Oxybicyclo[2.1.1]hexanes **130** units were proposed by Mykhailiuk and co-workers in 2020 as *meta*-substituted benzene bioisosteres, showing improved experimental logD, solubility and metabolic stability compared to the parent arene — although **134** was only tested against the *para*-substituted arene **133** (Figure 68).[125] Synthetically they were accessed from **131** *via* iodonium ion-mediated ring closure, or by photochemical [2+2] cyclisation of diene **132**.[126]

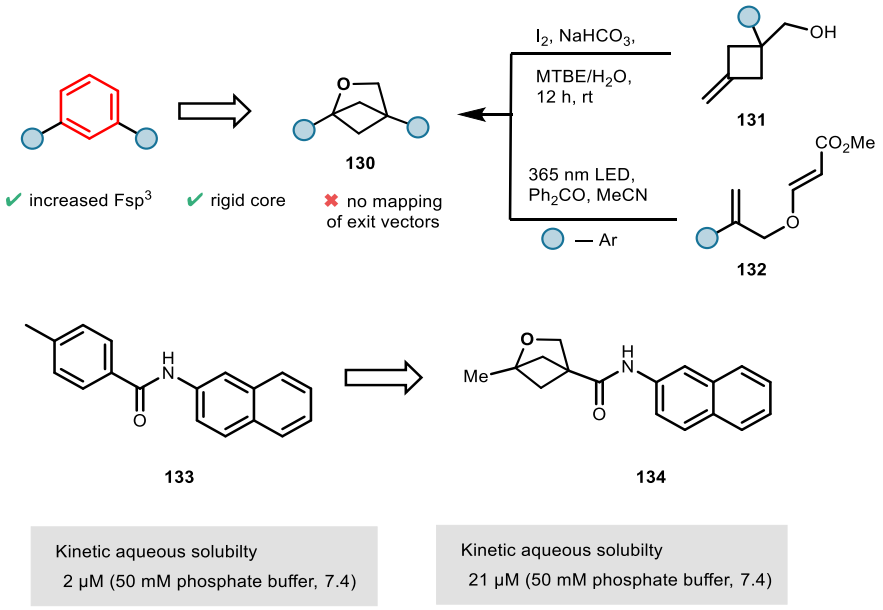


Figure 68. Mykhailiuk's and co-workers proposed oxa-BCHex bioisostere for meta-benzene systems.

Similar carbocyclic bicyclo[2.1.1]hexane BCHex units **135** have also been proposed and synthesised as *meta*-benzene bioisosteres by Mykhailiuk and co-workers in 2020 (Figure 69A).[71] Recent advances to access those BCHex structures through insertion of alkenes into BCB, were made by Glorius,[127] Procter,[128] and Brown,[129] independently. This formal [2π + 2σ] cycloaddition was achieved either through triplet sensitising (EnT transfer) with thioxanthones (Glorius and Brown) or through SmI_2 mediated processes (Procter, Figure 69A). Similarly, Leitch reported in 2022 the synthesis of azabiyclo[2.1.1]hexanes **136** through similar cycloadditions of imines to BCB (Figure 69B).[130] All of those were cautiously proposed as *meta*-substituted arene bioisosteres.

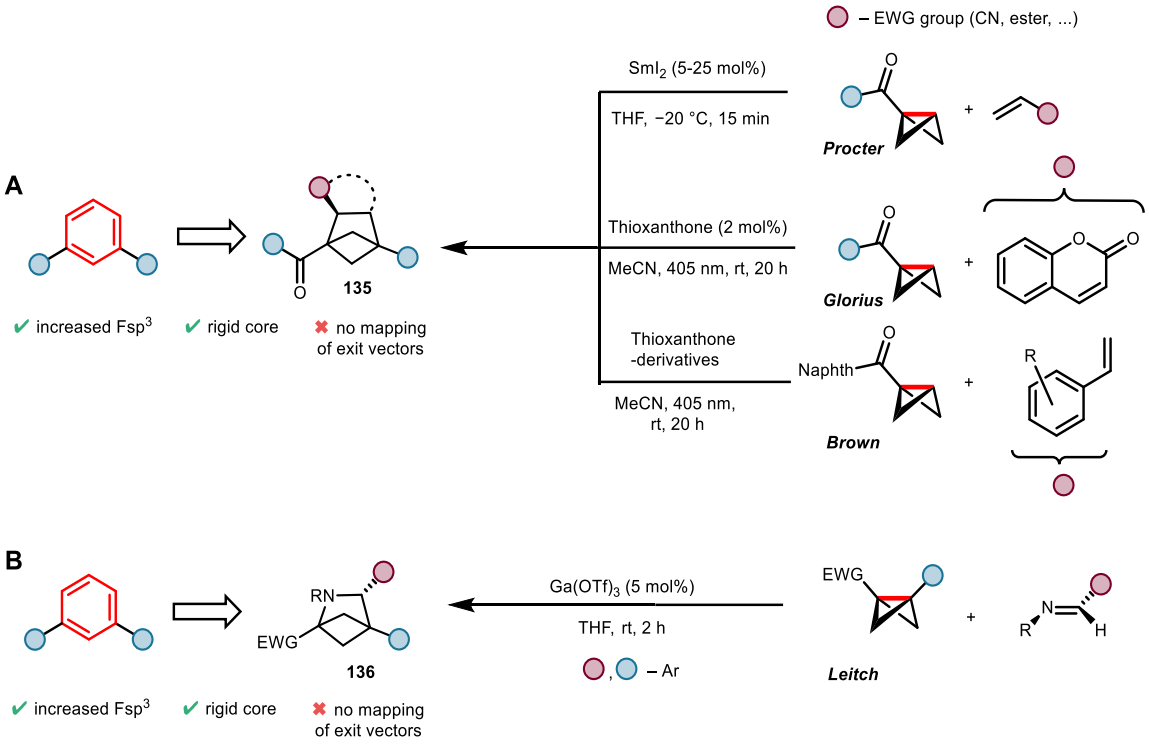


*Figure 69. (**A**) New routes to BCHex and their potential use as bioisosteres. (**B**) New route to azabicyclo[2.1.1]hexanes*

Baran and co-workers investigated 1,2-difunctionalised BCPs **137**, derived from bridge-substituted TCPs, as 'long-thought-after mimetics for *ortho*/*meta* substituted arenes' (Figure 70A). They prepared a set of *meta*- and *ortho*-substituted bioisosteric drug analogues, such as the *meta*-substituted systems Sonidegib or Meclizine (Figure 70B and C). In cooperation with Pfizer, these compounds were tested for lipophilicity (logD), kinetic aqueous solubility, permeability (Ralph Russ canine kidney) and were submitted to human hepatocyte stability tests. Indeed, beneficial ADME properties were found for most examples, for example the improved logD values and reduced clearance rate demonstrated by BCP-Sonidegib. In 2021, Qin and co-workers reported a Barluenga-Valéz methodology to bypass the laborious use of TCP derivatives (Section 1.2.1).

Notably, these proposed bioisosteres offer limited access to structural diversity and involve lengthy synthesis, which makes their implementation in drug discovery programs

unattractive. Further, they are on the limit of required structural parameters to be true *meta*-arene bioisosteres (see Section 3.2).

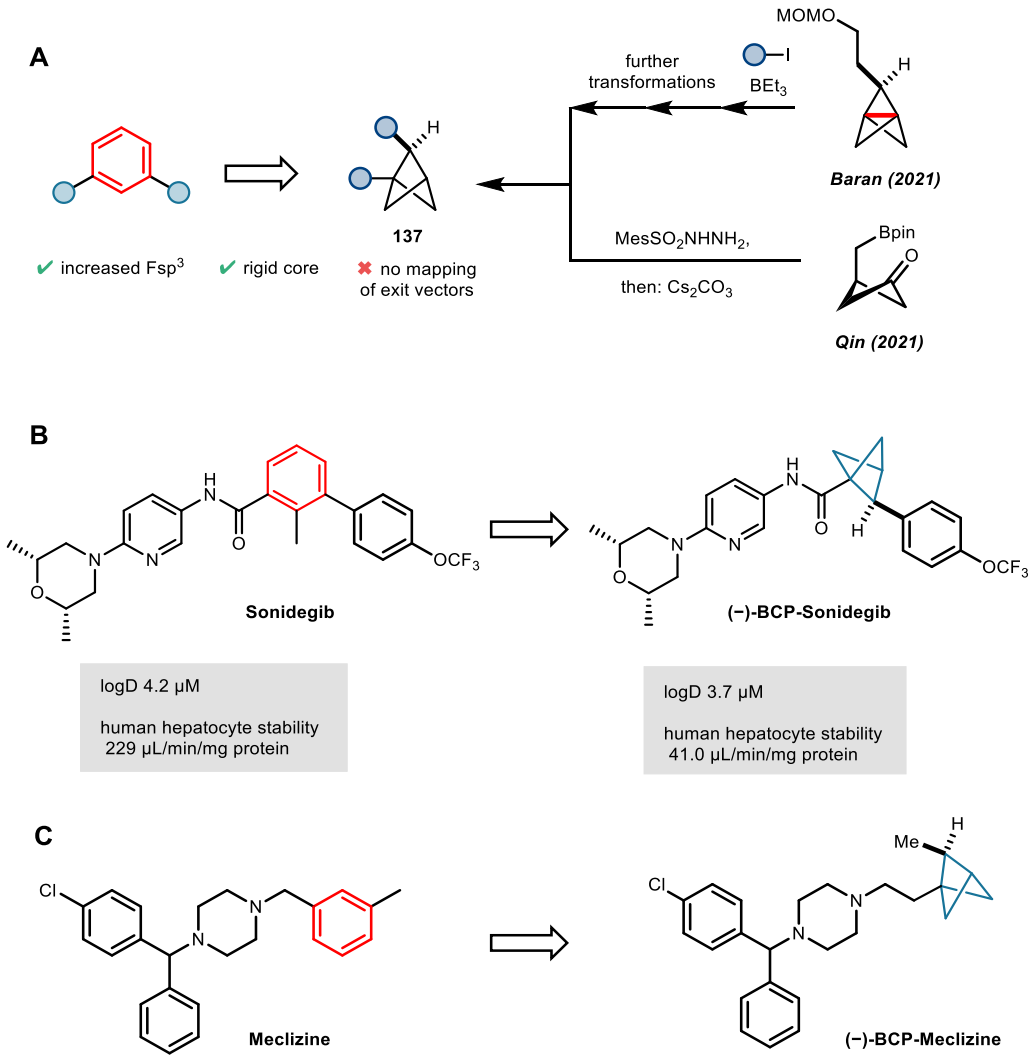


*Figure 70. 1,2-Bridgesubstituted BCPs as bioisosteres for meta- (and ortho)-substituted arene systems. (**A**) Routes to bridgesubstituted BCPs. Two exemplary tested bioisosteres are shown: (**B**) BCP-Sonidegib and (**C**) BCP-Meclizine*

3.2. Crystallographic and *in silico* evidence for isosterism

These structures, and BCHeps, can be evaluated computationally to compare their optimised geometries and test the hypothesis of BCHep units being the ideal bioisosteres for *meta*-substituted arene systems.[131] Four crucial parameters were investigated: the inner-core distance r_1 and outer-distance r_2, comparing the spatial expansion of the systems. Most importantly, the angle between the two bonds α — spanned by the two exit vectors $\vec{r}$ and $\vec{v}$ — and their 'out-of-plane' (dihedral) angle ϕ are compared (Figure 71).

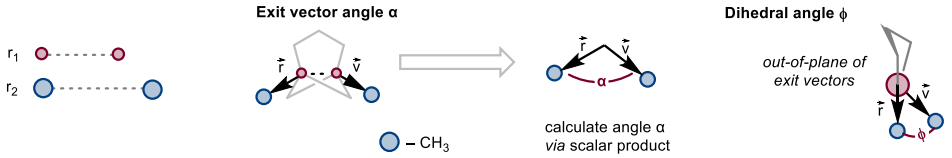


Figure 71. Definition of parameters crucial for comparing geometric bioisosteric features.

For calculating the angles, the cartesian coordinates were extracted from the obtained .xyz file, the associated vectors $\vec{r}$ and $\vec{v}$ were derived, and the angle they incorporated was calculated with their normed scalar product (see equation (III) and (IV)):

$$cos(\beta) = \frac{\vec{r} \cdot \vec{v}}{\|\vec{r}\| \cdot \|\vec{v}\|} \qquad \text{(III)}$$

$$\beta = \arccos\left(\frac{\vec{r} \cdot \vec{v}}{\|\vec{r}\| \cdot \|\vec{v}\|}\right) \qquad \text{(IV)}$$

In Table 5, inner r_1 and outer r_2 distance values of the rigid core can be found. All bridgehead-substituted bicyclic cage-system are generally compressed by 30–40 pm in r_1 compared to a *meta*-arene. r_2 deviates less, however it is interesting to note that BCHex units (4.91–4.95 Å) achieve closer parameters to the arene distance of 5.04 Å than BCHep units (4.75 Å), albeit at a cost of vector angle. Comparing these values to the compression

found for BCPs ($\Delta r_1 \approx \Delta r_2 \approx 1.0$ Å), BCHep deviates less from a spatial expansion perspective.

Table 5. r_1 and r_2 values determined at B2PLYP-D3BJ/def2-TZVP level of theory.

	r_1 [Å]	**r_2 [Å]**
meta-xylene	2.42	5.04
BCHep	2.14	4.75
O-substituted BCHex	2.03	4.95
Bridgesubstituted BCP	1.57	3.50
All-carbon BCHex *(1,2 bridge-substituted)*	1.55	3.18
All-carbon BCHex *(1,3 bridge-substituted)*	2.37	4.91
All-carbon BCHex *(bridgehead-substituted)*	2.07	4.93
N-substituted BCHex	2.04	4.94

Critically, Figure 72 shows the values of the angles α and ϕ verifying that the above published proposed *meta*-substituted bioisosteres do *not* structurally resemble a *meta*-benzene ring. Only for the bridge-substituted hetero- and carbocyclic BCHex structures do the exit vectors lie in the same plane (dihedral angle ϕ = 0) but these still deviate extensively from the required 120°.

Bridge-substituted BCP- and BCHex units do not possess angle values that qualify them as geometric mimics of *meta*-substituted benzene drugs. On the other hand, BCHep does indeed include a dihedral angle ϕ of ~0° and an exit vector angle α of ~119°. From an angle perspective, BCHep, therefore, perfectly matches a *meta*-substituted benzene.

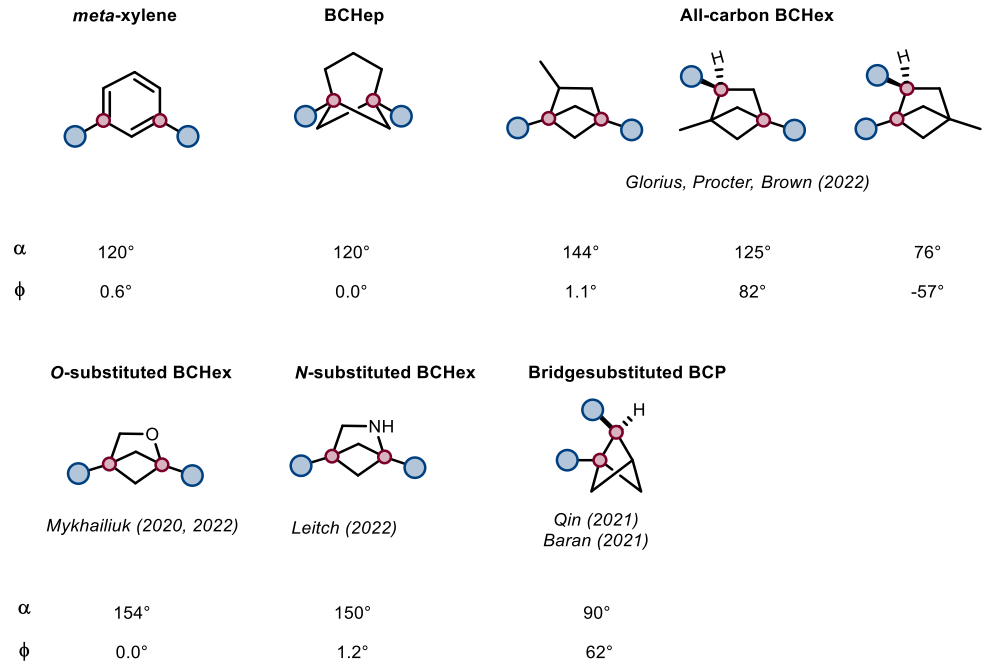


Figure 72. Angle data α and ϕ determined at B2PLYP-D3BJ/def2-TZVP level of theory.

So far, only dimethyl substituted motifs were compared computationally. Crystallographic data would give additional insight into the special arrangement of more complex substituents, although acknowledging the fact that solid-state structures do not necessarily resemble the ensemble of structures in solutions. Indeed, it was possible to collect crystallographic data (measured by DPhil student Helena Pickford) for five of the BCHeps presented in Chapters 2 and Section 3.3.5. For completeness, the same BCHep structure and its corresponding parent *meta*-arene were computed.

The following findings were made: Firstly, the *m*-Ar_{calc} angles indicate that the classical *meta*-substituted benzene angle of α = 120° is just an idealisation, and that angles in specific examples can deviate by up to 3°; Secondly, the 'out-of-plane' angle ϕ varies by up to 4° for *meta*-benzenes. The X-ray α- and ϕ-angle values of the BCHep unit fit perfectly within those windows, with only **72** as an exception, deviating considerably by 6°. Further, the X-ray geometry of **56** differs by 9° in its dihedral 'out-of-plane' angle ϕ,

which is also verified by large deviations of 6° in the computed structure. For all other investigated structures, pleasingly well-fitting angle values were obtained (Figure 73).

In summary, BCHep units excel in replicating a *meta*-substituted arene's structural profile, with the exit vector angles α and the out-of-plane angle ϕ being almost identical. Admittingly, inner- and outer-core distances r_1 and r_2 are more compressed for BCHep by ~0.3 Å. In our view, BCHep therefore structurally surpasses others scaffolds as a mimic of *meta*-substituted arenes. To truly validate this statement, the reactivity presented in Chapter 2 should be tested and diversified on 'real-world' targets to demonstrate its potential as a bioisosteric platform.

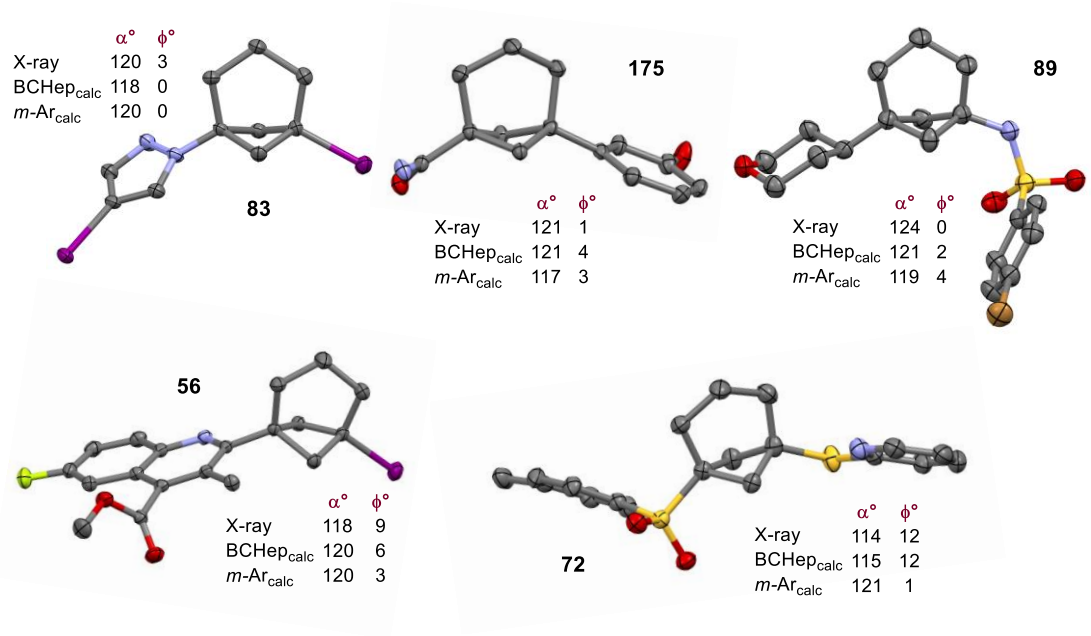


*Figure 73. Comparison of α and ϕ from single-crystal X-ray structures ('X-ray') and computed values for BCHeps ('BCHep$_{calc}$') and their parent meta-substituted arenes ('m-Ar$_{calc}$'), calculated at CPCM(THF)-B2PLYP-D3BJ/def2-TZVP level of theory. Crystallographic data was collected by Dr Helena Pickford. Crystal of **72** was grown by Dr Jeremy Nugent.*

3.3. Functionalisation of *C,I*–Bicyclo[3.1.1]heptanes

3.3.1. Target Drug Selection

Chapter 2 explored the broad reactivity and functional group tolerance of TCHep as a convenient reagent to access BCHep motifs. This section aims to apply this chemistry to the synthesis of genuine drug analogues. Ideally, the aim of developing this new bioisosteric platform is that *any meta*-substituted drug example can be carried out reliably yielding the bioisosteric drug which incorporated a BCHep unit instead of a *meta*-substituted arene. Figure 74 gives a diverse selection of *meta*-substituted pharmaceutical drug examples classifying them into three major categories A, B and C:

A. **Carbonyl substitution.** A carbonyl group is directly attached in a *meta*-substitution pattern on the arene, e.g. a terminal carboxylic acid, amide or ketyl functionalities. Examples include Olaparib by AstraZeneca which is used to treat ovarian cancer as a PARP inhibitor,[132] Lumacaftor (a treatment for cibric fibrosis)[133] and the pain-relieving agent Ketoprofen.[134]

B. Arene-substitution. Another arene system is directly attached to the central arene system forming a biaryl. The other substituent is not limited to a specific group, e.g. an acyl-substitution can be found here too.

C. Aliphatic- & Heteroatom-substitution *Meta*-benzene systems in which the substitution pattern does not feature an acyl or arene substituent. Examples include *S*- or *N*-substituted arenes like Belinostat, a drug against T-cell lymphoma,[135] or alkenyl- or alkynyl-substituents as in Benfluorex, which is used as an anorectic and hypolipidemic agent.[136]

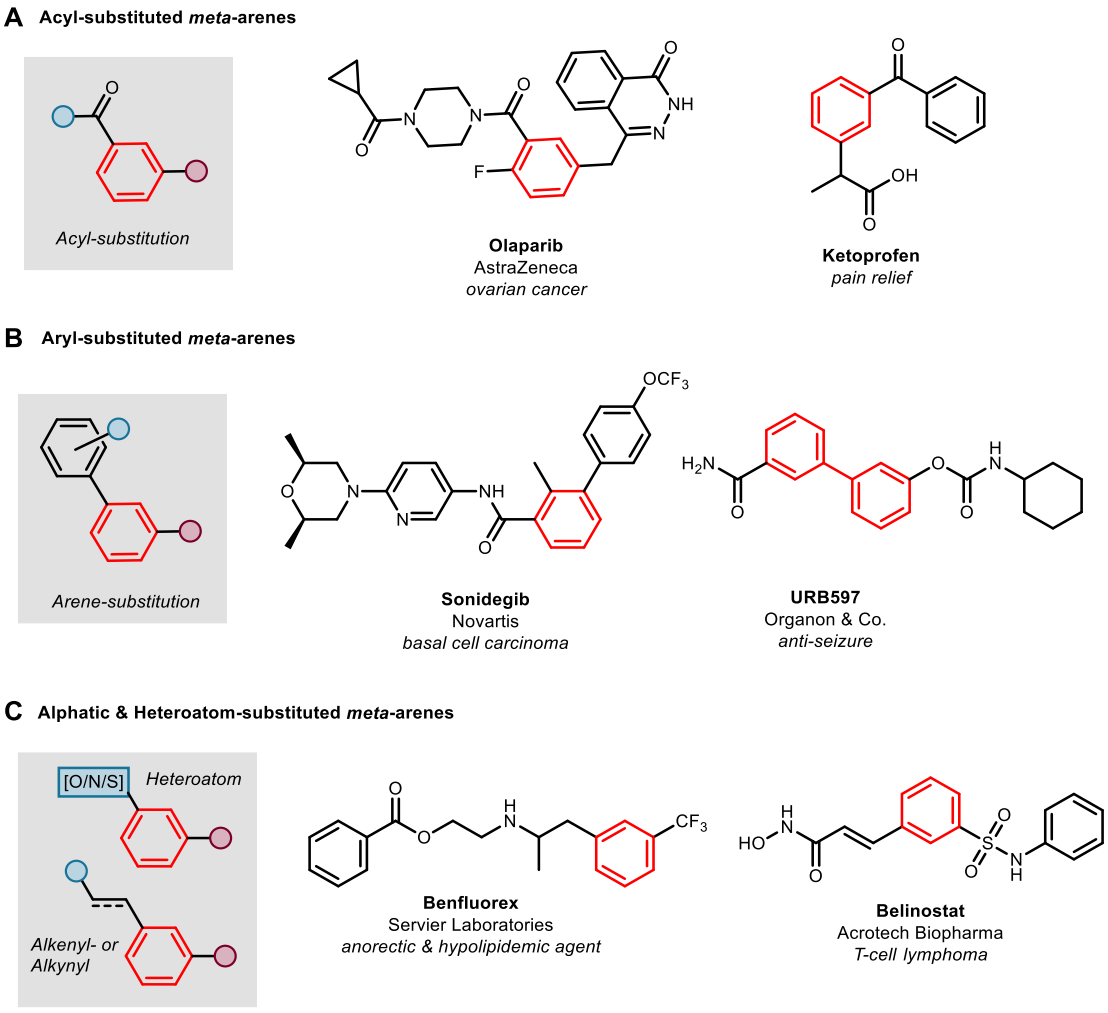


Figure 74. Drug examples and their structural categorisation.

In the subsequent chapters, it will become apparent why these classifications have been made. These categories are built around the strategies which will rely heavily on the insertion of organic iodides (see Section 2.3.1), being among the most versatile methodologies probed. Of key relevance is that our group has investigated and developed methods to functionalise BCP iodides (Figure 75, Section 1.2.3); it is the logical next step to examine these reactions on BCHep iodides.

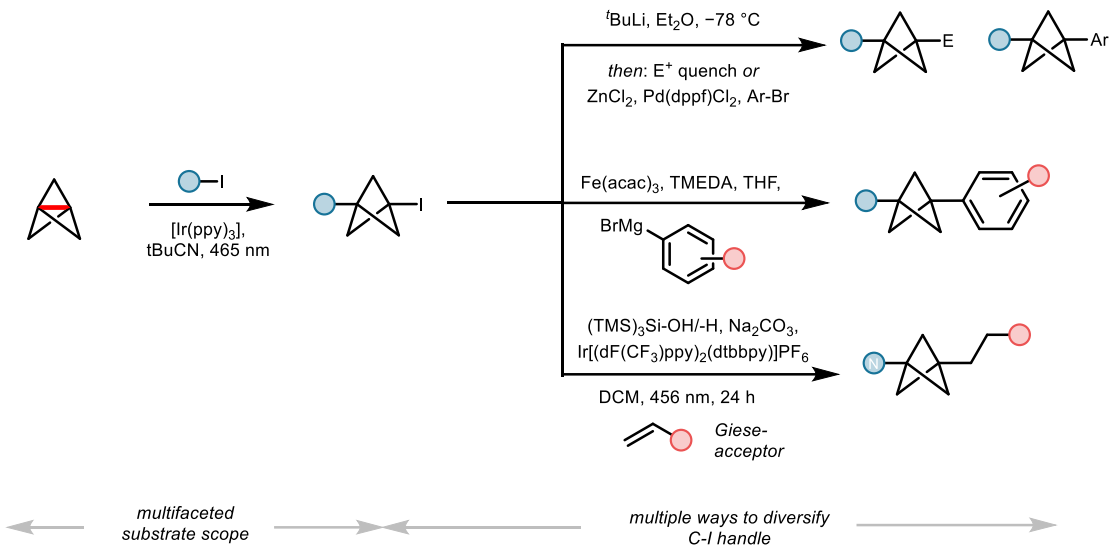


Figure 75. Diversification strategy and methodology for BCP iodides (see also Chapter 2.3.1).

3.3.2. Lithiation strategy

The lithiation of the BCHep iodides could be achieved through halogen-lithium exchange with *tert*-BuLi at −78 °C in an ethereal solution, quenching it various electrophiles. DPhil student Bethany Shire found that **48** can be lithiated and quenched either with CO_2 affording **138**, or *via* a borylation quench which allowed installation of a bridgehead hydroxy group after oxidation to yield **139** with sodium perborate (Figure 76).

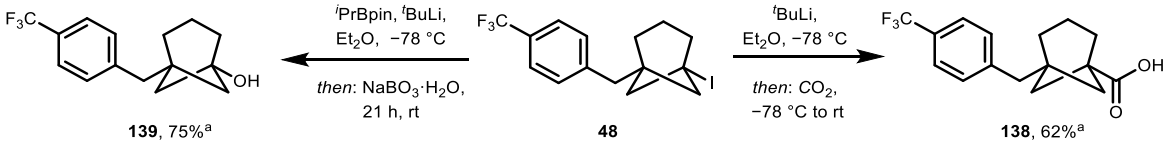


Figure 76. Successfully employed lithiation strategy. [a]Compound synthesised and characterised by DPhil student Bethany Shire.

Based on these encouraging results, syntheses of the BCHep drug analogues of Ketoprofen and Olaparib (bearing acyl substituents, Category A) commenced. Starting

with Ketoprofen, Figure 77 shows the envisioned bioisosteric replacement with the associated retrosynthetic plan.

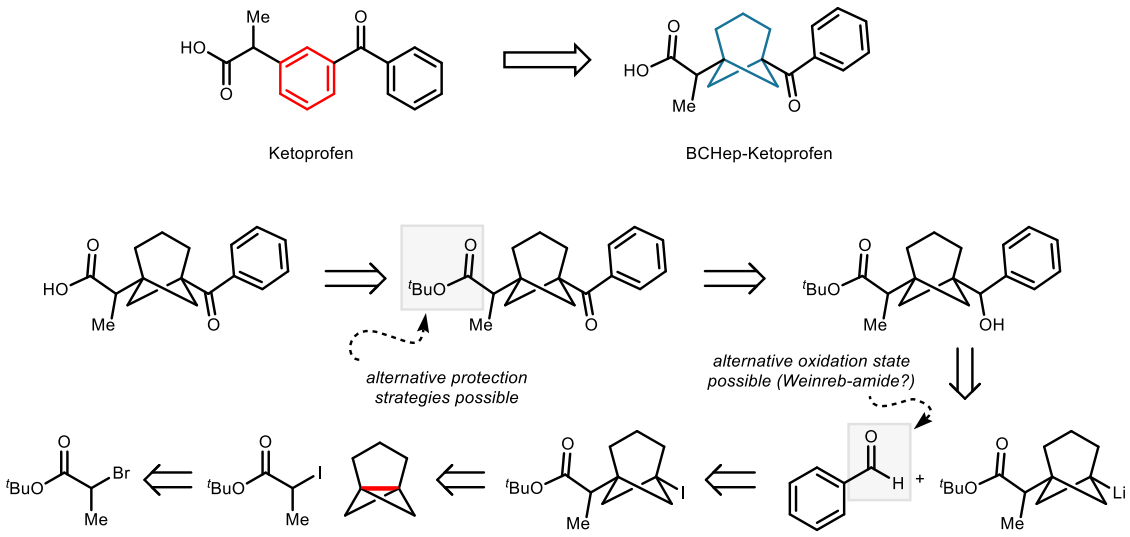


Figure 77. Retrosynthesis for BCHep-Ketoprofen.

The western fragment can be easily installed through C–I insertion chemistry and was already successfully shown in Figure 29 to be high-yielding. Lithiation of the resulting BCHep iodide and trapping with benzaldehyde was proposed — to yield the alcohol, which then can be easily oxidised towards the targeted ketoprofen-functionality. A protection strategy of the free carboxylic acid as a *tert*-butyl ester was deemed necessary to avoid problems in the metallation step, and was envisioned to be cleaved by TFA in a last step.

The synthesis of **46** proved straightforward, but sadly, the lithiation did not work regardless of the quenching agent used (benzaldehyde, benzoyl chloride or Weinreb amide, Figure 78). No starting material was left; only decomposition of the reaction mixture from which no BCHep compounds could be isolated.

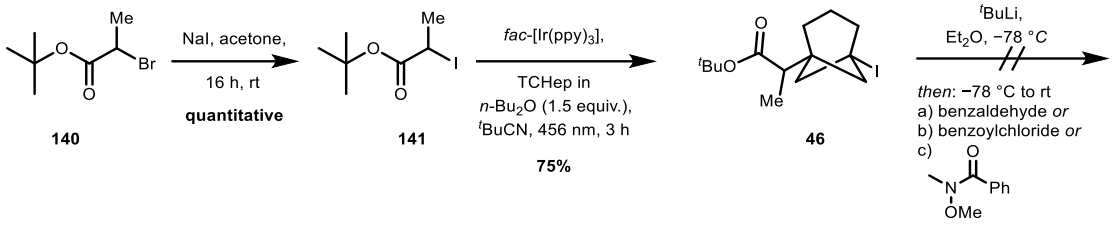


Figure 78. Failed use of a tert-Bu-protecting group in the forward synthesis of BCHep-Ketoprofen. 2.0 equiv. of tert-BuLi solution (Et_2O, 1.5 M) was used. Different electrophilic trapping reagents were tested after lithiation: a) benzaldehyde, b) benzoyl chloride or c) a Weinreb amide.

It can be reasoned that the ester group might pose problems in combination with *tert*-BuLi; therefore, the ester group was converted into a TBDMS-protected alcohol **142** (Figure 79). But also here, decomposition was observed, and quenching the reaction at −78 °C did not improve the crude reaction profile.

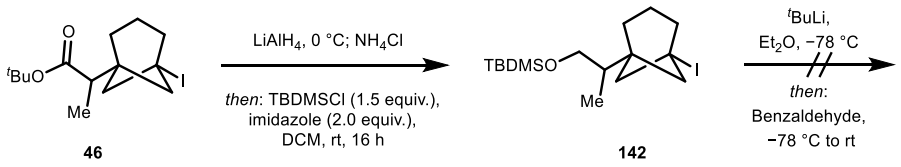


Figure 79. Failed approach towards BCHep-Ketoprofen using a silyl protecting group. Consistently 2.0 equiv. of tert-BuLi solution (Et_2O, 1.5 M) was used.

To ensure inertness towards the strong base *tert*-BuLi, a protecting group strategy employing an ortho ester was chosen, which is known to be stable towards bases but highly labile towards acids. First, the triethyl orthoester **143** was trialed but found to not undergo Finkelstein iodination to **144** (Figure 80A). Therefore, a switch to the OBO ortho ester **148** was made. Figure 80B shows this route, using the bicyclic ortho ester OBO. However, once again, lithiation failed at the final step for this ortho ester.

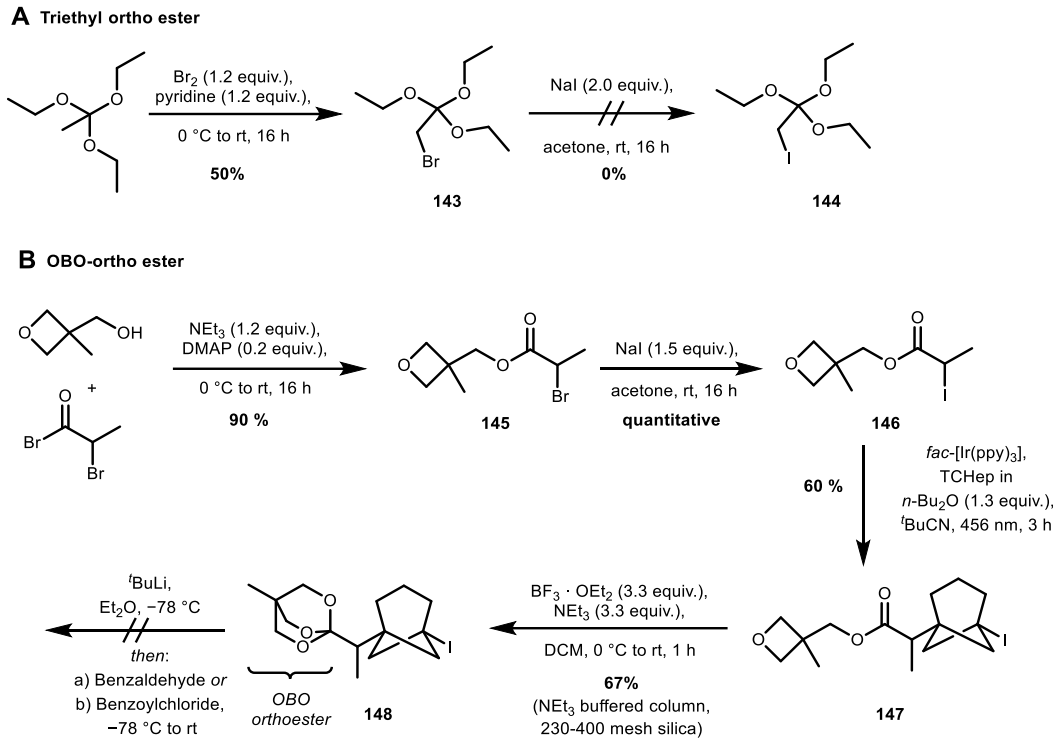


Figure 80. Approaching BCH-Ketoprofen with an ortho ester protecting group, which also failed at the lithiation stage.

The synthesis of BCH-Olaparib was next pursued. Focusing on the synthesis of the eastern fragment (Figure 81), which after addition and lithiation/carboxylation of the BCHep iodide, could be coupled to the western fragment, which is commercially available, *via* amide bond formation. The key disconnection and strategies are C-I insertion, lithiation and carboxylation. The phthalazinone unit can be synthesised *via* hydrazine ring-closure. A protection strategy might be necessary to protect the phthalazinone unit from the *tert*-BuLi. Further, it would assist potential solubility issues.

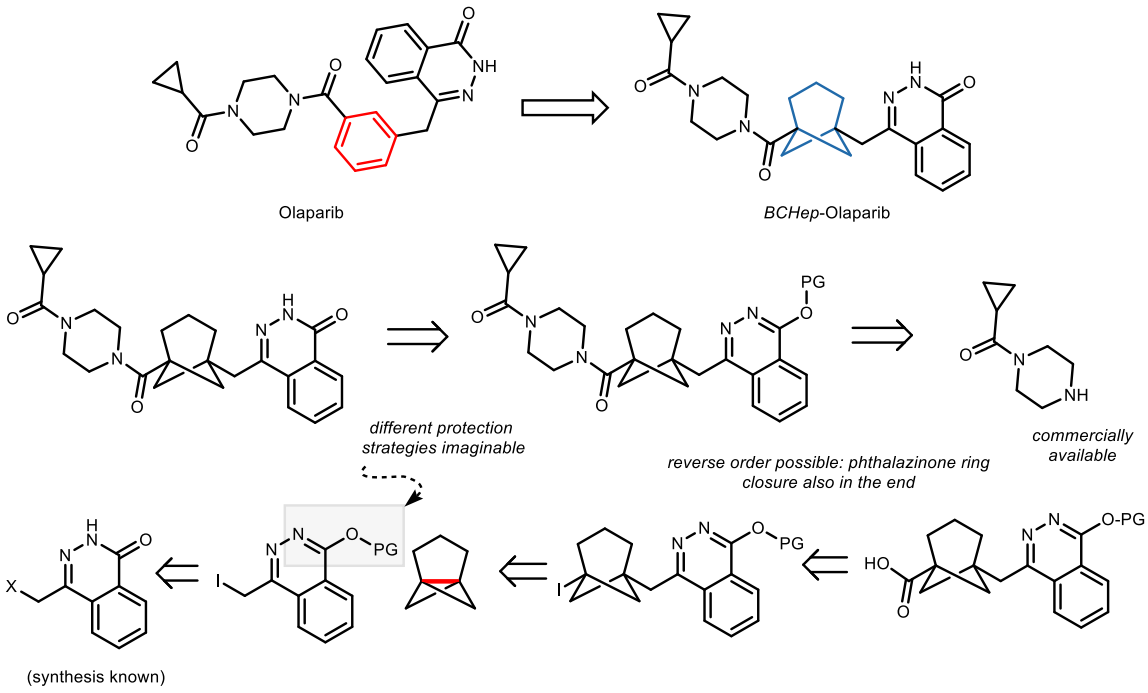


Figure 81. Retrosynthesis of BCHep-Olaparib.

Retrosynthetically, it was initially thought to ring-close the eastern phthalazinone unit before the addition of TCHep to reduce the length of the linear sequence after the BCHep unit was installed, and presented in Figure 82. However, **151** proved too insoluble to undergo productive ATRA chemistry, without protecting groups, with either BEt_3 initiation or mediated by *fac*-[$Ir(ppy)_3$]. An additive solvent like DMSO and DMF improved the solubility of **151** but was found to not have a significant impact on the yield (< 20 %).

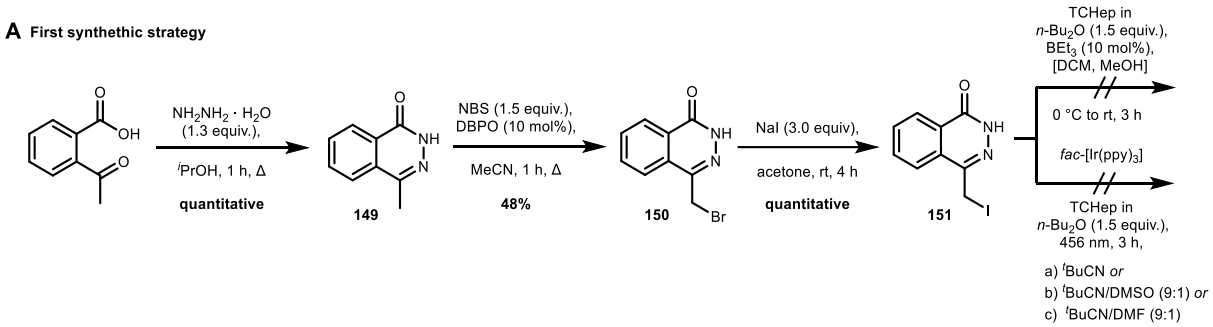


*Figure 82. Synthesis of **151**.*

Therefore, strategies were probed to install a protecting group on **150**. Little precedent is known for the protection of phthalazinones, and even for the amide substructure (highlighted in red in Figure 83), only niche examples are known.[137] As a result, several conditions were screened for installing a TBDMS protecting group hoping to achieve product **152**. All approaches were unsuccessful, using imidazole or pyridine, which returned starting material **150** even at elevated temperatures, or ultimately NaH, which resulted in decomposition. Acylation of **150** was unsuccessful too.

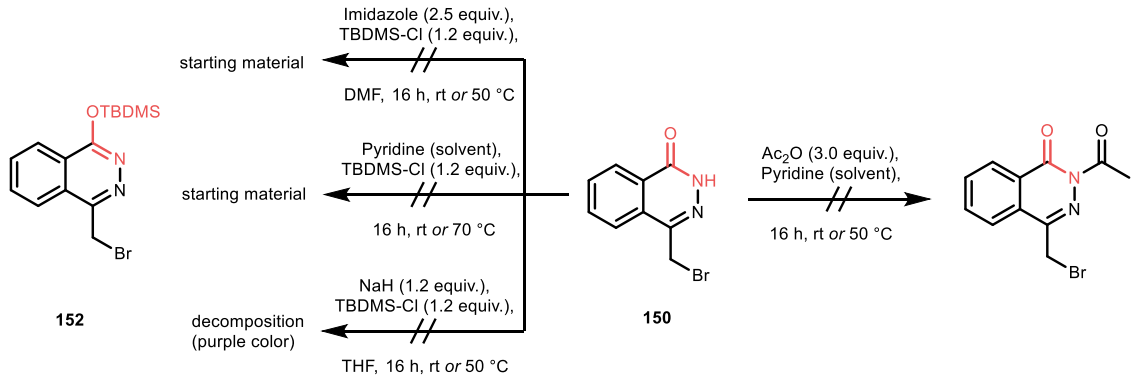


Figure 83. Failed Protection strategy.

At that stage, it was deemed productive to change the strategy so that the ring-closure to form the phthalazinone unit happens after installing the BCHep, using substrate **155** in the ATRA chemistry with TCHep. **155** was derived by esterification of commercially available starting material **153** and subsequent CuO-mediated iodination. After installation of the BCHep unit, the system was closed towards the phthalazinone **157** using hydrazine (Figure 84). However, initial lithiation trials without a protecting group yielded no product, nor returned starting material. Another approach that first attempted to deprotonate the phthalazine with NaH, and then proceeded with the lithiation failed too, possibly due to the insoluble nature of the intermediate sodium phthalazinone salt.

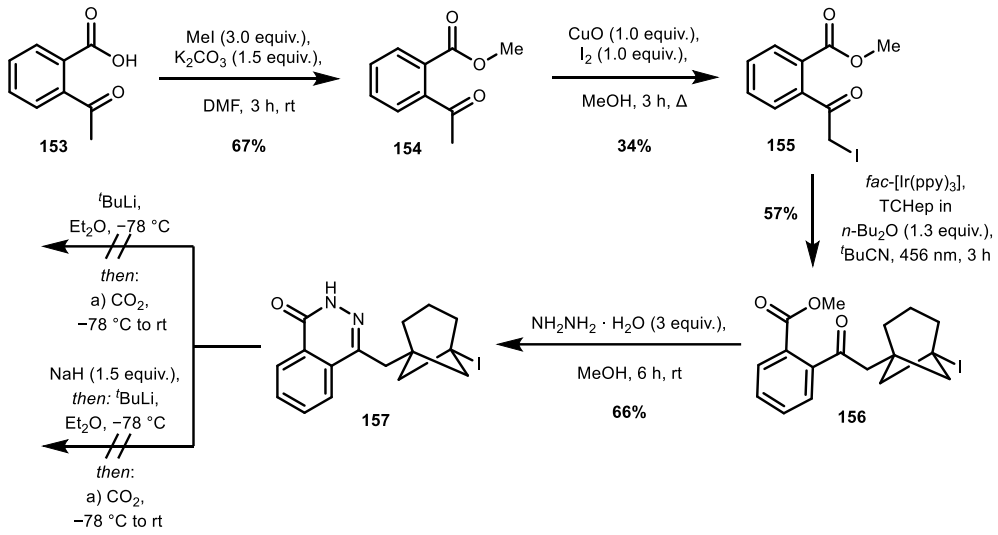


Figure 84. Revised strategy towards BCH-Olaparib.

Trying to install a TBDMS group to protect the heterocyclic core was again unsuccessful. At any stage during these synthetic trials, reasons for the failure of the lithiation were considered. Neither starting material nor a viable reduced BCHep-H product were observed (typically visible as a characteristic heptet by ^{1}H NMR spectroscopy). Attempts to isolate by-products of these reactions did not deliver valuable insights.

Probing the lithiation on two more substrates (Figure 85) strengthens the conclusion that lithiation strategies are only successful in the limited case of **48**. In retrospect, it appears surprising that substrate **48** was lithiated and trapped successfully.

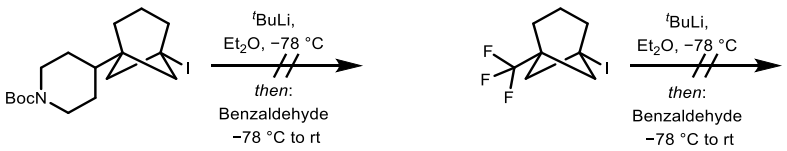


Figure 85. Unsuccessfully probed substrates in tert-BuLi (2.0 equiv.) lithiations.

Lithiations are usually driven by their thermodynamic driving force, e.g. a hybridisation change of the organolithium from sp^3 to sp^2. For the BCP iodides, for which lithiations are successful, a structural change from a destabilised *tert*-butyl anion towards a 'tied-

back’ and hence rehybridised carbanion intermediate affords sufficient differentiation to favour one over the other. Solvation effects may be important here too.

Indeed, computation of Gibbs free energies confirmed that a BCP anion **158** is 5.6 kcal mol^{-1} more stable than a *tert*-butyl anion **160** (Figure 86). For a BCHep carbanion, being a model for an organolithium system, computation suggests that a BCHep anion **159** is 2.1 kcal mol^{-1} *less* stable than a *tert*-butyl anion. That bridgehead BCP carbanions **158** are not intrinsically favoured was discussed in Section 2.5.4 and can be traced down to fewer possibilities for hyperconjugative stabilisation of already electronically congested bicyclic systems. Further, destabilisation effects can be imagined for the BCHep anion which are not prevalent for the BCP-core: The [3.1.1]-core forces overlap between bridged σ_1- and σ_2-orbital carbanionic orbital destabilising the overall unit (Figure 86, inlay). The Gibbs free energy would correspond to an equilibration constant K of 0.03 and explains why the above-performed lithiation failed — although not why **48** is the sole example of successful lithiations. These computational insights appear to rule out lithiation as a viable strategy to diversify BCHep iodides.

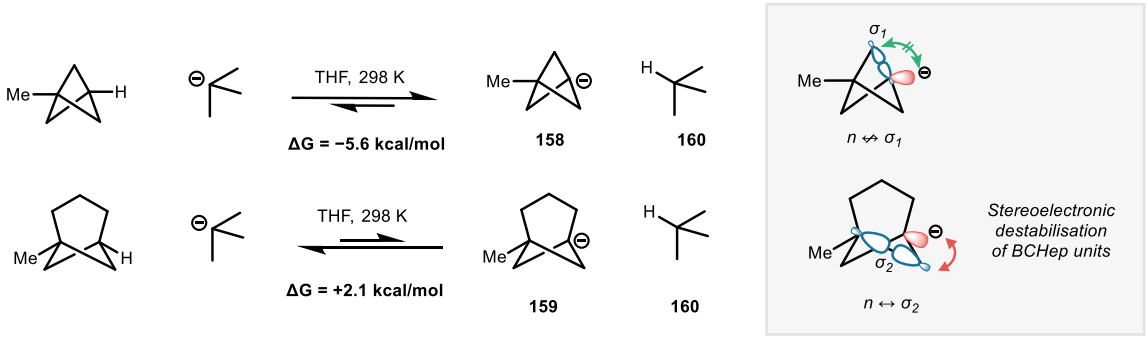


Figure 86. Gibbs free energies for proton-transfer indicating relative stability between carbanions. Inlay: Hypothesis of hyperconjucative destabilisation of the BCHep-units through aligned bridge σ-orbital and free carbanion. Computations were performed at DLPNO-CCSD(T)/def2-QZVPP//CPCM(THF)-B2PLYP-D3BJ/def2-TZVP 298 K / 1M level of theory.

3.3.3. Alternative metalation strategies

Having no access to drugs of category A (see Section 3.3.2) puts a severe limitations on the TCHep – BCHep system as a platform to access *meta*-substituted arene bioisosteres. We therefore sought other ways to metalate the BCHep iodide to approach the same units.

Besides lithium-halogen exchange, another classical way to generate organometallic compounds is through Grignard reagents. BCHep iodide **46** was submitted to common Grignard (Figure 87A) and Turbo-Grignard (Figure 87B) formation conditions. Only starting material was obtained in all cases, even though diverse activation methods were screened. Further, a protocol reported by Knochel and co-workers employing elemental zinc and various additives also failed (Figure 87C).[138]

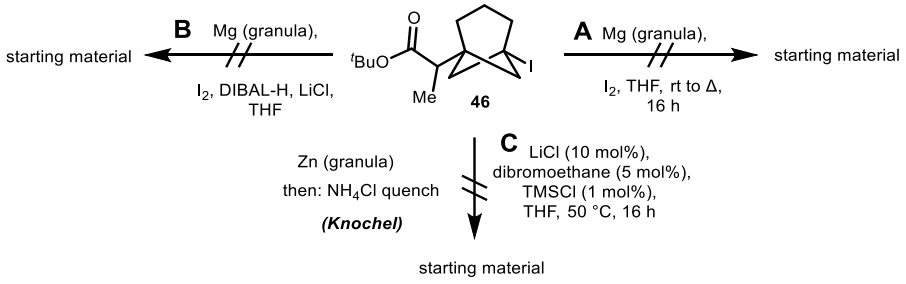


Figure 87. Tests on various metalation conditions.

Knowing how crucial the used metal supplier, metal surface and granularity of the elemental metal is,[35] it was hypothesised that freshly prepared Rieke-metal might offer a solution. Rieke metals are highly reactive elemental metal powders generated by *in situ* reduction of a metal salt with, e.g. lithium naphthalenide. They are used as a suspension in their mother liquor, are finely dispersed, and lack an oxide surface, enabling high reactivity.[139] They are known for undergoing the formation of 'impossible Grignard reagents', such as the insertion of magnesium into 2-chloronorbornane and its

carboxylation with CO_2.[140] A similar structural example was found for the insertion of Rieke calcium into 1-adamantyl chloride.[141]

Rieke magnesium,[140] Rieke calcium[141-142] and Rieke zinc[35] were synthesised with freshly prepared stoichiometric amounts of lithium biphenylenide or lithium naphthalenide solution in THF (Figure 88). Experimentally, only Rieke zinc was prepared with confidence, as Rieke magnesium and Rieke calcium either formed aggregates, or no precipitate was visible, respectively. It was found that Rieke magnesium and Rieke calcium do not undergo addition into BCHep iodide **48** — possibly due to inexpert preparation.

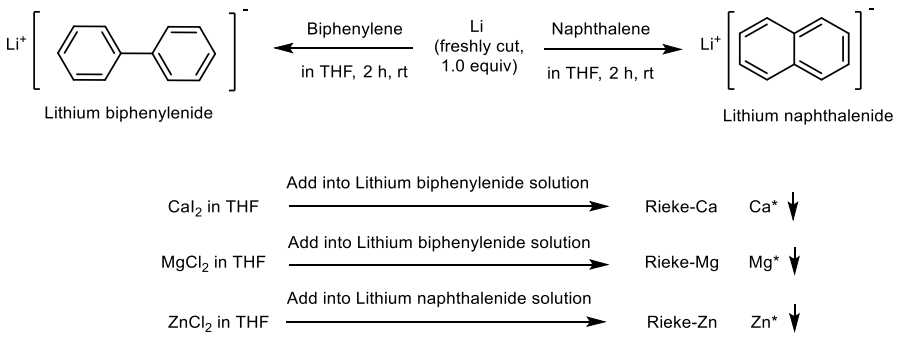


Figure 88. Preparation of Rieke metals in THF solution.

On the other hand, Rieke zinc was observed to insert into the BCHep iodo-bond reliably and reproducibly. ^{1}H NMR aliquots (NH_4Cl quench) showed that this zinc insertion process begins at room temperature, although complete conversion is not achieved after 24 h. At 50 °C reaction temperature and after 16 h reaction time, Rieke zinc was fully inserted into the BCHep iodide bond and can be cleanly quenched with NH_4Cl to **162**. An intermediate organozincate species $RZnX_2^-$ Li^+ **161** might be proposed as investigated by Fleckenstein and Koszinowski[143] as well as Blum and coworkers,[144] highlighting the vital effect of the remaining LiCl in the Rieke zinc suspension.

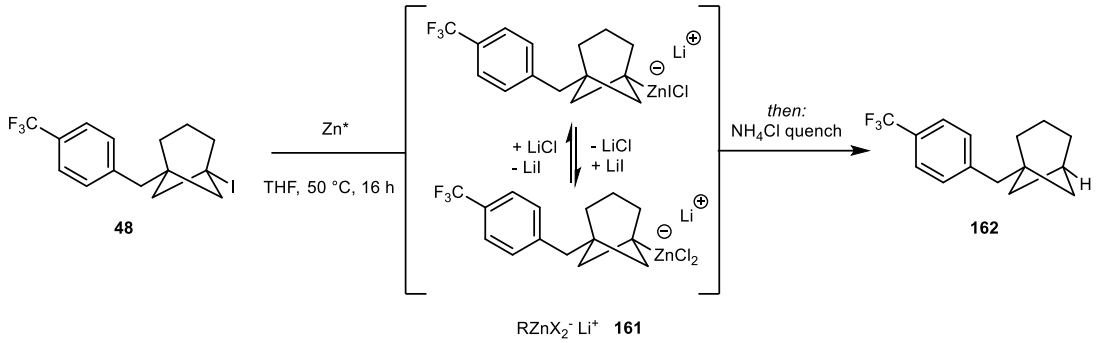


*Figure 89. Successful insertion of Rieke zinc into **48** being quenched to **162**.*

Organozinc reagents are valued for their mild reactivity and associated regioselectivity.[35] Trapping with benzaldehyde was possible, although in low (isolated) yields of 10% (Figure 90A). Several common cross-coupling and other transformations were probed without any success and, in all cases, reduced BCHep-H was observed. Switching to 2-MeTHF and increasing the temperature to 80 °C did not significantly change this yield, neither did the addition of different Lewis-acids ($MgBr_2$, $BF_3{\cdot}OEt_2$). Further, adding TMS-Cl, which is often beneficial for increasing yields in organozinc chemistry,[145] did not alter the results.

Using a Negishi-cross coupling protocol did not afford any 2-iodo pyridine cross-coupled product (Figure 90B) and instead only reduced starting material. Similar no S_N2' reactivity was observed with allyl bromide, a reaction which is otherwise well-established for organozinc reagents (Figure 90C).

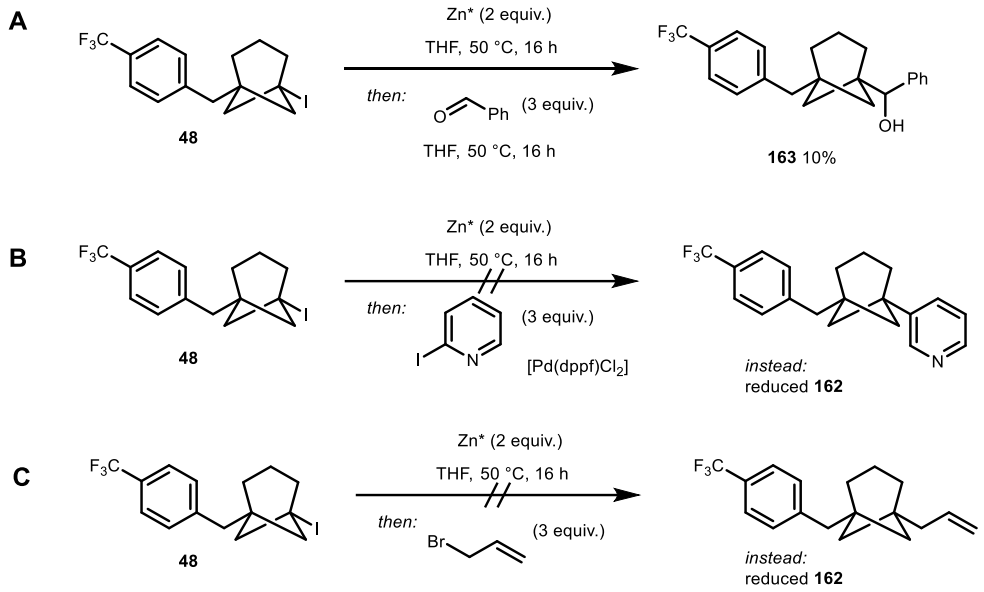


Figure 90. Unsuccessful approaches towards trapping of the generated organozincates.

It is important to note that often organozincates are too stabilised to react efficiently and are thus transmetalated to organocuprates using CuCN which possess higher reactivity. This strategy was considered beneficial in this situation: metalating a BCHep iodide needs enough driving force to shift the equilibrium to the BCHep-metalate side. On the one hand, this is indeed the case in the reactions mentioned above, producing stabilised enough zincates. On the other hand, these intermediates seem too stabilised — too unreactive — to be quenched by electrophilic trapping reagents. To circumvent this dilemma, transmetalation to cuprates could come to the rescue.

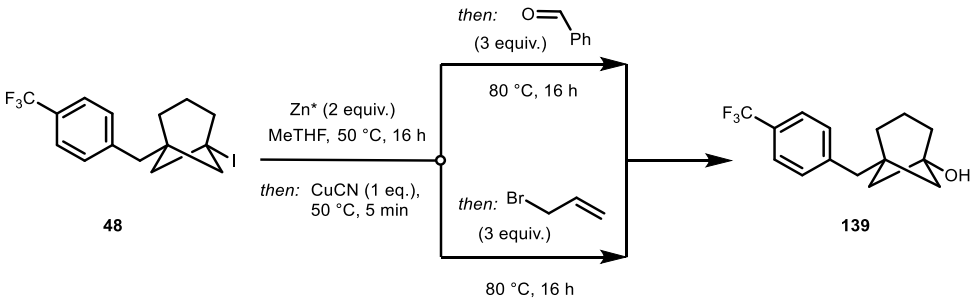


*Figure 91. Unexpected product **139** unambiguously identified by matching characterisation data of **139** on p. 114.*

Several reactions were probed using either solid CuCN or CuCN · LiCl solution. A new product was observed and isolated in both cases (Figure 91) whose characterisation data fits alcoholic product **139** in Section 3.2.2. Conducted under an inert atmosphere, the oxygen source is not clear. Further investigations are needed to clarify what role the CuCN plays, and if this serendipitously discovered reaction is helpful in any broader context.

3.3.4. Miscellaneous reactions

It should be mentioned that several other reactions were probed without any success. First, the photoredox-catalysed Giese reaction developed by DPhil student Helena Pickford for BCP iodides is of potential interest to be used in synthesising drug examples from Category C. Attempted application of this methodology to BCHep iodides did not meet with success, and solely the reduced BCHep-H product was observed (Figure 92A). A possible alternative is hydrolysis of **64** into a carboxylic acid, however this either returned starting material or led to decomposition (Figure 92B).

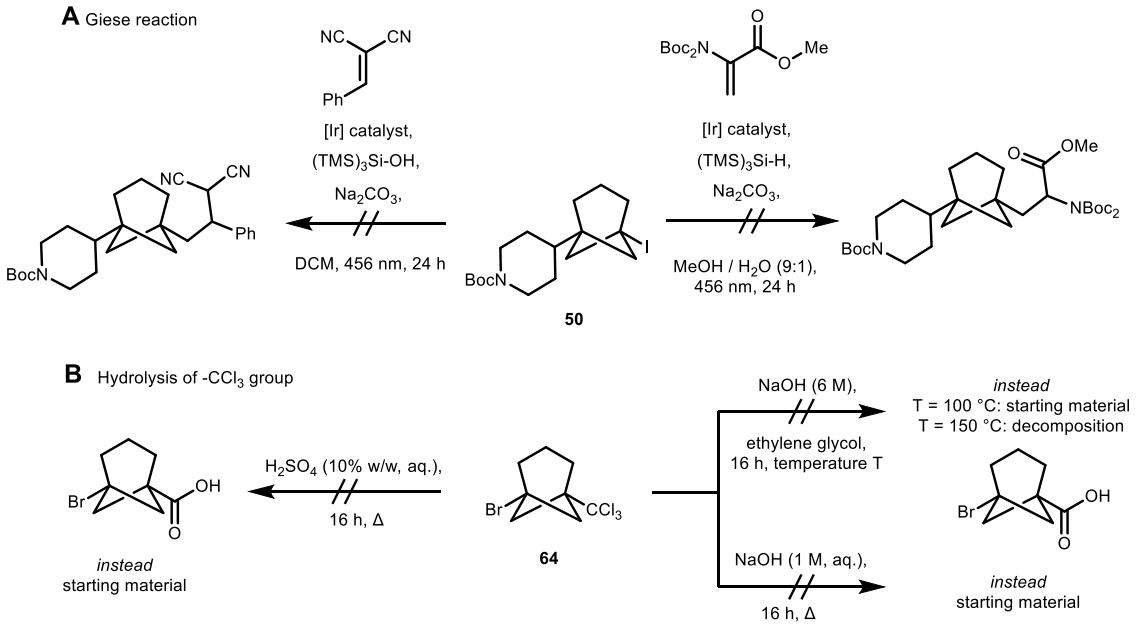


Figure 92. Miscellaneous probed derivatisation reactions. [Ir]-catalyst: Ir[dF(CF)$_3$ppy]$_2$(dtbbpy)PF$_6$.

3.3.5. Kumada cross-example strategy

Drugs out of the defined 'Category A' appeared inaccessible so far. Luckily, DPhil student Bethany Shire discovered that BCHep iodides can undergo Kumada cross-coupling in excellent yields, even superseding the yields obtained for BCP iodides.[46] Further, more electron-deficient aromatics were better tolerated than for BCP iodides. Figure 93 shows the substrate scope which ranges from electron-rich anisoles **164** to electron-deficient pyridines **169**.

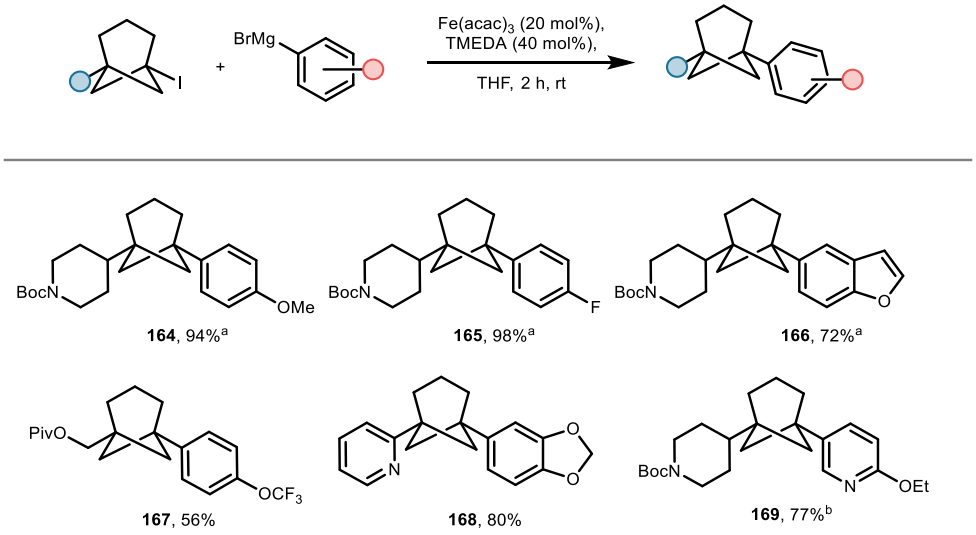


Figure 93. Substrate scope of the Fe-catalysed Kumada-cross coupling on BCHep iodides. [a]*Synthesised and characterised by DPhil student Bethany Shire.* [b]*Synthesised and characterised by Dr Jeremy Nugent.*

It becomes apparent that these cross-coupled products fall into 'Category B' of envisioned drugs. Encouraged by those results, the drugs BCHep-Sonidegib and BCHep-URB597 were tackled synthetically (Figure 94). The retrosynthetic analysis in Figure 94 shows the crucial conceptual trick[146] to use a pivalic ester as a latent carboxyl group (after hydrolysis and oxidation).

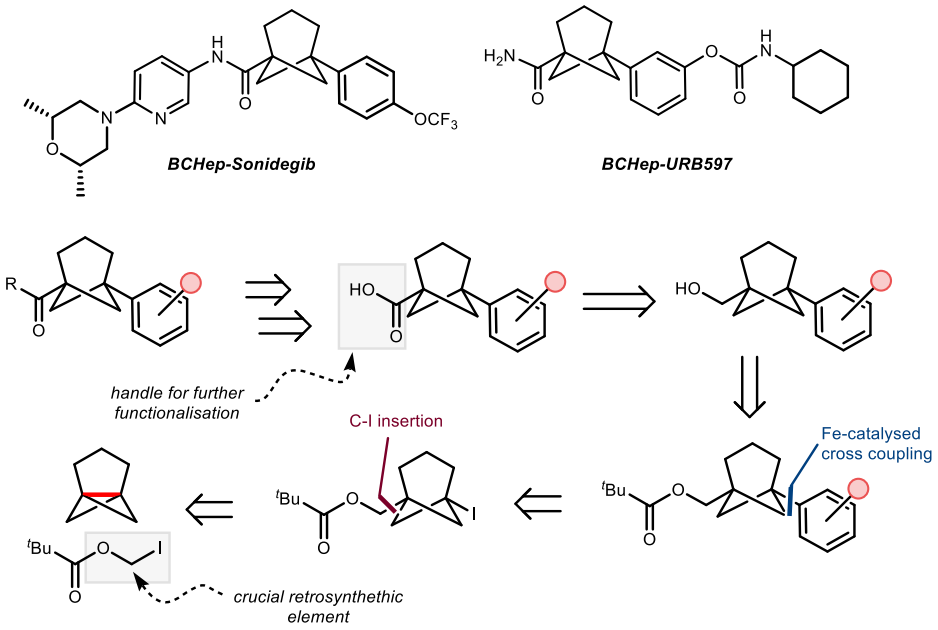


Figure 94. Retrosynthetic analysis of the structural motifs of Category B drug examples.

The synthesis of BCHep-Sonidegib proved straightforward, as presented in Figure 95. **52** can be synthesised by the photoredox-catalysed insertion of pivalic iodide in 64% yield, as described in Section 2.3.1. The BCHep iodides can be subjected to the Kumada cross coupling with 56%. The pivalic ester was hydrolysed by aqueous sodium hydroxide solution and subsequently oxidised with $RuCl_3/NaIO_4$ (Figure 95). Finally, amide coupling with **171** afforded BCHep-Sonidegib in 77%. In total BCHep-Sonidegib was synthesised in over 4 steps in 30% (starting from **52**).

The successful synthesis of BCHep-URB597 is shown in Figure 96. In this synthesis, the cyclohexyl carbamate was thought be introduced at a late stage, with the phenol precursor proteced as a benzyl ether through the iron-catalysed Kumada cross-coupling giving **172**. The corresponding product was unpurified taken into the following hydrolysis and oxidation yielding **173** in 36% over three steps. An amidation using ethyl chloroformate produced **174** in 88% yield. A subsequent benzyl deprotection used cyclohexene as a hydrogen source, avoiding the direct use of H_2 gas, afforded **175** in 71%.[147] Final

condensation of cyclohexyl isocyanate yielded BCHep-URB597 in 70%. Overall, BCHep-URB597 was synthesised in 16% yield over 6 steps (starting from **52**).

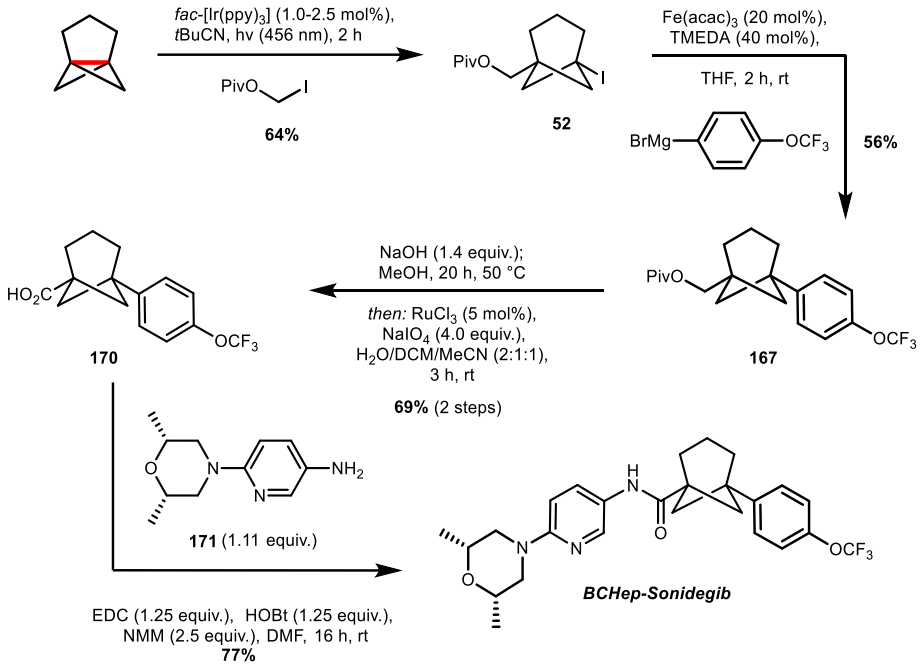


*Figure 95. Synthesis of BCHep-Sonidegib using **52** as starting material (see Figures 29 and 93).*

Both drug analogues were obtained in amounts of ca. 50 mg, and were purified by reversed-phase HPLC to obtain the compounds in purities suitable for ADME testing.

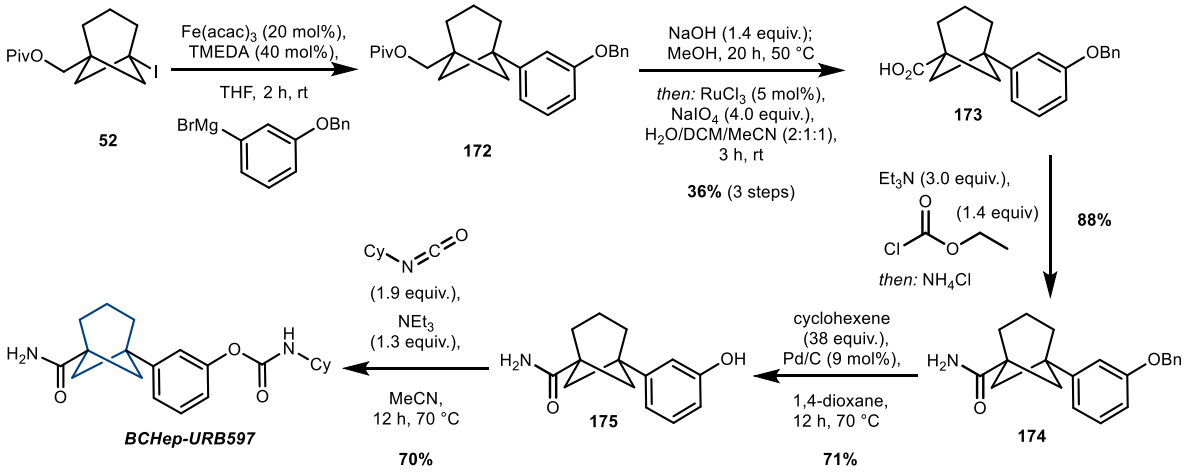


Figure 96. Synthesis of BCHep-URB597.

3.4. Physicochemical and metabolic evidence for bioisosterism

The two drug analogues synthesised above offer the possibility to test the bioisosteric promises that were only hypothesised so far. Besides the exit vector angles, which were compared for several simple examples in Section 3.2, the overall drug shape and topology is essential to be maintained so that the bioisosteric drug is capable of binding correctly in its target protein environment (see Section 1.1).[68] It can be imagined that replacing the planar arene with a bicyclic BCHep unit might distort the drug's ability to do so.

For Sonidegib and BCHep-Sonidegib, a computed conformer search was carried out. The conformational space was sampled *via autodE*[148] using ETKDGv2 (RDKit[149]) and afterwards optimised in ORCA at a CPCM(THF)-PBE0-D3BJ/def2-SVP level of theory (version 4.2.1).[150-151] The lowest-lying conformer was selected, and a constrained scan around the dihedral angle ψ was carried out. ψ quantifies how the two quasi-planar western and eastern fragments attached to the central *meta*-substituted arene system or BCHep-unit are oriented towards each other (Figure 97).

The incontinuities visible in these scans (Figure 97) can be explained by a change in the global conformation around fixed ψ. Interestingly, BCHep-Sonidegib appears to have no significant conformational preference for ψ, within a range of 1.6 kcal mol^{-1}. This can be rationalised by the sterically-congested bicyclic BCHep unit, which is different to the planar benzene system of Sonidegib itself, for which clearer local minima were observed. In the case of the BCHep, it is reasonable that no clear preference arises for a substituent bonded to a pseudo-symmetric saturated quaternary carbon centre.

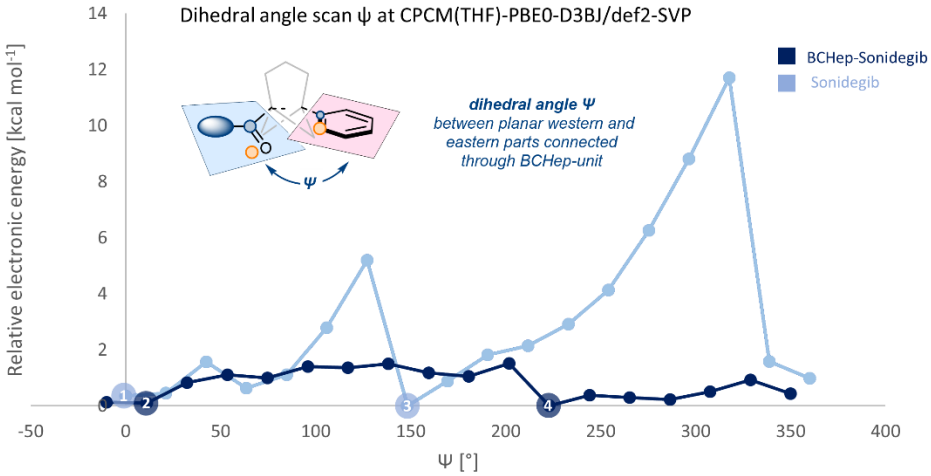


Figure 97. Constrained scan showing the angular relation of the two pseudoplanar western and eastern parts of BCHep-Sonidegib. The angle ψ is defined as the dihedral angle between the orange and blue spots. Scan performed at CPCM(THF)-PBE0-D3BJ/def2-TZVP level of theory.

For Sonidegib, two low-energy zones were found around $\psi \approx 0°$ and $\psi \approx 150°$, related to the orientation of the amide into the front and back space. Similar zones were identified for BCHep-Sonidegib: $\psi \approx 11°$ and $\psi \approx 223°$. All four structures were put through another geometry optimisation at the higher CPCM(THF)-B2PLYP-D3BJ/def2-TZVP level of theory to verify both local minima. These calculations confirm that the local minima are of comparable energy and are equally populated at room temperature: ΔE(BCHep-Sonidegib pair ② and ④) = 0.12 kcal mol^{-1} and ΔE(Sonidegib pair ① and ③) = 0.07 kcal mol^{-1}.

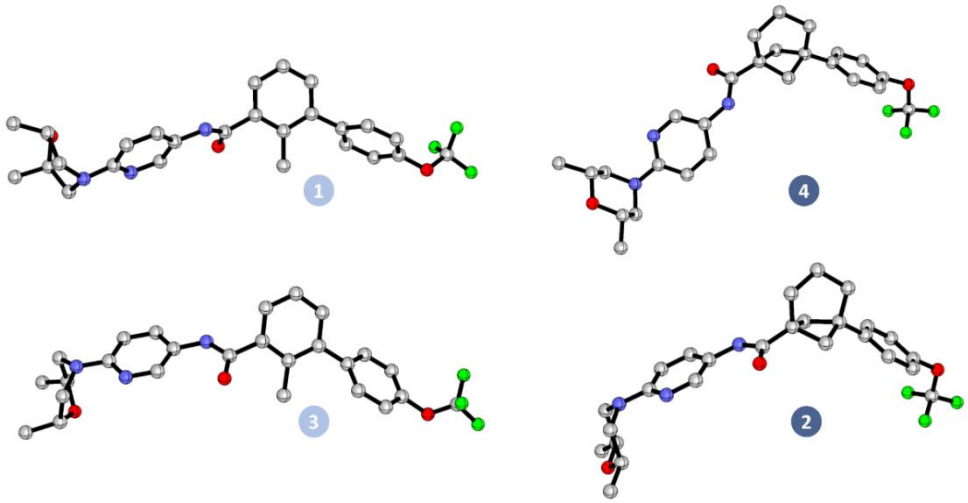


Figure 98. Reoptimised geometries of two local minima for Sonidegib (① and ③) and BCHep-Sonidegib (② and ④) corresponding to the carbonyl-group oriented in front- and hind-space. Geometries optimised at CPCM(THF)-B2PLYP-D3BJ/def2-TZVP level of theory.

Comparison of the α, ρ, and ψ shows a similar molecular van-der-Waals volume and reasonable agreement with the largest deviation in ψ of approximately 10° (Figure 99).

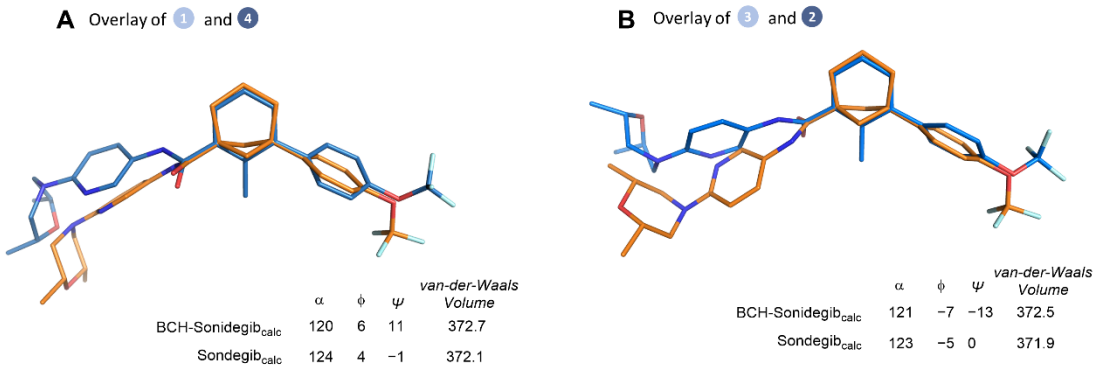


*Figure 99. **(A)** Overlay of BCHep-Sonidegib ① and Sonidegib ④, both with the carbonyl-system oriented in the front space, **(B)** Overlay of BCHep-Sonidegib ③ and Sonidegib ②, both with the carbonyl-system oriented in the hind space. For both the α, ρ, and ψ parameters as well as the van-der-Waals volume are displayed in a table.*

An overlay of the Sonidegib and BCHep-Sonidegib geometries is shown in Figure 99. The effect of the 10° deviation in ψ propagates into further regions of the molecule,

showing the most significant structural deviations of the terminal morpholine unit. Interestingly, the RDKit[149] calculated van-der-Waals volume of each pair is nearly the same, indicating similar overall steric demand of the BCHep-bioisostere.

In collaboration with Dr Tryfon Zarganes-Tzitzikas of the Prof. Brennan group, BCHep-Sonidegib, Sonidegib (commercial sample), BCHep-URB597 and URB597 (commercial sample) were tested for aqueous solubility, microsomal stability in mouse and human livers, cell permeability and cytochrome inhibition assays at WuXi AppTec (HongKong) Limited.

Table 6 shows the obtained results for BCHep-Sonidegib and Sonidegib and Table 7 for BCHep-URB597 and URB597. The computed clog(P) and the topological surface area (TPSA) are very similar for both pairs. Interestingly, these predicted values would mean that BCHep-units do not change the hydrophilicity as much as might have been anticipated, at least in these compounds. Somewhat to our dismay, the solubilities of all four compounds were too low to be measured. Therefore, no conclusion can be drawn if the BCHep unit increases solubility compared to the parent arene. This has to be either verified on other drug examples for which aqueous solubilities are measurable, or a salt-formulation of the herein tested drugs has to be prepared to increase solubility, as reported in the literature for Sonidegib diphosphate.[152-153] More meaningful results were obtained for the mouse liver microsomal (MLM) and human liver microsomal (HLM) stability assays. The BCHep analogues showed higher stability, meaning a longer half-life $T_{1/2}$ or lower clearance rate Cl_i.

Table 6. Obtained molecular properties and ADME properties for Sonidegib and BCHep-Sonidegib. Molecular weight, clog(P) and the topological surface area (TPSA) were computed with ChemAxon 22.9.

	Sonidegib	**BCHep-Sonidegib**
Molecular weight [Da]	485.51	489.56
clog(P)	6.75	6.22
Topological surface area (TPSA) [$Å^2$]	63.69	63.69
Aqueous solubility [µg/mL] / [µM]	< 0.759 / < 1.59	< 0.756 / < 1.56
Mouse liver microsomal (MLM) stability Cl_i [µL/min/mg protein] / $T_{1/2}$ [min]	26 / 53	19 / 75
Human liver microsomal (HLM) stability Cl_i [µL/min/mg protein] / $T_{1/2}$ [min]	20 / 70	18 / 76
Caco-2, AB/BA P_{app} [10^{-6} cm s^{-1}]	0.6 / 0.7	3.7 / 2.7
Caco-2, efflux ratio (ER)	1.1	0.7
CYP1A2 inhibition , IC_{50} [µM]	> 50	> 50
CYP2C9 inhibition , IC_{50} [µM]	4.2	18.5
CYP1A19 inhibition , IC_{50} [µM]	> 50	13.9
CYP2D6 inhibition , IC_{50} [µM]	> 50	> 50
CYP3A4 inhibition , IC_{50} [µM]	> 50	> 50

Especially BCHep-Sonidegib shows substantial higher cell-permeability (Caco-2) compared to the parent drug sample. For BCHep-URB597 cell permeability is maintained. Similarly, the CYP inhibition tests show improved values for the BCHep-analogues compared to the parent arenes, except for CYP1A19 for BCHep-Sonidegib.

BCHep-URB597 especially is 7- and 3-fold weaker in inhibition against CYP1A2 and CYP2C9 enzymes.

Table 7. Obtained molecular properties and ADME properties for URB597 and BCHep-URB597. Molecular weight, clog(P), and (TPSA) were computed with ChemAxon 22.9.

	URB597	**BCHep-URB597**
Molecular weight [Da]	338.41	356.47
clog(P)	3.76	3.74
Topological surface area (TPSA) [$Å^2$]	81.41	81.41
Aqueous solubility [µg/mL] / [µM]	< 0.529 / < 1.56	< 0.557 / < 1.56
Mouse liver microsomal (MLM) stability Cl_i [µL/min/mg protein] / $T_{1/2}$ [min]	180 / 8	77 / 18
Human liver microsomal (HLM) stability Cl_i [µL/min/mg protein] / $T_{1/2}$ [min]	54 / 26	17 / 80
Caco-2, AB/BA P_{app} [10^{-6} cm s^{-1}]	18.7 / 11.1	15.3 / 24.4
Caco-2, efflux ratio (ER)	0.6	1.6
CYP1A2 inhibition , IC_{50} [µM]	6.51	46.9
CYP2C9 inhibition , IC_{50} [µM]	5.7	16.9
CYP1A19 inhibition , IC_{50} [µM]	11.7	21.2
CYP2D6 inhibition , IC_{50} [µM]	> 50	> 50
CYP3A4 inhibition , IC_{50} [µM]	> 50	> 50

3.5. Conclusion

This chapter describes how BCHep iodides, derived from TCHep (Chapter 2), can be used in diversification and the synthesis of 'real-world' examples in which an isosteric BCHep unit replaces a *meta*-substituted arene system.

Despite many trials, it was shown that lithiation of BCHep iodides is not a reliable strategy for deriving BCHep-acyl systems. Unfavoured thermodynamics, namely the lack of a driving force towards the sterically congested BCHep-lithium, was proposed as a reason. Iron-catalysed Kumada cross coupling, developed by our group for iodo BCP-systems, proved to be successful and reliable on iodo BCHeps. Further, metalation *via* Rieke zinc was discovered as an interesting new avenue to functionalised BCHeps, however this still needs further work to be brought into use by improving subsequent reactivity. Using a pivalic ester iodomethyl reagent, in combination with the successfully employed Kumada-cross coupling of aryl Grignard reagents onto the pivalic BCHep iodide, was a successful strategy to synthesise the drug analogues BCHep-Sonidegib and BCHep-URB597.

Both bioisosteric drug geometries were analysed computationally, and their ADME properties evaluated experimentally. The two examples BCHep-Sonidegib and BCHep-URB597 show how BCHep-units retain structural integrity and, more importantly, increase metabolic stability — one of the key benefits of the bioisosteric paradigm for cage hydrocarbons. Needless to say, to verify the BCHep unit as a reliable bioisosteric replacement, more BCHep / parent drug pairs have to be synthesised and probed on their ADME properties. Assays testing the specific activity against e.g. cancer, need to show that BCHep-replacements maintain biological activity. For this, the *meta*-substituted benzene is not allowed to form, forming specific interactions with the target enzyme *in vivo*, contributing to the activity (Section 1.3.2). In an ideal scenario, drug candidates to

trial the BCHep unit would be selected with this requirement in mind. However, often structure-activity relationships and the mode of action of the drug are not known, thus making this an unattainable goal. For that, a bigger test set of BCHep-drug samples have to be prepared and tested, giving statistically significant claims (and decreasing that of unlucky outliers) on the bioisosteric ability of BCHep units.

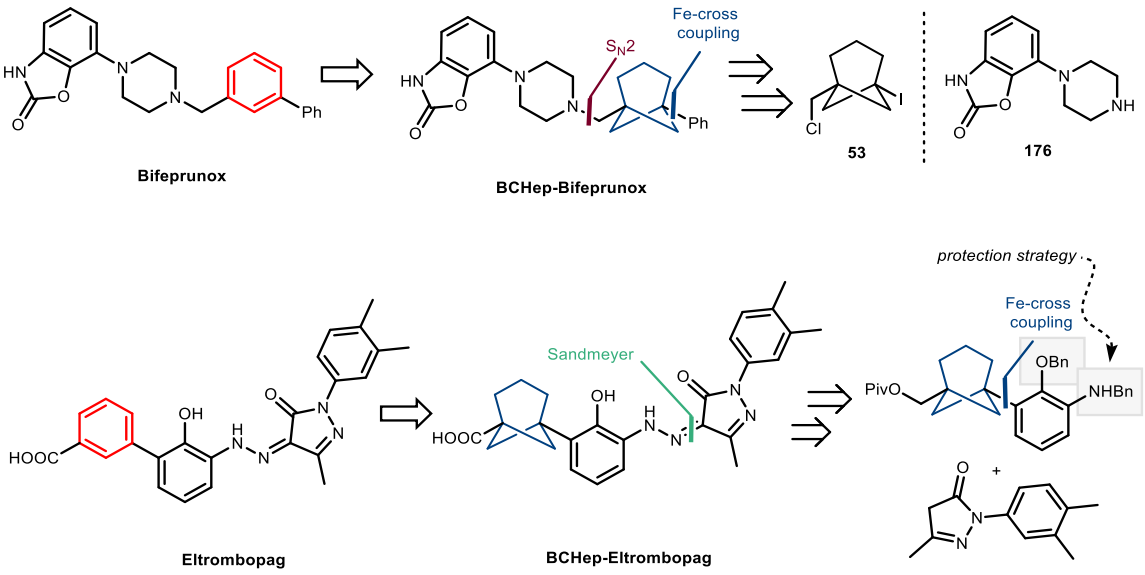


Figure 100. Bioisosteric replacement and retrosynthetic analysis of the synthesis BCHep-Bifeprunox and BCHep-Eltrombopag.

Two further examples of Category B could be synthesised: antipsychotic BCHep-Bifeprunox[154] and BCHep-Eltrombobag,[155] a treatment for thrombocytopenia. The precursor **53** of BCHep-Bifeprunox was already prepared in Section 2.3.1; a final S_N2 reaction could with amine **176** would furnish the target structure, although potential steric problems could of course arise in this step. Preliminary experiments showed difficulties in the synthesis of **176**. BCHep-Eltrombobag could be synthesised like BCHep-URB597 using a benzyl-protected aminophenol in the Kumada-cross coupling, and a late stage Sandmeyer-type reaction which is precedented in the literature.[156]

4.

Conclusion and further work

Since the seminal work of Stepan et al. showed how bicyclo[1.1.1]pentanes can be employed as bioisosteres for *para*-substituted benzene rings, increasing aqueous solubility and metabolic stability, the molecule [1.1.1]propellane (TCP) gained momentum in medicinal and synthetic chemistry. Numerous works have appeared, establishing TCP as a mature 'strain-releasing' reagent in the synthesis of BCP units. With recent advances in synthetic methodology, incorporating BCP units is now in principle possible for any larger pharmaceutical molecules in a bioisosteric fashion.

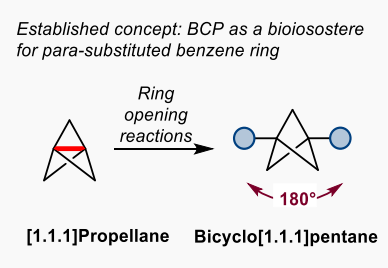


Figure 101. The established strain-release reagent TCP.

Although not only motivated by this success of TCP, [3.1.1]propellane (TCHep) was envisioned to act similarly. Chapter 2 presents a much-improved synthesis of TCHep which is scalable and practical, conveniently deriving TCHep in 5 steps from commercially available starting materials with only one chromatographic and one distillative purification. Further, Chapter 2 explores the reactivity of TCHep, finding that especially photoredox methodology published for TCP translates well onto TCHep. Other

methods, especially addition to nucleophiles, under numerous conditions, did not proceed with TCHep. Nonetheless, it was possible to show a diverse scope of different structures containing the BCHep unit derived from various methodologies. A propellane was used in a physiological environment to label cysteine-containing peptides for the first time — albeit rearranged products, and not the expected BCHep, were obtained.

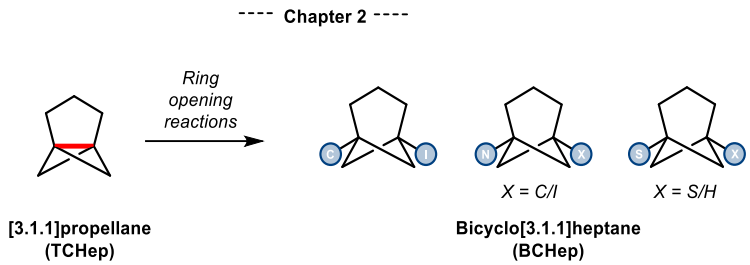


Figure 102. Chapter 2 explored the reactivity of TCHep (TCHep) to afford bicyclo[3.1.1]heptane (BCHep) units.

Chapter 2 rationalises the observed similarities and differences in reactivity between TCHep and TCP. Although many questions remain, one of the main reasons for reactivity difference has to be traced back to the missing fused, third cyclopropane unit (present in TCP), which limits delocalisation effects, especially in anionic methodology. Further, the enhanced stabilisation of BCHep bridgehead radicals, compared to BCP bridgehead radicals, has to be acknowledged because as this has proven important in BCHep radical chemistry, and likely the avoidance of staffane byproducts.

Chapter 3 explores methods to derivatise the BCHep iodides prepared in Chapter 2. A halogen-lithium exchange strategy turned out to be unreliable. Advances were made in using Rieke zinc, which quantitatively inserts into BCHep iodides, but subsequent reactvity behaviour has yet to be optimised. Only an iron-catalysed Kumada cross-coupling was versatile enough to make the synthesis of the two-drug analogues BCHep-

Sonidegib and BCHep-URB597 possible. Both analogues were tested on ADME properties fulfilling the hope of higher metabolic stability.

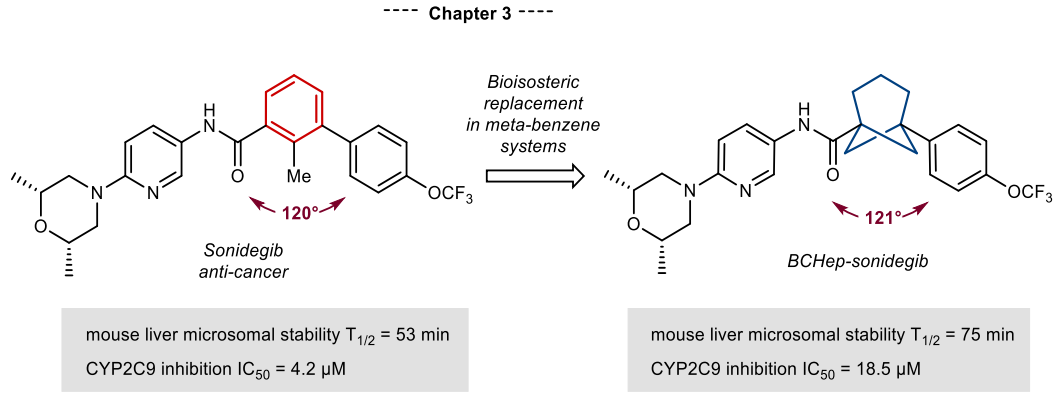


Figure 103. Chapter 3 realised bioisosteric example BCHep-Sonidegib synthetically achieved and tested on ADME properties.

This thesis presented work which has made the first steps of elevating the TCHep/BCHep-unit into the toolbox of medicinal chemistry by offering a scalable and practical synthesis of TCHep and a panoply of reactivity reaching otherwise hard-to-obtain BCHep units. It is hoped for wide use in drug-discovery programs side by side with TCP as equal partners in conquering new chemical space.

To apply BCHep as a bioisostere in drug design, novel reaction modes of BCHep must yet be developed. Two different possibilities are evident and promising. Firstly, if the trapping step of benzaldehyde can be improved in yield (Figure 90), drug analogues from Category A (e.g. BCHep-Ketoprofen and BCHep-URB597) should become accessible. Even though a preliminary condition screen did not deliver much improvement in yields, this Rieke activation pathway might be the most promising one so far.

Secondly, moving away from BCHep iodides, novel activation modes of the bridgehead position of bicyclic systems have been proposed. Hartwig and co-workers reported a [Ir]-catalysed borylation of the bridgehead C–H bond in BCPs and BCHex, which could

potentially be used for testing other cross-coupling conditions on BCHep-H systems (Figure 104A).[42] MacMillan and co-workers' coupling was shown to be successful in undergoing installing azarenes on TCHep; a recently publication by Pan and co-workers[157] expands this work by replacing the azarenes with terminal alkynes (Figure 104B). If the same reaction can be translated to TCHep, it would afford bridgehead-substituted alkynyl BCHeps which can further be easily derivatised as exemplified by Pan and co-workers, accessing drugs from Category C.[157]

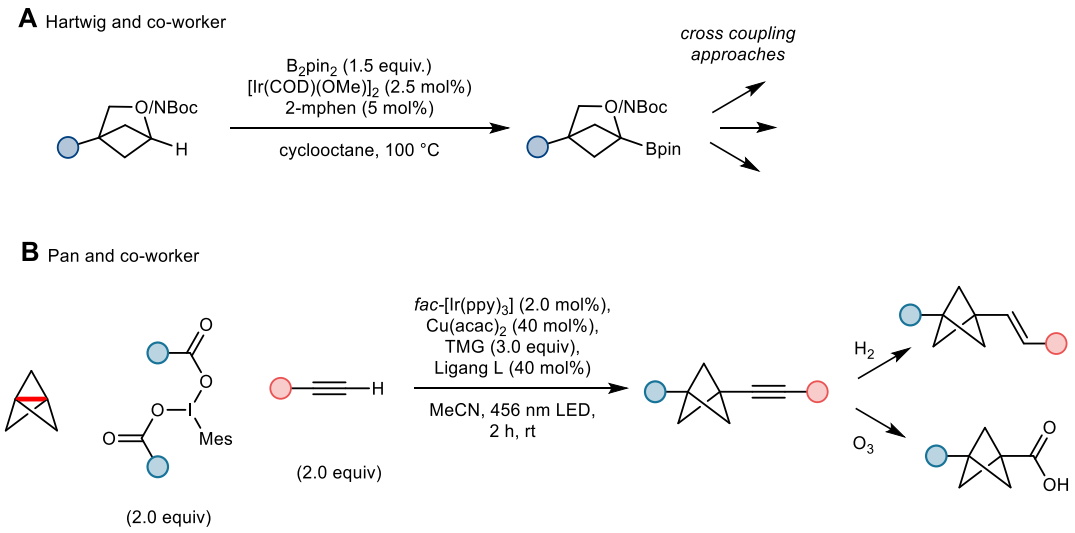


Figure 104. Recently published work being of potential interest for TCHep. Ligang L is 4,4-dimethoxy-2,2-bipyridine.

Considering the BCHep unit itself, the most radical approach might be to avoid TCHep at all and build up the BCHep core *via* the route explored by Gassman et al. (Figure 22). Indeed, a Part II project in our group by Benjamin Whitaker dealt with this approach, improving the synthesis of **36** and differentiating and selectively functionalising each bridgehead carboxylate.[158] For example, using redox-active ester **177**, a Minisci-like C–H functionalisation of azarenes was achieved while retaining an ester functionality on the other side of the BCHep (Figure 105). This complements the Kumada-cross coupling of BCHep iodides by employing more electron-deficient coupling partners or aromatics

which do not readily undergo the formation of Grignard reagents. It was also shown that **178** undergoes successful Curtius rearrangement. Although **178** was not yet successfully employed in classical carbonyl chemistry, e.g. Friedel-Craft acylations or DIBAL-H reduction, it can be imagined that further exploration can open up new entry vectors into the BCHep drug space unachieved by TCHep, e.g. making the synthesis of the drugs BCHep-LT-2300559 or BCH-Zaleplon possible.

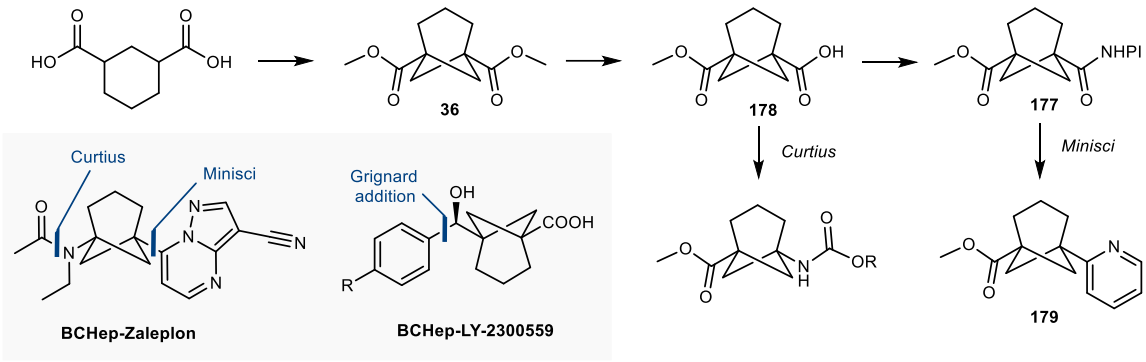


Figure 105. Use of BCHep diesters as building blocks to derive BCHep units.

Leaving bioisosteric space, TCHep might offer unique reactivity in the field of material sciences beyond our group's expertise. Specifically, TCP can be used to prepare BCP 'rods' *via* polymerisation, the so-called [*n*]staffanes (Figure 106). [*n*]Staffanes were shown to have a five times higher Young's modulus than diamond,[159] and have also been explored as liquid crystals.[160] Similar investigations of TCHep may unleash the same exotic material properties as TCP, although no linear rods are expected, rather helical secondary structures of a [*n*]-BCHep-staffane. In short, TCHep undoubtedly remains a strained molecule with unreleased potential.

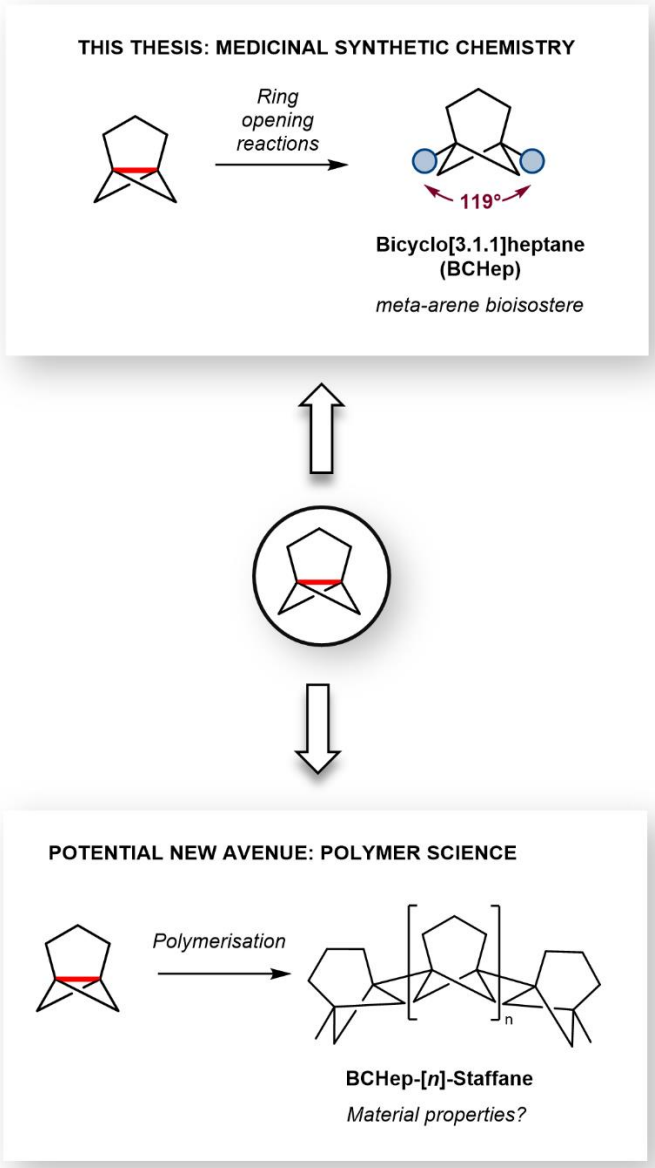


Figure 106. Potential new avenues of research for TCHep.

5.

Supporting information

5.1. General Experimental Considerations

NMR Spectroscopy

^{1}H, ^{13}C and ^{19}F NMR spectra were recorded on Bruker AVIIIHD 400 (nanobay) or Bruker AVIIIHD 500 spectrometers using TOPSPIN software, with the deuterated solvent acting as the internal deuterium lock. ^{1}H NMR spectra were recorded at 400 or 500 MHz, ^{13}C NMR spectra were recorded at 101 or 126 MHz with ^{1}H decoupling, and ^{19}F NMR spectra were recorded at 376 or 470 MHz. Assignments were determined either on the basis of unambiguous chemical shift / coupling patterns, or from 2D COSY, HMBC, and / or HSQC experiments. Peak multiplicities are defined as: s = singlet, d = doublet, t = triplet, q = quartet, quin. = quintet, dd = doublet of doublet, dt= doublet of triplet, m = multiplet, br. = broad, app. = apparent; coupling constants (J) are reported to the nearest 0.1 Hz.

NMR experiments on the labelled ACV tripeptide were recorded using a Bruker AVIII HD 700 equipped with a TCI H/C/N He CryoProbe at the respective frequency. Samples for NMR were prepared in 5 mm tubes and recorded at 298 K. Chemical shifts (δ) are reported in parts per million (ppm) and referenced to the respective H_2O resonance (δ_H = 4.79 ppm). NMR spectra were processed with 3 Hz Lorentzian line broadening using MestReNova 14.1 (MestReLabs, Spain; www.mestrelab.com) and TopSpin 3.6.1 (Bruker, Germany; www.bruker.com).

Infrared Spectroscopy

Infrared spectra were recorded on a Bruker Tensor 27 FT-IR spectrometer with the sample being prepared as a thin film on a diamond ATR module. Absorption maxima (ν_{max}) are quoted in wavenumbers (cm^{-1}).

Mass Spectrometry

Low resolution mass spectra were recorded on a Micromass LCT Premier Open Access using electrospray ionisation (ESI). Accurate mass (HRMS) data was determined under conditions of ESI, EI and CI on a Bruker MicroTOF. High resolution values are calculated to 4 decimal places from the molecular formula, and all values are within a tolerance of 5 ppm.

Samples for LC-MS analysis of reactions involving the ACV tripeptide (see Chapter 13) were prepared by dilution of the reaction mixture to 20 μM. LC-MS analysis was conducted using a Xevo G2-XS mass spectrometer to confirm labelling efficiency of the ACV tripeptide. The peptide solutions were injected to a ACE Equivalence 3 C18 column (2.1 x 50 mm).

Melting Points

Melting points were obtained using a Gallenkamp melting point apparatus and are uncorrected.

Reagents, solvents and techniques

All reagents were used directly as supplied. Solvents were either used as commercially supplied, or purified by standard techniques. Anhydrous Et_2O, CH_2Cl_2, 1,4-dioxane, tetrahydrofuran, dimethylformamide and toluene were obtained from solvent dispenser units having been passed through an activated alumina column under argon. Unless otherwise stated, non-aqueous reactions were performed using heat gun-dried glassware under a N_2 atmosphere. Reactions were monitored by thin layer chromatography on pre-coated aluminium-backed plates (Merck Kieselgel 60 with fluorescent indicator UV254). Spots were visualised by quenching of UV fluorescence or by staining with potassium permanganate, phosphomolybdic acid (PMA) stain or vanillin, and retention factors are reported with the solvent system in parentheses. Flash column chromatography was performed on silica gel obtained from Merck (Silica gel Si 60, 0.04-0.063 mm) under a positive pressure of nitrogen, using the stated solvent system.

X-ray Crystallography

Low temperature single crystal X-ray diffraction data were collected for **83**, **175**, **89**, **56** and **72** using Oxford Diffraction (Rigaku) SuperNova diffractometers at 150 K. These data were reduced using CrysAlisPro, solved using SuperFlip66 and the structures were refined using CRYSTALS. Further details about the refinements are documented in the CIF and Chapter 9.

Photochemical set-ups

Under optimised conditions, reactions on <0.15 mmol scale were irradiated with the specified LED lamp in an Evoluchem™ PhotoRedOx box (Figure 107, left). Reactions performed on ≥0.15 mmol scale were irradiated directly with the specified LED lamp from a distance of 5 cm with fan cooling (Figure 107, right).



Fig. 107. Photochemical (LED) set-ups.

5.2. General Procedures

General procedure 1: ATRA with BEt_3 [161]

Under air, a solution of alkyl iodide (1.0 equiv.) in [3.1.1]propellane (1.1 to 1.5 equiv. of a solution in *n*-Bu_2O) was cooled to 0 °C and Et_3B (10 mol%, 1.0 M in hexane) was added *via* syringe (needle tip in the solution). The mixture was stirred until the reaction reached completion as monitored by thin layer chromatography. The reaction mixture was then concentrated and the residue purified by column chromatography.

General procedure 2: Photoredox-catalysed ATRA [45]

To a flame dried, screw-capped vial equipped with a stirrer bar was added *fac*-$Ir(ppy)_3$ (2.5 mol%), alkyl or aryl halide (1.0 equiv.), *t*-BuCN (0.1 M) and [3.1.1]propellane (1.1 to 2.0 equiv. of a solution in *n*-Bu_2O). The vial was placed under nitrogen, and the solution was degassed *via* a modified freeze-pump-thaw cycle (vacuum was only applied while the reaction mixture was frozen due to TCH volatility). The stirred mixture was irradiated with blue LEDs (Kessil PR160 456 nm) with fan cooling for the indicated time. The reaction mixture was concentrated, and the residue was purified by column chromatography.

General procedure 3: Addition of thiols

To a solution of thiol (1.1 equiv.) in anhydrous diethyl ether was added [3.1.1]propellane (1.0 equiv., of a solution in *n*-Bu_2O) dropwise. The mixture was stirred for 1 h then the mixture was diluted with diethyl ether, washed with 1 M aqueous NaOH solution (3 ×).

The organic layer was dried over Na_2SO_4, filtered and concentrated *in vacuo*. The obtained crude product was either purified by column chromatography or trituration.

General procedure 4: Generation of iodomesitylene biscarboxylic acid [106]

A round-bottomed flask was equipped with iodomesitylene diacetate (1.0 equiv.), carboxylic acid (2.1 equiv.) and toluene (0.05 M). The toluene was removed on a rotary evaporator at 50 °C over 10 min. This was repeated another 4 times. Residual toluene was removed under high vacuum at 50 °C. The final product was >90% pure and used without further purification.

General procedure 5: Ir/Cu catalysed additions to [3.1.1]propellane [52]

To a flame dried, screw-capped vial equipped with a stirrer bar was added *fac*-$Ir(ppy)_3$ (2.0 mol%), amine starting material (1.0 equiv.), iodomesitylene biscarboxylic acid (2.0 equiv.), $Cu(acac)_2$ or $Cu(TMHD)_2$ (0.60 equiv), 2-*tert*-butyl-1,1,3,3-tetramethylguanidine BTMG (3.0 equiv.) and anhydrous 1,4-dioxane (0.03 M). The solution was sparged with Ar for 10 min then [3.1.1]propellane (1.5 equiv. of a solution in *n*-Bu_2O) was added, the vial capped and sealed with parafilm. The mixture was stirred and irradiated with blue LEDs (Kessil PR160 456 nm) with fan cooling for 16 h. The reaction mixture was diluted with EtOAc and washed with 30% aqueous ammonia solution. The phases were separated, and the aqueous phase was extracted with EtOAc (3 ×). The combined organics were dried (Na_2SO_4), filtered and concentrated *in vacuo.* The residue was purified by column chromatography.

General procedure 6: Disulfide addition [162]

To a flame dried, screw-capped vial was added disulfide (3.0 equiv.) and [3.1.1]propellane (1.0 equiv. of a solution in *n*-Bu_2O). The mixture was irritated with a LED lamp (HepatoChem Evoluchem HCK1012-01-011 365 nm) with fan cooling for 20 h. The solvents were removed *in vacuo* and the resulting residue was purified by column chromatography.

General procedure 7: Formation of aryl Grignard reagents

Mg turnings (88 mg, 3.6 mmol, 1.2 equiv.) were added to a flask which then was heated (heat gun) under vacuum for 2 min with stirring. To the cooled (room temperature) flask was added anhydrous THF (2.5 mL) and I_2 (one crystal) before dropwise addition of the aryl bromide (3.0 mmol, 1.0 equiv.). The mixture was heated at reflux for 2 h (unless specified otherwise). The concentration of the resulting Grignard reagent was determined *via* iodometric titration and directly used in *General procedure 9*.

General procedure 8: Formation of Turbo Grignard reagents

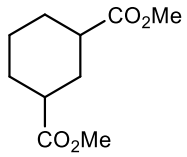
Mg turnings (146 mg, 6.0 mmol, 2.0 equiv.) and LiCl (150 mg, 3.6 mmol, 1.2 equiv.) were added to a flask that was then heated (heat gun) under vacuum for 2 min with stirring. To the cooled (room temperature) flask was added anhydrous THF (2.5 mL) and DIBAL-H (0.15 mL, 1 M in hexanes, 0.15 mmol, 0.05 equiv.). After 5 min at room temperature, the halide (3.0 mmol, 1.0 equiv.) was added at the specified temperature and stirred for the specified time. The concentration of the resulting Turbo Grignard reagent was determined *via* iodometric titration.

General procedure 9: Iron-catalysed Kumada coupling [46]

To a flame-dried vial was added BCHep iodide (1.0 equiv.) and $Fe(acac)_3$ (20 mol%). The vial was then evacuated and refilled with N_2 (g) three times. To this was added anhydrous THF (0.2 mL) and TMEDA (40 mol%), and the resulting mixture was stirred for 5 min. The Grignard reagent (1.6 equiv.) was then added *via* syringe pump over approximately 1 h at room temperature. The reaction was stirred for a further 1 h, then quenched by addition of aqueous NH_4Cl (2 mL, saturated). The layers were separated, and the aqueous layer was extracted with Et_2O (3 × 1 mL). The combined organic layers were washed with brine, dried over $MgSO_4$, filtered and concentrated *in vacuo*. The crude product was purified by column chromatography.

5.3. Synthesis of [3.1.1]Propellane (Section 2.2)

Dimethyl cyclohexane-1,3-dicarboxylate, 24



Cyclohexane-1,3-dicarboxylic acid (5.00 g, 29.0 mmol, 1.00 equiv.) was dissolved in MeOH (50 mL). The mixture was refluxed for 16 h. The reaction mixture was cooled down to room temperature and the solvent was removed *in vacuo*. The resulting residue was diluted with EtOAc (70 mL). This organic layer was washed with cold $NaHCO_3$ (sat., aq., 30 mL) and brine (2 x 20 mL). Subsequently, the organic layer was dried over Na_2SO_4, filtered and concentrated *in vacuo* to affords the crude product. Purification by column chromatography (SiO_2, pentane / EtOAc, 1:4) gave **24** (5.02 g, 25 mmol, 86%) as a yellow oil.

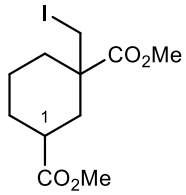
R_f 0.59 (EtOAc / pentane, 1:4).

Note: Diastereomeric mixture of cyclohexane-1,3-dicarboxylic acid was used as starting material reflecting above reporting peaks.

^{1}H NMR (400 MHz, $CDCl_3$) δ_H 3.66 (s, 6H, O*Me*), 3.65 (s, 6H, O*Me*), 2.67 (p, *J* = 5.9 Hz, 2H), 2.31 (tt, *J* = 11.9, 3.5 Hz, 2H), 2.21 (m, 1H), 2.00-1.92 (m, 4H), 1.91-1.84 (m, 1H), 1.79-1.64 (m, 4H), 1.60-1.47 (m, 3H), 1.40-1.29 (m, 3H).

^{13}C NMR (101 MHz, $CDCl_3$) δ_C 175.8, 175.6, 51.8, 51.7, 42.6, 39.1, 31.1, 29.4, 28.4, 28.0, 24.9, 22.1.

Dimethyl 1-(iodomethyl)cyclohexane-1,3-dicarboxylate, 25



Prepared according to a literature procedure.[163]

Diisopropylamine (2.74 mL, 19.5 mmol, 1.30 equiv.) and THF (15 mL) were added to a flame-dried two-necked round-bottomed flask. The mixture was cooled down to –78 °C. *n*-BuLi (7.50 mL of 2.4 M solution in THF, 18.0 mmol, 1.20 equiv.) was added dropwise *via syringe.* Subsequently, the solution was warmed up to 0 °C for 5 min and then re-cooled to –67 °C. DMPU (4.80 mL, 39.5 mmol, 2.64 equiv.) was added dropwise. Afterwards, a THF-solution (7.8 mL) of dimethyl cyclohexane-1,3-dicarboxylate **24** (3.00 g, 15.0 mmol, 1.00 equiv.) was added dropwise. The reaction mixture was stirred for 1 h at –67 °C. Then, CH_2I_2 (4.41 mL, 20.3 mmol, 1.36 equiv.) in a THF-solution (10 mL) was added dropwise. The reaction was warmed up to room temperature and stirred for 17 h. The reaction was cooled with an ice bath to 0 °C and quenched with NH_4Cl (sat., aq., 10 mL). The aqueous layer was extracted with Et_2O (3 x 50 mL). The combined organic layers were washed with brine (50 mL), dried over Na_2SO_4, filtered and concentrated *in vacuo.* Purification by column chromatography (SiO_2, pentane / EtOAc, gradient 8:1 to 8:2) gave **25** (3.16 g, 9.31 mmol, 62%) as a yellow oil.

R_f 0.50 (Pentane / EtOAc, 8:1).

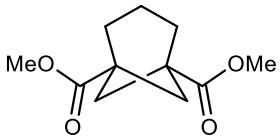
^{1}H NMR (400 MHz, $CDCl_3$) δ_H 3.74 (s, 1H, H1), 3.67 (m, 6H, O*Me*), 2.60-2.46 (m, 2H), 2.08-1.94 (m, 4H), 1.96-1.86 (m, 2H), 1.86-1.78 (m, 2H).

^{13}C NMR (101 MHz, $CDCl_3$) δ_C 175.7, 173.5, 52.4, 51.9, 47.8, 40.4, 36.5, 34.7, 28.6, 23.2, 16.2.

Note: Above data reflects only one diastereomer.

Analytical data matches that previously reported.[163]

Dimethyl bicyclo[3.1.1]heptane-1,5-dicarboxylate, 36



Prepared according to a literature procedure.[163]

Dimethyl 1-(iodomethyl)cyclohexane-1,3-dicarboxylate **25** (3.16 g, 9.31 mmol, 1.00 equiv.), distilled DMPU (5.0 ml, 41.3 mmol, 4.44 equiv.) and anhydrous THF (21 mL) were added to a flame-dried two-necked flask. The mixture was cooled down to −78 °C. Diisopropylamine (1.74 mL, 12.4 mmol, 1.33 equiv.) and anhydrous THF (14 mL) were added to a second flame-dried round-bottomed flask. This round-bottomed flask was cooled down to −78 °C. Subsequently, *n*-BuLi solution (4.31 mL, 2.4 M in THF, 10.3 mmol, 1.11 equiv.) was added to the second round-bottomed flask dropwise to produce LDA. The mixture was warmed up to 0 °C for 5 min and re-cooled to −78 °C. This freshly prepared solution (of LDA) was transferred dropwise to the first two-necked flask *via* syringe at –78 °C. This mixture was stirred for 30 min at –78 °C, warmed up to room temperature and stirred for further 20 h at room temperature. Finally, the mixture was cooled to 0 °C and quenched with NH_4Cl (aq., sat., 15 mL). The organics were removed *in vacuo.* The residue was extracted with hexane (3 x 40 mL). The combined organic

layers were washed with water, dried over $MgSO_4$, filtered and concentrated *in vacuo*. The residue was dissolved in DCM and filtered through an Alumina pad. Purification by column chromatography (SiO_2, pentane / EtOAc, 4:1) gave **36** (1.09 g, 5.14 mmol, 55%) as a colorless oil.

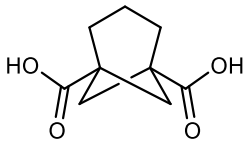
R_f 0.50 (Pentane / EtOAc, (8:1)).

^{1}H NMR (400 MHz, $CDCl_3$) δ_H 3.67 (s, 6H, O*Me*), 2.55-2.46 (m, 2H), 2.03-1.94 (m, 4H), 1.96-1.86 (m, 2H), 1.86-1.77 (m, 2H).

^{13}C NMR (101 MHz, $CDCl_3$) δ_C 175.6, 51.9, 42.4, 38.1, 29.6, 16.1.

Analytical data matches that previously reported.[163]

Bicyclo[3.1.1]heptane-1,5-dicarboxylic acid, 37



Prepared according to a literature procedure.[163]

Dimethyl bicyclo[3.1.1]heptane-1,5-dicarboxylate **36** (1.09 g, 5.14 mmol, 1.00 equiv.) was dissolved in ^{i}PrOH (4.6 mL) and THF (14 mL). LiOH · H_2O (1.20 g, 28.7 mmol, 5.58 equiv.) was dissolved in H_2O (14 mL) and added to the above solution. The solution was heated for 20 h at 65 °C. Finally, the organic solvents were mostly removed *in vacuo*. The aqueous residue was cooled to 0 °C and HCl (7.2 mL, 6 M) was added. The resulting solid was filtered, rinsed with ice-cold water, and dried *in vacuo*. The aqueous phase was extracted with EtOAc (2 x 10 mL). The organic layer was dried over $MgSO_4$, filtered and

concentrated *in vacuo.* The resulting solid was triturated with small amounts of diethyl ether. The combined solids yield the pure product **37** (410 mg, 2.23 mmol, 43%) as a pale-yellow solid.

^{1}H NMR (400 MHz, $(CD_3)_2CO$) δ_H 2.46 (dt, *J* = 7.4, 3.7 Hz, 2H), 2.04-1.88 (m, 6H), 1.85-1.77 (m, 2H).

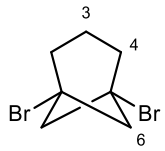
Note: -COOH not visible.

^{13}C NMR (101 MHz, $CDCl_3$) δ_C 176.4, 42.7, 38.6, 16.6.

Note: one quaternary carbon not visible.

Analytical data matches that previously reported.[163]

1,5-Dibromobicyclo[3.1.1]heptane, 38



Prepared according to a literature procedure.[96]

Bicyclo[3.1.1]heptane-1,5-dicarboxylic acid **37** (250 mg, 1.36 mmol, 1.00 equiv.), thionyl chloride (0.88 mL, 11.5 mmol, 8.46 equiv.), DMF (1 drop) and anhydrous DCM (0.6 mL) were heated under reflux for 90 min. The mixture was cooled to room temperature and the organics removed *in vacuo*. The residue was taken up in halothane $C_2HBrClF_3$ (0.2 mL). This solution is added to a refluxing suspension of 2-thioxopyridin-1(2*H*)-olate (515 mg, 3.05 mmol, 2.24 equiv) and 4-dimethylaminopyridine DMAD (11 mg, 0.090 mmol, 7 mol%) in Halothane (1.6 mL) while being irridated with a natural light lamp (300 W). The reaction mixture was refluxed for 1 h. The reaction mixture was

cooled down to room temperature, washed with H_2O (2 x 1 mL), washed with concentrated HCl (2 x 0.5 mL), then dried (Na_2SO_4), filtered and concentrated *in vacuo* to afford the crude product. Purification by column chromatography (SiO_2, pentane) gave **38** (137 mg, 0.54 mmol, 40 %) as a yellow oil.

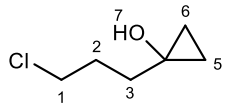
R_f 0.50 (100% pentane).

^{1}H NMR (400 MHz, $CDCl_3$) δ_H 3.23-2.94 (m, 2H, H6), 2.86-2.69 (m, 2H, H6), 2.31-2.17 (4H, m, H4), 2.10-1.91 (2H, m, H3).

^{13}C NMR (101 MHz, $CDCl_3$) δ_C 55.8, 52.0, 38.0, 20.6.

Analytical data matches that previously reported.[97]

1-(3-Chloropropyl)cyclopropan-1-ol, 40



Prepared according to a literature procedure.[97]

A solution of ethyl 4-chlorobutanoate **39** (5.60 mL, 40.0 mmol, 1.0 equiv.), and Ti(O*i*-Pr)$_4$ (1.20 mL, 4.0 mmol, 0.10 equiv.) in dry diethyl ether (60 mL) was cooled to 0 °C and a solution of EtMgBr (33.3 mL, 3.0 M in Et_2O, 100 mmol, 2.5 equiv.) was added dropwise over 90 min. The mixture was stirred for further 30 min at 0 °C, then the mixture was *slowly* quenched by dropwise addition of 10% aqueous H_2SO_4 (50 mL). The organic layer was washed sequentially with H_2O (70 mL), $NaHCO_3$ (sat., aq., 70 mL), brine (70 mL), then dried (Na_2SO_4), filtered and concentrated *in vacuo* to afford **40** (4.73 g, 35.1

mmol, 88%) as a colourless oil which was used without further purification.

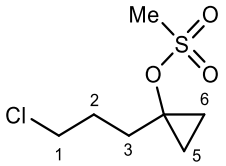
R_f 0.38 (pentane / EtOAc, 7:3).

^{1}H NMR (400 MHz, $CDCl_3$) δ_H 3.65 (t, *J* = 6.5 Hz, 2H, H1), 2.11-1.97 (m, 2H, H2), 1.74 (br, 1H, H7), 1.85-1.65 (m, 2H, H3), 0.87-0.67 (m, 2H, H5, H6), 0.59-0.44 (m, 2H, H5, H6).

^{13}C NMR (101 MHz, $CDCl_3$) δ_C 55.2, 45.2, 35.6, 29.3, 13.8.

Analytical data matches that previously reported.[97]

1-(2-Chloroethyl)cyclopropyl methanesulfonate, 41



Prepared according to a literature procedure.[97]

A solution of **40** (4.73 g, 35.1 mmol, 1.00 equiv.), and triethylamine (7.05 mL, 50.7 mmol, 1.44 equiv.) in anhydrous CH_2Cl_2 (60 mL) was cooled to 0 °C and methanesulfonyl chloride (3.08 mL, 40.0 mmol, 1.14 equiv.) was added dropwise over 30 min. The mixture was stirred for further 30 min at 0 °C, then quenched with water (30 mL). The layers were separated, and the organic layer was washed sequentially with H_2O (60 mL), 10% H_2SO_4 (aq., 50 mL), $NaHCO_3$ (sat., aq., 50 mL) and brine (50 mL), then dried (Na_2SO_4), filtered and concentrated *in vacuo* to afford **41** (7.20 g, 33.9 mmol, 96%) as a pale-yellow oil which was used without further purification.

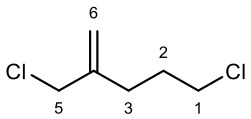
R_f 0.38 (pentane / EtOAc, 7:3).

^{1}H NMR (400 MHz, $CDCl_3$) δ_H 3.64 (t, *J* = 6.1 Hz, 2H, H1), 2.99 (s, 3H, *Me*), 2.16-1.96 (m, 4H, H2, H3), 1.34-1.24 (m, 2H, H5, H6), 0.84-0.73 (m, 2H, H5, H6).

^{13}C NMR (101 MHz, $CDCl_3$) δ_C 66.0, 44.6, 40.0, 33.4, 28.9, 12.0.

Analytical data matches that previously reported.[97]

5-Chloro-2-(chloromethyl)pent-1-ene, 42



To solution of **41** (7.20 g, 33.8 mmol, 1.0 equiv.) in anhydrous CH_2Cl_2 (60 mL) was slowly added $TiCl_4$ (5.72 mL, 52.4 mmol, 1.55 equiv.) at room temperature over 20 min. The mixture was stirred at room temperature for 3 h, then slowly quenched with H_2O (60 mL) at 0 °C with vigorous stirring. The layers were separated, and the organic layer was washed sequentially with H_2O (2 × 70 mL), $NaHCO_3$ (sat., aq., 70 mL), brine (70 mL), then dried ($MgSO_4$), filtered and concentrated *in vacuo* (300 mbar, 30 °C) to afford **42** (4.46 g, 29.1 mmol, 86%) as a clear pale-yellow liquid.

Note: Product is volatile under reduced pressure (isolated with residual solvent) and was taken forward without further purification.

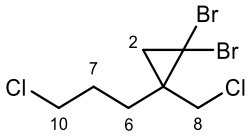
R_f 0.70 (100% Pentane).

^{1}H NMR (400 MHz, $CDCl_3$) δ_H 5.19 (app. q, *J* = 0.9 Hz, 1H, H6), 5.01 (app. q, *J* = 1.3 Hz, 1H, H6), 4.05 (d, *J* = 1.0 Hz, 2H, H5), 3.57 (t, *J* = 6.5 Hz, 2H, H1), 2.39-2.31 (m, 2H, H3), 2.06-1.87 (m, 2H, H2).

^{13}C NMR (101 MHz, $CDCl_3$) δ_C 143.8, 115.5, 48.3, 44.3, 30.43, 30.36.

Analytical data matches that previously reported.[164]

1,1-Dibromo-2-(chloromethyl)-2-(3-chloropropyl)cyclopropane, 27



Adapted from a literature procedure.[100]

To a vigorously stirred (1000 rpm) solution of **42** (4.46 g, 29.1 mmol, 1.00 equiv.), $CHBr_3$ (20.4 mL, 233 mmol, 8.00 equiv.), dibenzo-18-crown-6 (524 mg, 1.47 mmol, 0.05 equiv.) and pinacol (137 mg, 1.15 mmol, 0.04 equiv.) in CH_2Cl_2 (37 mL) was added 50% NaOH solution (22 mL) dropwise over 20 min at 50 °C. The resulting mixture was stirred for 5 h at 50 °C, then cooled to room temperature and diluted with *n*-pentane (100 mL) and distilled water (100 mL). The resulting suspension was filtered through a pad of celite and washed with additional *n*-pentane (100 mL). Additional distilled water (100 mL) was added to the filtrate. The layers were separated and the organic layer was washed with brine (150 mL), then dried (Na_2SO_4), filtered and concentrated *in vacuo*. The crude product was purified by column chromatography (⌀ 4 cm, 40 g SiO_2, gradient 100%

pentane to 95:5 pentane / EtOAc) to afford **27** (7.50 g, 23.1 mmol, 79%) as a colorless oil.

R_f 0.40 (100% Pentane). [*Phosphomolybdic acid PMA* stain]

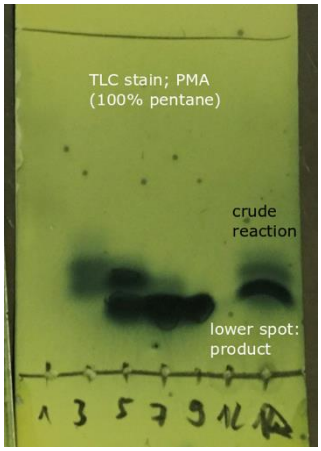
^{1}H NMR (400 MHz, $CDCl_3$) δ_H 3.77 (s, 2H, H8), 3.65-3.53 (m, 2H, H10), 2.14-1.86 (m, 4H), 1.75-1.59 (m, 2H).

^{13}C NMR (101 MHz, $CDCl_3$) δ_C 49.5, 44.5, 34.9, 34.1, 33.3, 31.4, 29.2.

Analytical data matches that previously reported.[165]

Note:

The picture depicted on the right-hand side of a thin layer chromatography plate exemplifies a typical column purification. It shows the crucial separation between two closely eluting fractions of which the latter one is the product.



[3.1.1]Propellane, 10



To a cooled (–78 °C) solution of **27** (9.74 g, 30.0 mmol, 1.0 equiv.) in anhydrous Et_2O (160 mL) was slowly added phenyllithium (31.8 mL, 60.4 mmol, 2.01 equiv., 1.9 M in *n*-Bu_2O). The resulting mixture was stirred at −78 °C for 15 min then warmed to room temperature and stirred for 7 h. The mixture was then distilled using a rotary evaporator (25 °C water bath temperature) equipped with a dry-ice cold finger condenser, with the receiving flask immersed in a dry ice / acetone bath. The Et_2O fraction was removed by slowly decreasing the applied pressure to 150 mbar. This fraction was then discarded. The remaining solution was distilled by slowly reducing the applied pressure to <10 mbar to afford a solution of [3.1.1]propellane **10** in *n*-Bu_2O which was stored under an inert atmosphere at −20 °C. The yield was determined by ^{1}H NMR spectroscopy using 1,2-dichloroethane as an internal standard (see below). The concentration of the [3.1.1]propellane solution ranged between 0.25 M and 0.50 M, with yields of 43-61%.

Note: The resulting TCH stock solution contains bromobenzene which does not influence the reactions presented herein.

^{1}H NMR (400 MHz, d_6-C_6D_6 with *n*-Bu_2O) δ_H 2.27 (p, J = 6.8 Hz, 2H), 2.23 (t, J = 1.5 Hz, 2H).

Note: Other signals of [3.1.1]propellane overlap with *n*-Bu_2O peaks

^{13}C NMR (126 MHz, d_6-C_6D_6 with *n*-Bu_2O) δ_C 52.9, 42.4, 31.0, 24.6.

Analytical data matches that previously reported.[165]

Determination of the concentration of [3.1.1]propellane (n-Bu_2O/Et_2O solution)

An aliquot of the [3.1.1]propellane solution (0.20 mL), d_6-benzene (0.30 mL) and 1,2-dichloroethane (50 µL, 0.63 mmol) was added to an NMR tube. A ^{1}H NMR spectrum was measured immediately and the 1,2-dichloroethane peak (3.06 ppm, 4 × H) was integrated against the [3.1.1]propellane peaks between 2.35 and 2.20 ppm (4 × H):

$$\frac{\text{Integral(Propellane)}}{\text{Integral(DCE)}} = \frac{\text{n(Propellane)}}{\text{n(DCE)}} \quad \text{(V)}$$

Therefore, the concentration of [3.1.1]propellane can be calculated as follows:

$$\text{n(Propellane)} = \frac{\text{n(Propellane)}}{\text{V(Propellane)}} = \frac{\frac{\text{Integral(Propellane)}}{\text{Integral(DCE)}} \cdot \text{n(DCE)}}{\text{V(Propellane)}} \quad \text{(VI)}$$

This is illustrated in an example calculation: Using the above amounts of 1,2-dichloroethane, [3.1.1]propellane solution volume and an integral ratio of 0.17 we can calculate the concentrate as follows:

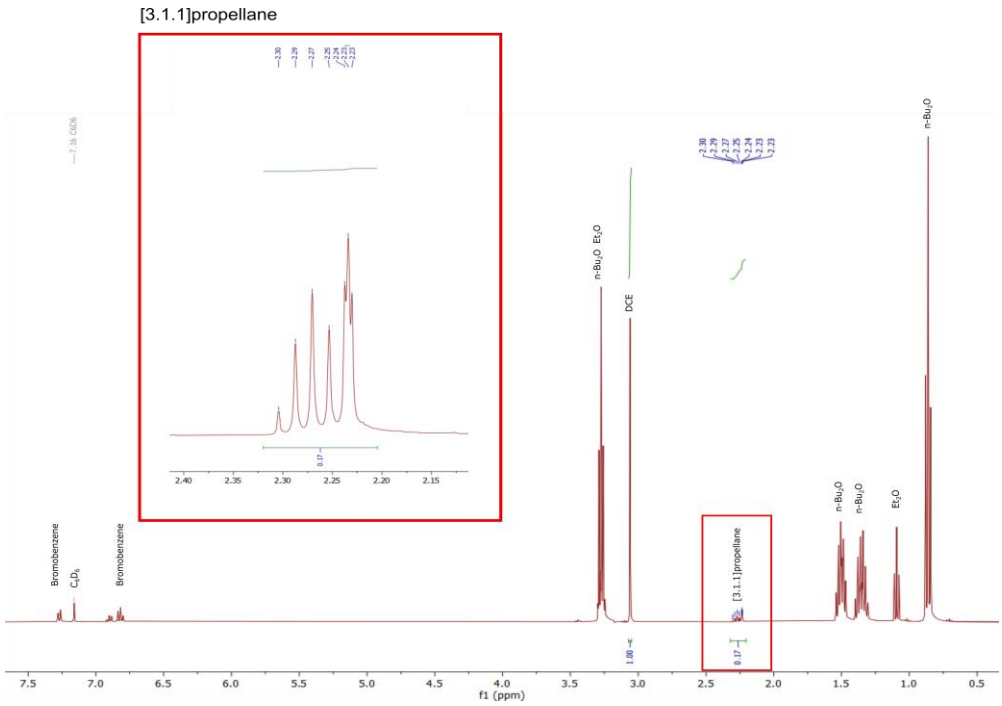
$$\text{n(Propellane)} = \frac{\text{n(Propellane)}}{\text{V(Propellane)}} = \frac{\frac{\text{Integral(Propellane)}}{\text{Integral(DCE)}} \cdot \text{n(DCE)}}{\text{V(Propellane)}} \quad \text{(VII)}$$

$$= \frac{0.17 \cdot 0.63\ \text{mmol}}{0.2\ \text{mL}}$$

$$= 0.54\ \text{M}$$

Spectral data of tricyclo[3.1.1.0^{1,5}]heptane- ([3.1.1]propellane-, TCH-) solution, 10

(400 MHz, C_6D_6 with *n*-Bu_2O)



Depending on the exact concentration of TCH inside the NMR tube the reported pentet and triplet are better separated.

A ^{13}C NMR (126 MHz, C_6D_6 with *n*-Bu_2O) spectra was recorded showing the reported signals[25,26] of [3.1.1]propellane. Further it contains the signals of co-isolated bromobenzene and the ethereal solvent (*n*-Bu_2O and Et_2O).

The relevant area from 0 to 100 ppm is depicted below and only the signals of [3.1.1]propellane are picked (*n*-Bu_2O and Et_2O solvent peaks annotated).

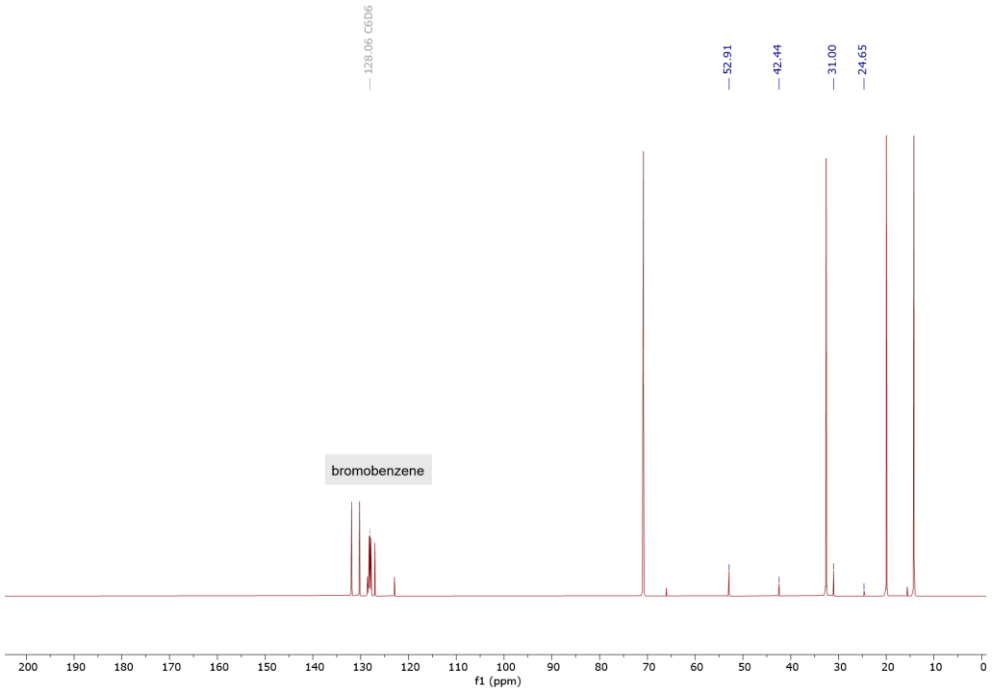


Figure 108

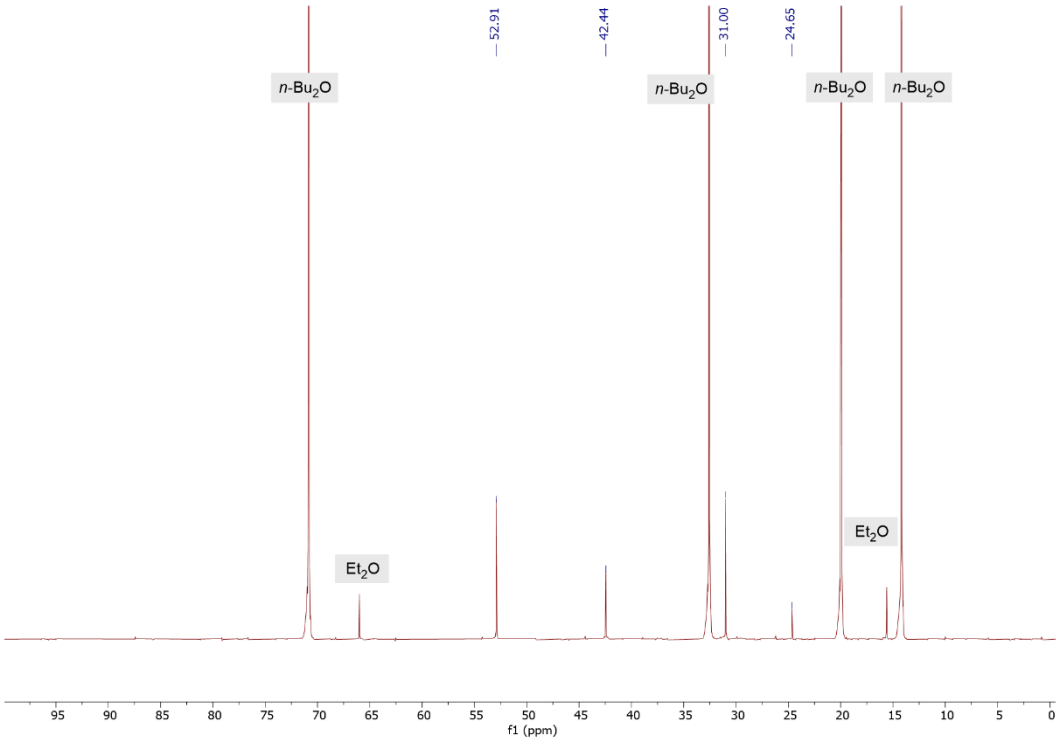
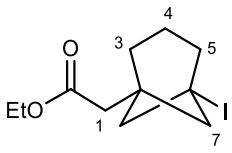


Figure 109

5.4. Characterisation of the BCHep compounds (Section 2.3)

Ethyl 2-(5-iodobicyclo[3.1.1]heptan-1-yl)acetate, 43



BEt_3-initiated

Ethyl 2-iodoacetate (11 µL, 0.09 mmol, 1.0 equiv.), [3.1.1]propellane solution (0.18 mL, 0.55 M in *n*-Bu_2O, 0.10 mmol, 1.1 equiv.) and BEt_3 (9.0 µL, 1.0 M in hexane, 10 mol%) were submitted to *General procedure 1* at 0 °C for 15 min. Purification by column chromatography (SiO_2, pentane / EtOAc, 99:1 to 95:5) gave **43** (20 mg, 0.064 mmol, 73%) as a yellow oil.

Photoredox-catalysed

Ethyl 2-iodoacetate (12 µL, 0.10 mmol, 1.0 equiv.), [3.1.1]propellane solution (0.68 mL, 0.22 M in *n*-Bu_2O, 0.15 mmol, 1.5 equiv.), *fac*-$Ir(ppy)_3$ (1.6 mg, 2.5 µmol, 2.5 mol%) and *t*-BuCN (1.0 mL) were submitted to *General procedure 2* for 1 h at room temperature. Purification by column chromatography (SiO_2, pentane / EtOAc, 99:1 to 95:5) gave **43** (29 mg, 0.094 mmol, 94%) as a yellow oil.

R_f 0.39 (pentane / EtOAc, 9:1).

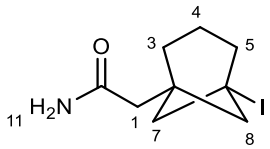
^{1}H NMR (400 MHz, $CDCl_3$) δ_H 4.11 (q, *J* = 7.1 Hz, 2H, CH_3-C*H*$_2$-O), 2.60-2.56 (m, 2H, H7), 2.56-2.48 (m, 2H, H3/H5), 2.43-2.37 (m, 2H, H7), 2.37 (s, 2H, H1), 1.90-1.83 (m, 2H, H4), 1.74-1.66 (m, 2H, H3/H5), 1.25 (t, *J* = 7.1 Hz, 3H, C*H*$_3$-CH_2-O).

^{13}C NMR (101 MHz, $CDCl_3$) δ_C 171.1, 60.4, 51.9, 45.3, 44.0, 43.1, 33.7, 31.3, 19.7, 14.5.

IR (thin film, ν_{max} / cm^{-1}) 2864, 2949, 1732, 1451, 1189, 1035, 818.

HRMS (ESI^+) calc. for $C_{11}H_{18}IO_2$ $[M+H]^+$ 309.0346, found 309.0347.

2-(5-Iodobicyclo[3.1.1]heptan-1-yl)acetamide, 44



BEt_3-initiated

2-Iodoacetamide (28 mL, 0.15 mmol, 1.0 equiv.), [3.1.1]propellane solution (0.46 mL, 0.42 M in *n*-Bu_2O, 0.20 mmol, 1.3 equiv.), MeOH (0.1 mL) and BEt_3 (15 µL, 1.0 M in hexane, 10 mol%) were submitted to *General procedure 1* at room temperature for 3 h. Purification by column chromatography (SiO_2, EtOAc) gave **44** (29 mg, 0.104 mmol, 69%) as a yellow oil.

Photoredox-catalysed

2-Iodoacetamide (19 mg, 0.10 mmol, 1.0 equiv.), [3.1.1]propellane solution (0.68 mL, 0.22 M in *n*-Bu_2O, 0.15 mmol, 1.5 equiv.), *fac*-$Ir(ppy)_3$ (1.6 mg, 3.8 µmol, 2.5 mol%) and *t*-BuCN (1.0 mL) were submitted to *General procedure 2* for 2 h at room temperature. Purification by column chromatography (SiO_2, EtOAc) gave **44** (21 mg, 0.075 mmol, 75%) as a brown oil.

R_f 0.22 (pentane / EtOAc, 1:1).

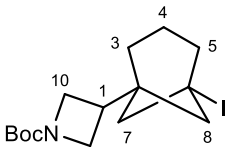
^{1}H NMR (400 MHz, $CDCl_3$) δ_H 5.59-5.28 (m, 2H, H11), 2.65-2.56 (m, 2H, H7), 2.57-2.49 (m, 2H, H3/H5), 2.47-2.40 (m, 2H, H7), 2.30 (s, 2H, H1), 1.94-1.82 (m, 2H, H4), 1.78-1.69 (m, 2H, H3/H5).

^{13}C NMR (101 MHz, $CDCl_3$) δ_C 172.6, 52.0, 46.7, 44.2, 43.1, 33.6, 31.3, 19.7.

IR (thin film, ν_{max} / cm^{-1}) 3334, 3189, 2945, 1659, 1450, 1401, 1148, 757.

HRMS (ESI^+) calc. for $C_9H_{15}INO$ $[M+H]^+$ 280.0193, found 280.0195.

Tert-butyl 3-(5-iodobicyclo[3.1.1]heptan-1-yl)azetidine-1-carboxylate, 45



BEt$_3$-catalysed

Tert-butyl 3-iodoazetidine-1-carboxylate (57 mg, 0.20 mmol, 1.0 equiv.), [3.1.1]propellane solution (0.55 mL, 0.55 M in *n*-Bu_2O, 0.30 mmol, 1.5 equiv.), and BEt_3 (20 µL, 0.020 mmol, 1.0 M in hexane, 10 mol%) were submitted to *General procedure 1* at room temperature for 5 h. Purification by column chromatography (SiO_2, pentane / EtOAc, gradient 99:1 to 90:10) gave **45** (52 mg, 0.138 mmol, 69%) as a pale-yellow oil.

Photoredox-catalysed

Tert-butyl 3-iodoazetidine-1-carboxylate (28 mg, 0.10 mmol, 1.0 equiv.), [3.1.1]propellane solution (0.68 mL, 0.22 M in *n*-Bu_2O, 0.15 mmol, 1.5 equiv.), *fac*-$Ir(ppy)_3$ (1.6 mg, 2.5 µmol, 2.5 mol%) and *t*-BuCN (1.0 mL) were submitted to *General*

procedure 2 for 3 h at room temperature. Purification by column chromatography (SiO_2, pentane / EtOAc, gradient 99:1 to 90:10) gave **45** (22 mg, 0.058 mmol, 58%) as a pale-yellow oil.

R_f 0.19 (pentane / EtOAc, 9:1).

^{1}H NMR (400 MHz, $CDCl_3$) δ_H 3.85 (t, *J* = 8.8 Hz, 2H, H10), 3.64 (dd, *J* = 8.8, 5.7 Hz, 2H, H10), 2.65-2.50 (m, 4H, H7, H3/5), 2.42-2.35 (m, 1H, H1), 2.28-2.18 (m, 2H, H7), 1.97-1.83 (pent, *J* = 7.3 Hz, 2H, H4), 1.55 (t, *J* = 7.3 Hz, 2H, H3/5), 1.44 (s, 9H, *tBu*).

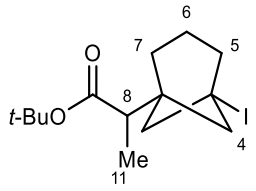
^{13}C NMR (101 MHz, $CDCl_3$) δ_C 156.4, 79.6, 49.9, 47.35, 47.27, 43.7, 35.1, 33.4, 29.8, 28.6, 19.6.

IR (thin film, ν_{max} / cm^{-1}) 2949, 2881, 1701, 1394, 1162, 816.

HRMS (ESI^+) calc. for $C_{15}H_{25}INO_2$ $[M+Na]^+$ 400.0744, found 400.0745.

m.p. 73-76 °C.

Tert-butyl 2-(5-iodobicyclo[3.1.1]heptan-1-yl)propanoate, 46



Tert-butyl 2-iodopropanoate (38 mg, 0.15 mmol, 1.0 equiv.), [3.1.1]propellane solution (0.64 mL, 0.35 M in *n*-Bu_2O, 0.23 mmol, 1.5 equiv.), *fac*-$Ir(ppy)_3$ (2.5 mg, 3.8 µmol, 2.5 mol%) and *t*-BuCN (1.5 mL) were submitted to *General procedure II* at room

temperature for 3 h. Purification by column chromatography (SiO_2, toluene) gave **46** (38 mg, 0.108 mmol, 73%) as a yellow oil.

Millimole scale

Tert-butyl 2-iodopropanoate (390 mg, 1.5 mmol, 1.0 equiv.), [3.1.1]propellane solution (5.57 mL, 0.35 M in *n*-Bu_2O, 1.95 mmol, 1.3 equiv.), *fac*-$Ir(ppy)_3$ (9.8 mg, 15 µmol, 1.0 mol%) and *t*-BuCN (7.5 mL) were submitted to *General procedure II* at room temperature for 3 h. Purification by column chromatography (SiO_2, toluene) gave **46** (394 mg, 1.13 mmol, 75%) as a yellow oil.

R_f 0.50 (toluene / EtOAc, 9:1).

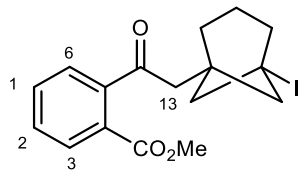
^{1}H NMR (400 MHz, $CDCl_3$) δ_H 2.68 (d, *J* = 9.5 Hz, 1H), 2.56-2.44 (m, 3H), 2.45-2.29 (m, 3H), 1.84 (app. dt, *J* = 14.1, 7.2 Hz, 2H), 1.72-1.59 (m, 1H), 1.61-1.49 (m, 1H), 1.43 (d, *J* = 1.0 Hz, 9H, *t*-Bu), 0.94 (d, *J* = 7.2 Hz, 3H, H11).

^{13}C NMR (101 MHz, $CDCl_3$) δ_C 173.2, 80.5, 51.9, 51.1, 49.2, 48.1, 43.5, 33.9, 28.3, 27.7, 19.8, 11.5.

IR (thin film, ν_{max} / cm^{-1}) 2975, 1724, 1367, 1157, 1140, 813.

HRMS (APCI, ESI, EI) Not found.

Methyl 2-(2-(5-iodobicyclo[3.1.1]heptan-1-yl)acetyl)benzoate, 47



Methyl 2-(2-iodoacetyl)benzoate **155** (46 mg, 0.15 mmol, 1.0 equiv.), [3.1.1]propellane solution (0.64 mL, 0.35 M in *n*-Bu_2O, 0.23 mmol, 1.5 equiv.), *t*-BuCN (1.5 mL) and *fac*-$Ir(ppy)_3$ (2.5 mg, 3.8 µmol, 2.5 mol%) were submitted to *General procedure 2* for 3 h at room temperature. Purification by column chromatography (SiO_2, pentane / EtOAc, 9:1) afforded **47** (42 mg, 0.106 mmol, 71%) as a yellow oil.

Millimole scale

Methyl 2-(2-iodoacetyl)benzoate **155** (304 mg, 1.0 mmol, 1.0 equiv.), [3.1.1]propellane solution (4.80 mL, 0.27 M in *n*-Bu_2O, 1.30 mmol, 1.3 equiv.), *t*-BuCN (10.0 mL) and *fac*-$Ir(ppy)_3$ (6.5 mg, 10 µmol, 1 mol%) were submitted to *General procedure 2* for 3 h at room temperature. Purification by column chromatography (SiO_2, pentane / EtOAc, 9:1) afforded **155** (226 mg, 0.567 mmol, 57%) as a yellow oil.

R_f 0.26 (pentane / EtOAc, 9:1).

^{1}H NMR (400 MHz, $CDCl_3$) δ_H 7.87 (ddd, *J* = 7.6, 1.4, 0.5 Hz, 1H, *Ar*H), 7.55 (app. td, *J* = 7.6, 1.4 Hz, 1H, *Ar*H), 7.49 (app. td, *J* = 7.6, 1.4 Hz, 1H, *Ar*H), 7.30 (ddd, *J* = 7.6, 1.4, 0.5 Hz, 1H, *Ar*H), 3.89 (s, 3H, *Me*), 2.94 (s, 2H, H13), 2.61-2.45 (m, 6H), 1.97-1.85 (m, 2H), 1.87-1.79 (m, 2H).

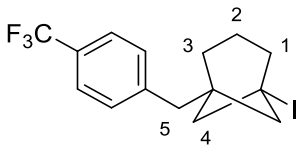
^{13}C NMR (101 MHz, $CDCl_3$) δ_C 203.2, 167.2, 143.4, 132.3, 130.13, 130.05, 128.7, 126.5, 52.7, 52.5, 44.2, 43.3, 35.0, 31.2, 19.9.

Note: One ^{13}C peak overlapping at 52.7 ppm.

IR (thin film, ν_{max} / cm^{-1}) 2948, 2864, 1721, 1280, 1133, 1088, 816, 760, 708.

HRMS (ESI^+) calc. for $C_{17}H_{20}IO_3$ $[M+H]^+$ 399.0451, found 399.0452.

1-Iodo-5-(4-(trifluoromethyl)benzyl)bicyclo[3.1.1]heptane, 48



1-(Iodomethyl)-4-(trifluoromethyl)benzene (43 mg, 0.15 mmol, 1.0 equiv.), [3.1.1]propellane solution (0.64 mL, 0.28 M in *n*-Bu_2O, 0.18 mmol, 1.20 equiv.), *t*-BuCN (1.5 mL) and *fac*-$Ir(ppy)_3$ (2.5 mg, 3.8 µmol, 2.5 mol%) were submitted to *General procedure 2* for 4 h at room temperature. Purification by column chromatography (SiO_2, 100% pentane) afforded **48** (35 mg, 0.092 mmol, 62%) as yellow oil.

R_f 0.71 (100% pentane).

^{1}H NMR (400 MHz, $CDCl_3$) δ_H 7.53 (d, 2H, *J* = 8.0 Hz, Ar*H*), 7.16 (d, 2H, *J* = 8.0 Hz, Ar*H*), 2.75 (s, 2H, H5), 2.61-2.52 (m, 2H, H4), 2.54-2.48 (m, 2H, H1/H3), 2.38-2.27 (m, 2H, H4), 1.89-1.73 (m, 2H, H2), 1.60-1.47 (m, 2H, H1/H3).

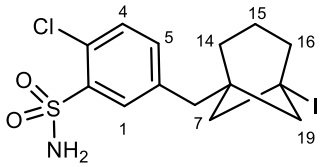
^{13}C NMR (101 MHz, $CDCl_3$) δ_C 142.3, 129.8, 128.8 (q, ^2J = 31.8 Hz), 125.3 (q, ^1J = 3.9 Hz), 123.4 (q, ^3J = 271.8 Hz), 51.8, 47.1, 47.0, 43.5, 34.3, 31.0, 19.7.

^{19}F NMR (377 MHz, $CDCl_3$) δ_F –62.34.

IR (thin film, ν_{max} / cm^{-1}) 2980, 2863, 2361, 1322, 1161, 1120, 1103, 1066, 1019, 820.

HRMS (APCI, ESI, EI) Not found.

Methyl 6-fluoro-2-(5-iodobicyclo[3.1.1]heptan-1-yl)-3-methylquinoline-4-carboxylate, 49



2-Chloro-5-(iodomethyl)benzenesulfonamide (50 mg, 0.15 mmol, 1.0 equiv.), [3.1.1]propellane solution (0.56 mL, 0.40 M in *n*-Bu_2O, 0.23 mmol, 1.5 equiv.), *fac*-$Ir(ppy)_3$ (2.5 mg, 3.8 µmol, 2.5 mol%) and *t*-BuCN (1.5 mL) were submitted to *General procedure 2* at room temperature for 3 h. Purification by column chromatography (SiO_2, DCM / MeOH, 95:5) gave **49** (42 mg, 0.100 mmol, 66%) as a pale yellow oil.

R_f 0.33 (pentane / EtOAc, 1:1).

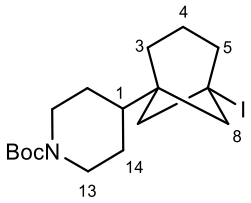
^{1}H NMR (400 MHz, CD_3OD) δ_H 7.81 (d, *J* = 2.2 Hz, 1H, H1), 7.51 (d, *J* = 8.1 Hz, 1H, H4), 7.32 (dd, *J* = 8.1, 2.2 Hz, 1H, H5), 2.79 (s, 2H, H7), 2.56 (dd, *J* = 6.9, 2.8 Hz, 2H, H19), 2.50 (t, *J* = 7.1 Hz, 2H, H14/16), 2.32 (dd, *J* = 6.9, 2.8 Hz, 2H, H19), 1.84 (p, *J* = 7.1 Hz, 2H, H15), 1.57 (t, *J* = 7.3 Hz, 2H, H14/16).

^{13}C NMR (101 MHz, CD_3OD) δ_C 141.7, 139.3, 135.5, 132.4, 131.2, 130.3, 52.4, 48.0, 46.8, 44.8, 34.8, 31.9, 20.5.

IR (thin film, ν_{max} / cm^{-1}) 2980, 2889, 1473, 1383, 1252, 1158, 1073, 954, 817.

HRMS (ESI^+) calc. for $C_{14}H_{18}ClINO_2S$ $[M+Na]^+$ 447.9605, found 447.9607.

Tert-butyl 4-(5-iodobicyclo[3.1.1]heptan-1-yl)piperidine-1-carboxylate, 50



Tert-butyl 4-iodopiperidine-1-carboxylate (47 mg, 0.15 mmol, 1.0 equiv.), [3.1.1]propellane solution (0.56 mL, 0.40 M in *n*-Bu_2O, 0.23 mmol, 1.5 equiv.), *fac*-$Ir(ppy)_3$ (2.5 mg, 3.8 µmol, 2.5 mol%) and *t*-BuCN (1.5 mL) were submitted to *General procedure 2* at room temperature for 3 h. Purification by column chromatography (SiO_2, pentane / EtOAc, 9:1) gave **50** (40 mg, 0.100 mmol, 66%) as a yellow oil.

Millimole scale

Tert-butyl 4-iodopiperidine-1-carboxylate (467 mg, 1.5 mmol, 1.0 equiv.), [3.1.1]propellane solution (5.6 mL, 0.35 M in *n*-Bu_2O, 1.95 mmol, 1.3 equiv.), *fac*-$Ir(ppy)_3$ (9.3 mg, 15 µmol, 1.0 mol%) and *t*-BuCN (15 mL) were submitted to *General*

procedure 2 at room temperature for 3 h. Purification by column chromatography (SiO_2, pentane / EtOAc, 9:1) gave **50** (370 mg, 0.913 mmol, 61%) as a yellow oil.

R_f 0.25 (pentane / EtOAc, 9:1).

^{1}H NMR (400 MHz, $CDCl_3$) δ_H 4.17-4.13 (m, 2H, H13), 2.63-2.48 (m, 4H, H13, H3/H5), 2.47-2.38 (m, 2H, H8), 2.33-2.26 (m, 2H, H8), 1.93-1.78 (m, 2H, H4), 1.55 (t, *J* = 7.2 Hz, 2H, H3/H5), 1.48-1.35 (m, 12H, *t-Bu*, H1, H14), 1.08 (app. qd, *J* = 12.0, 11.0, 4.2 Hz, 2H, H14).

^{13}C NMR (101 MHz, $CDCl_3$) δ_C 154.9, 79.5, 50.8, 49.6, 46.3, 44.2, 43.9, 35.2, 28.6, 27.9, 26.6, 19.9.

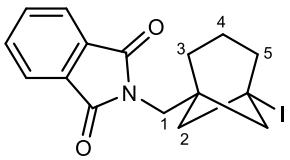
IR (thin film, ν_{max} / cm^{-1}) 2936, 2861, 1692, 1423, 1167.

HRMS (APCI, ESI, EI) Not found.

m.p. 78-81 °C.

2-((5-Iodobicyclo[3.1.1]heptan-1-yl)methyl)isoindoline-1,3-dione, 51

This compound was synthesised and characterised by Dr Jeremy Nugent.



N-(Iodomethyl)phthalimide (43 mg, 0.15 mmol, 1.0 equiv.), [3.1.1]propellane solution (0.49 mL, 0.40 M in *n*-Bu_2O, 0.20 mmol, 1.3 equiv.), *fac*-$Ir(ppy)_3$ (2.5 mg, 3.8 µmol, 2.5 mol%) and *t*-BuCN (1.5 mL) were submitted to *General procedure 2* for 3 h at room

temperature. Purification by column chromatography (SiO_2, pentane / EtOAc, 9:1) gave **51** (45 mg, 0.118 mmol, 79%) as a colourless oil.

R_f 0.49 (pentane / EtOAc, 4:1).

^{1}H NMR (400 MHz, $CDCl_3$) δ_H 7.51-7.33 (m, 2H, Ar*H*), 7.29-7.20 (m, 2H, Ar*H*), 3.13 (s, 2H, H1), 2.19-2.08 (m, 2H, H2), 2.03 (t, *J* = 7.1 Hz, 2H, H3/5), 1.84-1.75 (m, 2H, H2), 1.46-1.30 (m, 2H, H4), 1.18 (t, *J* = 7.1 Hz, 2H, H3/5).

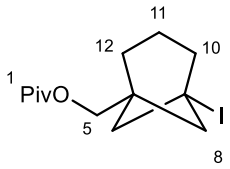
^{13}C NMR (101 MHz, $CDCl_3$) δ_C 168.7, 134.2, 132.1, 123.6, 50.1, 47.1, 45.4, 43.3, 33.1, 29.7, 19.5.

HRMS (APCI, ESI, EI): Not found.

IR (film, ν_{max}/cm^{-1}) 2938, 2861, 1715, 1392, 1353, 726.

m.p. 96-98 °C.

(5-Iodobicyclo[3.1.1]heptan-1-yl)methyl pivalate, 52



Iodomethyl pivalate **141** (36 mg, 0.15 mmol, 1.0 equiv.), [3.1.1]propellane solution (0.45 mL, 0.50 M in *n*-Bu_2O, 0.23 mmol, 1.50 equiv.), *t*-BuCN (1.5 mL) and *fac*-$Ir(ppy)_3$ (2.5 mg, 3.8 µmol, 2.5 mol%) were submitted to *General procedure 2* for 5 h at room temperature. Purification by column chromatography (SiO_2, pentane / EtOAc, gradient 100:0 to 99:1) afforded **52** (32 mg, 0.095 mmol, 64%) as a yellow oil.

Millimole scale

Iodomethyl pivalate **141** (363 mg, 1.5 mmol, 1.0 equiv.), [3.1.1]propellane solution (4.50 mL, 0.50 M in *n*-Bu_2O, 2.3 mmol, 1.50 equiv.), *t*-BuCN (10 mL) and *fac*-$Ir(ppy)_3$ (9.8 mg, 15 µmol, 1 mol%) were submitted to *General procedure 2* for 5 h at room temperature. Purification by column chromatography (SiO_2, pentane / EtOAc, gradient 100:0 to 99:1) afforded **52** (280 mg, 0.833 mmol, 56%) as a yellow oil.

R_f 0.38 (pentane / EtOAc, 95:5).

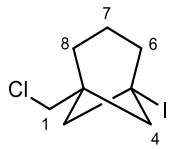
^{1}H NMR (400 MHz, $CDCl_3$) δ_H 3.85 (s, 2H, H5), 2.63-2.52 (m, 4H, H8, H12/10), 2.28-2.21 (m, 2H, H8), 1.89 (app. p, *J* = 7.2 Hz, 2H, H11), 1.65 (app. t, *J* = 7.2 Hz, 2H, H12/H10), 1.22 (s, 9H, *t*-Bu).

^{13}C NMR (101 MHz, $CDCl_3$) δ_C 178.3, 68.5, 48.7, 46.3, 43.5, 39.1, 33.1, 28.9, 27.4, 19.4.

IR (thin film, ν_{max} / cm^{-1}) 2953, 2986, 1729, 1479, 1457, 1282, 1152.

HRMS (APCI, ESI, EI) Not found.

1-(Chloromethyl)-5-iodobicyclo[3.1.1]heptane, 53



Chloroiodomethane (11.0 µL, 0.15 mmol, 1.0 equiv.), [3.1.1]propellane solution (0.45 mL, 0.50 M in *n*-Bu_2O, 0.225 mmol, 1.5 equiv.), *t*-BuCN (1.5 mL) and *fac*-$Ir(ppy)_3$ (2.5 mg, 3.8 µmol, 2.5 mol%) were submitted to *General procedure 2* for 7 h at room

temperature. Purification by column chromatography (SiO_2, pentane) afforded **53** (19 mg, 0.070 mmol, 47%) as a colourless oil.

Millimole scale

Chloroiodomethane (73.0 µL, 1.00 mmol, 1.0 equiv.), [3.1.1]propellane solution (3.00 mL, 0.50 M in *n*-Bu_2O, 1.50 mmol, 1.5 equiv.), *t*-BuCN (10 mL) and *fac*-$Ir(ppy)_3$ (6.5 mg, 10 µmol, 1 mol%) were submitted to *General procedure 2* for 7 h at room temperature. Purification by column chromatography (SiO_2, pentane) afforded **53** (172 mg, 0.636 mmol, 64%) as a colourless oil.

R_f 0.31 (100% pentane).

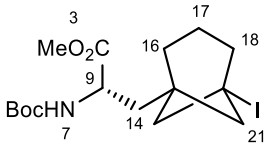
^{1}H NMR (400 MHz, $CDCl_3$) δ_H 3.42 (s, 2H, H1), 2.64-2.50 (m, 4H, H4+H8/H6), 2.37-2.26 (m, 2H, H4), 1.93-1.84 (m, 2H, H7), 1.74 (dd, *J* = 7.6, 0.7 Hz, 2H, H8/H6).

^{13}C NMR (101 MHz, $CDCl_3$) δ_C 52.1, 49.7, 47.3, 43.3, 32.0, 29.5, 19.5.

IR (thin film, ν_{max} / cm^{-1}) 2948, 2964, 1451, 1252, 1169, 955, 926, 913, 819, 729.

HRMS (APCI, ESI, EI) Not found.

Methyl (S)-2-((tert-butoxycarbonyl)amino)-3-(5-iodobicyclo[3.1.1]heptan-1-yl)propanoate, 54



Methyl *(S)*-2-((*tert*-butoxycarbonyl)amino)-3-iodopropanoate (41 mg, 0.15 mmol, 1.0 equiv.), [3.1.1]propellane solution (0.56 mL, 0.40 M in *n*-Bu_2O, 0.23 mmol, 1.5 equiv.), *fac*-$Ir(ppy)_3$ (2.5 mg, 3.8 µmol, 2.5 mol%) and *t*-BuCN (1.5 mL) were submitted to *General procedure 2* at room temperature for 3 h. Purification by column chromatography (SiO_2, pentane / EtOAc, 9:1) gave **54** (42 mg, 0.115 mmol, 76%) as a yellow oil.

R_f 0.37 (pentane / EtOAc, 8:2).

^{1}H NMR (400 MHz, $CDCl_3$) δ_H 4.84 (d, *J* = 9.2 Hz, 1H, N*H*), 4.31 (td, *J* = 9.2, 4.6 Hz, 1H, H9), 3.71 (s, 3H, O*Me*), 2.49 (m, 3H, H21, H16/18), 2.42 (m, 1H, H21), 2.41-2.29 (m, 2H, H21), 2.01-1.75 (m, 4H, H14, H17, H16/18), 1.66 (m, 2H, H14, H16/18), 1.43 (s, 9H, *t*-Bu).

^{13}C NMR (101 MHz, $CDCl_3$) δ_C 173.5, 155.2, 80.2, 52.6, 52.5, 50.8, 45.0, 43.8, 43.4, 34.5, 30.2, 28.5, 19.8.

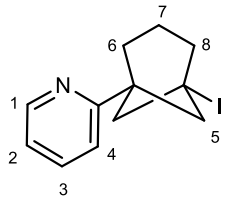
IR (thin film, ν_{max} / cm^{-1}) 3364, 2949, 1745, 1712, 1366, 1166, 1053.

HRMS (ESI^+) calc. for $C_{16}H_{27}INO_4$ $[M+Na]^+$ 446.0799, found 446.0798.

$[a]_D^{25}$ +15.5 (c = 0.7, $CHCl_3$).

2-(5-Iodobicyclo[3.1.1]heptan-1-yl)pyridine, 55

This compound was synthesised and characterised by Dr Jeremy Nugent.



2-Iodopyridine (31 mg, 0.15 mmol, 1.0 equiv.), [3.1.1]propellane solution (0.56 mL, 0.40 M in *n*-Bu_2O, 0.23 mmol, 1.5 equiv.), *fac*-$Ir(ppy)_3$ (2.5 mg, 3.8 µmol, 2.5 mol%) and *t*-BuCN (1.5 mL) were submitted to *General procedure 2* for 3 h at room temperature. Purification by column chromatography (SiO_2, pentane / EtOAc, 9:1) gave **55** (32 mg, 0.107 mmol, 71%) as a colourless oil.

R_f 0.44 (pentane / EtOAc, 4:1).

^{1}H NMR (400 MHz, $CDCl_3$) δ_H 8.52 (ddd, *J* = 4.9, 1.9, 1.0 Hz, 1H, H1), 7.61 (app. td, *J* = 7.7, 1.9 Hz, 1H, H3), 7.10 (ddd, *J* = 7.7, 4.9, 1.0 Hz, 1H, H2), 7.02 (app. dt, *J* = 7.7, 1.0 Hz, 1H, H4), 3.04-2.95 (m, 2H, H5), 2.75-2.60 (m, 4H, H5, H6/8), 2.09-1.94 (m, 4H, H7, H6/8).

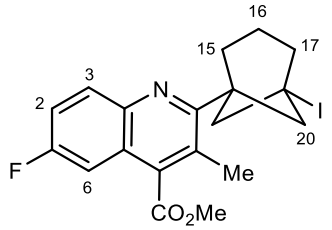
^{13}C NMR (101 MHz, $CDCl_3$) δ_C 165.2, 149.3, 136.7, 121.4, 119.3, 51.5, 51.0, 43.2, 33.2, 33.0, 19.7.

HRMS (ESI^+) calc. for $C_{12}H_{15}NI$ $[M+H]^+$ 300.0244, found 300.0243.

IR (film, ν_{max}/cm^{-1}) 3395 (br), 2936, 2862, 1589, 1472, 1431, 1214, 917, 815, 730, 750.

m.p. 44-47 °C.

Methyl 6-fluoro-2-(5-iodobiyclo[3.1.1]heptan-1-yl)-3-methylquinoline-4-carboxylate, 56



Methyl 6-fluoro-2-iodo-3-methylquinoline-4-carboxylate (34 mg, 0.10 mmol, 1.0 equiv.), [3.1.1]propellane solution (0.28 mL, 0.40 M in *n*-Bu_2O, 0.11 mmol, 1.1 equiv.), *fac*-$Ir(ppy)_3$ (1.6 mg, 2.5 µmol, 2.5 mol%) and *t*-BuCN (1.0 mL) were submitted to *General procedure 2* at room temperature for 3 h. Purification by column chromatography (SiO_2, pentane / EtOAc, 9:1) gave **56** (27 mg, 0.061 mmol, 62%) as a yellow-green solid.

The starting material Methyl 6-fluoro-2-iodo-3-methylquinoline-4-carboxylate was prepared according to a published procedure.[45]

R_f 0.25 (pentane / EtOAc, 9:1).

^{1}H NMR (400 MHz, $CDCl_3$) δ_H 8.02 (dd, *J* = 9.2, 5.5 Hz, 1H, Ar*H*), 7.42 (ddd, *J* = 9.2, 8.1, 2.7 Hz, 1H, Ar*H*), 7.25 (dd, *J* = 9.5, 2.7 Hz, 1H, Ar*H*), 4.06 (s, 3H, CO_2*Me*), 3.16-3.11 (m, 2H, H20), 2.97-2.88 (m, 2H, H20), 2.69 (app. t, *J* = 6.3 Hz, 2H, H15/H16), 2.34 (s, 3H, Ar-*Me*), 2.10-1.97 (m, 4H, H15/H16, H17).

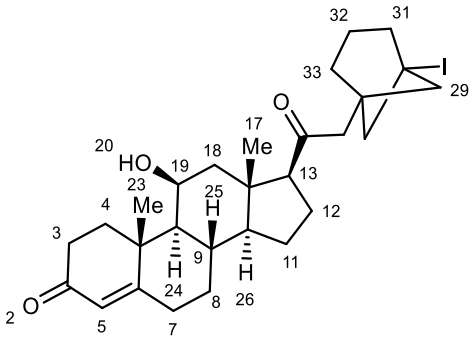
^{13}C NMR (101 MHz, $CDCl_3$) δ_C 168.3, 163.2 (d, ^3J = 3.0 Hz), 161.0 (d, ^1J = 248.2 Hz), 143.2, 139.0 (d, ^3J = 5.6 Hz), 132.1 (d, ^3J = 9.4 Hz), 125.8, 123.8 (d, ^3J = 10.1 Hz), 119.4 (d, ^2J = 25.5 Hz), 107.8 (d, ^2J = 23.4 Hz), 53.4, 52.9, 51.8, 43.2, 32.6, 31.6, 19.8, 16.5.

IR (thin film, ν_{max} / cm^{-1}) 2950, 2866, 1732, 1497, 1375, 1216, 969, 831.

HRMS (ESI$^+$) calc. for $C_{19}H_{20}FINO_2$ $[M+H]^+$ 440.0517, found 440.0512.

m.p. 128-130 °C.

(8S,9S,10R,11S,13S,14S,17S)-11-Hydroxy-17-(2-(5-iodobicyclo[3.1.1]heptan-1-yl)acetyl)-10,13-dimethyl-1,2,6,7,8,9,10,11,12,13,14,15,16,17-tetradecahydro-3H-cyclopenta[a]phenanthren-3-one, 57



(8*S*,9*S*,10*R*,11*S*,13*S*,14*S*,17*S*)-11-Hydroxy-17-(2-iodoacetyl)-10,13-dimethyl-1,2,6,7,8,9,10,11,12,13,14,15,16,17-tetradecahydro-3*H*-cyclopenta[*a*]phenanthren-3-one (29 mg, 0.063 mmol, 1.0 equiv.), [3.1.1]propellane solution (0.23 mL, 0.40 M in *n*-Bu_2O, 0.094 mmol, 1.5 equiv.), *fac*-$Ir(ppy)_3$ (1.0 mg, 1.6 µmol, 2.5 mol%) and *t*-BuCN (0.63 mL) were submitted to *General procedure 2* at room temperature for 3 h. Purification by column chromatography (SiO_2, pentane / EtOAc, 8:2) gave **57** (24 mg, 0.044 mmol, 70%) as a yellow oil.

R_f 0.40 (100% EtOAc).

^{1}H NMR (400 MHz, $CDCl_3$) δ_H 5.67 (s, 1H, H5), 4.41-4.38 (m, 1H, H20), 2.65-2.41 (m, 9H), 2.40-2.35 (m, 1H), 2.35-2.28 (m, 2H), 2.27-2.09 (m, 3H), 2.06-1.93 (m, 2H), 1.91-

1.81 (m, 3H), 1.78-1.69 (m, 2H), 1.71-1.59 (m, 4H), 1.44 (s, 3H, H17), 1.39-1.24 (m, 1H), 1.18-0.95 (m, 4H), 0.87 (s, 3H, H23).

^{13}C NMR (101 MHz, $CDCl_3$) δ_C 209.1, 199.5, 172.0, 122.6, 68.3, 63.7, 57.7, 56.5, 54.3, 52.7, 52.6, 48.6, 44.2, 43.4, 39.3, 35.2, 34.9, 34.0, 32.7, 32.2, 31.43, 31.38, 24.5, 22.7, 21.1, 19.8, 16.2.

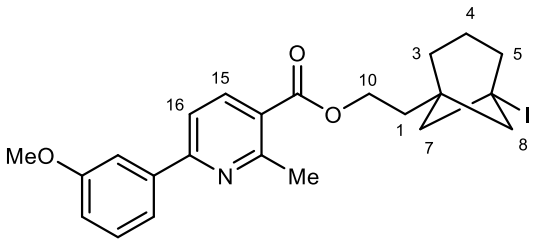
IR (thin film, ν_{max} / cm^{-1}) 3492, 2935, 2866, 2360, 1659.

HRMS (ESI^+) calc. for $C_{28}H_{40}IO_3$ $[M+H]^+$ 551.2017, found 551.2015.

$[a]_D^{25}$ +127.1 (c = 1.9, $CHCl_3$).

2-(5-Iodobicyclo[3.1.1]heptan-1-yl)ethyl 6-(3-methoxyphenyl)-2-methylnicotinate, 58

This compound was synthesised and characterised by Dr Jeremy Nugent.



2-Iodoethyl 6-(3-methoxyphenyl)-2-methylnicotinate (60 mg, 0.15 mmol, 1.0 equiv.), [3.1.1]propellane solution (0.41 mL, 0.55 M in *n*-Bu_2O, 0.23 mmol, 1.5 equiv.), *fac*-$Ir(ppy)_3$ (2.5 mg, 3.8 µmol, 2.5 mol%) and *t*-BuCN (1.5 mL) were submitted to *General procedure 2* at room temperature for 16 h. Purification by column chromatography (SiO_2, pentane / Et_2O, gradient 100:0 to 95:5) gave **58** (44 mg, 0.090 mmol, 60%) as a yellow oil.

The starting material 2-Iodoethyl 6-(3-methoxyphenyl)-2-methylnicotinate was prepared according to a known procedure.[45]

R_f 0.39 (pentane / EtOAc, 95:5).

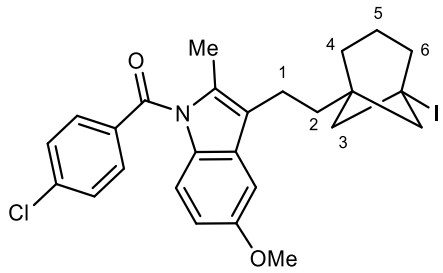
^{1}H NMR (400 MHz, $CDCl_3$) δ_H 8.22 (d, *J* = 8.2 Hz, 1H, Ar*H*), 7.78-7.55 (m, 3H, Ar*H*), 7.40 (app. t, *J* = 7.9 Hz, 1H, Ar*H*), 7.00 (ddd, *J* = 8.2, 2.6, 0.9 Hz, 1H, Ar*H*), 4.31 (t, *J* = 6.8 Hz, 2H, H10), 3.91 (s, 3H, O*Me*), 2.92 (s, 3H, *Me*), 2.60-2.51 (m, 4H, H7, H3/H5), 2.42-2.36 (m, 2H, H7), 1.93-1.86 (m, 4H, H4, H3/H5), 1.72 (t, *J* = 7.2 Hz, 2H, H1).

^{13}C NMR (101 MHz, $CDCl_3$) δ_C 166.5, 160.26, 160.25, 159.1, 139.9, 139.4, 130.0, 123.5, 119.9, 117.8, 115.9, 112.8, 62.0, 55.6, 52.2, 45.0, 43.4, 39.4, 34.3, 31.1, 25.4, 19.8.

IR (thin film, ν_{max} / cm^{-1}) 2949, 1719, 1584, 1458, 1263, 1083, 776.

HRMS (ESI^+) calc. for $C_{23}H_{27}INO_3$ $[M+H]^+$ 492.1030, found 492.1030.

(4-Chlorophenyl)(3-(2-(5-iodobicyclo[3.1.1]heptan-1-yl)ethyl)-5-methoxy-2-methyl-1H-indol-1-yl)methanone, 59



(4-Chlorophenyl)(3-(2-iodoethyl)-5-methoxy-2-methyl-1*H*-indol-1-yl)methanone (68 mg, 0.15 mmol, 1.0 equiv.), [3.1.1]propellane solution (0.56 mL, 0.40 M in *n*-Bu_2O, 0.23 mmol, 1.5 equiv.), *fac*-$Ir(ppy)_3$ (2.5 mg, 3.8 µmol, 2.5 mol%) and *t*-BuCN (1.5 mL) were submitted to *General procedure 2* for 3 h at room temperature. Purification by column chromatography (SiO_2, pentane / EtOAc, 9:1) gave **59** (51 mg, 0.093 mmol, 62%) as a colourless foam.

The starting material (4-chlorophenyl)(3-(2-iodoethyl)-5-methoxy-2-methyl-1H-indol-1-yl)methanone was prepared according to a published procedure.[45]

R_f 0.31 (pentane / EtOAc, 9:1).

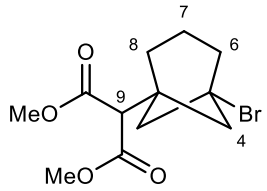
^{1}H NMR (400 MHz, $CDCl_3$) δ_H 7.64 (d, *J* = 8.5 Hz, 2H, Ar*H*), 7.47 (d, *J* = 8.5 Hz, 2H, Ar*H*), 6.91-6.83 (m, 2H, Ar*H*), 6.66 (dd, *J* = 9.0, 2.6 Hz, 1H, Ar*H*), 3.85 (s, 3H, O*Me*), 2.57 (t, *J* = 7.2 Hz, 2H, H4/6), 2.54-2.47 (m, 4H, H1, H3), 2.43-2.35 (m, 2H, H3), 2.30 (s, 3H, Ar*Me*), 2.00-1.85 (m, 2H, H5), 1.76 (t, *J* = 7.2 Hz, 2H, H4/6), 1.71-1.64 (m, 2H, H2).

^{13}C NMR (101 MHz, $CDCl_3$) δ_C 168.4, 156.0, 139.1, 134.4, 133.8, 131.23, 131.19, 131.1, 129.2, 119.6, 115.2, 110.8, 101.8, 55.9, 52.0, 47.0, 43.5, 40.9, 35.0, 31.0, 20.0, 19.2, 13.4.

IR (film, ν_{max}/cm^{-1}) 2929, 2866, 1679, 1456, 1327, 1220, 1116, 1068, 733.

HRMS (ESI^+) calc. for $C_{26}H_{28}NO_2ClI$ $[M+H]^+$ 548.0853, found 548.0848.

Dimethyl 2-(5-bromobicyclo[3.1.1]heptan-1-yl)malonate, 60



Dimethyl 2-bromomalonate (19.8 µL, 0.15 mmol, 1.0 equiv.), [3.1.1]propellane solution (0.90 mL, 0.25 M in *n*-Bu_2O, 0.23 mmol, 1.5 equiv.), *fac*-$Ir(ppy)_3$ (2.5 mg, 3.8 µmol, 2.5 mol%) and *t*-BuCN (1.50 mL) were submitted to *General procedure 2* at room temperature for 3 h. Purification by column chromatography (SiO_2, pentane / EtOAc, 9:1) gave **60** (26 mg, 0.085 mmol, 57%) as a colourless oil.

R_f 0.23 (pentane / EtOAc, 9:1).

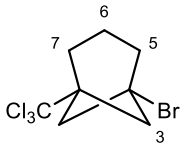
^{1}H NMR (400 MHz, $CDCl_3$) δ_H 3.73 (s, 6H, O*Me*), 3.45 (s, 1H, H9), 2.58-2.42 (m, 2H, H4), 2.40-2.30 (m, 4H, H4, H8/H6), 2.00-1.85 (m, 2H, H7), 1.83-1.74 (dd, *J* = 7.4, 0.7 Hz, 2H, H8/H6).

^{13}C NMR (101 MHz, $CDCl_3$) δ_C 168.0, 59.8, 56.0, 52.4, 48.9, 42.0, 39.8, 29.2, 19.1.

IR (thin film, ν_{max} / cm^{-1}) 2953, 2868, 1735, 1435, 1320, 1250, 1157.

HRMS (APCI$^+$) calc. for $C_{12}H_{18}BrO_4$ $[M+H]^+$ 305.0383, found 305.0383.

1-Bromo-5-(trichloromethyl)bicyclo[3.1.1]heptane, 64



A solution of [3.1.1]propellane (0.33 mL, 0.35 M in *n*-Bu_2O, 0.10 mmol, 1.0 equiv.) was cooled to −78 °C then $BrCCl_3$ (65 mg, 33 µL, 0.33 mmol, 3.3 equiv.) was added dropwise. The mixture was stirred for 15 min at −78 °C then slowly warmed up to room temperature and stirred for 1 h. The solvent was removed *in vacuo* and purified by column chromatography (SiO_2, pentane / Et_2O, 95:5) to afford **64** (20 mg, 0.068 mmol, 68%) as a white solid.

R_f 0.45 (100% pentane).

^{1}H NMR (400 MHz, $CDCl_3$) δ_H 2.99-2.91 (m, 2H, H3), 2.42-2.33 (m, 2H), 2.33-2.25 (m, 2H, H3), 2.18-2.08 (m, 2H), 2.07-1.92 (m, 2H, H6).

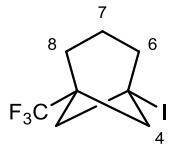
^{13}C NMR (101 MHz, $CDCl_3$) δ_C 105.2, 57.4, 51.9, 46.2, 39.6, 29.0, 19.2.

IR (thin film, ν_{max} / cm^{-1}) 2956, 1453, 1329, 1160, 945, 894, 788, 771.

HRMS (APCI, ESI, EI) Not found.

m.p. 34-36 °C.

1-Iodo-5-(trifluoromethyl)bicyclo[3.1.1]heptane, 65



A solution of [3.1.1]propellane (0.30 mL, 0.50 M in n-Bu_2O, 0.15 mmol, 1.0 equiv.) was cooled to –78 °C then CF_3I·2DMSO (0.10 mL, 0.45 mmol, 3.00 equiv.) was added. The resulting mixture was allowed to warm up to room temperature and stirred for 1 h. The mixture was diluted with Et_2O and washed with LiCl solution (1 mL, 10% aq.), dried ($MgSO_4$), filtered and concentrated *in vacuo* (150 mbar, 30 °C). Purification by column chromatography (SiO_2, pentane) afforded **65** (22 mg, 0.076 mmol, 51%) as a colorless oil. As the product is volatile, a ^{1}H NMR yield of **65** was determined using $CHBr_3$ as an internal standard (74%, 0.11 mmol).

*Note: **65** is not detectable via TLC. **65** eluates from the column in the first few fractions. It coalesces with the bromobenzene fraction which is detectable by UV. Bromobenzene can be removed in vacuo under partial sacrificial loss of **65**.*

R_f 0.80 (100% pentane).

^{1}H NMR (500 MHz, $CDCl_3$) δ_H 2.83 (app. dt, J = 7.6, 3.8 Hz, 2H, H4), 2.64-2.44 (m, 2H, H6/8), 2.42-2.26 (m, 2H, H4), 2.01-1.82 (m, 4H, H6/8, H7).

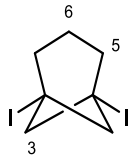
^{13}C NMR (126 MHz, $CDCl_3$) δ_C 125.0 (q, $^1J_{C\text{-}F}$ = 277.6 Hz), 47.8 (q, $^2J_{C\text{-}F}$ = 31.0 Hz), 45.6 (q, $^3J_{C\text{-}F}$ = 2.2 Hz), 42.8, 28.0, 24.8 (q, $^3J_{C\text{-}F}$ = 2.4 Hz), 18.6.

^{19}F NMR (377 MHz, $CDCl_3$) δ_F –78.02.

IR (thin film, ν_{max} / cm^{-1}) 2957, 2924, 2849, 2358, 2341, 2329, 672, 664.

HRMS (APCI, ESI, EI) Not found.

1,5-Diiodobicyclo[3.1.1]heptane, 66



A solution of [3.1.1]propellane (0.29 mL, 0.35 M in *n*-Bu_2O, 0.10 mmol, 1.0 equiv.) was cooled down to −78 °C and a solution of I_2 in DCM (51 mg I_2 dissolved in 0.5 mL DCM to yield a 0.2 M solution) was added dropwise *via syringe* until a violet colour persists. The organics were removed *in vacuo*. Purification by column chromatography (SiO_2, pentane) gave **66** (13 mg, 0.037 mmol, 37%) as a white solid.

R_f 0.50 (100% pentane).

^{1}H NMR (400 MHz, $CDCl_3$) δ_H 3.36-3.26 (m, 2H, H3), 2.96 (dd, *J* = 7.4, 2.9 Hz, 2H, H3), 2.54-2.42 (m, 4H, H5), 2.00-1.91 (m, 2H, H6).

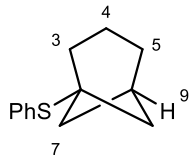
^{13}C NMR (101 MHz, $CDCl_3$) δ_C 59.7, 41.3, 28.9, 22.5.

IR (thin film, ν_{max} / cm^{-1}) 2950, 2859, 1448, 1320, 1218, 1080, 893, 809.

HRMS (APCI, ESI, EI) Not found.

m.p. 55-58 °C.

Bicyclo[3.1.1]heptan-1-yl(phenyl)sulfane, 68



Thiophenol (22 µL, 0.22 mmol, 1.1 equiv.), diethyl ether (0.50 mL) and [3.1.1]propellane solution (0.57 mL, 0.35 M in *n*-Bu_2O, 0.20 mmol, 1.0 equiv.) were submitted to *General procedure 3* at room temperature for 1 h. Trituration with *n*-pentane afforded **68** (41 mg, 0.200 mmol, 99%) as a yellow oil.

R_f 0.23 (100% pentane).

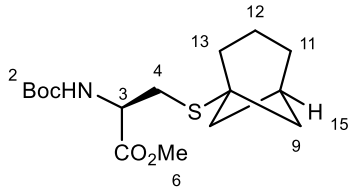
^{1}H NMR (400 MHz, $CDCl_3$) δ_H 7.44-7.39 (m, 2H, *Ar*-H), 7.31 (m, 3H, *Ar*-H), 2.34 (tt, *J* = 6.8, 3.1 Hz, 1H, H9), 2.05 (app. td, *J* = 6.8, 2.5 Hz, 2H, H7), 2.00-1.92 (m, 2H, H3), 1.82 (m, 2H, H4), 1.74– 1.66 (m, 4H, H5, H7).

^{13}C NMR (101 MHz, $CDCl_3$) δ_C 135.3, 133.1, 128.7, 127.9, 52.1, 39.7, 35.6, 31.2, 28.0, 17.8.

IR (thin film, ν_{max} / cm^{-1}) 2980, 2888, 1473, 1383, 1251, 1153, 1085, 954.

HRMS (ESI^+) calc. for $C_{13}H_{17}S$ $[M+H]^+$ 205.1045, found 205.1048.

Methyl S-(bicyclo[3.1.1]heptan-1-yl)-N-(tert-butoxycarbonyl)-L-cysteinate, 69



N-Boc-*L*-cysteine methyl ester (45 µL, 0.22 mmol, 1.1 equiv.), [3.1.1]propellane solution (0.63 mL, 0.32 M in *n*-Bu_2O, 0.20 mmol, 1.0 equiv.) were submitted to *General procedure 3* at room temperature for 1 h. Purification by column chromatography (SiO_2, pentane / EtOAc, 9:1) gave **69** (45 mg, 0.137 mmol, 69%) as a colourless oil.

R_f 0.39 (pentane / EtOAc, 8:2).

^{1}H NMR (400 MHz, $CDCl_3$) δ_H 5.29 (d, *J* = 7.9 Hz, 1H, N*H*), 4.56-4.46 (m, 1H, H3), 3.75 (s, 3H, O*Me*), 2.99-2.88 (m, 2H, H4), 2.41 (tt, *J* = 6.7, 3.2 Hz, 1H, H15), 2.08-2.01 (m, 2H, H9), 1.99-1.90 (m, 2H, H13), 1.84 (app. dq, *J* = 8.5, 6.4 Hz, 2H, H12), 1.77-1.67 (m, 2H, H11), 1.69-1.63 (m, 2H, H9), 1.44 (s, 9H, *t-Bu*).

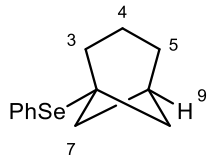
^{13}C NMR (101 MHz, $CDCl_3$) δ_C 171.6, 155.2, 80.2, 53.5, 52.6, 49.2, 39.6, 39.4, 35.9, 31.0, 30.7, 28.5, 27.8, 17.6.

IR (thin film, ν_{max} / cm^{-1}) 3375, 2944, 1747, 1715, 1501, 1352, 1165.

HRMS (ESI^+) calc. for $C_{16}H_{27}NO_4SNa$ $[M+Na]^+$ 352.1553, found 352.1553.

$[\alpha]_D^{25}$ +8.6 (c = 2.6, $CHCl_3$).

Bicyclo[3.1.1]heptan-1-yl(phenyl)selane, 70



A solution of benzeneselenol (16 µL, 0.15 mmol, 1.0 equiv.) in Et_2O (0.15 mL) was added to [3.1.1]propellane solution (0.57 mL, 0.35 M in *n*-Bu_2O, 0.20 mmol, 1.3 equiv.) at –78 °C. The mixture was warmed to room temperature, stirred for 2 h and then concentrated. Purification by column chromatography (SiO_2, pentane) gave **70** (37 mg, 0.147 mmol, 99%) as a colourless oil.

R_f 0.28 (100% pentane).

^{1}H NMR (400 MHz, $CDCl_3$) δ_H 7.58-7.53 (m, 2H, Ar*H*), 7.37-7.25 (m, 3H, Ar*H*), 2.40 (tt, J = 6.6, 3.1 Hz, 1H, H9), 2.14 (td, J = 6.7, 2.6 Hz, 2H, H7), 2.08 (m, 2H, H3/H5), 1.89-1.79 (m, 2H, H4), 1.78-1.70 (m, 4H, H7, H3/H5).

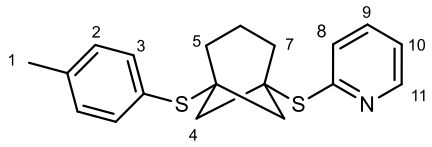
^{13}C NMR (101 MHz, $CDCl_3$) δ_C 137.0, 128.8, 128.3, 128.0, 48.9, 40.6, 36.6, 32.9, 27.9, 18.3.

IR (thin film, ν_{max} / cm^{-1}) 2940, 2859, 1475, 1086, 917, 739, 693.

HRMS (ESI^+) calc. for $C_{13}H_{17}Se$ $[M+H]^+$ 253.0490, found 253.0491.

2-((5-Tosylbicyclo[3.1.1]heptan-1-yl)thio)pyridine, 72

This compound was synthesised and characterised by Dr Jeremy Nugent.



To a solution of *S*-2-pyridyl tolylthiosulfonate (27 mg, 0.10 mmol) in anhydrous MeCN (1.5 mL) was added [3.1.1]propellane solution (0.43 mL, 0.35 M in *n*-Bu_2O, 0.15 mmol, 1.5 equiv.). The flask was sealed and heated to 60 °C for 16 h, then cooled to room temperature and concentrated *in vacuo*. Purification by column chromatography (SiO_2, pentane / EtOAc, 4:1) gave **72** (31 mg, 0.095 mmol, 95%) as a colourless solid.

R_f 0.26 (pentane / EtOAc, 4:1).

^{1}H NMR (400 MHz, $CDCl_3$) δ_H 8.42-8.36 (m, 1H, H11), 7.67 (d, *J* = 8.0 Hz, 2H, H3), 7.49 (td, *J* = 7.7, 1.9 Hz, 1H, H9), 7.32 (d, *J* = 8.0 Hz, 2H, H2), 7.17 (d, *J* = 7.7 Hz, 1H, H8), 7.01 (m, 1H, H10), 2.90-2.77 (m, 2H, H4), 2.44 (s, 3H, H1), 2.18-2.08 (m, 4H, H4), 1.96-1.83 (m, 4H).

^{13}C NMR (101 MHz, $CDCl_3$) δ_C 157.9, 149.8, 144.7, 136.3, 133.1, 129.8, 129.5, 125.1, 120.5, 62.5, 46.6, 40.1, 34.6, 27.1, 21.8, 18.0.

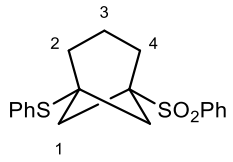
HRMS (ESI) calc. for $C_{19}H_{22}O_2NS_2$ $[M+H]^+$ 360.1086, found 360.1086.

IR (film, ν_{max}/cm^{-1}) 2921, 2861, 1575, 1449, 1417, 1300, 1154, 1118, 760, 673.

m.p. 120-124 °C.

Phenyl(5-(phenylsulfonyl)bicyclo[3.1.1]heptan-1-yl)sulfane, 73

This compound was synthesised and characterised by Dr Jeremy Nugent.



To a solution of *S*-phenyl benzenethiosulfonate (25 mg, 0.10 mmol) in anhydrous MeCN (1.5 mL) was added [3.1.1]propellane solution (0.43 mL, 0.35 M in *n*-Bu_2O, 0.15 mmol, 1.5 equiv.). The flask was sealed and heated to 60 °C for 16 h, then cooled to room temperature and concentrated *in vacuo*. Purification by column chromatography (SiO_2, pentane / EtOAc, 9:1) gave **73** (31 mg, 0.090 mmol, 90%) as a colourless solid.

R_f 0.31 (pentane / EtOAc, 9:1).

^{1}H NMR (400 MHz, $CDCl_3$) δ_H 7.75-7.69 (m, 2H, Ar*H*), 7.64-7.57 (m, 1H, Ar*H*), 7.53-7.46 (m, 2H, Ar*H*), 7.42-7.36 (m, 2H, Ar*H*), 7.36-7.29 (m, 3H, Ar*H*), 2.57-2.45 (m, 2H, H1), 1.94-1.77 (m, 8H, H1, H2, H3, H4).

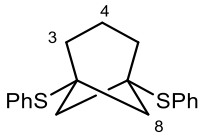
^{13}C NMR (101 MHz, $CDCl_3$) δ_C 135.95, 135.93, 133.8, 131.0, 129.4, 129.13, 129.10, 128.9, 60.9, 47.6, 39.3, 34.3, 27.1, 17.7.

HRMS (ESI) calc. for $C_{19}H_{20}O_2S_2Na$ $[M+Na]^+$ 367.0797, found 367.0798.

IR (film, ν_{max}/cm^{-1}) 2921, 2852, 1447, 1303, 1154, 751, 722, 691, 633.

m.p. 101-103 °C.

1,5-Bis(phenylthio)bicyclo[3.1.1]heptane, 74



Diphenyl disulfide (66 mg, 0.30 mmol, 3.0 equiv.), [3.1.1]propellane solution (0.31 mL, 0.32 M in *n*-Bu_2O, 0.10 mmol, 1.0 equiv.) were submitted to *General procedure 6* at room temperature for 16 h. Purification by column chromatography (SiO_2, pentane) gave **74** (10 mg, 0.032 mmol, 32%) as a colourless oil.

R_f 0.30 (100% pentane).

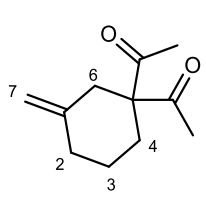
^{1}H NMR (400 MHz, $CDCl_3$) δ_H 7.32-7.11 (m, 10H, Ar*H*), 1.93-1.82 (m, 2H, H8), 1.96-1.88 (m, 2H, H8), 1.79 (m, 6H, H3, H4).

^{13}C NMR (101 MHz, $CDCl_3$) δ_C 135.4, 132.0, 128.9, 128.4, 48.7, 45.7, 34.5, 19.0.

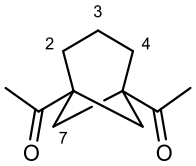
IR (thin film, ν_{max} / cm^{-1}) 2946, 2859, 1582, 1473, 1438, 1322, 1230, 744, 691.

HRMS (APCI, ESI, EI) Not found.

1,1'-(3-Methylenecyclohexane-1,1-diyl)bis(ethan-1-one), 81 and 1,1'-(bicyclo[3.1.1]heptane-1,5-diyl)bis(ethan-1-one), 80



81



80

To a flame dried, screw-capped vial was added diacetyl (13 µL, 0.15 mmol, 1.0 equiv.) and [3.1.1]propellane (0.47 mL, 0.32 M solution in *n*-Bu_2O, 0.15 mmol, 1.0 equiv). The mixture was irritated with a LED lamp (HepatoChem Evoluchem HCK1012-01-011 365 nm) with fan cooling for 20 h at ambient temperature. The solvents were removed *in vacuo*. Purification by column chromatography (SiO_2, pentane / EtOAc, gradient 10:0 to 7:3) to afford **80** (2 mg, 0.011 mmol, 7%) and **81** (3 mg, 0.016 mmol, 11%).

1,1'-(3-Methylenecyclohexane-1,1-diyl)bis(ethan-1-one), ***81***

R_f 0.45 (100% pentane).

^{1}H NMR (400 MHz, $CDCl_3$) δ_H δ 4.76 (app. d, 2H, H7), 2.68 (s, 2H, H6) 2.11 (s, 6H, *Me*), 2.09 – 2.06 (m, 2H, H2), 2.05 – 2.00 (m, 2H, H3/H4), 1.65 – 1.57 (m, 2H, H3/H4).

^{13}C NMR (101 MHz, $CDCl_3$) δ_C *not enough material available.*

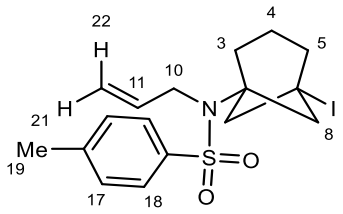
1,1'-(Bicyclo[3.1.1]heptane-1,5-diyl)bis(ethan-1-one), ***80***

R_f 0.43 (pentane / EtOAc, 8:2).

^{1}H NMR (400 MHz, $CDCl_3$) δ_H 2.26 – 2.21 (m, 2H, H7), 2.07 (s, 6H, *Me*), 2.00 – 1.90 (m, 6H, H2+H3+H4), 1.83 – 1.74 (m, 2H, H7).

^{13}C NMR (101 MHz, $CDCl_3$) δ_C *not enough material available.*

N-Allyl-N-(5-iodobicyclo[3.1.1]heptan-1-yl)-4-methylbenzenesulfonamide, 82



Adapted from a published procedure.[47]

2-(Iodomethyl)-1-tosylaziridine (51 mg, 0.15 mmol, 1.0 equiv.), [3.1.1]propellane solution (0.70 mL, 0.32 M in *n*-Bu_2O, 0.23 mmol, 1.5 equiv.), *fac*-$Ir(ppy)_3$ (2.5 mg, 3.8 µmol, 2.5 mol%) and *t*-BuCN (1.5 mL) were submitted to *General procedure 2* at room temperature for 3 h. Purification by column chromatography (SiO_2, pentane / EtOAc, 95:5) gave **82** (27 mg, 0.063 mmol, 42%) as a yellow oil.

Starting material prepared according to a known procedure. [47]

R_f 0.30 (pentane / EtOAc, 9:1).

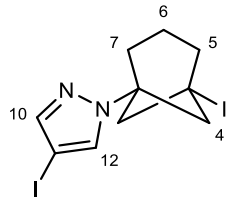
^{1}H NMR (400 MHz, $CDCl_3$) δ_H 7.72-7.68 (d, *J* = 8.0 Hz, 2H, H18), 7.29 (d, *J* = 8.0 Hz, 2H, H17), 5.76 (ddt, *J* = 16.6, 10.1, 6.3 Hz, 1H, H11), 5.14-5.04 (m, 2H, H21, H22), 3.72 (app. dt, *J* = 6.3, 1.5 Hz, 2H, H10), 2.86 (app. dt, *J* = 7.9, 3.9 Hz, 2H, H8), 2.71-2.62 (m, 2H, H8), 2.43 (s, 3H, H19), 2.42-2.38 (m, 2H, H3/5), 2.10-1.94 (m, 2H, H3/5), 1.89-1.74 (m, 2H, H4).

^{13}C NMR (101 MHz, $CDCl_3$) δ_C 143.4, 139.1, 135.8, 129.8, 127.4, 117.8, 64.0, 52.9, 48.9, 42.3, 32.7, 27.5, 21.7, 19.7.

IR (thin film, ν_{max} / cm^{-1}) 2950, 2866, 1598 (weak), 1494, 1334, 1152.

HRMS (ESI^+) calc. for $C_{17}H_{22}INO_2SNa$ $[M+Na]^+$ 454.0308, found 454.0307.

4-Iodo-1-(5-iodobicyclo[3.1.1]heptan-1-yl)-1H-pyrazole, 83



Adapted from a published procedure.[105]

A flame-dried vial equipped with a stir bar was charged with 4-iodo-1*H*-pyrazole (19 mg, 0.095 mmol, 1.0 equiv.), I_2 (25 mg, 0.10 mmol, 1.05 equiv.), Cs_2CO_3 (62 mg, 0.19 mmol, 2.0 equiv.) and anhydrous MeCN (0.47 mL). The mixture was stirred for 30 min at room temperature then a solution of [3.1.1]propellane (0.36 mL, 0.32 M in *n*-Bu_2O, 0.11 mmol, 1.2 equiv.) was added. The mixture was stirred for a further 16 h at room temperature, then diluted with 1 mL MeCN and filtered through Celite. The solution was dried (Na_2SO_4), filtered and concentrated *in vacuo.* Purification by column chromatography (SiO_2, EtOAc / pentane, gradient 99:1 to 98:2) followed by an acid/base extraction afforded **83** (12 mg, 0.029 mmol, 31%) as a white solid.

R_f 0.28 (pentane / EtOAc, 99:1).

^{1}H NMR (400 MHz, $CDCl_3$) δ_H 7.52 (d, *J* = 0.6 Hz, 1H), 7.40 (d, *J* = 0.6 Hz, 1H), 3.19-3.09 (m, 2H, H4), 2.82-2.70 (m, 2H, H4), 2.60-2.48 (m, 2H), 2.20-2.10 (m, 2H), 2.08-1.94 (m, 2H, H6).

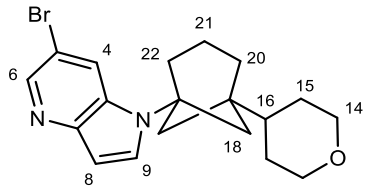
^{13}C NMR (101 MHz, $CDCl_3$) δ_C 144.5, 130.4, 63.9, 56.3, 51.9, 42.3, 32.7, 24.3, 19.2.

IR (thin film, ν_{max} / cm^{-1}) 2947, 2866, 955, 611.

HRMS (ESI^+) calc. for $C_{10}H_{13}I_2N_2$ $[M+H]^+$ 414.9163, found 414.9163.

m.p. 70-73 °C.

6-Bromo-1-(5-(tetrahydro-2H-pyran-4-yl)bicyclo[3.1.1]heptan-1-yl)-1H-pyrrolo[3,2-b]pyridine, 84



6-Bromo-1*H*-pyrrolo[3,2-*b*]pyridine (29 mg, 0.15 mmol, 1.0 equiv.), iodomesitylene bis(tetrahydro-2*H*-pyran-4-carboxylate) **182** (152 mg, 0.30 mmol, 2.0 equiv.), $Cu(acac)_2$ (24 mg, 0.090 mmol, 0.6 equiv.), *fac*-$Ir(ppy)_3$ (2.0 mg, 3.0 µmol, 2.0 mol%), anhydrous 1,4-dioxane (5.0 mL), BTMG (0.09 mL, 0.45 mmol, 3.0 equiv.) and [3.1.1]propellane solution (0.64 mL, 0.35 M in *n*-Bu_2O, 0.23 mmol, 1.5 equiv.) were submitted to *General procedure 5* at room temperature for 16 h. Purification by column chromatography (SiO_2, pentane / EtOAc, 7:3) followed by acid-bash extraction gave **84** (28 mg, 0.075 mmol, 50%) as a yellow oil.

R_f 0.25 (pentane / EtOAc, 1:1).

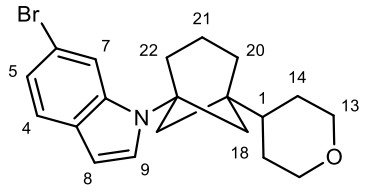
^{1}H NMR (400 MHz, $CDCl_3$) δ_H 8.47 (br. s, 1H, H6), 7.75 (dd, *J* = 2.0, 0.9 Hz, 1H, H4), 7.24 (d, *J* = 3.3 Hz, 1H, H9), 6.65 (dd, *J* = 3.3, 0.9 Hz, 1H, H8), 4.02 (app. dd, *J* = 11.2, 3.8 Hz, 2H, H14), 3.33 (td, *J* = 11.2, 2.2 Hz, 2H, H14), 2.28-2.24 (m, 2H, H18), 2.14-2.03 (m, 4H, H18, H20/H22), 2.03-1.91 (m, 2H, H21), 1.73 (t, *J* = 7.1 Hz, 2H, H20/H22), 1.58-1.31 (m, 5H, H15, H16).

^{13}C NMR (101 MHz, $CDCl_3$) δ_C 145.5, 143.5, 129.1, 128.4, 120.7, 112.3, 102.3, 68.3, 57.8, 44.4, 42.1, 40.9, 35.7, 29.4, 27.4, 17.5.

IR (thin film, ν_{max} / cm^{-1}) 2980, 1411, 1385, 1154, 1089, 954.

HRMS (ESI^+) calc. for $C_{19}H_{24}BrN_2O$ $[M+H]^+$ 375.1067, found 375.1050.

5-Bromo-1-(5-(tetrahydro-2H-pyran-4-yl)bicyclo[3.1.1]heptan-1-yl)-1H-indole, 85



5-Bromo-*1H*-indole (29 mg, 0.15 mmol, 1.0 equiv.), iodomesitylene bis(tetrahydro-2*H*-pyran-4-carboxylate) **182** (152 mg, 0.30 mmol, 2.0 equiv.), $Cu(acac)_2$ (24 mg, 0.090 mmol, 0.6 equiv.), *fac*-$Ir(ppy)_3$ (2.0 mg, 3.0 µmol, 2.0 mol%), anhydrous 1,4-dioxane (5.0 mL, 0.03 M), BTMG (0.09 mL, 0.45 mmol, 3.0 equiv.) and [3.1.1]propellane solution (0.64 mL, 0.35 M in *n*-Bu_2O, 0.23 mmol, 1.5 equiv.) were submitted to *General procedure 5* at room temperature for 16 h. Purification by column chromatography (SiO_2, pentane / EtOAc, 9:1) gave **85** (36 mg, 0.096 mmol, 64%) as a brown solid.

R_f 0.39 (pentane / EtOAc, 8:2).

^{1}H NMR (400 MHz, $CDCl_3$) δ_H 7.73 (d, *J* = 1.1 Hz, 1H, Ar*H*), 7.24-7.16 (m, 2H, Ar*H*), 7.01 (d, *J* = 3.1 Hz, 1H, Ar*H*), 6.39 (d, *J* = 3.1 Hz, 1H, Ar*H*), 4.01 (app. dd, *J* = 11.3, 4.1 Hz, 2H, H13), 3.34 (td, *J* = 11.3, 2.1 Hz, 2H, H13), 2.26 (app. dt, *J* = 7.3, 3.7 Hz, 2H, H18), 2.08 (app. t, *J* = 7.5 Hz, 4H, H18, H20/22), 2.01-1.89 (m, 2H, H21), 1.72 (app. t, *J* = 7.1 Hz, 2H, H20/H22), 1.51-1.32 (m, 5H, H1, H14).

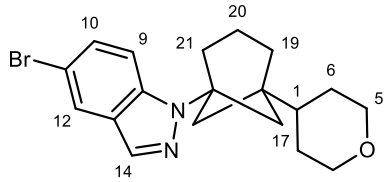
^{13}C NMR (101 MHz, $CDCl_3$) δ_C 133.4, 130.9, 125.9, 123.9, 123.6, 112.6, 112.5, 100.5, 68.3, 57.4, 44.4, 41.8, 41.0, 35.4, 29.6, 27.4, 17.6.

IR (thin film, ν_{max} / cm^{-1}) 2917, 2845, 1462, 1331, 1274, 1229, 1124, 1089.

HRMS (ESI^+) calc. for $C_{20}H_{25}BrNO$ $[M+H]^+$ 374.1114, found 374.1116.

m.p. 114-117 °C.

6-Bromo-1-(5-(tetrahydro-2H-pyran-4-yl)bicyclo[3.1.1]heptan-1-yl)-1H-pyrazolo[4,3-b]pyridine, 86



6-Bromo-1*H*-pyrazolo[4,3-*b*]pyridine (30 mg, 0.15 mmol, 1.0 equiv.), iodomesitylene bis(tetrahydro-2*H*-pyran-4-carboxylate) **182** (152 mg, 0.30 mmol, 2.0 equiv.), $Cu(acac)_2$ (24 mg, 0.090 mmol, 0.6 equiv.), *fac*-$Ir(ppy)_3$ (2.0 mg, 3.0 µmol, 2.0 mol%), anhydrous 1,4-dioxane (5.0 mL, 0.03 M), BTMG (0.09 mL, 0.45 mmol, 3.0 equiv.) and [3.1.1]propellane solution (0.70 mL, 0.32 M in *n*-Bu_2O, 0.23 mmol, 1.5 equiv.) were submitted to *General procedure 5* at room temperature for 16 h. Purification by column chromatography (SiO_2, pentane / EtOAc, gradient 95:5 to 94:7) gave **86** (29 mg, 0.077 mmol, 52%) as a yellow oil.

R_f 0.54 (pentane / EtOAc, 3:2).

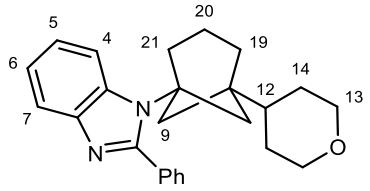
^{1}H NMR (400 MHz, $CDCl_3$) δ_H 7.89 (d, *J* = 0.8 Hz, 1H, H14), 7.85 (dd, *J* = 1.8, 0.8 Hz, 1H, H12), 7.37 (dd, *J* = 8.9, 1.8 Hz, 1H, H10), 7.30 (app. dt, *J* = 8.9, 0.8 Hz, 1H, H9), 4.05-3.97 (m, 2H, H5), 3.33 (app. td, *J* = 11.4, 2.1 Hz, 2H, H5), 2.33-2.28 (m, 2H, H17), 2.28-2.20 (m, 2H, H17), 2.16-2.08 (m, 2H, H21/H19), 2.00 (app. dt, *J* = 13.8, 6.8 Hz, 2H, H20), 1.73 (app. t, *J* = 7.1 Hz, 2H, H21/H19), 1.55-1.34 (m, 5H, H1, H6).

^{13}C NMR (101 MHz, $CDCl_3$) δ_C 136.6, 131.9, 128.9, 126.1, 123.7, 113.6, 111.7, 68.4, 59.9, 44.3, 42.0, 40.7, 34.9, 29.6, 27.4, 17.5.

IR (thin film, ν_{max} / cm^{-1}) 2945, 2844, 2361, 1483, 1442, 1409.

HRMS (ESI^+) calc. for $C_{19}H_{24}BrN_2O$ $[M+H]^+$ 375.1067, found 375.1067.

2-Phenyl-1-(5-(tetrahydro-2H-pyran-4-yl)bicyclo[3.1.1]heptan-1-yl)-1H-benzo[d]imidazole, 87



2-Phenyl-1*H*-benzo[*d*]imidazole (30 mg, 0.15 mmol, 1.0 equiv.), iodomesitylene bis(tetrahydro-2*H*-pyran-4-carboxylate) **182** (152 mg, 0.30 mmol, 2.0 equiv.), $Cu(TMHD)_2$ (39 mg, 0.090 mmol, 0.6 equiv.), *fac*-$Ir(ppy)_3$ (2.0 mg, 3.0 µmol, 2.0 mol%), anhydrous 1,4-dioxane (5.0 mL, 0.03 M), BTMG (0.09 mL, 0.45 mmol, 3.0 equiv.) and [3.1.1]propellane solution (0.64 mL, 0.35 M in *n*-Bu_2O, 0.23 mmol, 1.5 equiv.) were submitted to *General procedure 5* at room temperature for 16 h. Purification by column chromatography (SiO_2, pentane / EtOAc, 1:1) followed by trituration (Et_2O) gave **87** (20 mg, 0.054 mmol, 36%) as a pale-yellow solid.

R_f 0.20 (pentane / EtOAc, 1:1).

^{1}H NMR (400 MHz, $CDCl_3$) δ_H 7.82-7.78 (m, 1H, Ar*H*), 7.66-7.54 (m, 2H, Ar*H*), 7.53-7.40 (m, 4H, Ar*H*), 7.36-7.19 (m, 2H, Ar*H*), 3.97-3.84 (app. dd, *J* = 11.0, 3.5 Hz, 2H, H13), 3.22 (app. t, *J* = 11.1 Hz, 2H, H13), 2.46 (app. t, *J* = 7.2 Hz, 2H, H19/H21), 2.15-1.93 (app. pent, *J* = 7.2 Hz, 4H, H20, H9), 1.76-1.68 (m, 2H, H19/H21), 1.60 (app. t, *J* = 7.2 Hz, 2H, H9), 1.33-1.17 (m, 5H, H12, H14).

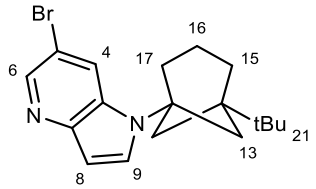
^{13}C NMR (101 MHz, $CDCl_3$) δ_C 153.0, 142.9, 134.7, 132.4, 130.0, 129.8, 128.2, 122.5, 122.4, 120.1, 111.9, 68.2, 58.0, 44.0, 42.5, 41.7, 35.8, 29.2, 27.2, 17.8.

IR (thin film, ν_{max} / cm^{-1}) 2942, 2850, 1454, 1454, 1368, 1124, 1089, 744, 700.

HRMS (ESI^+) calc. for $C_{25}H_{29}N_2O$ $[M+H]^+$ 373.2274, found 373.2276.

m.p. 211-214 °C.

6-Bromo-1-(5-(tert-butyl)bicyclo[3.1.1]heptan-1-yl)-1H-pyrrolo[3,2-b]pyridine, 88



6-Bromo-1*H*-pyrrolo[3,2-*b*]pyridine (29 mg, 0.15 mmol, 1.0 equiv.), di-*tert*-butyl mesityl-λ^3-iodanedicarboxylate **183** (134 mg, 0.30 mmol, 2.0 equiv.), $Cu(acac)_2$ (24 mg, 0.090 mmol, 0.6 equiv.), *fac*-$Ir(ppy)_3$ (2.0 mg, 3.0 µmol, 2.0 mol%), anhydrous 1,4-dioxane (5.0 mL, 0.03 M), BTMG (0.09 mL, 0.45 mmol, 3.0 equiv.) and [3.1.1]propellane solution (0.64 mL, 0.35 M in *n*-Bu_2O, 0.23 mmol, 1.5 equiv.) were submitted to *General procedure 5* at room temperature for 16 h. Purification by column chromatography (SiO_2, pentane / EtOAc, 9:1) gave **88** (27 mg, 0.078 mmol, 52%) as a yellow solid.

R_f 0.25 (pentane / EtOAc, 8:2).

^{1}H NMR (400 MHz, $CDCl_3$) δ_H 8.47 (br. s, 1H, H6), 7.78 (dd, *J* = 1.9, 0.8 Hz, 1H, H4), 7.27 (d, *J* = 3.3 Hz, 1H, H9), 6.67 (d, *J* = 3.3 Hz, 1H, H8), 2.28 (app. dt, *J* = 7.2, 3.6 Hz, 2H, H13), 2.14-2.07 (m, 2H, H13), 2.07-1.99 (m, 2H, H15/H17), 2.01-1.90 (m, 2H, H16), 1.81 (app. t, *J* = 6.8 Hz, 2H, H15/H17), 0.86 (s, 9H, *t*-Bu).

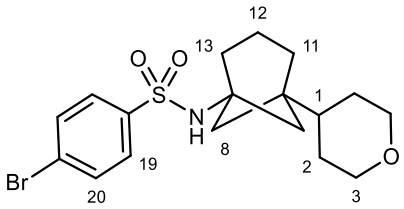
^{13}C NMR (101 MHz, $CDCl_3$) δ_C 145.9, 143.8, 129.0, 128.3, 120.5, 112.2, 102.3, 56.7, 45.6, 37.9, 35.6, 33.3, 29.0, 25.4, 18.0.

IR (thin film, ν_{max} / cm^{-1}) 2980, 2888, 1473, 1462, 1383, 1252, 1152, 1073, 954.

HRMS (ESI$^+$) calc. for $C_{18}H_{24}BrN_2$ $[M+H]^+$ 347.1117, found 374.1120.

m.p. 90-92 °C.

4-Bromo-N-(5-(tetrahydro-2H-pyran-4-yl)bicyclo[3.1.1]heptan-1-yl)benzenesulfonamide, 89



4-Bromobenzenesulfonamide (35 mg, 0.15 mmol, 1.0 equiv.), iodomesitylene bis(tetrahydro-2*H*-pyran-4-carboxylate) **182** (152 mg, 0.30 mmol, 2.0 equiv.), $Cu(acac)_2$ (24 mg, 0.090 mmol, 0.6 equiv.), *fac*-$Ir(ppy)_3$ (2.0 mg, 3.0 µmol, 2.0 mol%), anhydrous 1,4-dioxane (5.0 mL, 0.03 M), BTMG (0.09 mL, 0.045 mmol, 3.0 equiv.) and [3.1.1]propellane solution (0.70 mL, 0.32 M in *n*-Bu_2O, 0.23 mmol, 1.5 equiv.) were submitted to *General procedure 5* at room temperature for 16 h. Purification by column chromatography (SiO_2, pentane / acetone, gradient 95:5 to 80:20) gave **89** (19 mg, 0.046 mmol, 31%) as a yellow oil.

R_f 0.33 (pentane / EtOAc, 1:1).

^{1}H NMR (400 MHz, $CDCl_3$) δ_H 7.76-7.72 (m, 2H, H19), 7.65-7.61 (m, 2H, H20), 4.97 (s, 1H, N*H*), 3.96 (dd, *J* = 11.2, 4.1 Hz, 2H, H3), 3.29 (app. td, *J* = 11.2, 2.1 Hz, 2H, H3), 1.84-1.67 (m, 6H, H8, H11/H13, H12), 1.62-1.58 (m, 2H, H8), 1.45 (app. t, *J* = 6.9 Hz, 2H, H11/H13), 1.35-1.19 (m, 5H, H1, H2).

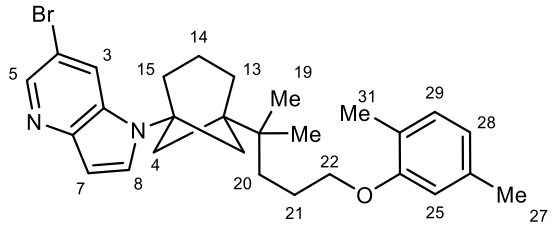
^{13}C NMR (101 MHz, $CDCl_3$) δ_C 142.2, 132.4, 128.7, 127.4, 68.3, 55.0, 44.2, 41.5, 41.1, 35.1, 29.0, 27.4, 17.3.

IR (thin film, ν_{max} / cm^{-1}) 3273, 2946, 2856, 1575, 1389, 1329, 1090, 1018, 913, 822, 739.

HRMS (ESI^+) calc. for $C_{18}H_{25}BrNO_3S$ $[M-H]^-$ 412.0660, found 412.0588.

m.p. 157-159 °C.

6-Bromo-1-(5-(5-(2,5-dimethylphenoxy)-2-methylpentan-2-yl)bicyclo[3.1.1]heptan-1-yl)-1H-pyrrolo[3,2-b]pyridine, 90



6-Bromo-1*H*-pyrrolo[3,2-*b*]pyridine (29 mg, 0.15 mmol, 1.0 equiv.), phenyl-λ^3-iodanediyl bis(5-(2,5-dimethylphenoxy)-2,2-dimethylpentanoate) **184** (223 mg, 0.30 mmol, 2.0 equiv.), $Cu(acac)_2$ (24 mg, 0.090 mmol, 0.6 equiv.), *fac*-$Ir(ppy)_3$ (2.0 mg, 3.0 µmol, 2.0 mol%), anhydrous 1,4-dioxane (5.0 mL, 0.03 M), BTMG (0.09 mL, 0.45 mmol, 3.0 equiv.) and [3.1.1]propellane solution (0.70 mL, 0.32 M in *n*-Bu_2O, 0.23 mmol, 1.5 equiv.) were submitted to *General procedure 5* at room temperature for 16 h. Purification by column chromatography (SiO_2, first column: pentane / EtOAc, 9:1, second column: toluene / EtOAc, 9:1) gave **90** (24 mg, 0.048 mmol, 32%) as a yellow oil.

R_f 0.39 (pentane / EtOAc, 8:2).

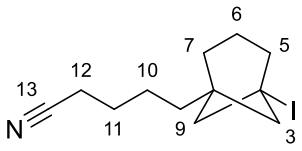
^{1}H NMR (500 MHz, $CDCl_3$) δ_H 8.47 (d, *J* = 1.9 Hz, 1H, H5), 7.75 (d, *J* = 1.2 Hz, 1H, H3), 7.25 (d, *J* = 3.3 Hz, 1H, H7/H8), 7.01 (d, *J* = 7.4 Hz, 1H, H29/H28), 6.67 (d, *J* = 7.4 Hz, 1H, H29/H28), 6.64 (d, *J* = 3.3 Hz, 1H, H7/H8), 6.63 (s, 1H, H25), 3.92 (t, *J* = 6.2 Hz, 2H, H22), 2.36-2.30 (m, 5H, H4, Ar*Me*), 2.19 (s, 3H, Ar*Me*), 2.16-2.12 (m, 2H, H4), 2.06-2.02 (m, 2H), 1.97 (app. dt, *J* = 13.9, 6.8 Hz, 2H), 1.86 (app. t, *J* = 6.8 Hz, 2H), 1.82-1.69 (m, 2H, H21), 1.47-1.39 (m, 2H, H20), 0.88 (s, 6H, H19).

^{13}C NMR (126 MHz, $CDCl_3$) δ_C 157.1, 145.9, 143.8, 136.6, 130.5, 129.0, 128.3, 123.7, 120.8, 120.4, 112.3, 112.1, 102.3, 68.6, 57.2, 45.8, 38.5, 35.7, 35.6, 34.5, 28.8, 24.9, 22.7, 21.6, 17.9, 15.9.

IR (thin film, ν_{max} / cm^{-1}) 2951, 2865, 1508, 1412, 1285, 1264, 1130, 904, 782, 729.

HRMS (ESI^+) calc. for $C_{28}H_{36}BrN_2O$ $[M+H]^+$ 495.2006, found 495.2006.

5-(5-Iodobicyclo[3.1.1]heptan-1-yl)pentanenitrile, 113



5-iodopentanenitrile **186** (30 mg, 0.15 mmol, 1.00 equiv.), [3.1.1]propellane solution (0.74 mL, 0.23 M in *n*-Bu_2O, 0.225 mmol, 1.5 equiv.), *fac*-$[Ir(ppy)_3]$ (2.5 mg, 4 µmol, 0.025 equiv.) and *tert*-BuCN (1.5 mL) were submitted to *General procedure II* at 25 °C for 5 h. . Purification by column chromatography (SiO_2, pentane / EtOAc, 95:5) gave **113** (20 mg, 0.066 mmol, 44%) as a yellow oil.

R_f 0.25 (pentane / EtOAc, 8:2).

^{1}H NMR (400 MHz, $CDCl_3$) δ_H 2.52 (t, J = 7.2 Hz, 2H, H12), 2.47 – 2.38 (m, 2H, H3), 2.34 (t, J = 7.1 Hz, 2H, H9), 2.32 – 2.27 (m, 2H, H3), 1.86 (p, J = 7.1 Hz, 2H, H6), 1.68 – 1.52 (m, 4H), 1.46 – 1.36 (m, 2H), 1.40 – 1.27 (m, 2H).

^{13}C NMR (101 MHz, $CDCl_3$) δ_C 119.7, 52.0, 46.7, 43.5, 40.3, 34.9, 31.1, 25.7, 23.9, 19.9, 17.3.

IR (thin film, ν_{max} / cm^{-1}) 2942, 2915, 2861, 1452, 1250, 1161, 814.

HRMS (APCI, ESI, EI) Not found.

5.5. Reactivity under Physiological Conditions (Section 2.6)

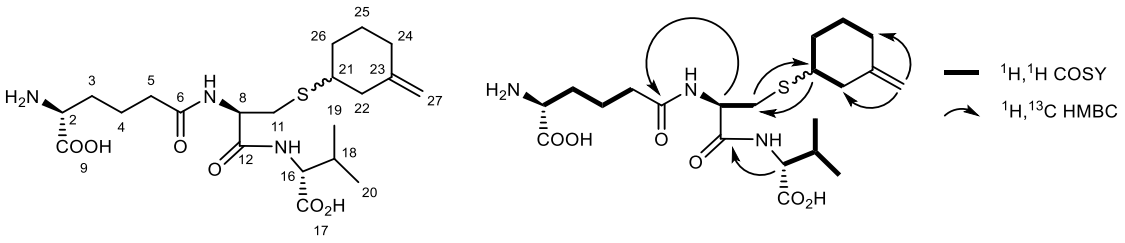
Following procedures and characterisations were carried out with the help of Dr Patrick Rabe (group of Prof. Schofield):

The substrate ACV was synthesised by solid-phase peptide synthesis as reported.[121] A solution of the ACV tripeptide (1 mM, initial stock: 100 mM in water) was incubated with [3.1.1]propellane (50 mM, 50 eq.) in phosphate or tris buffer (50 mM in water at pHs 5.0-9.0, for 1 hour at 4 °C or 22 °C). Samples for LC-MS analysis were prepared by dilution of the reaction mixture to 20 μM. LC-MS analysis was conducted using a Xevo G2-XS mass spectrometer to confirm labelling efficiency of the ACV tripeptide. The peptide solutions were injected to a ACE Equivalence 3 C18 column (2.1 x 50 mm). The labelled ACV was eluted with a gradient of acetonitrile in H_2O (with H_2O and acetonitrile supplemented with formic acid, 0.1 %): 0 – 1 min (1%), 1 – 7 min (1 - 50%), 7– 8 min (50 - 95%), 8 – 10 min (95%), 10 – 10.1 min (95 - 1%), 10.1 -12 min (1%). The obtained mass spectra were analysed using MassLynx v4.1.

For large scale reactions, labelling of ACV (1 mM, 0.011 mmol, 4 mg) with [3.1.1]propellane (50 mM, 50 eq.) was performed in phosphate buffer (50 mM in water pH 8.0) for 12 h at 22 °C. The reaction was monitored by LC-MS analysis. After completeness of the reaction, the solvent was removed under reduced pressure and the crude mixture was dissolved in 1 mL water. Purification was done using a Shimadzu HPLC system, equipped with a SunFireTM semi prep column (C18, 5 μm, 150 mm length, 10 mm diameter), LC20AR HPLC pumps, a LC SIL 10A autosampler, a LC SPD-20A UV detector and a LC CBM-20A controller unit. The peptide was purified using a gradient of acetonitrile in H_2O supplemented with formic acid (0.1% v/v): 0 – 5 min (20%

v/v, acetonitrile), 5 –32 min (20 – 65%), 32 – 34 min (65 – 98%), 34 – 36 min (98%), 36 – 38 min (98 – 20%), 38 – 40 min (2%).

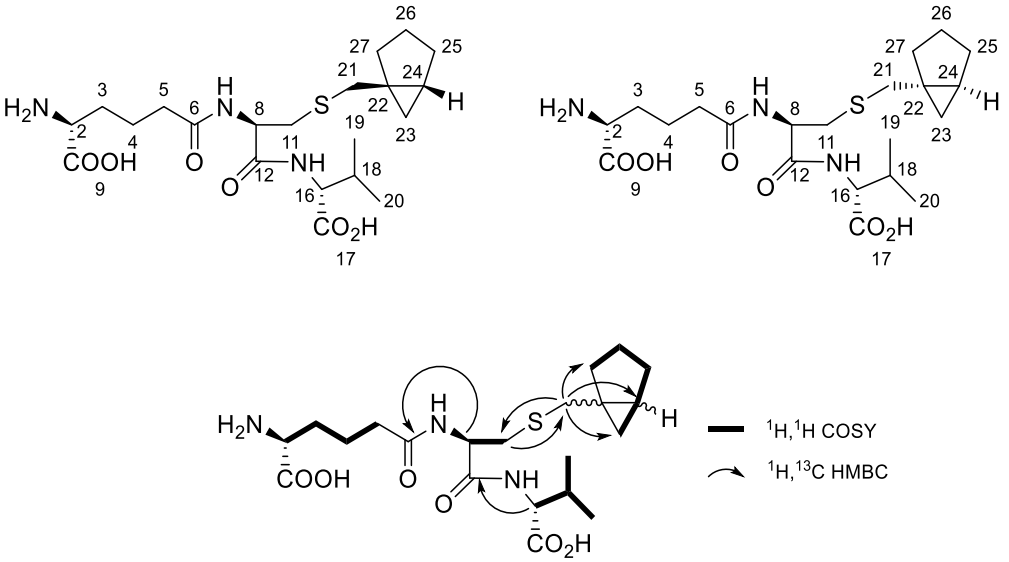
2-Amino-6-(((2R)-1-(((R)-1-carboxy-2-methylpropyl)amino)-3-((3-methylenecyclohexyl)thio)-1-oxopropan-2-yl)amino)-6-oxohexanoic acid, 121



^{1}H NMR (700 MHz, D_2O) δ_H 4.71(2H, CH_2 in HSQC, H27, covered by solvent peak), 4.62 (dd, *J* = 6.8, 6.8 Hz, 1H, H8), 4.19 (dd, *J* = 5.8, 2.0 Hz, 1H, H16), 3.78 (dd, *J* = 6.2, 6.2 Hz, 1H, H2), 3.04 (dd, *J* = 13.9, 6.2 Hz, 1H, H11), 2.99 – 2.91 (m, 2H, H11 and H21), 2.61 (dd, *J* = 13.4, 4.0 Hz, 1H, H22), 2.42 (ddd, *J* = 7.3, 7.3, 2.3 Hz, 2H, H5), 2.26 – 2.21 (m, 1H, H24), 2.20 – 2.00 (m, 4H, H18, H26, H24, H22), 1.95 – 1.80 (m, 3H, H3, H25), 1.78 – 1.67 (m, 2H, H4),1.56 – 1.49 (m, 1H, H26), 1.48 – 1.39 (m, 1H, H25), 0.97 (dd, *J* = 6.9, 3.6 Hz, 3H, H19), 0.94 (dd, *J* = 6.8, 4.8 Hz, 3H, H20).

^{13}C NMR (correlated from ^{1}H,^{13}C-HSQC and ^{1}H,^{13}C-HMBC experiments, 700 MHz, D_2O) δ_C 176.7 (C17), 175.7 (C6), 174 (C9), 171.9 (C12), 148.0 (C23), 108.6 (C27), 53.3 (C8), 59.5 (C16), 54.1 (C2), 44.1 (C21), 40.8 (C22), 34.7 (C5), 33.6 (C24), 31.5 (C26), 30.9 (C11), 30.5 (C18), 29.7 (C3),25.4 (C25), 21.3 (C4), 18.9 (C19), 17.5 (C20).

2-amino-6-(((R)-3-((((1R,5R)-bicyclo[3.1.0]hexan-1-yl)methyl)thio)-1-(((R)-1-carboxy-2-methylpropyl)amino)-1-oxopropan-2-yl)amino)-6-oxohexanoic acid and 2-amino-6-(((R)-3-((((1S,5S)-bicyclo[3.1.0]hexan-1-yl)methyl)thio)-1-(((R)-1-carboxy-2-methylpropyl)amino)-1-oxopropan-2-yl)amino)-6-oxohexanoic acid, 122



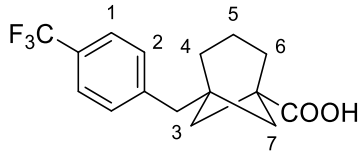
^{1}H NMR (700 MHz, D_2O) δ_H 4.62 (dd, *J* = 7.0 Hz, 7.0 Hz, 1H, H8), 4.11 (dd, *J* = 5.9, 2.2 Hz, 1H, H16), 3.77 (dd, *J* = 6.7, 6.7 Hz, 1H, H2), 3.07 (td, *J* = 13.0, 5.8 Hz, 1H, H11), 2.93 (td, *J* = 13.1, 6.0 Hz, 1H, H11), 2.90 (t, *J* = 13.1 Hz, 1H, H21), 2.77 (t, *J* = 13.2 Hz, 1H, H21), 2.43 (td, *J* = 7.3, 1.4 Hz, 2H, H5), 2.13 (q, *J* = 6.7 Hz, 1H, H18), 1.95 – 1.85 (m, 2H, H3), 1.78 – 1.57 (m, 7H, 2xH4, 1xH25, 2xH26, 2xH27), 1.24 – 1.14 (m, 2H, 1xH24, 1 x H25), 0.94 (d, *J* = 6.9 Hz, 3H, H19), 0.90 (d, *J* = 6.8 Hz, 3H, H20), 0.55 – 0.53 (m, 1H, H23), 0.46 – 0.37 (m, 1H, H23).

^{13}C NMR (correlated from ^{1}H,^{13}C-HSQC and ^{1}H,^{13}C-HMBC experiments, 700 MHz, D_2O) δ_C 176.6 (C17), 175.5 (C6), 173.9 (C9), 171.7 (C12), 52.9 (C8), 59.7 (C16), 53.9 (C2), 39.1 (C21), 34.3 (C5), 30.0 (C25/26/27), 32.5 (C11), 30.2 (C18), 29.4 (C3), 27.5 (C22), 23.5 (C24), 26.6 (C25/26/27), 20.6 (C4), 20.5 (C25/26/27), 18.5 (C19), 17.3

5.6. Lithiation strategy (Section 3.3.2)

5-(4-(Trifluoromethyl)benzyl)bicyclo[3.1.1]heptane-1-carboxylic acid, 138

This compound was synthesised and characterised by Bethany Shire.



To a flame dried vial were added **48** (57 mg, 0.15 mmol, 1 equiv.) and diethyl ether (1.5 mL) and the mixture cooled to –78 °C. *t*-BuLi (0.19 mL, 1.6 M in pentane, 0.30 mmol, 2.0 equiv.) was then added dropwise to the reaction and the mixture stirred for 30 min. $CO_{2\ (g)}$ was then bubbled through the reaction mixture for 30 min. The resulting solution was warmed to room temperature and quenched with NH_4Cl (5 mL, sat. aq.) The mixture was then acidified to pH = 1 with HCl (1M, aq.) and extracted with EtOAc (3 × 10 mL), and the combined organic layers concentrated *in vacuo*. Purification by column chromatography (SiO_2, pentane / EtOAc, gradient 7:3 to 0:1) afforded **138** (28 mg, 0.094 mmol, 62%) as a yellow oil.

R_f 0.20 (pentane / EtOAc, 1:1).

^{1}H NMR (400 MHz, $CDCl_3$) δ_H 7.53 (d, *J* = 7.9 Hz, 2H, Ar*H*), 7.18 (d, *J* = 7.9 Hz, 2H, Ar*H*), 2.70 (s, 2H, H3), 2.06 (m, 2H, H7), 1.95 (m, 2H, H4/H6), 1.79 (app. p, 2H, H5), 1.69-1.63 (m, 2H, H7), 1.57 (m, 2H, H4/H6).

^{13}C NMR (101 MHz, $CDCl_3$) δ_C 182.1, 142.8, 129.9, 128.6 (q, ^2J = 32.2 Hz), 125.9 (q, ^1J = 272.0), 125.2 (q, ^3J = 3.8 Hz), 47.0, 43.1, 39.7, 39.6, 32.6, 29.9, 16.5.

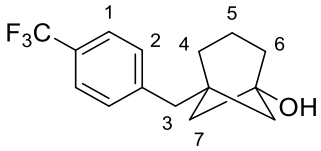
^{19}F NMR (377 MHz, $CDCl_3$) δ_F –62.31.

IR (thin film, ν_{max} / cm^{-1}) 3649, 2980, 2917, 2360, 1697, 1619, 1324, 1163, 1122, 1067.

HRMS (ESI$^-$) calc. for $C_{16}H_{16}F_3O_2$ $[M-H]^-$ 297.1108, found 297.1108.

5-(4-(Trifluoromethyl)benzyl)bicyclo[3.1.1]heptan-1-ol, 139

This compound was synthesised and characterised by Bethany Shire.



A solution of **48** (76 mg, 0.2 mmol, 1.0 equiv.) in a mixture of anhydrous toluene and THF (1 mL, 4:1) was cooled to –78 °C. To this was added isopropoxy-4,4,5,5-tetramethyl-1,3,2-dioxaborolane (45 μL, 0.22 mmol, 1.1 equiv.) followed by dropwise addition of *t*-BuLi (0.15 mL, 1.6 M in pentane, 0.24 mmol, 1.2 equiv.). The resultant mixture was stirred for 1 h then warmed to room temperature and quenched with H_2O (1 mL). The layers were separated, and the aqueous layer was extracted with Et_2O (3 × 10 mL). The combined organic layers were then dried ($MgSO_4$), filtered and concentrated *in vacuo*. The residue was then dissolved in a mixture of THF and H_2O (3 mL, 1:1) then $NaBO_3 \cdot H_2O$ (60 mg, 0.6 mmol, 3.0 equiv.) was added and maintained at this temperature for 21 h. The reaction mixture was quenched with H_2O (2 mL), the layers separated, and the aqueous layer extracted with Et_2O (3 × 10 mL) and the combined organic layers were dried ($MgSO_4$), filtered and concentrated *in vacuo*. Purification by column chromatography (SiO_2, pentane / EtOAc, gradient 9:1 to 1:1) afforded **139** (40.6 mg, 0.150 mmol, 75%) as a colourless oil.

R_f 0.37 (pentane / EtOAc, 8:2)

^{1}H NMR (400 MHz, $CDCl_3$) δ_H 7.53 (d, *J* = 7.9 Hz, 2H, Ar*H*), 7.19 (d, *J* = 7.9 Hz, 2H, Ar*H*), 2.72 (s, 2H, H3), 1.76 (m, 6H, H7, H4/H5/H6), 1.68-1.60 (m, 2H, H7), 1.44 (t, *J* = 6.7 Hz, 2H, H4/H5/H6).

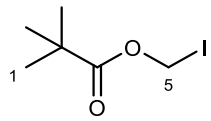
^{13}C NMR (101 MHz, $CDCl_3$) δ_C 143.3, 130.0, 128.5 (q, ^2J = 32.2 Hz), 125.1 (q, ^3J = 3.8 Hz), 124.5 (q, ^1J = 271.7 Hz), 71.9, 46.6, 45.4, 36.2, 35.7, 32.2, 17.7.

^{19}F NMR (377 MHz, $CDCl_3$) δ_F –62.29.

IR (thin film, ν_{max} / cm^{-1}) 3333, 2917, 2859, 2360, 1618, 1323, 1162, 1068, 848.

HRMS (APCI, ESI, EI) Not found.

Iodomethyl pivalate, 141



To a solution of chloromethyl pivalate (0.96 mL, 6.63 mmol, 1.0 equiv.) in acetone (7.0 mL) was added NaI (1.89 g, 12.6 mmol, 1.9 equiv.). The resulting mixture was stirred at room temperature for 16 h while protected from light. The resulting mixture was concentrated *in vacuo* then dissolved in EtOAc (15 mL), filtered and the organic filtrate washed with $Na_2S_2O_3$ solution (aq., 10%), dried over $MgSO_4$, filtered and concentrated *in vacuo* to afford **141** (1.30 g, 5.37 mmol, 81%) as a yellow oil.

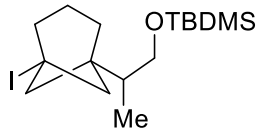
R_f 0.43 (100% pentane).

^{1}H NMR (400 MHz, $CDCl_3$) δ_H 5.93 (s, 2H, H5), 1.19 (s, 9H, H1).

^{13}C NMR (101 MHz, $CDCl_3$) δ_C 176.5, 39.0, 31.5, 26.7.

Analytical data matches that previously reported. [166]

Tert-butyl(2-(5-iodobicyclo[3.1.1]heptan-1-yl)propoxy)dimethylsilane, 142



Tert-butyl 2-(5-iodobicyclo[3.1.1]heptan-1-yl)propanoate **46** (350.0 mg, 1.00 mmol, 1.00 equiv.) was dissolved in Et_2O (5.0 mL) under inert conditions and cooled down to 0 °C. $LiAlH_4$-solution (0.350 mL, 3.5 M in THF, 1.21 mmol, 1.20 equiv.) was added dropwise. The resulting mixture was allowed to warm-up to room temperature and stirred further 2 h. The mixture was diluted with Et_2O, cooled down to 0 °C and carefully quenched by the sequential addition of H_2O (49 µL), an aqueous solution of NaOH (15% aq., 49 µL) and H_2O (147 µL). Subsequently, the mixture was stirred for 15 min at room temperature. Anhydrous $MgSO_4$ was added and stirred for another 15 min. The combined organics were dried over Na_2SO_4 and filtered through a plug of celite before being concentrated *in vacuo*. Purification by column chromatography (SiO_2, pentane / EtOAc, 8:2) afforded the alcoholic intermediate (213 mg, 0.76 mmol, 76%) as a yellow oil.

This intermediate was used directly in the next step

TBDMSCl (40 mg, 0.27 mmol, 1.50 equiv.), the crude 2-(5-iodobicyclo[3.1.1]heptan-1-yl)propan-1-ol intermediate (50 mg, 0.18 mmol, 1.00 equiv.) and imidazole (24 mg, 0.35 mmol, 2.00 equiv.) in DCM (1.5 mL). The mixture was stirred 16 h at room temperature. Subsequently, the mixture was diluted with EtOAc (2 mL) and H_2O (3 mL). The aqueous layer was extracted with EtOAc (2 x 5 mL). The combined organic layers were washed with brine, dried over Na_2SO_4, filtered and concentrated *in vacuo*. Purification by column chromatography (SiO_2, pentane / EtOAc, 99:1) afforded **142** (51 mg, 0.13 mmol, 72%) as a yellow oil.

R_f 0.37 (100% pentane).

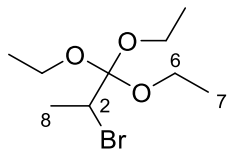
^{1}H NMR (400 MHz, $CDCl_3$) δ_H 4.09 (dtd, *J* = 11.3, 6.4, 5.0 Hz, 1H), 3.69 (dd, *J* = 10.7, 5.0 Hz, 1H), 3.56 (dd, *J* = 10.7, 5.0 Hz, 1H), 3.11-2.88 (m, 2H), 2.41 (t, *J* = 6.8 Hz, 2H), 2.40-2.31 (m, 2H), 1.92-1.76 (m, 4H), 1.17 (d, *J* = 6.4 Hz, 3H), 0.91 (d, *J* = 0.7 Hz, 9H, Si-^{t}*Bu*), 0.07 (s, 6H, Si-*Me*).

^{13}C NMR (101 MHz, $CDCl_3$) δ_C 65.0, 53.3, 51.6, 49.1, 45.4, 44.1, 36.5, 26.9, 26.1, 20.0, 18.4, 11.8, -5.3.

IR (thin film, ν_{max} / cm^{-1}) 2931, 2859, 1713, 1453, 1374, 1251, 1082, 1034, 837, 1034, 837, 776, 705.

HRMS (APCI, ESI, EI) Not found.

2-Bromo-1,1,1-triethoxyethane, 143



1,1,1-Triethoxypropane (6.05 mL, 30 mmol, 1.00 equiv.) was dissolved in pyridine (2.91 mL, 36 mmol, 1.20 equiv.) at −10 °C. Br_2 (1.84 mL, 36 mmol, 1.20 equiv.) was added dropwise so that the temperature does not exceed 10 °C. The resulting suspension was stirred 16 h at room temperature. Finally, the mixture was diluted with Et_2O and stirred for 15 min. The salt was filtered off and washed with Et_2O. The organics were removed *in vacuo* to afford the product **143** (3.83 g, 15 mmol, 50%).

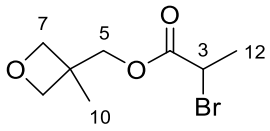
R_f 0.36 (100% pentane).

^{1}H NMR (400 MHz, $CDCl_3$) δ_H 4.22 (q, *J* = 6.8 Hz, 1H, H2), 3.92-3.57 (m, 6H, H6), 1.72 (d, *J* = 6.8 Hz, 3H, H8), 1.20 (t, *J* = 7.1 Hz, 9H, H7).

^{13}C NMR (101 MHz, $CDCl_3$) δ_C 112.1, 58.9, 50.0, 21.0, 15.4.

Analytical data matches that previously reported.[167]

(3-Methyloxetan-3-yl)methyl 2-bromopropanoate, 145



3-Methyl-3-oxetanemethanol (3.10 mL, 31.1 mmol, 1.00 equiv.), triethylamine (5.10 mL, 36.3 mmol, 1.17 equiv.) and *N*,*N*-dimethylaminopyridine (615 mg, 5.02 mmol, 6.20 equiv.) were dissolved in anhydrous DCM (100 mL). The reaction mixture was cooled to 0 °C and 2-bromopropionyl bromide (3.97 mL, 37.4 mmol, 1.20 equiv.) was added slowly over 10 min. The reaction mixture was stirred overnight at room temperature. Finally, the reaction mixture was poured into 100 mL of $NaHCO_3$ solution (sat. aq.). The aqueous layer was extracted 3 times with DCM. The organics were combined, dried with Na_2SO_4, filtered and concentrated *in vacuo*. Purification by column chromatography (SiO_2, pentane / EtOAc, 9:1) afforded **145** (6.63 g, 28 mmol, 90%) as a colourless oil.

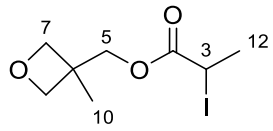
Analytical data matches that previously reported[168].

R_f 0.23 (100% pentane).

^{1}H NMR (400 MHz, $CDCl_3$) δ_H 4.54 (d, *J* = 3.0 Hz, 1H), 4.53 (d, *J* = 3.0 Hz, 1H), 4.45-4.35 (m, 3H), 4.30 (d, *J* = 11.1 Hz, 1H), 4.23 (d, *J* = 11.1 Hz, 1H), 1.84 (m, 3H), 1.36 (s, 3H).

^{13}C NMR (101 MHz, $CDCl_3$) δ_C 170.4, 79.53, 79.51, 70.0, 39.9, 39.4, 21.7, 21.2.

(3-Methyloxetan-3-yl)methyl 2-iodopropanoate, 146



(3-Methyloxetan-3-yl)methyl 2-bromopropanoate **145** (2.51 g, 10.6 mmol, 1.00 equiv.) was dissolved in acetone (25 mL). Subsequently, NaI (2.80 g, 18.7 mmol, 1.76 equiv.) was added as a solid. The reaction mixture was stirred at room temperature for 16 h covered in aluminium foil. Finally, the organics were removed *in vacuo*. The residue was taken up in EtOAc (30 mL), filtered, and the organic filtrate was washed with $Na_2S_2O_3$ solution (aq., 10%), dried over $MgSO_4$ and concentrated *in vacuo*. Purification by column chromatography (SiO_2, pentane / EtOAc, 8:2) afforded **146** (2.50 g, 8.80 mmol, 83%) as an orange oil.

R_f 0.23 (100% pentane).

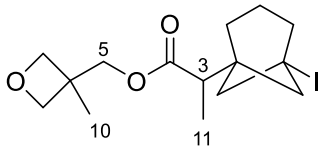
^{1}H NMR (400 MHz, $CDCl_3$) δ_H 4.60-4.48 (m, 3H, H5+H3), 4.40 (dd, *J* = 6.0, 1.9 Hz, 2H, H7), 4.27 (dd, *J* = 11.1, 1.7 Hz, 1H, H7), 4.19 (dd, *J* = 11.1, 1.7 Hz, 1H, H7), 2.01-1.94 (m, 3H, H10), 1.37 (d, *J* = 1.5 Hz, 3H, H12).

^{13}C NMR (101 MHz, $CDCl_3$) δ_C 172.1, 79.58, 79.56, 69.9, 39.5, 23.4, 21.3, 12.5.

IR (thin film, ν_{max} / cm^{-1}) 2964, 2872, 1732, 1446, 1378, 1333, 1253, 1207, 1132, 1056, 979.

HRMS (APCI, ESI, EI) Not found.

(3-Methyloxetan-3-yl)methyl 2-(5-iodobicyclo[3.1.1]heptan-1-yl)propanoate, 147



(3-Methyloxetan-3-yl)methyl 2-iodopropanoate **146** (284 mg, 1.00 mmol, 1.00 equiv.), [3.1.1]propellane solution (4.80 mL, 0.27 M in *n*-Bu_2O, 1.5 mmol, 1.50 equiv.), *t*-BuCN (10.0 mL) and *fac*-[$Ir(ppy)_3$] (7 mg, 0.01 mmol, 0.01 equiv.) were submitted to *General Procedure II* for 3 h at room temperature. Purification by column chromatography (SiO_2, pentane / EtOAc, 8:2) afforded **147** (226 mg, 0.60 mmol, 60%) as a yellow oil.

R_f 0.43 (pentane / EtOAc, 8:2).

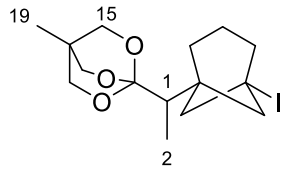
^{1}H NMR (400 MHz, $CDCl_3$) δ_H 4.52-4.36 (m, 4H), 4.10 (qq, *J* = 10.9, 7.1 Hz, 2H, H5), 2.72-2.64 (m, 1H, H3), 2.55-2.43 (m, 4H), 2.41-2.28 (m, 2H), 1.91-1.78 (m, 2H), 1.64 (dtd, *J* = 14.6, 7.3, 1.8 Hz, 1H), 1.54 (dddd, *J* = 13.1, 8.1, 6.4, 1.8 Hz, 1H), 1.24 (t, *J* = 7.1 Hz, 3H, H10), 0.99 (d, *J* = 7.1 Hz, 3H, H11).

^{13}C NMR (101 MHz, $CDCl_3$) δ_C 174.0, 79.7, 79.6, 68.9, 51.3, 51.2, 48.4, 47.8, 43.3, 39.1, 33.0, 27.8, 21.5, 19.7, 11.7.

IR (thin film, ν_{max} / cm^{-1}) 2977, 2940, 2864, 1730, 1450, 1376, 1336, 1248, 1206, 1177, 1141, 1093, 818.

HRMS (APCI, ESI, EI) Not found.

1-(1-(5-Iodobicyclo[3.1.1]heptan-1-yl)ethyl)-5-methyl-2,7,8-trioxabicyclo[3.2.2]nonane, 148



1-(1-Iodoethyl)-4-methyl-2,6,7-trioxabicyclo[2.2.2]octane **147** (42 mg, 0.15 mmol, 1.00 equiv.), [3.1.1]propellane solution (0.45 mL, 0.50 M in *n*-Bu_2O, 0.225 mmol, 1.5 equiv.) and BEt_3 (9.7 µL, 0.0093 mmol, 1.0 M in hexane, 0.10 equiv.) were submitted to *General procedure I* at 0 °C for 15 min, allowed to warm up to room temperature and stirred for another hour. Purification by column chromatography (SiO_2, pentane / EtOAc / NEt_3, 94:5:1) afforded **148** (25 mg, 0.066 mmol, 44%) as a white solid.

R_f 0.32 (pentane / EtOAc, 9:1).

^{1}H NMR (400 MHz, $CDCl_3$) δ_H 3.80 (s, 6H, H15), 2.67 (d, *J* = 9.5 Hz, 1H), 2.53-2.45 (m, 2H), 2.45-2.33 (m, 3H), 1.86 (q, *J* = 7.2 Hz, 1H, H1), 1.79 (tdt, *J* = 8.2, 6.1, 3.2 Hz, 3H), 1.73-1.61 (m, 1H), 0.80 (d, *J* = 7.2 Hz, 3H, H2), 0.76 (s, 3H, H19).

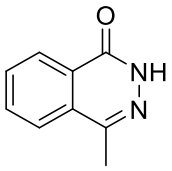
^{13}C NMR (101 MHz, $CDCl_3$) δ_C 110.5, 72.3, 51.7, 49.1, 48.3, 44.0, 37.0, 30.3, 27.1, 20.1, 14.7, 10.0.

IR (thin film, ν_{max} / cm^{-1}) 2946, 2872, 1455, 1396, 1273, 1086, 1045, 992, 950, 919, 816.

HRMS (ESI^+) calc. for $C_{15}H_{24}IO_3$ $[M+H]^+$ 379.0765, found 379.0763.

m.p. 93 – 95 °C

4-Methylphthalazin-1(2H)-one, 149



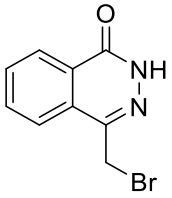
Hydrazine hydrate (1.02 mL, 15.9 mmol, 1.30 equiv., 64-65 %) was added to a solution 2-acetylbenzoic acid (2.00 g, 12.2 mmol, 1.00 equiv.) in ^{i}PrOH (12 mL). The mixture was stirred at 65 °C for 1 h. The organics were removed *in vacuo*, the resulting solid was washed with water (3 x 10 mL), dried *in vacuo* to afford **149** (1.46 g, 9.12 mmol, 58%) without any further purification.

R*f* 0.33 (100% DCM).

^{1}H NMR (400 MHz, $CDCl_3$) δ_H 10.62 (s, 1H, N*H*), 8.61-8.28 (m, 1H, Ar*H*), 8.00-7.57 (m, 3H, Ar*H*), 2.60 (s, 3H, *Me*).

Analytical data matches that previously reported.[169]

4-(Bromomethyl)phthalazin-1(2H)-one, 150



4-Methyl phthalazin-1(2*H*)-one **149** (1.46 g, 9.12 mmol, 1.00 equiv), *N*-bromosuccinimide (2.44 g, 13.7 mmol, 1.50 equiv.) and dibenzoyl peroxide (296 mg, 1.22 mmol, 0.13 mmol) were dissolved in MeCN (15 mL). The reaction mixture was

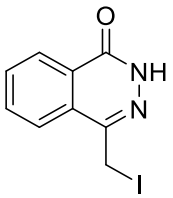
refluxed for 1 h. Finally, the reaction mixture was diluted with MeCN (10 mL) and H_2O (20 mL). The organics were separated, dried over anhydrous Na_2SO_4, filtered and concentrated *in vacuo* to afford **150** (1.04 g, 4.35 mmol, 48%) without any further purification.

R_f 0.25 (DCM / MeOH, 95:5).

^{1}H NMR (400 MHz, $CDCl_3$) δ_H 9.96 (s, 1H, N*H*), 8.98-8.27 (m, 1H, Ar*H*), 8.24-7.57 (m, 3H, Ar*H*), 4.70 (s, 2H, CH_2Br).

Analytical data matches that previously reported.[169]

4-(Iodomethyl)phthalazin-1(2H)-one, 151



4-(Bromomethyl)phthalazin-1(2*H*)-one **150** (200 mg, 0.84 mmol, 1.00 equiv.), NaI (376 mg, 2.51 mmol, 3.0 equiv.) and acetone (8 mL) were submitted to *General procedure X* under reflux for 20 h. Purification by column chromatography (SiO_2, DCM / MeOH, 95:5) afforded **151** (126 mg, 0.44 mmol, 52%) as a white solid.

R_f 0.25 (DCM / MeOH, 95:5).

^{1}H NMR (400 MHz, *d*$_6$-DMSO) δ_H 12.74 (s, 1H, N*H*), 8.45-7.98 (m, 3H), 7.95-7.82 (m, 2H), 4.84-4.78 (m, 2H).

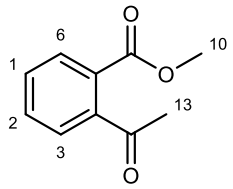
^{13}C NMR (101 MHz, *d*$_6$-DMSO) δ_C 159.4, 143.9, 133.5, 132.1, 127.8, 127.7, 126.2, 106.8, 2.4.

IR (thin film, ν_{max} / cm^{-1}). 3403, 2509, 1648, 1457.

HRMS (APCI, ESI, EI) Not found.

m.p. 205 – 210 °C.

Methyl 2-acetylbenzoate, 154



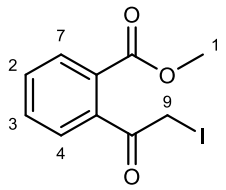
To a solution of 2-acetylbenzoic acid (2.00 g, 12.0 mmol, 1.0 equiv.) and K_2CO_3 (2.50 g, 18.0 mmol, 1.5 equiv.) in DMF (10 mL) was added MeI (2.24 mL, 36.0 mmol, 3.0 equiv.) in DMF (8 mL) over 10 min. The reaction mixture was stirred for 3 h the concentrated *in vacuo.* The residue was dissolved in DCM (120 mL) and washed with H_2O (3 × 30 mL). The organic layer was dried over anhydrous Na_2SO_4, filtered and concentrated *in vacuo*. Purification by column chromatography (SiO_2, pentane / EtOAc, 8:2) afforded **154** (1.43 g, 8.03 mmol, 67%) as a colorless oil.

R$_f$ 0.47 (pentane / EtOAc, 7:3).

^{1}H NMR (400 MHz, $CDCl_3$) δ_H 7.89-7.82 (m, 1H, Ar*H*), 7.57 (app. td, *J* = 7.6, 1.4 Hz, 1H, Ar*H*), 7.50 (app. td, *J* = 7.6, 1.4 Hz, 1H, Ar*H*), 7.46-7.39 (m, 1H, Ar*H*), 3.90 (s, 3H, H10), 2.54 (s, 3H, H13).

Analytical data matches that previously reported. [170]

Methyl 2-(2-iodoacetyl)benzoate, 155



A solution of methyl 2-acetylbenzoate (1.43 g, 8.00 mmol, 1.0 equiv.), CuO (636 mg, 8.00 mmol, 1.0 equiv.) and I_2 (2.03 g, 8.00 mmol, 1.0 equiv.) in MeOH (30 mL) was heated at reflux for 3 h then concentrated *in vacuo.* The residue was taken up in EtOAc (30 mL), filtered, and washed with $Na_2S_2O_3$ solution (20 mL, 10% aq.), dried over $MgSO_4$, filtered and concentrated *in vacuo*. Purification by column chromatography (SiO_2, pentane / EtOAc, 8:2) followed by recrystallisation in hot *n*-hexane afforded **155** (830 mg, 2.73 mmol, 34%) as orange crystals.

R_f 0.44 (pentane / EtOAc, 7:3).

^{1}H NMR (400 MHz, $CDCl_3$) δ_H 7.98 (dd, *J* = 7.6, 1.0 Hz, 1H, Ar*H*), 7.61 (app. td, *J* = 7.6, 1.4 Hz, 1H, Ar*H*), 7.54 (app. td, *J* = 7.6, 1.4 Hz, 1H, Ar*H*), 7.48 (dd, *J* = 7.6, 1.0 Hz, 1H, Ar*H*), 4.27 (s, 2H, H9), 3.92 (s, 3H, H1).

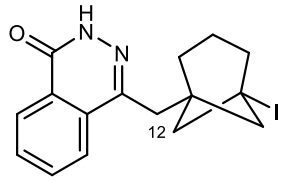
^{13}C NMR (101 MHz, $CDCl_3$) δ_C 198.6, 166.7, 140.5, 132.8, 130.4, 130.2, 129.0, 127.9, 53.0, 7.8.

IR (thin film, ν_{max} / cm^{-1}) 1713, 1435, 1285, 1115, 1081, 1007, 988, 962.

HRMS (ESI^+) calc. for $C_{10}H_{10}IO_3$ $[M+H]^+$ 304.9669, found 304.9670.

m.p. 49-51 °C.

4-((5-Iodobicyclo[3.1.1]heptan-1-yl)methyl)phthalazin-1(2H)-one, 156



Methyl 2-(2-(5-iodobicyclo[3.1.1]heptan-1-yl)acetyl)benzoate **155** (135 mg, 0.34 mmol, 1.00 equiv.), was dissolved in MeOH (3 mL). Hydrazine monohydrate (24 µL, N_2H_4 64-65 %, 0.50 mmol, 1.50 equiv.) was added dropwise at room temperature. The reaction mixture was stirred for 16 h at room temperature. Finally, the white precipitation was filtered off and triturated with cold *n*-pentane to obtain 7.7 mg (20 %) of **156** as a white solid without further purification.

R_f 0.26 (pentane / EtOAc, 85:15).

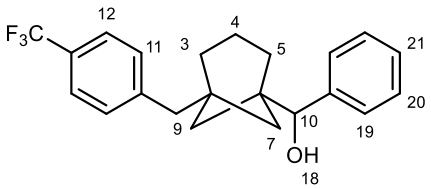
^{1}H NMR (400 MHz, $CDCl_3$) δ_H 10.49 (s, 1H, N*H*), 8.52 – 8.45 (m, 1H, *Ar*H), 7.82 (dqd, *J* = 15.0, 7.4, 1.4 Hz, 2H, *Ar*H), 7.75 – 7.70 (m, 1H, *Ar*H), 3.01 (s, 2H, H12), 2.62 – 2.56 (m, 2H), 2.52 (t, *J* = 7.1 Hz, 2H), 2.43 – 2.35 (m, 2H), 1.92 – 1.80 (m, 2H), 1.72 (t, *J* = 7.0 Hz, 2H).

^{13}C NMR (101 MHz, $CDCl_3$) δ_C 160.3, 145.0, 133.6, 131.6, 130.7, 128.2, 127.3, 125.1, 51.9, 46.3, 43.3, 41.2, 33.9, 31.9, 19.8.

IR (thin film, ν_{max} / cm^{-1}) 2940, 2910, 1674, 1336, 1147, 813, 781.

HRMS (ESI^+) calc. for $C_{16}H_{17}IN_2O$ $[M+H]^+$ 381.0458, found 381.0458.

5-(4-(Trifluoromethyl)benzyl)bicyclo[3.1.1]heptan-1-ol, 163



Preparation of Rieke Zinc metal

Lithium metal (42 mg, 6.12 mmol, 1.00 equiv., granular, 4-10 mesh particle size) was cut into to smaller pieces and approximately weighed in *n*-pentane and immediately immersed in anhydrous THF (3 mL). Naphthalene (800 mg, 6.23 mmol, 1.02 equiv.) was added under inert atmosphere. The mixture was stirred for 3 h at room temperature. In the meantime, $ZnCl_2$ (418 mg, 2.00 mmol, 3.06 equiv.) was weighed out, melted *in vacuo*, and dissolved in anhydrous THF under inert atmosphere. After 3 h this $ZnCl_2$-solution was transferred into the lithium naphthalenide solution *via* syringe slowly dropwise (every 3 seconds a drop). The mixture was stirred for further 20 min. Finally, stirring was stopped, the supernatant removed *via* syringe and refilled with a fresh portion of 3 mL of anhydrous THF assuming a concentration of c = 2 mmol / 3 mL = 0.67 M.

Zn-Insertion and trapping step

This Rieke Zn-solution (0.23 mL, 0.15 mmol, 2.00 equiv.) was added to a solution of **48** (29 mg, 0.076 mmol, 1.00 equiv.) in anhydrous THF (1 mL). The reaction mixture was stirred for 16 h at 50 °C under an inert atmosphere. Subsequently, benzaldehyde (24 μL, 0.23 mmol, 3.00 equiv.) was added. The reaction mixture was stirred at 50 °C for another 16 h. Finally, the reaction mixture was quenched with NH_4Cl (aq. sat., 1 mL), the organic layer dried over anhydrous Na_2SO_4, filtered and concentrated *in vacuo* to afford the crude reaction mixture. Purification by column chromatography (SiO_2, pentane / EtOAc, 8:2) afforded **163** (3 mg, 0.0076 mmol, 10%) as a yellow oil.

Rf 0.26 (pentane / EtOAc, 7:3).

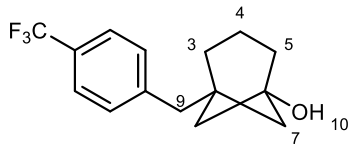
^{1}H NMR (400 MHz, $CDCl_3$) δ_H 7.94 (d, *J* = 7.4 Hz, 2H, Ar*H*), 7.58 (t, *J* = 7.4 Hz, 2H, Ar*H*), 7.48 (t, *J* = 7.7 Hz, 1H, Ar*H*), 7.31 (m, 4H, Ar*H*), 3.08 (s, 2H, H9), 2.05 – 1.95 (m, 2H, H7), 1.88 – 1.81 (m, 4H, H3/H4/H5), 1.79 – 1.73 (m, 2H, H7), 1.72 – 1.68 (m, 1H, H10), 1.65 (t, *J* = 6.5 Hz, 2H, H3/H4/H5), 1.28 (s, 1H, O*H*).

^{13}C NMR (101 MHz, $CDCl_3$) δ_C *not enough material available.*

IR (thin film, ν_{max} / cm^{-1}) 3408, 2945, 1676, 1449, 1324, 1260, 1217, 1056, 692.

HRMS (APCI, ESI, EI) Not found.

5-(4-(trifluoromethyl)benzyl)bicyclo[3.1.1]heptan-1-o via Rieke metal, 139



Preparation of Rieke Zinc metal

See procedure for **163**.

Zn-Insertion and trapping step

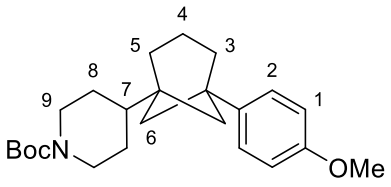
This Rieke Zn-solution (0.23 mL, 0.15 mmol, 2.00 equiv.) was added to a solution of **48** (29 mg, 0.076 mmol, 1.00 equiv.) in anhydrous THF (1 mL). The reaction mixture was stirred for 16 h at 50 °C under an inert atmosphere. Subsequently, benzaldehyde (8.0 µL, 0.076 mmol, 1.00 equiv.) or allylbromide (6.6 µL, 0.076 mmol, 1.00 equiv.) and CuCN (7 mg, 0.076 mmol, 1.00 equiv.) were added. The reaction mixture was stirred at 50 °C for another 16 h. Finally, the reaction mixture was quenched with NH_4Cl (aq. sat., 1 mL), the organic layer dried over anhydrous Na_2SO_4, filtered and concentrated *in vacuo* to afford the crude reaction mixture. Purification by column chromatography (SiO_2, pentane / EtOAc, 95:5) afforded **139** (6 mg, 0.021 mmol, 28%) as a yellow oil.

*Characterisation data identical with the ones reported for **139** on p. 213/214.*

5.7. Kumada-cross coupling products (Section 3.3.5)

Tert-butyl 4-(5-(4-methoxyphenyl)bicyclo[3.1.1]heptan-1-yl)piperidine-1-carboxylate, 164

This compound was synthesised and characterised by Bethany Shire.



4-Methoxyphenylmagnesium bromide

4-Bromoanisole (0.38 mL, 3.0 mmol, 1.0 equiv.) and Mg turnings (88 mg, 3.6 mmol, 1.2 equiv.) were submitted to *General procedure 7* to give 4-methoxyphenylmagnesium bromide as a 1.3 M solution in THF.

50 (41 mg, 0.10 mmol, 1.0 equiv.), $Fe(acac)_3$ (7.1 mg, 0.02 mmol, 0.2 equiv.), TMEDA (6.0 μL, 0.04 mmol, 0.4 equiv.) and 4-methoxyphenylmagnesium bromide (0.12 mL, 1.3 M in THF, 0.16 mmol, 1.6 equiv.) were submitted to *General procedure 9* at room temperature. Purification by column chromatography (SiO_2, pentane / EtOAc, 95:5) afforded **164** (36 mg, 0.094 mmol, 94%) as a white solid.

R_f 0.41 (pentane / EtOAc, 9:1).

^{1}H NMR (400 MHz, $CDCl_3$) δ_H 7.07-6.97 (m,), 6.86-6.80 (m, 2H, Ar*H*), 4.15 (app. s, 2H, H9), 3.78 (s, 3H, O*Me*), 2.63-2.51 (m, 2H, H9), 1.92-1.76 (m, 6H, H6, H5/H4/H3), 1.71 (dt, *J* = 6.6, 3.6 Hz, 2H, H6), 1.62 (t, *J* = 6.5 Hz, 2H, H5/H4/H3), 1.53-1.46 (m, 2H, H8), 1.45 (s, 9H, *t*-Bu), 1.30-1.20 (m, 1H, H7), 1.13 (qd, *J* = 12.2, 4.3 Hz, 2H, H8).

^{13}C NMR (101 MHz, $CDCl_3$) δ_C 157.5, 155.0, 143.3, 126.0, 113.7, 79.3, 55.4, 46.2, 44.5, 42.0, 41.5, 40.4, 38.1, 29.8, 28.6, 26.5, 17.8.

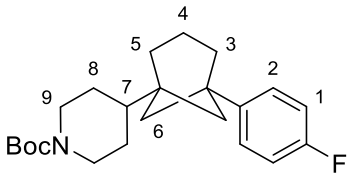
IR (thin film, ν_{max} / cm^{-1}) 2936, 2854, 2360, 1691, 1580, 1448, 1243, 1170, 826.

HRMS (ESI^+) calc. for $C_{24}H_{35}O_3NNa$ $[M+Na]^+$ 408.2509, found 408.2509.

m.p. 59-61 °C.

Tert-butyl 4-(5-(4-fluorophenyl)bicyclo[3.1.1]heptan-1-yl)piperidine-1-carboxylate, 165

This compound was synthesised and characterised by Bethany Shire.



4-Fluorophenylmagnesium bromide

1-Bromo-4-fluorobenzene (0.33 mL, 3.0 mmol, 1.0 equiv.) and Mg turnings (88 mg, 3.6 mmol, 1.2 equiv.) were submitted to *General Procedure XII* at room temperature for 1 h to give 4-fluorophenylmagnesium bromide as a 0.67 M solution in THF.

50 (41 mg, 0.10 mmol, 1.0 equiv.), $Fe(acac)_3$ (7.1 mg, 0.02 mmol, 0.2 equiv.), TMEDA (6.0 μL, 0.04 mmol, 0.4 equiv.) and 4-fluorophenylmagnesium bromide (0.24 mL, 0.67 M in THF, 0.16 mmol, 1.6 equiv.) were submitted to *General procedure 9* at room temperature. Purification by column chromatography (SiO_2, pentane / diethyl ether, 9:1) afforded **165** (37 mg, 0.098 mmol, 98%) as a white gum.

R_f 0.23 (pentane / EtOAc, 9:1)

^{1}H NMR (400 MHz, $CDCl_3$) δ_H 7.06-7.00 (m, 2H, Ar*H*), 6.98-6.92 (m, 2H, Ar*H*), 4.15 (app. s, 2H, H9), 2.57 (app. t, *J* = 12.6 Hz, 2H, H9), 1.90-1.78 (m, 6H, H6, H5/H4/H3), 1.71 (dt, *J* = 6.5, 3.7 Hz, 2H, H6), 1.63 (t, *J* = 6.8 Hz, 2H, H5/H4/H3), 1.52-1.48 (m, 2H, H8), 1.45 (s, 9H, *t*-Bu), 1.31-1.20 (m, 1H, H7), 1.13 (qd, *J* = 12.3, 4.4 Hz, 2H, H8).

^{13}C NMR (101 MHz, $CDCl_3$) δ_C 161.0 (d, ^1J = 242.9 Hz), 155.0, 146.7 (d, ^3J = 3.0 Hz), 126.4 (d, ^2J = 7.7 Hz), 114.9 (d, *J* = 21.0 Hz), 79.3, 46.2, 44.5, 42.1, 41.5, 40.3, 38.1, 29.7, 28.6, 26.5, 17.7.

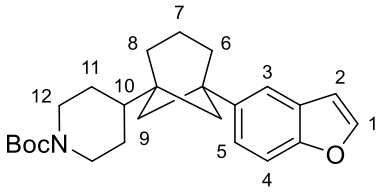
^{19}F NMR (377 MHz, $CDCl_3$) δ_F –118.32.

IR (thin film, ν_{max} / cm^{-1}) 3650, 2980, 2856, 2360, 2340, 1692, 1510, 1424, 1244, 1163, 830.

HRMS (ESI^+) calc. for $C_{23}H_{32}O_2NFNa$ $[M+Na]^+$ 396.2309, found 396.2309.

Tert-butyl 4-(5-(benzofuran-5-yl)bicyclo[3.1.1]heptan-1-yl)piperidine-1-carboxylate, 166

This compound was synthesised and characterised by Bethany Shire.



Benzofuran-5-ylmagnesium bromide lithium chloride complex

5-Bromobenzofuran (0.38 mL, 3.0 mmol, 1.0 equiv.), Mg turnings (120 mg, 4.9 mmol, 1.7 equiv.) and LiCl (153 mg, 3.6 mmol, 1.2 equiv.) were submitted to *General procedure*

8 at 65 °C for 2 h to give benzofuran-5-yl magnesium bromide lithium chloride complex as a 1.1 M solution in THF.

50 (41 mg, 0.10 mmol, 1.0 equiv.), $Fe(acac)_3$ (7.1 mg, 0.02 mmol, 0.2 equiv.), TMEDA (6.0 μL, 0.04 mmol, 0.4 equiv.) and benzofuran-5-yl magnesium bromide lithium chloride complex (0.15 mL, 1.1 M in THF, 0.16 mmol, 1.6 equiv.) were submitted to *General procedure 9* at room temperature. Purification by column chromatography (SiO_2, pentane / EtOAc, 95:5) afforded **166** (28 mg, 0.072 mmol, 72%) as a pale-yellow solid.

R_f 0.46 (pentane / EtOAc, 9:1).

^{1}H NMR (400 MHz, $CDCl_3$) δ_H 7.59 (d, *J* = 2.2 Hz, 1H, Ar*H*), 7.41 (dt, *J* = 8.4, 0.7 Hz, 1H, Ar*H*), 7.29 (dd, *J* = 1.8, 0.7 Hz, 1H, Ar*H*), 7.04 (dd, *J* = 8.4, 1.8 Hz, 1H, Ar*H*), 6.71 (dd, *J* = 2.2, 1.0 Hz, 1H, Ar*H*), 4.23-4.08 (m, 2H, H12), 2.56 (m, 2H, H12), 1.95-1.84 (m, 6H, H9, H6/H7/H8), 1.78 (m, 2H, H9), 1.70-1.62 (m, 2H, H6/H7/H8), 1.53-1.47 (m, 2H, H11), 1.45 (s, *t*-Bu), 1.17 (m, 1H, H10), 0.89 (m, 2H, H11).

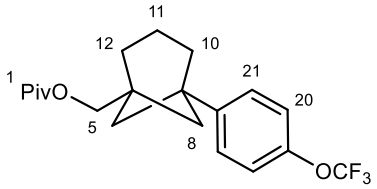
^{13}C NMR (101 MHz, $CDCl_3$) δ_C 155.0, 153.4, 145.9, 145.3, 127.3, 121.7, 117.1, 111.0, 106.6, 79.3, 46.2, 44.5, 42.7, 41.5, 40.6, 38.7, 29.9, 28.6, 26.5, 17.8.

IR (thin film, ν_{max} / cm^{-1}) 2927, 2854, 2359, 1693, 1424, 1169, 1032, 737.

HRMS (ESI^+) calc. for $C_{25}H_{33}O_3NNa$ $[M+Na]^+$ 418.2353, found 418.2353.

m.p. 67-69 °C.

(5-Iodobicyclo[3.1.1]heptan-1-yl)methyl pivalate, 167



(4-(Trifluoromethoxy)phenyl)magnesium bromide

1-Bromo-4-(trifluoromethoxy)benzene (0.45 mL, 3.00 mmol, 1.0 equiv.), Mg turnings (88 mg, 3.60 mmol, 1.20 equiv.) and anhydrous THF (2.5 mL) were subjected to *General procedure 7* for 2 h to give (4-(trifluoromethoxy)phenyl)magnesium bromide as a 0.73 M solution in THF.

52 (101 mg, 0.30 mmol, 1.0 equiv.), $Fe(acac)_3$ (21 mg, 0.06 mmol, 0.20 equiv.), TMEDA (18 µL, 0.12 mmol, 0.40 equiv.), (4-(trifluoromethoxy)phenyl)magnesium bromide (0.66 mL, 0.73 M in THF, 0.48 mmol, 1.60 equiv.) and anhydrous THF (0.40 mL) were submitted to *General procedure 9* at room temperature. Purification by column chromatography (SiO_2, pentane / EtOAc, gradient 100:0 to 99:1) afforded **167** (96 mg, 0.259 mmol, 86%) as yellow oil.

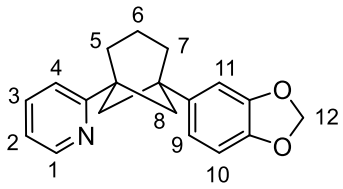
R_f 0.50 (pentane / EtOAc, 95:5).

^{1}H NMR (400 MHz, $CDCl_3$) δ_H 7.10 (t, J = 6.5 Hz, 4H, H20, H21), 3.90 (s, 2H, H5), 2.00-1.81 (m, 8H), 1.75 (app. t, J = 6.9 Hz, 2H, H10/12), 1.20 (s, 9H, *t*-Bu).

^{13}C NMR (101 MHz, $CDCl_3$) δ_C 178.6, 149.0, 147.3, 126.3, 120.9, 120.7 (q, ^1J = 256.7 Hz), 70.2, 42.8, 39.1, 38.9, 38.8, 37.6, 30.6, 27.4, 17.2.

IR (thin film, ν_{max} / cm^{-1}) 2949, 2862, 1730, 1510, 1260, 1223, 1160. **HRMS** (APCI, ESI, EI) Not found.

2-(5-(Benzo[d][1,3]dioxol-5-yl)bicyclo[3.1.1]heptan-1-yl)pyridine, 168



Benzo[d][1,3]dioxol-5-ylmagnesium bromide

1-Bromo-3,4-(methylenedioxy)benzene (0.36 mL, 3.00 mmol, 1.0 equiv.), Mg turnings (88 mg, 3.60 mmol, 1.20 equiv.) and anhydrous THF (2.5 mL) were subjected to *General procedure VII* for 2 h to give benzo[*d*][1,3]dioxol-5-ylmagnesium bromide as a 0.90 M solution in THF.

55 (60 mg, 0.20 mmol, 1.0 equiv.), $Fe(acac)_3$ (14 mg, 0.04 mmol, 0.20 equiv.), TMEDA (12 µL, 0.12 mmol, 0.40 equiv.), benzo[*d*][1,3]dioxol-5-ylmagnesium bromide (0.36 mL, 0.90 M in THF, 0.32 mmol, 1.60 equiv.) and anhydrous THF (0.20 mL) were submitted to *General procedure 9* at room temperature. Purification by column chromatography (SiO_2, pentane / EtOAc, gradient 9:1 to 4:1) afforded **168** (47 mg, 0.160 mmol, 80%) as a colourless oil.

R_f 0.34 (pentane / EtOAc, 4:1).

^{1}H NMR (400 MHz, $CDCl_3$) δ_H 8.53 (ddd, *J* = 4.9, 1.8, 1.0 Hz, 1H, H1), 7.59 (app. td, *J* = 7.7, 1.8 Hz, 1H, H3), 7.16-7.02 (m, 2H, H2, H4), 6.73 (d, *J* = 8.0 Hz, 1H, H10), 6.66 (d, *J* = 1.7 Hz, 1H, H11), 6.59 (dd, *J* = 8.0, 1.7 Hz, 1H, H9), 5.89 (s, 2H, H12), 2.35-2.24 (m, 4H, H8), 2.06-1.90 (m, 6H, H5, H6, H7).

^{13}C NMR (101 MHz, $CDCl_3$) δ_C 167.8, 149.2, 147.6, 145.4, 144.8, 136.4, 120.9, 119.5, 117.8, 108.1, 106.0, 100.9, 44.4, 42.5, 41.3, 37.6, 35.0, 17.7.

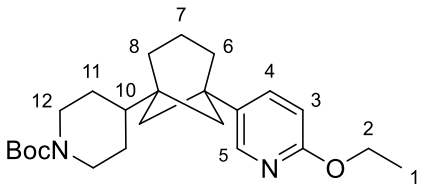
IR (thin film, ν_{max} / cm^{-1}) 2938, 2858, 1486, 1351, 1230, 1039, 936.

HRMS (ESI^+) calc. for $C_{19}H_{20}O_2N$ $[M+H]^+$ 294.1489, found 294.1485.

m.p. 43-45 °C.

Tert-butyl 4-(5-(6-ethoxypyridin-3-yl)bicyclo[3.1.1]heptan-1-yl)piperidine-1-carboxylate, 169

This compound was synthesised and characterised by Bethany Shire.



(6-Ethoxypyridin-3-yl)magnesium bromide lithium chloride complex

5-Bromo-2-ethoxypyridine (606 mg, 3.0 mmol, 1.0 equiv.), Mg turnings (146 mg, 6.0 mmol, 2.0 equiv.) and LiCl (153 mg, 3.6 mmol, 1.2 equiv.) were submitted to *General procedure 8* at 60 °C for 2 h to give (6-ethoxypyridin-3-yl)magnesium bromide lithium chloride complex as a 0.47 M solution in THF.

50 (41 mg, 0.10 mmol, 1.0 equiv.), $Fe(acac)_3$ (7.1 mg, 0.02 mmol, 0.20 equiv.), TMEDA (6.0 μL, 0.04 mmol, 0.4 equiv.) and (6-ethoxypyridin-3-yl)magnesium bromide lithium chloride complex (0.53 mL, 0.47 M in THF, 0.25 mmol, 2.5 equiv.) were submitted to *General procedure 9* at 45 °C. Purification by column chromatography (SiO_2, pentane / EtOAc, 95:5 to 80:20) afforded **169** (31 mg, 0.077 mmol, 77%) as a pale-yellow solid.

R_f 0.27 (pentane / EtOAc, 9:1)

^{1}H NMR (400 MHz, $CDCl_3$) δ_H 7.86 (d, *J* = 2.5 Hz,), 7.32 (dd, *J* = 8.5, 2.5 Hz, 1H, H4), 6.64 (d, *J* = 8.5 Hz, 1H, H3), 4.32 (q, *J* = 7.1 Hz, 2H, H2), 4.21-4.04 (m, 2H, H12), 2.57 (app. t, *J* = 12.7 Hz, 2H, H12), 1.84 (m, 6H, H9, H6/H7/H8), 1.71 (m, 2H, H9), 1.62 (m, 2H, H6/H7/H8), 1.49 (m, 2H, H11), 1.44 (s, 9H, *t*-Bu) 1.38 (t, *J* = 7.0 Hz, 3H, H1), 1.31-1.20 (m, 1H, H10), 1.13 (qd, *J* = 12.3, 4.3 Hz, 2H, H11).

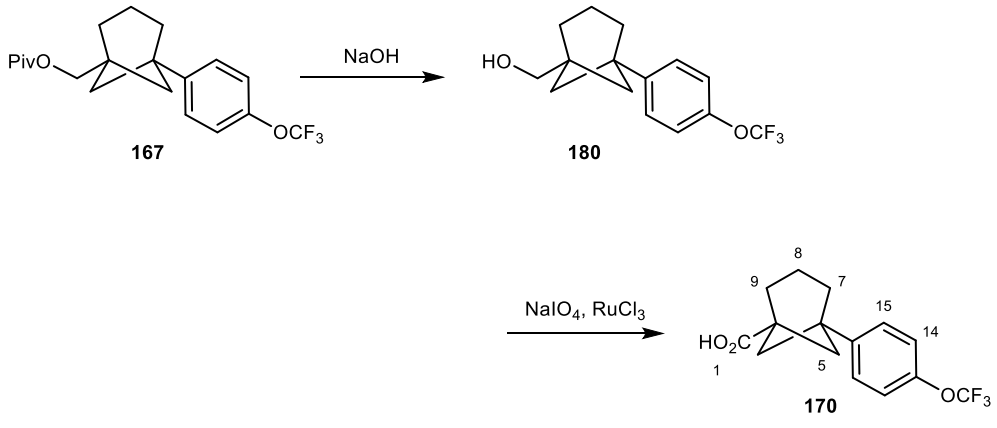
^{13}C NMR (101 MHz, $CDCl_3$) δ_C 162.1, 155.0, 143.2, 138.5, 136.1, 110.5, 79.3, 61.8, 46.2, 44.4, 42.1, 40.23, 40.21, 37.7, 29.8, 29.6, 28.6, 26.4, 17.6, 14.9.

IR (thin film, ν_{max} / cm^{-1}) 2975, 2934, 2855, 2360, 1692, 1607, 1493, 1315, 1166, 1043.

HRMS (ESI^+) calc. for $C_{24}H_{37}O_3N_2$ $[M+H]^+$ 401.2799, found 401.2798.

m.p. 77-79 °C.

5-(4-(Trifluoromethoxy)phenyl)bicyclo[3.1.1]heptane-1-carboxylic acid, 170



A solution of **167** (82 mg, 0.22 mmol, 1.0 equiv.) in MeOH (2.7 mL) was added NaOH (aq., 1M, 0.31 mL, 0.30 mmol, 1.4 equiv.) and the resulting mixture was heated at 50 °C for 20 h. The mixture was concentrated *in vacuo* and the residue was dissolved in EtOAc

(5 mL), then washed with H_2O (5 mL). The layers were separated and the aqueous layer was extracted with EtOAc (2 × 5 mL). The combined organic layers were dried (Na_2SO_4), filtered, and concentrated *in vacuo* to afford the alcoholic intermediate **180** (62 mg, 0.216 mmol, 98%) as a white solid which was used without further purification.

To a solution of **180** (62 mg, 0.22 mmol, 1.0 equiv.) in MeCN (0.27 mL), DCM (0.27 mL) and distilled water (0.54 mL) was added $NaIO_4$ (188 mg, 0.88 mmol, 4.0 equiv.) and $RuCl_3 \times H_2O$ (2.4 mg, 10.8 µmol, 0.05 equiv.). The resulting mixture was stirred for 3 h, then filtered through a pad of Celite which was subsequently rinsed with Et_2O and DCM. The filtrate was dried (Na_2SO_4), filtered, and concentrated *in vacuo*. 1 M NaOH (2 mL) was added to the residue and the aqueous layer was extracted with Et_2O (2 mL) which was then discarded, the aqueous layer was then acidified with 1 M HCl and then extracted with EtOAc (3 × 5 mL). The EtOAc layer was dried (Na_2SO_4), filtered, and concentrated *in vacuo* to afford **170** (45 mg, 0.150 mmol, 69%) as a white solid.

R_f 0.41 (pentane / EtOAc / AcOH, 70:29:1).

^{1}H NMR (400 MHz, $CDCl_3$) δ_H 7.19-7.06 (m, 4H, H15, H14), 2.39 (m, 2H, H5), 2.08 (m, 4H, H5, H7/9), 1.99-1.88 (m, 4H, H8, H7/9).

^{13}C NMR (101 MHz, $CDCl_3$) δ_C 181.7, 148.0, 147.5, 126.3, 120.7 (q, ^1J = 256.7 Hz), 121.0, 42.6, 42.3, 39.8, 36.7, 29.4, 16.9.

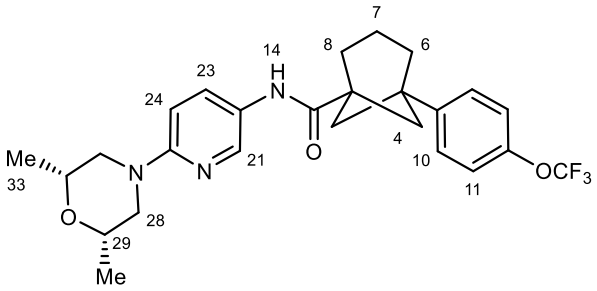
^{19}F NMR (377 MHz, $CDCl_3$) δ_F –57.9.

IR (thin film, ν_{max} / cm^{-1}) 2950, 2870, 1699, 1511, 1418, 1258, 1223, 1161.

HRMS (ESI^-) calc. for $C_{15}H_{14}F_3O_3$ $[M-H]^-$ 299.0901, found 299.0894.

m.p. 80-82 °C.

N-(6-((2R,6S)-2,6-Dimethylmorpholino)pyridin-3-yl)-5-(4-(trifluoromethoxy)phenyl)bicyclo[3.1.1]heptane-1-carboxamide, BCHep-Sonidegib



To a solution of **170** (11 mg, 0.037 mmol, 1.00 equiv.) in anhydrous DMF (0.2 mL) was added 1-hydroxybenzotriazole hydrate (7.1 mg, 0.046 mmol, 1.25 equiv.) and EDCI hydrochloride (8.8 mg, 0.046 mmol, 1.25 equiv.) and the resulting solution was stirred at room temperature for 1 h. In a separate flask, 6-((2*R*,6*S*)-2,6-dimethylmorpholino)pyridin-3-amine **14** (8.5 mg, 0.041 mmol, 1.11 equiv.) and 4-methylmorpholine (10.0 µL, 0.138 mmol, 2.50 equiv.) were dissolved in anhydrous DMF (0.1 mL) and the resulting solution was added dropwise to the first flask. The resulting mixture was stirred for 16 h at room temperature then EtOAc (1 mL) and distilled water (1 mL) was added to the reaction mixture. The layers were separated, and the organic layer was washed with brine and dried over anhydrous Na_2SO_4, filtered and concentrated *in vacuo*. Purification by column chromatography (SiO_2, pentane / EtOAc / HOAc, 50:49:1) afforded BCHep-Sonidegib (14 mg, 0.029 mmol, 77%) as a yellow solid.

R_f 0.28 (pentane / EtOAc, 6:4).

^{1}H NMR (400 MHz, $CDCl_3$) δ_H 8.11 (d, *J* = 2.7 Hz, 1H, H21), 7.87 (dd, *J* = 9.1, 2.7 Hz, 1H, H23), 7.20-7.08 (m, 4H, H10, H11), 6.96 (br s, 1H, NH), 6.61 (d, *J* = 9.1 Hz, 1H, H24), 3.98-3.93 (m, 2H, H28), 3.72 (app. dqd, *J* = 10.6, 6.2, 2.4 Hz, 2H, H29), 2.48 (dd, *J* = 12.6, 10.6 Hz, 2H, H28), 2.35 (m, 2H, H4), 2.17 (m, 2H, H4), 2.12 (m, 2H, H6/8),

2.12 (app. t, *J* = 6.9 Hz, 2H, H7), 1.93 (app. t, *J* = 6.9 Hz, 2H, H6/8), 1.25 (d, *J* = 6.2 Hz, 6H, H33).

^{13}C NMR (101 MHz, $CDCl_3$) δ_C 174.6, 156.9, 147.9, 147.5 (q, ^3J = 1.9 Hz), 140.3, 131.5, 126.3, 125.7, 121.1, 120.7 (q, ^1J = 256.6 Hz), 107.0, 71.7, 51.4, 44.4, 41.6, 39.7, 36.8, 31.2, 19.1, 17.1.

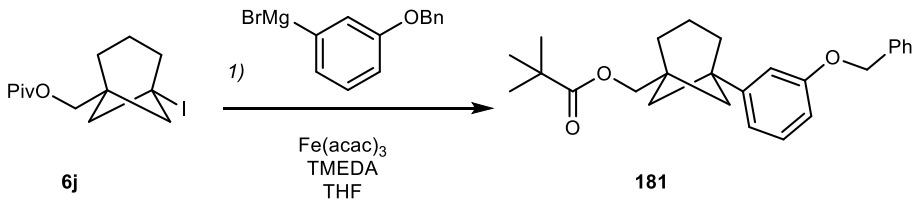
^{19}F NMR (470 MHz, $CDCl_3$) δ_F –57.9.

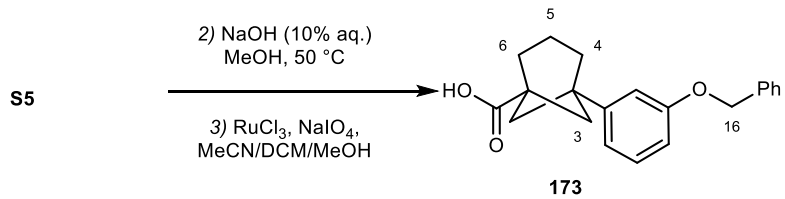
IR (thin film, ν_{max} / cm^{-1}) 3285, 2974, 2864, 1650, 1510, 1492, 1453, 1390, 1258, 1224, 1175, 1086.

HRMS (ESI^+) calc. for $C_{26}H_{31}F_3N_3O_3$ $[M+H]^+$ 490.2312, found 490.2307.

m.p. 214-217 °C.

(5-Iodobicyclo[3.1.1]heptan-1-yl)methyl pivalate, 173





1-(Benzyloxy)-3-bromobenzene (1.58 g, 6.00 mmol, 1.0 equiv.), Mg turnings (175 mg, 7.20 mmol, 1.2 equiv.) and anhydrous THF (5.0 mL) were subjected to *General*

procedure VII for 6 h to obtain a solution of (3-(benzyloxy)phenyl)magnesium bromide in THF. A concentration of 0.58 M was determined by iodometric titration.

52 (572 mg, 1.70 mmol, 1.0 equiv.), $Fe(acac)_3$ (120 mg, 0.34 mmol, 0.20 equiv.), TMEDA (102 µL, 0.68 mmol, 0.40 equiv.), (3-(benzyloxy)phenyl)magnesium bromide (4.7 mL, 0.58 M in THF, 2.72 mmol, 1.6 equiv.) and anhydrous THF (2.0 mL) were submitted to *General procedure 9* at room temperature. Purification by column chromatography (SiO_2, pentane / EtOAc, gradient 100:0 to 90:10) afforded a mixture of **181** and an aromatic byproduct (531 mg) as a white solid. This resulting mixture was used directly in the next step.

$\mathbf{R_f}$ 0.36 (pentane / EtOAc, 98:2)

To a solution of impure **181** (531 mg) in MeOH (16 mL) was added NaOH (aq., 1M, 1.80 mL, 1.8 mmol) and the resulting reaction mixture was heated at 50 °C for 20 h then concentrated *in vacuo*. To the resulting residue was added EtOAc (10 mL) and H_2O (10 mL) and the layers were separated. The aqueous layer was extracted with EtOAc (2 × 10 mL and the combined organic layers were dried over anhydrous Na_2SO_4, filtered and concentrated *in vacuo.* Purification *via* column chromatography (SiO_2, pentane / EtOAc, 7:3) afforded alcoholic intermediate (250 mg) as a white solid which was used directly in the next step.

$\mathbf{R_f}$ 0.46 (pentane / EtOAc, 6:4).

^{1}H NMR (400 MHz, $CDCl_3$) δ_H 7.48-7.41 (m, 2H), 7.43-7.34 (m, 2H), 7.37-7.28 (m, 1H), 7.22 (t, *J* = 8.0 Hz, 1H), 6.78 (ddd, *J* = 8.1, 2.6, 1.0 Hz, 1H), 6.77-6.69 (m, 2H), 5.05 (s, 2H), 3.44 (s, 2H), 2.02-1.84 (m, 6H), 1.85-1.76 (m, 2H), 1.73 (t, *J* = 6.6 Hz, 2H).

To a solution of the alcoholic intermediate (250 mg, 0.810 mmol, 1.0 equiv.) in MeCN (1.0 mL), DCM (1.0 mL) and distilled water (1.5 mL) were added $NaIO_4$ (693 mg, 3.24 mmol, 4.0 equiv.) and $RuCl_3 \times H_2O$ (9.0 mg, 40.0 µmol, 0.05 equiv.). The mixture was stirred for 3 h and filtered through a pad of Celite which was subsequently rinsed with DCM. The filtrate was dried over anhydrous Na_2SO_4, filtered, and concentrated *in vacuo* to afford **173** (200 mg, 0.620 mmol, 36% (over 3 steps)).

R_f 0.29 (pentane / EtOAc / HOAc, 70:29:1).

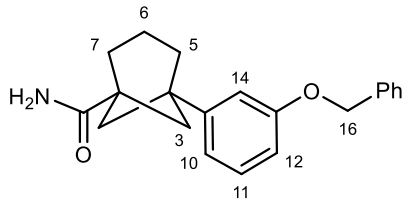
^{1}H NMR (400 MHz, $CDCl_3$) δ_H 7.45-7.31 (m, 5H, Ar*H*), 7.23 (t, *J* = 8.0 Hz, 1H, Ar*H*), 6.81 (dd, *J* = 8.0, 2.3 Hz, 1H, Ar*H*), 6.77-6.69 (m, 2H, Ar*H*), 5.05 (s, 2H, H16), 2.48-2.37 (m, 2H, H3), 2.16-1.87 (m, 8H, H4, H5, H6).

^{13}C NMR (101 MHz, $CDCl_3$) δ_C 182.1, 159.0, 151.1, 137.2, 129.5, 128.7, 128.1, 127.7, 117.6, 112.0, 111.8, 70.2, 42.7, 42.6, 39.8, 36.7, 29.5, 16.9.

IR (thin film, ν_{max} / cm^{-1}) 2947, 2916, 2867, 1696, 1609, 1581, 1454, 1294.

HRMS (ESI^-) calc. for $C_{21}H_{21}O_3$ $[M-H]^-$ 321.1496, found 321.1493.

5-(3-(Benzyloxy)phenyl)bicyclo[3.1.1]heptane-1-carboxamide, 174



A solution of **173** (200 mg, 0.62 mmol, 1.0 equiv.) and Et_3N (259 µL, 1.86 mmol, 3.0 equiv.) in anhydrous THF (7.4 mL) was cooled to 0 °C and ethyl chloroformate (83 µL, 0.87 mmol, 1.4 equiv.) was added dropwise. The reaction mixture was stirred for 30 min then a solution of NH_4Cl (0.93 mL, 1 M aq., 0.93 mmol, 1.5 equiv.) was added dropwise. The reaction mixture was stirred for further 30 min at 0 °C then distilled water (0.50 mL) was added and the solution was extracted with EtOAc (5 mL). The layers were separated, and the aqueous layer was extracted with EtOAc (5 mL). The combined organics were washed with brine, dried over $MgSO_4$, filtered and the organics removed *in vacuo.* Purification by column chromatography (SiO_2, pentane / EtOAc, 8:2) afforded **174** (175 mg, 0.544 mmol, 88%) as yellow oil.

R_f 0.41 (pentane / EtOAc / HOAc, 70:29:1).

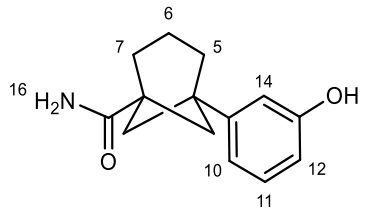
^{1}H NMR (500 MHz, $CDCl_3$) δ_H 7.47-7.28 (m, 5H, Ar*H*), 7.22 (t, *J* = 7.9 Hz, 1H, Ar*H*), 6.80 (ddd, *J* = 8.2, 2.5, 1.0 Hz, 1H, Ar*H*), 6.74-6.68 (m, 2H, Ar*H*), 5.40 (br. s, 2H, N*H*$_2$), 5.04 (s, 2H, H16), 2.27 (m, 2H, H3), 2.12-1.95 (m, 6H, H3, H6, H5/H7), 1.91 (t, *J* = 6.9 Hz, 2H, H5/7).

^{13}C NMR (126 MHz, $CDCl_3$) δ_C 179.1, 159.0, 151.1, 137.1, 129.5, 128.7, 128.1, 127.7, 117.6, 112.1, 111.7, 70.1, 43.5, 42.0, 39.7, 36.8, 31.1, 17.1.

IR (thin film, ν_{max} / cm^{-1}) 3350, 3191, 2945, 2914, 2862, 1656, 1607, 1581.

HRMS (ESI^+) calc. for $C_{21}H_{24}NO_2$ $[M+H]^+$ 322.1802, found 322.1801.

5-(3-(Benzyloxy)phenyl)bicyclo[3.1.1]heptane-1-carboxamide, 175



To a solution of **174** (175 mg, 0.54 mmol, 1.0 equiv.) and cyclohexene (2.1 mL, 20.5 mmol, 38 equiv.) in anhydrous 1,4-dioxane (6.0 mL) was added Pd/C (53 mg, 10 wt. % loading, 0.049 mmol, 9 mol%). The resulting mixture was heated at 70 °C for 12 h then another portion of Pd/C (53 mg, 10 wt. % loading, dry, 0.049 mmol, 9 mol%) was added and the reaction mixture heated for a further 12 h. The resulting mixture was cooled to room temperature, then filtered through a pad of celite and washed with 1,4-dioxane and ethanol. The combined organics were washed with brine, dried over $MgSO_4$, filtered and concentrated *in vacuo* to afford **175** (89 mg, 0.385 mmol, 71%) as a white solid which was used in the next step without further purification.

R_f 0.49 (EtOAc / MeOH, 95:5).

^{1}H NMR (400 MHz, *d*$_4$-MeOD) δ_H 7.08 (app. t, *J* = 7.8 Hz, 1H, H11), 6.59-6.51 (m, 3H, H10, H12, H14), 2.14 (m, 2H), 2.10-2.05 (m, 2H), 2.02-1.92 (m, 4H), 1.91-1.84 (m, 2H).

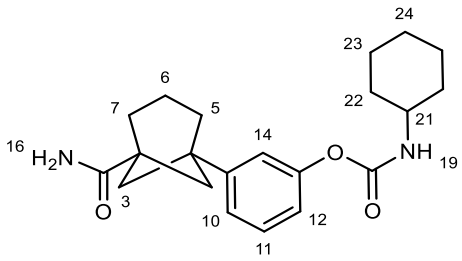
^{13}C NMR (101 MHz, *d*$_4$-MeOD) δ_C 182.9, 158.4, 152.6, 130.3, 116.9, 113.6, 112.6, 44.8, 42.6, 40.5, 37.9, 32.2, 17.9.

IR (thin film, ν_{max} / cm^{-1}) 2947, 2863, 2361, 2342, 1647, 1598, 1449, 987, 785, 733, 700.

HRMS (ESI^+) calc. for $C_{14}H_{18}NO_2$ $[M+H]^+$ 232.1332, found 232.1335.

m.p. 179 -181 °C.

3-(5-Carbamoylbicyclo[3.1.1]heptan-1-yl)phenyl cyclohexylcarbamate, BCHep-URB597



To a solution of **175** (19 mg, 0.084 mmol, 1.0 equiv.) and anhydrous NEt_3 (15 μL, 0.11 mmol, 1.3 equiv.) in anhydrous MeCN (0.45 mL) was added a solution of cyclohexylisocyanate (20 μL, 0.16 mmol, 1.9 equiv.) in anhydrous MeCN (0.30 mL) dropwise. The resulting mixture was stirred for 2 h then filtered through sintered funnel, the precipitate was then triturated with *n*-pentane and dried *in vacuo* to afford BCHep-URB597 (21 mg, 0.059 mmol, 70%) as a white solid.

R_f 0.10 (DCM / MeOH, 95:5).

^{1}H NMR (500 MHz, $CDCl_3$) δ_H 7.25 (t, *J* = 8.2 Hz, 1H, H11), 6.97-6.87 (m, 2H, H10, H12), 6.85 (app. t, *J* = 2.0 Hz, 1H, H14), 5.69 (br. s, 1H, N*H*$_2$), 5.58 (br. s, 1H, N*H*$_2$), 4.97 (br. s, 1H, N*H*), 3.61-3.48 (m, 1H, H21), 2.31-2.21 (m, 2H, H3), 2.10-1.86 (m, 10H), 1.77-1.68 (m, 2H), 1.66-1.57 (m, 1H), 1.45-1.28 (m, 2H), 1.28-1.11 (m, 3H).

^{13}C NMR (126 MHz, $CDCl_3$) δ_C 179.2, 153.9, 151.2, 150.8, 129.2, 121.7, 119.1, 118.3, 50.3, 43.5, 41.8, 39.7, 36.6, 33.4, 31.0, 25.6, 24.9, 17.0.

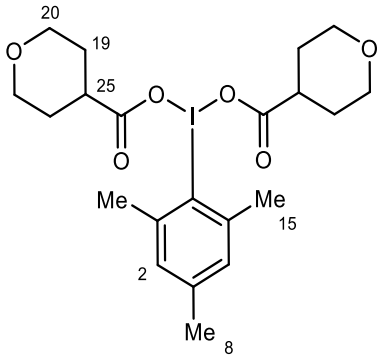
IR (thin film, ν_{max} / cm^{-1}) 3326, 3192, 2933, 2857, 1716, 1656, 1530, 1229, 1187, 1019, 732, 698.

HRMS (ESI^+) calc. for $C_{21}H_{29}N_2O_3$ $[M+H]^+$ 357.2173, found 357.2172.

m.p. 166-168 °C.

5.8. Preparation of starting material

Mesityl-λ^3-iodanediyl bis(tetrahydro-2H-pyran-4-carboxylate), 182



Mesityl-λ^3-iodanediyl diacetate (364 mg, 1.00 mmol, 1.0 equiv.), tetrahydro-2*H*-pyran-4-carboxylic acid (274 mg, 2.10 mmol, 1.05 mmol) and toluene (20 mL) were submitted to *General procedure 4* to obtain 499 mg of **182** (499 mg, 0.99 mmol, 99%) as a white solid.

Prepared according to a literature procedure. [106]

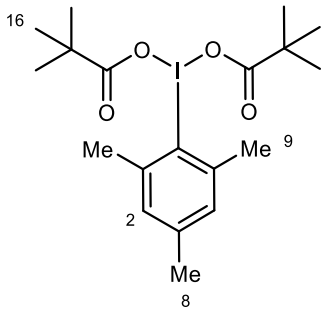
R$_f$ 0.05 (DCM / MeOH, 9:1).

^{1}H NMR (400 MHz, $CDCl_3$) δ_H 7.08 (s, 2H, H2), 3.85 (dt, *J* = 11.6, 3.7 Hz, 4H, H20), 3.34 (ddd, *J* = 11.6, 10.3, 3.3 Hz, 4H, H20), 2.70 (s, 6H, H15), 2.53-2.38 (m, 2H, H25), 2.36 (s, 3H, H8), 1.76-1.58 (m, 8H, H19).

^{13}C NMR (101 MHz, $CDCl_3$) δ_C 179.4, 143.3, 141.4, 130.1, 129.1, 67.3, 40.1, 29.5, 26.7, 21.3.

Analytical data matches that previously reported. [106]

Mesityl-λ^3-iodanediyl bis(2,2-dimethylpropanoate), 183



Mesityl-λ^3-iodanediyl diacetate (364 mg, 1.00 mmol, 1.0 equiv.), pivalic acid (0.242 mL, 2.10 mmol, 1.05 mmol) and toluene (20 mL) were submitted to *General procedure 4* to obtain **183** (440 mg, 0.812 mmol, 81%) as a yellow oil.

Prepared according to a literature procedure. [52]

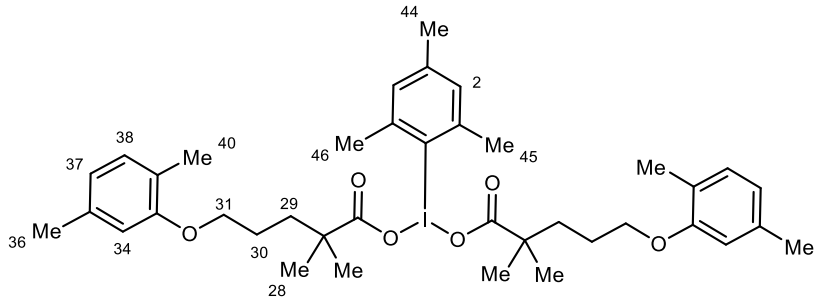
R$_f$ 0.05 (DCM / MeOH, 9:1).

^{1}H NMR (400 MHz, $CDCl_3$) δ_H 7.06 (br. s, 2H, H2), 2.70 (s, 6H, H9), 2.35 (s, 3H, H8), 1.06 (s, 18H, H16).

^{13}C NMR (101 MHz, $CDCl_3$) δ_C 183.6, 142.6, 141.4, 130.3, 128.8, 39.2, 27.9, 26.5, 21.3.

Analytical data matches that previously reported. [52]

Mesityl-λ^3-iodanediyl bis(5-(2,5-dimethylphenoxy)-2,2-dimethylpentanoate), 184



Mesityl-λ^3-iodanediyl diacetate (364 mg, 1.0 mmol, 1.0 equiv.), 5-(2,5-dimethylphenoxy)-2,2-dimethylpentanoic acid (526 mg, 2.10 mmol, 1.05 equiv.) and toluene (20 mL) were submitted to *General procedure 4* to obtain **184** (743 mg, 0.998 mmol, 99%) as a yellow oil.

R_f 0.05 (DCM / MeOH, 9:1).

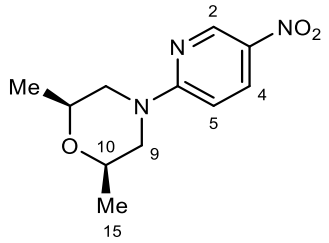
^{1}H NMR (400 MHz, $CDCl_3$) δ_H 7.00 (s, 3H, Ar*H*), 6.99 (s, 1H, Ar*H*), 6.65 (d, J = 7.4 Hz, 2H, Ar*H*), 6.56 (s, 2H, Ar*H*), 3.77 (t, *J* = 5.6 Hz, 4H, H31), 2.70 (s, 6H, Ar*Me*), 2.31 (s, 6H, Ar*Me*), 2.28 (s, 3H, H44), 2.13 (s, 6H, Ar*Me*), 1.61-1.49 (m, 8H, H30, H29), 1.09 (s, 12H, H28).

^{13}C NMR (101 MHz, $CDCl_3$) δ_C 182.6, 157.2, 142.8, 141.3, 136.6, 131.0, 130.4, 128.8, 123.7, 120.8, 112.1, 68.2, 42.6, 37.8, 26.6, 25.9, 25.5, 21.6, 21.2, 15.9.

IR (thin film, ν_{max} / cm^{-1}) 2955, 2922, 1645, 1509, 1471, 1364, 1264, 1200, 1156, 1130, 1045, 778.

HRMS (APCI, ESI, EI) Not found.

(2R,6S)-2,6-Dimethyl-4-(5-nitropyridin-2-yl)morpholine, 185



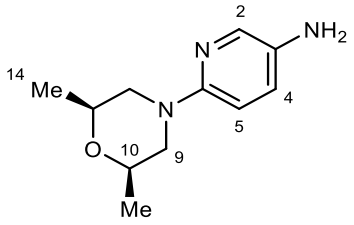
A solution of 2-chloro-5-nitro-pyridine (2.79 g, 17.6 mmol, 1.0 equiv.), *cis*-2,6-dimethylmorpholine (2.03 g, 17.6 mmol, 1.0 equiv.) and K_2CO_3 (4.86 g, 35.2 mmol, 2.0 equiv.) in anhydrous DMF (15 mL) was heated at 50 °C for 20 h then concentrated *in vacuo*. The resulting mixture was partitioned between EtOAc and water, the layers were separated and the organic layer was dried over anhydrous Na_2SO_4, filtered, and concentrated *in vacuo.* Purification by column chromatography (SiO_2, pentane / EtOAc, gradient 80:20 to 60:40, dry load) afforded **185** (3.76 g, 0.016 mmol, 90%) as a yellow solid.

R_f 0.50 (pentane / EtOAc, 7:3).

^{1}H NMR (400 MHz, d_6-DMSO) δ_H 8.96 (d, *J* = 2.8 Hz, 1H, H2), 8.24 (dd, *J* = 9.6, 2.8 Hz, 1H, H4), 6.98 (d, *J* = 9.6 Hz, 1H, H5), 4.43 (d, *J* = 13.1 Hz, 2H, H9), 3.58 (dtd, *J* = 12.5, 6.2, 2.6 Hz, 2H, H10), 2.65 (dd, *J* = 13.1, 10.6 Hz, 2H, H9), 1.16 (d, *J* = 6.2 Hz, 6H, H15).

Analytical data matches that previously reported. [171]

6-((2R,6S)-2,6-Dimethylmorpholino)pyridin-3-amine, 171



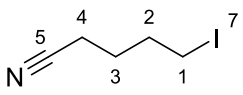
To a solution of **185** (1.00 g, 4.22 mmol, 1.0 equiv.) in anhydrous MeOH (16 mL) was added 10% Pd/C (135 mg, 0.127 mmol, 3 mol%). The flask was evacuated and flushed with H_2 (g) three times and then maintained at room temperature for 16 h. The suspension was filtered through Celite and concentrated *in vacuo*. Purification by column chromatography (SiO_2, EtOAc / MeOH, 9:1) afforded **171** (310 mg, 1.50 mmol, 35%) as a brown oil.

R_f 0.34 (EtOAc / MeOH, 9:1).

^{1}H NMR (400 MHz, $CDCl_3$) δ_H 7.79 (d, *J* = 2.9 Hz, 1H, H2), 6.99 (dd, *J* = 8.8, 2.9 Hz, 1H, H4), 6.55 (d, *J* = 8.8 Hz, 1H, H5), 3.89-3.77 (m, 2H, H9), 3.75 (dtd, *J* = 12.6, 6.2, 2.4 Hz, 2H, H10), 3.31 (s, 2H, N*H*$_2$), 2.41 (dd, *J* = 12.1, 10.3 Hz, 2H, H9), 1.25 (d, *J* = 6.2 Hz, 6H, H14).

Analytical data matches that previously reported. [172]

5-Iodopentanenitrile, 186



5-Iodopentanenitrile (30 mg, 0.15 mmol, 1.00 equiv.), NaI (0.74 mL, 0.23 M in *n*-Bu_2O, 0.225 mmol, 1.5 equiv.) and acetone (1.5 mL) were submitted to *General procedure X* at

25 °C for 20 h. Purification by column chromatography (SiO_2, pentane / EtOAc, 95:5) afforded **186** (20 mg, 0.096 mmol, 64%) as a yellow oil.

R_f 0.25 (pentane / EtOAc, 9:1)

^{1}H NMR (400 MHz, $CDCl_3$) δ_H 3.21 (t, J = 6.6 Hz, 2H, H1), 2.39 (t, J = 7.0 Hz, 2H, H4), 2.07 – 1.92 (m, 2H, H2/H3), 1.88 – 1.74 (m, 2H, H2/H3).

^{13}C NMR (101 MHz, $CDCl_3$) δ_C 119.2, 31.9, 26.3, 16.4, 4.5.

Analytical data matches that previously reported.[173]

5.9. Evaluation of ADME properties (Section 3.4)

These ADME studies were independently performed by WuXi AppTec (Shanghai, China).

Molecular properties (MW, clogP, TPSA) were calculated with ChemAxon 22.9. Selected compounds were screened for aqueous solubility in PBS (pH 7.4), metabolic stability in mouse liver microsomes (MLM) as a measure of clearance and finally inhibition of representative CYP450 enzymes.

Kinetic Solubility Studies in 50 mM Phosphate Buffer at pH 7.4

Medium

Preparation of 50 mM phosphate buffer (PB) with the pH at pH 7.4:

50 mM NaH_2PO_4: Dissolved 3.000 g of NaH_2PO_4 with 500 mL of water; the measured pH was about 4.5.

50 mM Na_2HPO_4: Dissolved 3.549 g of Na_2HPO_4 with 500 mL of water; the measured pH was about 9.4.

50 mM PB (pH 7.4): 15 mL of 50 mM Na_2HPO_4 was added into a 50 mL tube, and then adjusted pH to 7.4 with 50 mM NaH_2PO_4.

Experimental Procedure

10 μL of 10 mM of the test and control compounds in DMSO was added into the lower chambers of Whatman miniuniprep vials followed by 490 μL of 50 mM PB (pH 7.4) into the lower chambers of the Whatman miniuniprep vials, respectively. The samples were vortexed for at least 2 min. The vials were shaken for 24 h at room temperature (800 rpm),

then centrifuged for 20 min (4000 rpm) and compressed to prepare the filtrates for injection into the UPLC system in order to calculate the concentrations with a standard curve.

Miniuniprep (PTFE Filter Media with Polypropylene Housing) with Cat. No.UN203NPUORG purchased from GE Healthcare Whatman

Data Analysis method

Column: ACQUTY UPLC BEH C18 1.7 µm 50 mm

Mobile Phase A: 0.1% TFA and 5 mM NH_4OAc in water/ACN (v:v, 95:5)

Mobile Phase B: 0.1% TFA and 5 mM NH_4OAc in water/ACN (v:v, 5:95)

Results

Table 8. Kinetic solubility data. '<' means BQL (Below the lower limit of quantitation).

Compound ID	Batch	Media	Visual Appearance	Kinetic Solubility (µM)	Kinetic Solubility (µg/mL)
URB597	URB597	PB (pH 7.4)	many visible particles	<1.56	<0.529
Sonidegib	Sonidegib	PB (pH 7.4)	many visible particles	<1.56	<0.759
BCH-Sonidegib	BCH-Sonidegib	PB (pH 7.4)	many visible particles	<1.56	<0.765

Metabolic Stability in Mouse Liver Microsomes

Experimental procedure

Working solution: 5 μL of compound and control stock solution (10 mM in dimethyl sulfoxide (DMSO)) were diluted with 495 μL of MeCN (intermediate solution concentration: 100 μM, 99% CAN).

NADPH Cofactor Preparation

NADPH powder: β-Nicotinamide adenine dinucleotide phosphate reduced form, tetrasodium salt; NADPH·4Na (Vendor: BONTAC, Cat. No. BT04). The appropriate amount of NADPH powder was weighed and diluted into a 10 mM $MgCl_2$ solution (working solution concentration: 10 mM; final concentration in reaction system: 1 mM).

Liver Microsomes Preparation

The appropriate concentrations of microsome working solutions were prepared in 100 mM potassium phosphate buffer.

Table 9. Specification of Liver Microsomes.

Species	Product Information	Vendor	Abbreviation
CD-1 Mouse	Cat No. M1000 Lot No. 2110092	Xenotech	MLM

Stop Solution Preparation

Cold (4 °C) acetonitrile (MeCN) containing 200 ng/mL tolbutamide and 200 ng/mL labetalol as internal standards (IS) was used as the stop solution.

Assay Procedure

1. Pre-warm empty 'Incubation' plates T60 and NCF60 for 10 min.
2. Dilute liver microsomes to 0.56 mg/mL in 100 mM phosphate buffer.
3. Transfer 445 µL microsome working solutions (0.56 mg/mL) into pre-warmed 'Incubation' plates T60 and NCF60.
4. Pre-incubate 'Incubation' plates T60 and NCF60 for 10 min at 37°C with constant shaking.
5. Transfer 54 µL liver microsomes to blank plate.
6. Add 6 µL NAPDH cofactor to blank plate
7. Add 180 µL quenching solution to blank plate.
8. Add 5 µL compound working solution (100 µM) into 'incubation' plates (T60 and NCF60) containing microsomes and mix 3 times thoroughly.
9. For the NCF60 plate, add 50 µL of buffer and mix 3 times thoroughly.
10. Start timing; plate will be incubated at 37°C for 60 min while shaking.
11. In 'Quenching' plate T0, add 180 µL quenching solution and 6 µL NAPDH cofactor. Ensure the plate is chilled to prevent evaporation.
12. For the T60 plate, mix 3 times thoroughly, and immediately remove 54 µL mixture for the 0-min time point to 'Quenching' plate.
13. Add 44 µL NAPDH cofactor to incubation plate (T60).
14. Start timing; plate will be incubated at 37°C for 60 min while shaking.

Table 10. Final concentration of each component in the incubation medium.

Component	Concentration
Microsome	0.5 mg protein/mL
Test Compound	1 μM
Control Compound	1 μM
Acetonitrile	0.99%
DMSO	0.01%

At 5, 15, 30, 45, and 60 min, 180 μL of the quenching solution was added to the 'Quenching' plates. The solution was mixed once, and serially transfer 60 μL sample from T60 plate per time point to 'Quenching' plates.

Table 11. Reaction Plate Incubations.

Time Point	Start Time	End Time
Blank	1:00:00	0:00:00
T60	1:00:00	0:00:00
T45	0:45:00	0:00:00
T30	0:30:00	0:00:00
T15	0:15:00	0:00:00
T5	0:05:00	0:00:00
T0	mix 3 times and remove out to 'Quenching' plate	

For NCF60: mix once, and transfer 60 μL sample from the NCF60 incubation to 'Quenching' plate containing quenching solution at the 60-min time point.

Table 12. NCF60 Incubation.

Time Point	Start Time	End Time
NCF60	1:00:00	0:00:00

All sampling plates were shaken for 10 min, then centrifuged (4000 rpm, 20 min, 4°C). 80 µL supernatant was transferred into 240 µL HPLC water, and mixed using plate shaker for 10 min. Each bioanalysis plate was sealed and shaken for 10 min prior to LC-MS/MS analysis.

Data Analysis

First order kinetics (Eq. 1) was used to calculate $T_{1/2}$ and $CL_{int(mic)}$ (µL/min/mg):

$$C_t = \frac{1}{2}C_0 = C_0 \exp(-k_c \cdot t) \quad \text{(VIII)}$$

When $C_t = 0.5\ C_0$ the half life $T_{1/2}$ can be determined:

$$T_{1/2} = ln(2) \cdot \frac{1}{k_e} = \frac{0.693}{k_e} \quad \text{(IX)}$$

Intrinsic clearance $CL_{int(mic)} = \frac{0.693}{T_{1/2}\ (in\ vitro)} \cdot \frac{1}{mg/mL\ microsomal\ protein\ in\ reaction\ system}$ (X)

$$CL_{int(liver)} = CL_{int(mic)} \cdot \frac{mg\ microsomes}{g\ liver} \cdot \frac{g\ liver}{kg\ body\ weight} \quad \text{(XI)}$$

Results

Table 13. Summary of the Metabolic Stability in Mouse Liver Microsomes results. NCF: no co-factor added. No NADPH is added to NCF samples (replaced by buffer) during the 60 minute incubation. If the NCF remaining is less than 60%, then possibly non-NADPH dependent metabolism occurs. R2: correlation coefficient of the linear regression for the determination of kinetic constant.

			MLM 0.5			
Sample Name	**R2**	**T1/2 [min]**	**CLint(mic) [µL/min/mg]**	**CLint(liver) [mL/min/kg]**	**Remaining after T = 60min**	**Remaining after NCF = 60min**
URB597	0.9995	7.7	179.9	712.5	0.5%	83.8%
Sonidegib	0.9748	53.1	26.1	103.4	46.0%	96.1%
BCH-URB597	0.9977	18.1	76.7	303.6	9.9%	80.9%
BCH-Sonidegib	0.9776	74.8	18.5	73.3	57.4%	99.8%
Testosterone	0.9971	3.2	430.2	1703.7	0.0%	77.2%
Diclofenac	0.9829	41.8	33.2	131.4	36.9%	88.5%
Propafenone	0.9954	1.6	877.5	3475.0	0.0%	91.6%

Metabolic Stability in Human Liver Microsomes

The same protocol as in "Metabolic Stability in Mouse Liver Microsomes" was used with following liver microsomes:

Table 14 Used cell lines

Species	**Product Information**	**Vendor**	**Abbreviation**
Human	Cat No. 452117 Lot No. 38297	Corning	HLM

Cell permeability studies

Caco-2 Culture

Caco-2 cells purchased from ATCC were seeded onto polyethylene membranes (PET) in 96-well Corning Insert plates at 1 x 10^5 cells/ cm^2, and refreshed medium every 4~5 days until to the 21^{st} to 28^{th} day for confluent cell monolayer formation.

Transport Methods

The transport buffer in the study was HBSS with 10.0 mM HEPES at pH 7.40 ± 0.05. Test compound was tested at 2.00 µM bi-directionally in duplicate. Digoxin was tested at 10.0 µM bi-directionally in duplicate, while nadolol and metoprolol were tested at 2.00 µM in A to B direction in duplicate. Final DMSO concentration was adjusted to less than 1%.

1. The plate was incubated for 2 h in CO_2 incubator at 37 ± 1 °C, with 5% CO_2 at saturated humidity without shaking.
2. All samples were mixed with acetonitrile, containing an internal standard, and were centrifuged at 3200 g for 10 min.
3. For nadolol and metoprolol, 200 µL supernatant solution was diluted with 600 µL ultra-pure water for LC-MS/MS analysis. For digoxin and the tested compounds, 200 µL supernatant solution was diluted with 200 µL ultra-pure water for LC-MS/MS analysis.
4. Concentrations of test and control compounds in starting solution, donor solution, and receiver solution were quantified by LC-MS/MS methodologies, using peak area ratio of analyte/internal standard.
5. After transport assay, lucifer yellow rejection assay was applied to determine the Caco-2 cell monolayer integrity.

Data analysis

The apparent permeability coefficient P_{app} (cm/s) was calculated using the equation:

$$P_{app} = \frac{dC_r}{dt} \frac{V_r}{A \cdot C_0} \quad \text{(XII)}$$

Where dC_r/dt is the cumulative concentration of compound in the receiver chamber as a function of time (µM/s); V_r is the solution volume in the receiver chamber (0.075 mL on the apical side, 0.25 mL on the basolateral side); A is the surface area for the transport, i.e. 0.0804 cm^2 for the area of the monolayer; C_0 is the initial concentration in the donor chamber (µM).

The efflux ratio was calculated using the equation:

$$Efflux\ ratio = \frac{P_{app}\ (BA)}{P_{app}\ (AB)} \quad \text{(XIII)}$$

Percent recovery was calculated using the equation:

$$\%Solvent\ recovery = 100 \cdot \frac{(V_r \cdot C_r) + (V_d \cdot C_d)}{V_d \cdot C_0} \quad \text{(XIV)}$$

Where V_d is the volume in the donor chambers (0.075 mL on the apical side, 0.25 mL on the basolateral side); C_d and C_r are the final concentrations of transport compound in donor and receiver chambers, respectively.

CYP Inhibition in Human Liver Microsomes

Table 15. Used buffer. Water used in the assay and analysis is purified by ELGA Lab purification systems.

Reagent	Concentration [mM]
Potassium phosphate buffer (PB)	100
$MgCl_2$	33

Table 16. Used substrate stock solution. Organic solvents are AR or HPLC grade.

Compound name	Concentration (mM)	Solvent
Phenacetin	20	MeOH
Diclofenac	10	MeOH
S-Mephenytoin	20	MeOH
Dextromethorphan	20	MeOH
Midazolam	10	MeOH

Table 17. Standard inhibitors stock solutions.

Compound name	Concentration (mM)	Solvent
α-Naphthoflavone	3	DMSO
Sulfaphenazole	3	DMSO
(+)-N-3-Benzylnirvanol	1	DMSO
Quinidine	3	DMSO
Ketoconazole	3	DMSO

Table 18. Test compound stock solution.

Client substance ID / Batch No	MW	FW	Purity%	Concentration
URB597	338.41	338.41	95.00	10 mM in DMSO
Sonidegib	485.51	485.51	95.00	10 mM in DMSO
BCH-URB597	356.47	356.47	95.00	10 mM in DMSO
BCH-Sonidegib	489.54	489.54	95.00	10 mM in DMSO

Test compounds and positive controls preparation

Table 19. Preparation of test compound working solution (100x final concentration).

Concentrations of test compounds	Volume of solution [µL]	1:1 DMSO : MeOH [µL]	Working Conc. [mM]	Final Conc. in assay [µM]
10 mM	30.0	30.0 (MeOH)	5.00	50.0
5 mM	30.0	70.0	1.50	15.0
1.5 mM	30.0	60.0	0.500	5.000
0.5 mM	30.0	70.0	0.150	1.500
0.15 mM	30.0	60.0	0.0500	0.500
0.05 mM	30.0	70.0	0.01500	0.1500
0.015 mM	30.0	60.0	0.00500	0.0500

Table 20. Preparation of positive controls solution (100x final concentration).

Compounds	Stock Conc.(mM)	Vol. of solution [µL]	Vol. of MeOH [µL]	Working Conc. [µM]	Final Conc. [µM]
α-Naphthoflavone	3	10	90	300	3
Sulfaphenazole	3	10	90	300	3
(+)-N-3-Benzylnirvanol	1	10	90	100	1
Quinidine	3	10	90	300	3
Ketoconazole	3	10	90	300	3

Table 21. Preparation of cocktail substrate solution (10x final concentration).

CYP	Substrate	Stock Conc. [mM]	Working Conc. [µM]	Final Conc. [µM]	Vol. [µL]
1A2	Phenacetin	20	100	10	60
2C9	Diclofenac	10	50	5	60
2C19	S-Mephenytoin	20	300	30	180
2D6	Dextromethorphan	20	50	5	30
3A4	Midazolam	10	20	2	24
	PB	100 mM			11646
				Total vol:	**12 mL**

Table 22. Preparation of HLM working solution (1.27×) (final conc.: 0.2 mg/ml).

Microsomes	Product information	Source	Vol. of microsomes(mL)	Vol. of PB(mL)	Working Conc.
Human liver microsome	Cat No. 452117 Lot No. 38297	Corning	0.696	54.304	0.253 mg/mL

Table 23. Preparation of cofactor solution (10×) (final conc.: 1 mM).

NADPH	Product information	Source	Weight. of NADPH [mg]	Vol. for 33 mM $MgCl_2$ [mL]	NADPH Conc. [mM]
NADPH	Cat No. BT04 Lot No. BT04T120L003	BONTAC	127.6	15.0	10

Experimental procedure for CYP Inhibition in Human Liver Microsomes

1. Prepare test compounds and standard inhibitors working solution at (100×).
2. Remove microsomes from a –80°C freezer and thaw on ice.
3. Add 20 µL of the substrates solutions to the corresponding 2.2mL 96-well plates.
4. Add 20 µL PB to Blank wells.
5. Add 2 µL of the test compounds and positive control working solution to corresponding wells.
6. Add 2 µL solvent to No Inhibitor wells and Blank wells.
7. Prepare HLM working solution.

8. Add 158 µL of the HLM working solution to all wells of incubation plate.
9. Pre-warm the plate for about 10 min at 37 °C water bath.
10. Prepare NADPH cofactor solution.
11. Add 20 µL NADPH cofactor to all incubation wells. Mix and incubate for 10 min for all the CYPs at 37 °C water bath.
12. At the specific time point, terminate the reaction by adding 400 µL cold stop solution (200 ng/mL Tolbutamide and Labetalol in MeCN).
13. Centrifuged samples are at 4000 rpm for 20 min to precipitate protein.
14. Transfer 200 µL supernatant to 100 µL HPLC grade water and shake for 10 min.
15. Carry out LC/MS/MS analysis.

Data analysis

XL fit was used to plot the percent of vehicle control versus the test compound concentrations, and for non-linear regression analysis of the data. IC_{50} values were determined using 3- or 4- parameter logistic equation. IC_{50} values are reported as ">50 µM" when the % inhibition at the highest concentration (50 µM) is less than 50%.

Equation for three parameters logistic sigmoidal curve: $$y = \frac{max}{1 + \left(\frac{x}{IC_{50}}\right)^{-hillslope}}$$

Equation for four parameters logistic sigmoidal curve: $$y = \frac{max - min}{1 + \left(\frac{x}{IC_{50}}\right)^{-hillslope}}$$

Result summary

Table 24. Summary of the results.

Compound ID	IC_{50} [μM]				
	CYP1A2	**CYP2C9**	**CYP2C19**	**CYP2D6**	**CYP3A4-M**
URB597	6.51	5.68	11.7	>50	>50
Sonidegib	>50	4.20	>50	>50	>50
BCH-URB597	46.9	16.9	21.2	>50	>50
BCH-Sonidegib	>50	18.5	13.9	>50	>50

5.10. Computational details (Section 2.5, 2.6 and Chapter 3)

All calculations were carried out using the ORCA suite of programs (version 4.2.1).[150-151] Both optimisations and single-point energy calculations were carried out using "Tight" convergence criteria, corresponding to tolerances of 10^{-8} Hartrees for the SCF energy change, and 10^{-6} Hartrees for the optimisation step. To speed up the calculations, the resolution-of-identity chain-of-spheres exchange (RIJCOSX) approximation was employed.[174] The integration grid "Grid5" was employed for DFT energies, corresponding to a Lebedev-434 angular grid, and a radial integral accuracy (IntAcc) of 5.01. Calculations employing a RI approximation utilised the "GridX6" procedure, corresponding to IntAcc = 4.34 and a Lebedev-194 angular grid. For calculations of triple-z basis set quality, calculation of correlation integrals used the def2-TZVPP/C auxiliary basis set. Coulomb integrals were approximated using the def2/J auxiliary basis set.[175-178] All intermediate structures were verified to be minima by the absence of imaginary frequencies upon calculation of the Hessian. Grimme's quasiRRHO approach was used to calculate free energies at 298.15 K.[179] A 1 atm to 1 M standard state correction was applied by adding RTln(1/24.5) to the calculated free energy of each species. For calculating the thermodynamic potentials the python-script *otherm.py* was used.[180] Dispersion corrections to DFT energies were implemented using Grimme's D3 empirical method with Becke-Johnson damping (D3BJ).[181-182]

The Domain-based Local Pair Natural Orbital coupled cluster method with singles, doubles and perturbative triples (DLPNO-CCSD(T)) was used as a final single point providing reliable electronic energies using the def2-TZVPP basis set. [183] DLPNO-CCSD(T) calculations were run using "NormalPNO" cut-offs, corresponding to TCutPairs = 10^{-5} Hartrees, TCutPNO = 3.33 10^{-7} and TCutMKN = 10^{-3}, where TCutPairs is the correlation threshold for inclusion of a given electron pair in the CCSD calculation,

TCutPNO is the occupation threshold for each PNO (pair natural orbital) formed from an expansion of projected atomic orbitals (PAOs), and TCutMKN determines the threshold for the inclusion of each localised MO in the PNO expansion based on Mulliken population.[184]

Preliminary geometries of ground states as well as transition states were obtained *via autodE* using standard settings (PBE0-D3BJ/def2-TZVP//PBE0-D3BJ/def2-SVP) and GFN2-XTB for initial conformational sampling) for the implemented workflow.[185-186] *autodE* carries out conformational sampling on both ground and transition states using the ETKDGv2 algorithm,[149] using a similarity threshold of 0.3 Å on heavy atoms and an energy threshold of 1 kJ mol^{-1}.[148] The obtained geometries were then subjected high-level geometry optimisation as described above.

5.11. Methods (Section 2.5.2)

The quantum theory of atoms in molecules (QTAIM)

The quantum theory of atoms in molecules (QTAIM) by Bader[109] delivers the possibility to divide the total electronic density $\rho(\mathbf{r})$ into atomic basins opening a way to characterise bonds out of given a density distribution. The way it works is that the Hessian of $\rho(\mathbf{r})$ is diagonalisable at each stationary point of $\rho(\mathbf{r})$ into a set of three eigenvalues λ_1, λ_2 and λ_3, which identify the nature (ω, σ) of the stationary point. The rank ω counts the number of non-negative eigenvalues λ, and the signature σ is the sum over the signs of λ_1, λ_2 and λ_3. Three negative eigenvalues (3,-3) correspond to so-called basin attractors, which are maxima of $\rho(\mathbf{r})$ in all three directions (often resembling the position of the nuclei). Between these basin attractors, stationary points with one, two or three positive eigenvalues are found. They correspond to the so-called bond critical point (3,-1), ring critical point (3,+1) and cage critical point (3,+3), respectively. For example, a bond critical point possesses a minimum in $\rho(\mathbf{r})$ in the direction of the basin attractor and two maxima in the perpendicular direction. More pictorially speaking, the surfaces of zero flux in the gradient vector field towards the attractors $\nabla\rho(\mathbf{r})\mathbf{n}(\mathbf{r}) = 0$ divide $\rho(\mathbf{r})$ into basins with all critical points (ω, σ) lying on these surfaces.[187] The ellipticity $\epsilon(\mathrm{r})$ is defined by $\epsilon(\mathbf{r}) = \left(\lambda_1(\mathbf{r})/\lambda_2(\mathbf{r})\right) - 1$ (with $\lambda_1(\mathbf{r}) < \lambda_2(\mathbf{r}) < \lambda_3(\mathbf{r})$).

Table 25. Quantitative analysis of bond critical point in the inter-bridgehead bond of TCHep and TCP performed with MultiWfn.

Bond critical point in inter-bridgehead bond	**TCHep**	**TCP**
Level of Theory	SCS-MP2	CASSCF(2,2)
Density ρ	0.196	0.178
Gradient (norm)	$0.128 \cdot 10^{-9}$	$0.485 \cdot 10^{-10}$
x	$0.126 \cdot 10^{-9}$	$-0.400 \cdot 10^{-11}$
y	$0.132 \cdot 10^{-10}$	$-0.296 \cdot 10^{-11}$
z	$0.184 \cdot 10^{-10}$	$-0.482 \cdot 10^{-10}$
Laplacian (norm)	– 0.0804	+ 0.167
x	– 0.279	$-0.442 \cdot 10^{-1}$
y	0.276	$-0.442 \cdot 10^{-1}$
z	– 0.0776	0.256
Ellipticity	2.59	0.00293
Geometric angle α_1	58.2°	58.4°
Bond path angle α_{b1}	74.4°	60.7°
$\Delta\alpha$	16.2°	2.3°

The NCI analysis uses the typical characteristics of non-covalent interaction: They possess only low electron density $\rho(\mathbf{r})$ combined with a small gradient $\nabla\rho(\mathbf{r})$. The Laplacian $\nabla^2\rho(\mathbf{r})$ and the corresponding eigenvalues $\lambda_1(\mathbf{r}) < \lambda_2(\mathbf{r}) < \lambda_3(\mathbf{r})$ are used to distinguish between repulsive (electron depletion) or attractive interaction (electron accumulation), qualified by the sign of the eigenvalues and quantified by the magnitude.

DORI-analysis tries to capture covalent- as well as non-covalent interactions. Essentially, DORI is an improved Single-Exponential-Decay Detector (SEDD) which reduces numerical noise in low-density areas and the basis set dependency of the SEDD. In contrast to QTAIM and NCI-analysis, which search for stationary points, the SEDD tries to capture the geometrical feature of a bond: The deviation from a localised, exponentially decaying (atomic wave) function which indicates bonding. This is mathematically captured in the local wave vector $\nabla\rho(\boldsymbol{r})/\rho(\boldsymbol{r})$. DORI slightly varied SEDD(**r**) to yield the DORI functions (XV), a normalised function ranging from 0 (non-bonding) to 1 (bonding). The DORI analysis uses the same interpretation of the signs of the eigenvalues of the Laplacian $\nabla^2\rho(\mathbf{r}) = \lambda_1(\mathbf{r}) + \lambda_2(\mathbf{r}) + \lambda_3(\mathbf{r})$ to obtain information about the kind of interaction.[188]

$$\mathrm{SEDD}(\mathbf{r}) = \ln\left(1 + \left(\frac{\nabla\left(\frac{\nabla\rho(\mathbf{r})}{\rho(\mathbf{r})}\right)^2}{\rho(\mathbf{r})}\right)^2\right) \qquad \text{(XV)}$$

The electrophilicity index ω is defined according to equation (XVI) using the ionisation energies E(Ionisation) and electron affinities E(Electron affinity) as well as orbital energies of the HOMO and LUMO.

$$\omega = \frac{\mu^2}{2\eta} = \frac{E(Ionisation) + E(Electron\ affinity)}{2\,[E(LUMO) - \mathrm{E(HOMO)}]} \qquad \text{(XVI)}$$

5.12. Crystallographic data (Section 3.2)

Crystallographic data have been deposited with the CCDC as entries CCDC 2175923 - 2175926 and CCDC 2176171.

*Table 26. Crystal data and structure refinement for **56**.*

CCDC Identification code	2175923	
Empirical formula	C19 H19 F1 I1 N1 O2	
Formula Weight	436.63	
Temperature	150 K	
Wavelength	1.54184	
Crystal system	Triclinic	
Space Group	P -1	
Unit cell dimensions	a = 8.1208 (3) Å	α = 87.000 (3) °
	b = 9.1923 (3) Å	β = 87.674 (3) °
	c = 12.3257(4) Å	γ = 72.303 (3) °
Volume	875.06 (5) $Å^3$	
Z	2	
Density (calculated)	1.667 Mg/m^3	
Absorption coefficient	14.559 mm^{-1}	
F(000)	436.0	
Crystal size	0.05 x 0.15 x 0.25 mm^3	
Theta range for data collection	3.56 to 75.98°	
Index ranges	-10<=h<=9, -11<=k<=10, -15<=l<=15	
Reflections collected	3601	
Independent reflections	3446 [R(int) = 0.0210]	
Completeness to theta = 76.30°	98.6%	
Absorption correction	Multi Scan	
Max. and min. transmission	0.48 and 0.15	
Refinement method	Full-matrix least-squares on F^2	
Data / restraints / parameters	3601 / 0 / 217	
Goodness-of-fit on F2	1.0236	
Final R indices [I>2sigma(I)]	R1 = 0.0210, wR2 = 0.0529	
R indices (all data)	R1 = 0.0223, wR2 = 0.0544	
Largest diff. peak and hole	0.50 and -0.59 e.$Å^{-3}$	

*Table 27. Crystal data and structure refinement for **89**.*

CCDC Identification code	2176171	
Empirical formula	C18 H23 Br1 N1 O3 S1	
Formula Weight	413.33	
Temperature	150 K	
Wavelength	1.54184	
Crystal system	Monoclinic	
Space Group	I 1 a 1	
Unit cell dimensions	a = 14.8723 (4) Å	α = 90°
	b = 12.4951 (3) Å	β = 102.455 (3)°
	c = 9.9629 (3) Å	γ = 90°
Volume	1807.84 (9) $Å^3$	
Z	4	
Density (calculated)	1.519 Mg/m^3	
Absorption coefficient	4.312 mm^{-1}	
F(000)	852.0	
Crystal size	0.05 x 0.08 x 0.20 mm^3	
Theta range for data collection	4.64 to 75.94°	
Index ranges	-18<=h<=17, -15<=k<=15, -12<=l<=12	
Reflections collected	7555	
Independent reflections	3156 [R(int) = 0.034]	
Completeness to theta = 76.475°	83%	
Absorption correction	Multi Scan	
Max. and min. transmission	0.66 and 0.81	
Refinement method	Full-matrix least-squares on F^2	
Data / restraints / parameters	3156 / 114 / 246	
Goodness-of-fit on F2	1.0026	
Final R indices [I>2sigma(I)]	R1 = 0.0310, wR2 = 0.0798	
R indices (all data)	R1 = 0.0310, wR2 = 0.0798	
Largest diff. peak and hole	0.28 and -0.22 e.$Å^{-3}$	

*Table 28. Crystal data and structure refinement for **83.***

CCDC Identification code	2175926	
Empirical formula	C10 H12 I2 N2	
Formula Weight	414.03	
Temperature	150 K	
Wavelength	1.54184	
Crystal system	Triclinic	
Space Group	P -1	
Unit cell dimensions	a = 5.7620 (3)Å	α = 66.033 (4)°
	b = 10.0072 (4) Å	β = 80.694 (3)°
	c = 11.6084 (4)Å	γ = 86.675 (4)°
Volume	603.57 (5) $Å^3$	
Z	2	
Density (calculated)	2.278 Mg/m^3	
Absorption coefficient	40.642 mm^{-1}	
F(000)	384.0	
Crystal size	0.058 x 0.114 x 0.259 mm^3	
Theta range for data collection	4.22 to 76.02°	
Index ranges	-7<=h<=7, -11<=k<=12, 0<=l<=14	
Reflections collected	2489	
Independent reflections	2372 [R(int) = 0.0375]	
Completeness to theta = 76.30°	98.6%	
Absorption correction	Multi Scan	
Max. and min. transmission	0.00 and 0.09	
Refinement method	Full-matrix least-squares on F^2	
Data / restraints / parameters	2489 / 0 / 127	
Goodness-of-fit on F2	1.0063	
Final R indices [I>2sigma(I)]	R1 = 0.0375, wR2 = 0.0932	
R indices (all data)	R1 = 0.0387, wR2 = 0.0954	
Largest diff. peak and hole	1.54 and -1.80 e.$Å^{-3}$	

*Table 29. Crystal data and structure refinement for **72**.*

CCDC Identification code	2175924	
Empirical formula	C19 H21 N1 O2 S2	
Formula Weight	359.49	
Temperature	150 K	
Wavelength	1.54184	
Crystal system	Monoclinic	
Space Group	I 1 a 1	
Unit cell dimensions	a = 14.0657 (11) Å	α = 90°
	b = 22.2956 (2) Å	β = 153.30 (2)°
	c = 12.4341 (10) Å	γ = 90°
Volume	1752.1 (12) $Å^3$	
Z	4	
Density (calculated)	1.363 Mg/m^3	
Absorption coefficient	2.841 mm^{-1}	
F(000)	760.0	
Crystal size	0.08 x 0.25 x 0.40 mm^3	
Theta range for data collection	3.93 to 76.13°	
Index ranges	-17<=h<=14, -27<=k<=27, -14<=l<=15	
Reflections collected	3432	
Independent reflections	3395 [R(int) = 0.0232]	
Completeness to theta = 76.475°	94%	
Absorption correction	Multi Scan	
Max. and min. transmission	0.69 and 0.80	
Refinement method	Full-matrix least-squares on F^2	
Data / restraints / parameters	3432 / 2 / 218	
Goodness-of-fit on F2	0.8994	
Final R indices [I>2sigma(I)]	R1 = 0.0235, wR2 = 0.0595	
R indices (all data)	R1 = 0.0236, wR2 = 0.0596	
Largest diff. peak and hole	0.13 and -0.16 e.$Å^{-3}$	

*Table 30. Crystal data and structure refinement for **175**.*

CCDC Identification code	2175925	
Empirical formula	C14 H17 N1 O2	
Formula Weight	231.29	
Temperature	150 K	
Wavelength	1.54180	
Crystal system	Triclinic	
Space Group	P -1	
Unit cell dimensions	a = 10.5730 (3) Å	α = 63.099 (3)°
	b = 11.5021 (4) Å	β = 67.797 (3)°
	c = 12.1280 (4) Å	γ = 75.429 (3)°
Volume	1211.96 (8) $Å^3$	
Z	4	
Density (calculated)	1.268 Mg/m^3	
Absorption coefficient	0.677 mm^{-1}	
F(000)	496.0	
Crystal size	0.08 x 0.14 x 0.28 mm^3	
Theta range for data collection	4.26 to 76.08°	
Index ranges	-11<=h<=13, -12<=k<=14, 0<=l<=15	
Reflections collected	5013	
Independent reflections	4750 [R(int) = 0.0340]	
Completeness to theta = 76.30°	98.7%	
Absorption correction	Multi Scan	
Max. and min. transmission	0.87 and 0.95	
Refinement method	Full-matrix least-squares on F^2	
Data / restraints / parameters	5013 / 16 / 415	
Goodness-of-fit on F2	1.0042	
Final R indices [I>2sigma(I)]	R1 = 0.0340, wR2 = 0.0876	
R indices (all data)	R1 = 0.0353, wR2 = 0.0890	
Largest diff. peak and hole	0.29 and -0.22 e.$Å^{-3}$	

5.13. Geometrical data (Section 3.2)

Table 31. Determined structural parameters based on crystallographic geometries (.xyz coordinates) shown in Figure 73.

Compound	r_1 [Å]	r_2 [Å]	exit vector angle α [°]	dihedral angle ρ [°]
175	2.12	4.75	121.3	0.5
89	2.12	4.76	124.0	0.0
72	2.10	5.11	114.1	11.7
83	2.08	5.22	119.7	-2.6
56	2.10	5.27	118.4	-8.6

Table 32. Determined structural parameters based on computational geometry optimisation at CPCM(THF)-B2PLYP-D3BJ/def2-TZVP level of theory. These values are shown in Figure 72 and 73 (Section 3.2).

Compound	r_1 [Å]	r_2 [Å]	exit vector angle α [°]	dihedral angle ρ [°]
175(BCHep)	2.12	4.74	121.0	3.7
175(*meta*-Benzene)	2.43	4.97	117.2	-2.5
56(BCHep)	2.09	5.28	119.3	-6.4
56(*meta*-Benzene)	2.41	5.53	120.4	-2.5
72(BCHep)	2.10	5.13	115.0	11.7
72(*meta*-Benzene)	2.40	5.46	119.7	1.3
89(BCHep)	2.12	4.72	120.7	-1.6
89(*meta*-Benzene)	2.43	4.96	119.0	-3.5
83(BCHep)	2.08	5.19	118.3	0.2
83(*meta*-Benzene)	2.40	5.45	119.8	0.0

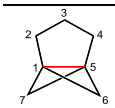
5.14. Data for Reactivity under Physiological Conditions (Section 2.6)

Table 33. Thermodynamic quantities of the investigated reaction in Figure 63. Thermodynamic calculations were carried out at the CPCM(water)-B2PLYP/def2-TZVP level of theory. Free energy G was calculated using the electronic energy of CPCM(water)-DLPNO-CCSD(T)/def2-QZVPP// CPCM(water)-B2PLYP/def2-TZVP level of theory via $G = E_{el}$*(DLPNO-CCSD(T)) + [G(B2PLYP) − *E_{el}*(B2PLYP)].*

	Electronic energy [Ha] B2PLYP	Electronic energy DLPNO-CCSD(T) [Ha]	Enthalpy H B2PLYP [Ha]	Free energy G [Ha]	ΔG rel.**16**+**5** [kcal mol^{-1}]
123	-272.9764029	-271.5055177	-272.8057389	-271.3692602	
124	-272.9610073	-271.5008662	-272.7939682	-271.3683095	0.60
125	-272.9669649	-271.5062077	-272.7995874	-271.3746353	-3.4

5.15. Computational Benchmarking Data (Section 2.5.1)

Table 34. Detailed Comparison of bond length of the tested methods. Bond lengths are in Å.



Level of theory	1-5	1-2 = 4-5	5-6 = 1-6	1-7=5-7	2-3 = 3-4	C2-H	C3-H
RI-MP2/def2-SVP	1.565	1.513	1.498	1.496	1.544	1.102	1.102
RI-MP2/def2-TZVP	1.583	1.509	1.499	1.498	1.541	1.094	1.093
RI-MP2/def2-TZVPP	1.583	1.509	1.499	1.498	1.541	1.091	1.090
RI-MP2/def2-QZVPP	1.580	1.507	1.497	1.495	1.538	1.090	1.090
RI-SCS-MP2/def2-SVP	1.564	1.518	1.499	1.500	1.549	1.103	1.103
RI-SCS-MP2/def2-TZVP	1.581	1.514	1.501	1.500	1.546	1.095	1.094
RI-SCS-MP2/def2-TZVPP	1.582	1.515	1.500	1.501	1.545	1.090	1.091
RI-SCS-MP2/def2-QZVPP	1.578	1.513	1.499	1.498	1.543	1.0910	1.090
HF/def2-QZVPP	1.515	1.514	1.487	1.485	1.546	1.082	1.083
RI-BLYP/def2-QZVPP	1.578	1.525	1.510	1.509	1.564	1.096	1.097
RI-B3LYP/def2-QZVPP	1.549	1.515	1.498	1.497	1.551	1.091	1.091
RI-B2PLYP/def2-QZVPP	1.563	1.512	1.497	1.498	1.546	1.090	1.090
RI-B2GP-PLYP/def2-QZVPP	1.558	1.510	1.494	1.493	1.542	1.088	1.088
RI-BLYP-D3BJ/def2-QZVPP	1.579	1.523	1.509	1.508	1.562	1.096	1.097
RI-B3LYP-D3BJ/def2-QZVPP	1.550	1.514	1.497	1.496	1.549	1.091	1.091
RI-B2PLYP-D3BJ/def2-QZVPP	1.563	1.512	1.497	1.496	1.545	1.090	1.089
RI-B2GP-PLYP-D3BJ/def2-QZVPP	1.558	1.509	1.494	1.493	1.542	1.088	1.070
RI-MP2/cc-pVTZ	1.584	1.510	1.499	1.498	1.541	1.091	1.090
RI-MP2/cc-pQTZ	1.579	1.508	1.496	1.495	1.538	1.090	1.090
RI-SCS-MP2/cc-pVTZ	1.583	1.515	1.501	1.500	1.546	1.092	1.091
RI-SCS-MP2/cc-pQTZ	1.577	1.513	1.499	1.497	1.543	1.091	1.090

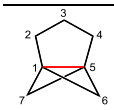
Table 35. Detailed comparison of angles of the tested methods. Angles are in °.

s							
Level of theory	**∠(6-1-2)**	**∠(7-1-2)**	**∠(1-2-3)**	**∠(2-3-4)**	**∠(1-5-6)**	**∠(1-5-7)**	**∠(7-1-6)**
RI-MP2/def2-SVP	106.7	121.3	105.4	104.0	58.5	58.5	98.2
RI-MP2/def2-TZVP	122.0	121.0	105.8	103.4	58.1	58.1	97.8
RI-MP2/def2-TZVPP	122.0	120.9	105.8	103.3	58.1	58.1	97.8
RI-MP2/def2-QZVPP	121.9	120.9	105.7	103.3	58.1	58.1	97.9
RI-SCS-MP2/def2-SVP	122.5	121.4	105.4	104.2	58.6	58.6	98.3
RI-SCS-MP2/def2-TZVP	122.1	121.1	105.8	103.7	58.2	58.2	97.9
RI-SCS-MP2/def2-TZVPP	122.1	121.1	105.8	103.6	58.2	58.2	97.9
RI-SCS-MP2/def2-QZVPP	122.0	121.1	105.7	103.6	58.2	58.2	98.0
HF/def2-QZVPP	123.4	122.4	105.1	104.5	59.4	59.3	98.6
RI-BLYP/def2-QZVPP	122.4	121.6	106.1	104.6	58.5	58.5	98.3
RI-B3LYP/def2-QZVPP	122.8	121.8	105.6	104.4	58.9	58.8	98.4
RI-B2PLYP/def2-QZVPP	122.5	121.4	105.7	104.0	58.5	58.5	98.2
RI-B2GP-PLYP/def2-QZVPP	122.5	121.4	105.6	103.9	58.6	58.5	98.2
RI-BLYP-D3BJ/def2-QZVPP	122.2	121.4	106.0	104.4	58.4	58.4	98.4
RI-B3LYP-D3BJ/def2-QZVPP	122.7	121.7	105.6	104.3	58.8	58.8	98.5
RI-B2PLYP-D3BJ/def2-QZVPP	122.4	121.3	105.7	104.0	58.5	58.5	98.3
RI-B2GP-PLYP-D3BJ/def2-QZVPP	122.5	121.3	105.6	103.9	58.6	58.5	98.3
RI-MP2/cc-pVTZ	122.0	120.9	105.8	103.3	58.1	58.1	97.8
RI-MP2/cc-pQTZ	122.0	120.9	105.7	103.3	58.2	58.1	97.9
RI-SCS-MP2/cc-pVTZ	122.1	121.0	105.8	103.6	58.2	58.2	97.9
RI-SCS-MP2/cc-pQTZ	122.1	121.1	105.8	103.7	58.3	58.2	98.0

Table 36. Relative comparison of selected dihedral angles d and selected distances of the tested methods.

	Dihedral angle [°]			**Distances [Å]**	
Level of theory	**d(H-C2-C3-H)**	**d(6-1-2-H2)**	**d(1-7-5-6)**	**H3-H6**	**H3'-H7**
RI-MP2/def2-SVP	-39.3	-153.3	44.9	4.061	2.295
RI-MP2/def2-TZVP	-40.6	-153.3	44.6	4.074	2.272
RI-MP2/def2-TZVPP	-40.9	-153.2	44.5	4.071	2.262
RI-MP2/def2-QZVPP	-41.0	-153.0	44.4	4.066	2.257
RI-SCS-MP2/def2-SVP	-38.2	-153.8	45.0	4.053	2.333
RI-SCS-MP2/def2-TZVP	-39.3	-153.8	44.7	4.065	2.312
RI-SCS-MP2/def2-TZVPP		-153.7	44.6	4.061	2.303
RI-SCS-MP2/def2-QZVPP	-39.6	-153.6	44.6	4.055	2.299
HF/def2-QZVPP	-35.4	-154.0	46.5	3.999	2.432
RI-BLYP/def2-QZVPP	-34.1	-156.1	44.9	4.006	2.474
RI-B3LYP/def2-QZVPP	-35.7	-154.6	45.5	4.013	2.421
RI-B2PLYP/def2-QZVPP	-37.7	-154.2	45.0	4.031	2.355
RI-B2GP-PLYP/def2-QZVPP	-38.4	-153.8	45.1	4.034	2.333
RI-BLYP-D3BJ/def2-QZVPP	-35.4	-155.6	44.6	4.013	2.472
RI-B3LYP-D3BJ/def2-QZVPP	-36.6	-154.3	45.4	4.015	2.388
RI-B2PLYP-D3BJ/def2-QZVPP	-37.9	-154.1	44.5	4.029	2.345
RI-B2GP-PLYP-D3BJ/def2-QZVPP	-37.4	-153.7	45.0	4.005	2.367
RI-MP2/cc-pVTZ	-41.0	-153.2	44.4	4.073	2.262
RI-MP2/cc-pQTZ	-40.9	-153.1	44.5	4.063	2.261
RI-SCS-MP2/cc-pVTZ	-39.7	-153.7	44.6	4.063	2.304
RI-SCS-MP2/cc-pQTZ	-39.5	-153.7	44.6	4.052	2.304

Table 37. Selected comparison of relative differences of bond lengths r and dihedral angles d.



	Distances [pm]			Dihedral angle [°]
Relative difference to SCS-MP2/def2-QZVPP	**r(1-5)**	**r(H3-H6)**	**r(H3'-H7)**	**d(1-7-5-6)**
RI-MP2/def2-SVP	-1.3	0.6	-0.4	0.3
RI-MP2/def2-TZVP	0.5	1.9	-2.7	0.0
RI-MP2/def2-TZVPP	0.5	1.6	-3.7	-0.1
RI-MP2/def2-QZVPP	0.2	1.1	-4.2	-0.2
RI-SCS-MP2/def2-SVP	-1.4	-0.2	3.4	0.4
RI-SCS-MP2/def2-TZVP	0.3	1.0	1.3	0.1
RI-SCS-MP2/def2-TZVPP	0.4	0.6	0.4	0.0
RI-SCS-MP2/def2-QZVPP	0.0	0.0	0.0	0.0
HF/def2-QZVPP	-6.3	-5.6	13.3	1.9
RI-BLYP/def2-QZVPP	0.0	-4.9	17.5	0.3
RI-B3LYP/def2-QZVPP	-2.9	-4.2	12.2	0.9
RI-B2PLYP/def2-QZVPP	-1.5	-2.4	5.6	0.4
RI-B2GP-PLYP/def2-QZVPP	-2.0	-2.1	3.4	0.5
RI-BLYP-D3BJ/def2-QZVPP	0.1	-4.2	17.3	0
RI-B3LYP-D3BJ/def2-QZVPP	-2.8	-4.0	8.9	0.8
RI-B2PLYP-D3BJ/def2-QZVPP	-1.5	-2.6	4.6	-0.1
RI-B2GP-PLYP-D3BJ/def2-QZVPP	-2.0	-5.0	6.8	0.4
RI-MP2/cc-pVTZ	0.6	1.8	-3.7	-0.2
RI-MP2/cc-pQTZ	0.1	0.8	-3.8	-0.1
RI-SCS-MP2/cc-pVTZ	0.5	0.8	0.5	0.0
RI-SCS-MP2/cc-pQTZ	-0.1	-0.3	0.5	0.0

5.16. Computational Thermodynamic Data (Section 2.5, 2.6 and 3.3.2)

Table 38. Thermodynamic quantities of the investigated reaction in Figure 50 for TCP. Thermodynamic calculations were carried out at the CPCM(THF)-B2PLYP/def2-TZVP level of theory. Free energy G was calculated using the electronic energy of CPCM(THF)-B2PLYP/def2-QZVPP// CPCM(THF)-B2PLYP/def2-TZVP level of theory via $G = E_{el}(def2\text{-}QZVPP) + [G(def2\text{-}TZVP) - E_{el}(def2\text{-}TZVP)]$

	Electronic energy [Ha] (def2-TZVP)	**Enthalpy H [Ha]**	**Free energy G [Ha]**	**Electronic energy [Ha] (def2-QZVPP)**	**Corrected Free energy G [Ha]**	
TCP	-193.9070	-193.8101	-193.8367	-193.9381	-193.8678	
	PhS·					
PhS·	-629.5798	-629.4822	-629.5148	-629.6307	-629.5657	
TS	not found					
Product	-823.4998	-823.3025	-823.3466	-823.5819	-823.4288	3.0
	I·					
I·	-297.5163	-297.5125	-297.5287	-297.5695	-297.5819	
TS	not found					
Product	-491.4421	-491.3409	-491.3759	-491.5271	-491.4609	-7.0
	CH3·					
CH_3·	-39.8102	-39.7777	-39.7959	-39.8190	-39.8047	
TS	-233.4077	-233.2734	-233.3070	-233.7505	-233.6497	14.3
Product	-233.7656	-233.6271	-233.6579	-233.8053	-233.6977	-15.8
	NH2					
NH_2^-	-55.9754	-55.9528	-55.9713	-55.9966	-55.9925	
TS	-249.8700	-249.7485	-249.7833	-249.9181	-249.8315	18.1
Product	-249.9049	-249.7802	-249.8118	-249.9505	-249.8575	1.8
	Ph-Anion					
Ph^-	-231.5548	-231.4632	-231.4923	-231.5917	-231.5292	
TS	-425.4478	-425.2582	-425.3011	-425.5145	-425.3678	18.3
Product	-425.5070	-425.3151	-425.3568	-425.5745	-425.4243	-17.1

Table 39. Thermodynamic quantities of the investigated reaction in Figure 50 for TCP. Thermodynamic calculations were carried out at the CPCM(THF)-B2PLYP/def2-TZVP level of theory. Free energy G was calculated using the electronic energy of CPCM(THF)-B2PLYP/def2-QZVPP// CPCM(THF)-B2PLYP/def2-TZVP level of theory via G = E_{el}(def2-QZVPP) + [G(def2-TZVP) − E_{el}(def2-TZVP)]

	Electronic energy [Ha] (def2-TZVP)	**Enthalpy H [Ha]**	**Free energy G [Ha]**	**Electronic energy [Ha] (def2-QZVPP)**	**Corrected Free energy G [Ha]**	
TCHep	-272.5215	-272.3632	-272.3959	-272.5675	-272.4418	
	PhS·					
PhS·	-629.5798	-629.4822	-629.5148	-629.6307	-629.5657	
TS	not found					
Product	-902.1379	-901.8796	-901.9270	-902.2349	-902.0239	-10.3
	I·					
I·	-297.5163	-297.5125	-297.5287	-297.5695	-297.5819	
TS	not found					
Product	-570.0698	-569.9085	-569.9476	-570.1699	-570.0477	-15.0
	CH_3·					
CH_3·	-39.8102	-39.7777	-39.7959	-39.8190	-39.8047	
TS	-312.3252	-312.1314	-312.1702	-312.3801	-312.2251	13.5
Product	-312.4033	-312.2041	-312.2400	-312.4580	-312.2946	-30.2
	NH_2^-					
NH_2^-	-55.9754	-55.9528	-55.9713	-55.9966	-55.9925	
TS	-328.4752	-328.2938	-328.3321	-328.5376	-328.3946	25.0
Product	-328.5203	-328.3351	-328.3712	-328.5813	-328.4322	1.4
	Ph^-					
Ph^-	-231.5548	-231.4632	-231.4923	-231.5917	-231.5292	
TS	-504.0558	-503.8065	-503.8527	-504.1375	-503.9345	22.9
Product	-504.1268	-503.8743	-503.9182	-504.2097	-504.0011	-18.9

Table 40. Thermodynamic quantities of the investigated reaction in Figure 53. Thermodynamic calculations were carried out at the CPCM(THF)-B2PLYP/def2-TZVP level of theory. Free energy G was calculated using the electronic energy of CPCM(THF)-B2PLYP/def2-QZVPP// CPCM(THF)-B2PLYP/def2-TZVP level of theory via $G = E_{el}(def2\text{-}QZVPP) + [G(def2\text{-}TZVP) - E_{el}(def2\text{-}TZVP)]$

	Electronic energy [Ha] (def2-TZVP)	**Enthalpy H [Ha]**	**Free energy G [Ha]**	**Electronic energy [Ha] (def2-QZVPP)**	**Corrected Free energy G [Ha]**	
TCHep	-272.5215	-272.3632	-272.3959	-272.5675	-272.4418	
Educt	-540.2224	-539.9751	-540.0214	-539.7084	-539.5075	
TS 99	-812.7430	-812.3373	-812.3990	-812.8733	-812.5293	11.5
Product 101	-812.8215	-812.4116	-812.4702	-812.9516	-812.6004	-33.2
TCP	-193.9070	-193.8086	-193.8355	-193.9381	-193.8667	
Educt	-461.5839	-461.3975	-461.4398	-461.6540	-461.5098	
TS 98	-655.4883	-655.2030	-655.2588	-655.5892	-655.3597	10.6
Product 100	-655.5507	-655.2630	-655.3146	-655.6511	-655.4150	-24.2

Table 41. Thermodynamic quantities of the investigated reaction in Figure 56. Thermodynamic calculations were carried out at the at CPCM(THF)-B2PLYP-D3BJ/def2-TZVP level of theory.

	Electronic energy E [Ha]	**Enthalpy H [Ha]**	**Free energy G [Ha]**	
TCHep	-272.522	-272.363	-272.399	
Radical				
BCB 103	-312.354	-312.158	-312.203	25.7
***Exo*-methylene 104**	-312.431	-312.233	-312.276	-20.1
BCHep 102	-312.403	-312.204	-312.244	0
Anionic				
BCB 102	-312.43	-312.23	-312.28	24.1
***Exo*-methylene 104**	-312.5	-312.3	-312.34	-18.9
BCHep 102	-312.5	-312.28	-312.31	0

Table 42. Thermodynamic quantities of the investigated reaction in Figure 57. Thermodynamic calculations were carried out at the at CPCM(THF)-B2PLYP-D3BJ/def2-TZVP level of theory.

	Electronic energy E [Ha]	**Enthalpy H [Ha]**	**Free energy G [Ha]**	
Biacetyl Anion				
107	-425.7843	-425.5762	-425.6179	
TS 106	-425.7710	-425.5645	-425.6056	7.8
104	-425.8720	-425.6629	-425.7053	-54.8
Biacetyl Radical				
107	-425.7098	-425.4989	-425.5408	
TS 106	-425.6842	-425.4753	-425.5170	15.0
104	-425.7523	-425.5418	-425.5852	-27.8
Methyl Anion				
102	-312.4712	-312.2751	-312.3113	
TS 106	-312.4279	-312.2349	-312.2710	25.3
104	-312.4986	-312.3039	-312.3413	-18.8
Methyl Radical				
102	-312.4033	-312.2041	-312.2407	
TS 106	-312.3639	-312.1673	-312.2043	22.8
104	-312.4312	-312.2333	-312.2727	-20.1

Table 43. Thermodynamic quantities of the investigated reaction in Figure 60. Thermodynamic calculations were carried out at the CPCM(THF)-B2PLYP/def2-TZVP level of theory. Free energy G was calculated using the electronic energy of CPCM(THF)-B2PLYP/def2-QZVPP// CPCM(THF)-B2PLYP/def2-TZVP level of theory via $G = E_{el}(def2\text{-}QZVPP) + [G(def2\text{-}TZVP) - E_{el}(def2\text{-}TZVP)]$

	Electronic energy [Ha] (def2-TZVP)	Enthalpy H [Ha]	Free energy G [Ha]	Electronic energy [Ha] (def2-QZVPP)	Corrected Free energy G [Ha]
TCP	-193.9070	-193.8086	-193.8355	-193.9381	-193.8667
TCHep	-272.5215	-272.3632	-272.3959	-272.5675	-272.4418
PhS· radical	-629.5798	-629.4822	-629.5148	-629.6307	-629.5657
Thiophenol	-630.2113	-630.1048	-630.1396	-630.2645	-630.1928
BCP-adduct 117	-823.4998	-823.3025	-823.3466	-823.5819	-823.4288
BCHep-adduct 116	-902.1379	-901.8796	-901.9270	-902.2349	-902.0239
HAT BCHep 68	-902.8071	-902.5354	-902.5827	-902.9063	-902.6819
HAT BCP 118	-824.1722	-823.9619	-824.0059	-824.2320	-824.0657
TCP ⟶ PhS-BCP·					2.3
TCHep ⟶ PhS-BCHep·					-10.3
PhS-BCP· ⟶ PhS-BCP-H					-6.2
PhS-BCHep· ⟶ PhS-BCHep-H					-19.4

Table 44. Thermodynamic quantities of the investigated reaction in Figure 86. Thermodynamic calculations were carried out at the CPCM(THF)-B2PLYP/def2-TZVP level of theory. Free energy G was calculated using the electronic energy of DLPNO-CCSD(T)/def2-QZVPP//CPCM(THF)-B2PLYP-D3BJ/def2-TZVP level of theory via $G = E_{el}(def2\text{-}QZVPP) + [G(def2\text{-}TZVP) - E_{el}(def2\text{-}TZVP)]$

	Electronic energy [Ha] (def2-TZVP)	Enthalpy H [Ha]	Free energy G [Ha]	Electronic energy [Ha] (def2-QZVPP)	Corrected Free energy G [Ha]
BCHep-H	-313.0722	-312.8599	-312.8958	-313.1288	-312.9524
BCHep anion 158	-312.4711	-312.2750	-312.3112	-312.5302	-312.3703
BCP-H	-234.4391	-234.2880	-234.3188	-234.4807	-234.3604
BCP anion 159	-233.8517	-233.7161	-233.7471	-233.8952	-233.7905
^{t}Bu-H	-158.3492	-158.2109	-158.2422	-158.3826	-158.2755
^{t}Bu anion 160	-157.7521	-157.6309	-157.6604	-157.7885	-157.6968
BCHep-H + ^{t}Bu anion					2.1
BCHep-H + ^{t}Bu anion					-5.6

References

[1] A. Baeyer, *Chem. Ber.* **1885**, *18*, 2269-2281.
[2] H. C. Brown, *Science* **1946**, *103*, 385-387.
[3] J. Clayden, N. Greeves, S. Warren, *Organic Chemistry* **2012**.
[4] J. L. Franklin, *Industrial & Engineering Chemistry* **2002**, *41*, 1070-1076.
[5] S. W. Benson, J. H. Buss, *Chem. Phys.* **1958**, *29*, 546-572.
[6] T. Dudev, C. Lim, *J. Am. Chem. Soc.* **1998**, *120*, 4450-4458.
[7] W. E. Brittin, *J. Chem. Educ.* **1945**, *22*, 145.
[8] C. A. Wurtz, *C. R. Acad. Sci.* **1859**, *48*, 101-105.
[9] E. Reboul, *Ann. Chim.* **1878**, *14*, 496.
[10] A. Freund, *J. Prakt. Chem.* **1882**, *26*, 367-377.
[11] R. Willstätter, J. Bruce, *Chem. Ber.* **1907**, *40*, 3979-3999.
[12] K. B. Wiberg, G. M. Lampman, R. P. Ciula, D. S. Connor, P. Schertler, J. Lavanish, *Tetrahedron* **1965**, *21*, 2749-2769.
[13] K. B. Wiberg, D. S. Connor, *J. Am. Chem. Soc.* **1966**, *88*, 4437-4441.
[14] P. E. Eaton, T. W. Cole, *J. Am. Chem. Soc.* **1964**, *86*, 3157-3158.
[15] G. Maier, S. Pfriem, U. Schäfer, R. Matusch, *Angew. Chem. Int. Ed.* **1978**, *17*, 520-521.
[16] A. Boudhar, M. Charpenay, G. Blond, J. Suffert, *Angew. Chem. Int. Ed.* **2013**, *52*, 12786-12798.
[17] H. Hopf, *Classics in Hydrocarbon Chemistry: Syntheses, Concepts, Perspectives*, Wiley-VCH, **2000**.
[18] C. A. Coulson, W. E. Moffitt, *Lond. Edinb. Dublin philos. mag. j. sci.* **1949**, *40*, 1-35.
[19] A. D. Walsh, *Nature* **1947**, *159*, 165-165.
[20] M. L. M. M. J. S. Dewar, *Pure Appl. Chem.* **1980**, *52*, 1431-1441.
[21] A. Sterling, R. Smith, E. Anderson, F. Duarte, *ChemRxiv* **2022**.
[22] A. J. Sterling, A. B. Dürr, R. C. Smith, E. A. Anderson, F. Duarte, *Chem. Sci.* **2020**, *11*, 4895-4903.
[23] M. G. Evans, M. Polanyi, *J. Chem. Soc. Faraday Trans.* **1938**, *34*.
[24] *Proc. Math. Phys. Eng.* **1997**, *154*, 414-429.
[25] J. Meinwald, W. Szkrybalo, D. R. Dimmel, *Tetrahedron Lett.* **1967**, *8*, 731-733.
[26] R. Srinivasan, K. H. Carlough, *J. Am. Chem. Soc.* **2002**, *89*, 4932-4936.
[27] H. K. Hall, C. D. Smith, E. P. Blanchard, S. C. Cherkofsky, J. B. Sieja, *J. Am. Chem. Soc.* **2002**, *93*, 121-130.
[28] Y. Yang, J. Tsien, J. M. E. Hughes, B. K. Peters, R. R. Merchant, T. Qin, *Nat. Chem.* **2021**, *13*, 950-955.
[29] K. B. Wiberg, S. T. Waddell, *J. Am. Chem. Soc.* **1990**, *112*, 2194-2216.
[30] K. P. Dockery, W. G. Bentrude, *J. Am. Chem. Soc.* **1997**, *119*, 1388-1399.
[31] P. Kaszynski, J. Michl, *J. Org. Chem.* **1988**, *53*, 4593-4594.
[32] M. Messner, Sergei I. Kozhushkov, A. de Meijere, *Eur. J. Org. Chem.* **2000**, *2000*, 1137-1155.

[33] I. S. Makarov, C. E. Brocklehurst, K. Karaghiosoff, G. Koch, P. Knochel, *Angew. Chem. Int. Ed.* **2017**, *56*, 12774-12777.
[34] K. Schwärzer, H. Zipse, K. Karaghiosoff, P. Knochel, *Angew. Chem. Int. Ed.* **2020**, *59*, 20235-20241.
[35] *Organometallics in Synthesis: A Manual*, Wiley–Blackwell, **1996**.
[36] S. Yu, C. Jing, A. Noble, V. K. Aggarwal, *Angew. Chem. Int. Ed.* **2020**, *59*, 3917-3921.
[37] R. Gianatassio, J. M. Lopchuk, J. Wang, C. M. Pan, L. R. Malins, L. Prieto, T. A. Brandt, M. R. Collins, G. M. Gallego, N. W. Sach, J. E. Spangler, H. Zhu, J. Zhu, P. S. Baran, *Science* **2016**, *351*, 241-246.
[38] J. M. Lopchuk, K. Fjelbye, Y. Kawamata, L. R. Malins, C. M. Pan, R. Gianatassio, J. Wang, L. Prieto, J. Bradow, T. A. Brandt, M. R. Collins, J. Elleraas, J. Ewanicki, W. Farrell, O. O. Fadeyi, G. M. Gallego, J. J. Mousseau, R. Oliver, N. W. Sach, J. K. Smith, J. E. Spangler, H. Zhu, J. Zhu, P. S. Baran, *J. Am. Chem. Soc.* **2017**, *139*, 3209-3226.
[39] J. M. E. Hughes, D. A. Scarlata, A. C. Chen, J. D. Burch, J. L. Gleason, *Org. Lett.* **2019**, *21*, 6800-6804.
[40] R. A. Shelp, P. J. Walsh, *Angew. Chem. Int. Ed.* **2018**, *57*, 15857-15861.
[41] R. A. Shelp, A. Ciro, Y. Pu, R. R. Merchant, J. M. E. Hughes, P. J. Walsh, *Chem. Sci.* **2021**, *12*, 7066-7072.
[42] J. L. M. Isaac F. Yu, Alejandro Diéguez-vázquez, Antonio Misale, Alexander E. Pashenko, Sergey V. Ryabukhin, Dmitriy M. Volochnyuk, John F. Hartwig, *ChemRxiv* **2022**.
[43] N. Trongsiriwat, Y. Pu, Y. Nieves-Quinones, R. A. Shelp, M. C. Kozlowski, P. J. Walsh, *Angew. Chem. Int. Ed.* **2019**, *58*, 13416-13420.
[44] D. F. J. Caputo, C. Arroniz, A. B. Durr, J. J. Mousseau, A. F. Stepan, S. J. Mansfield, E. A. Anderson, *Chem. Sci.* **2018**, *9*, 5295-5300.
[45] J. Nugent, C. Arroniz, B. R. Shire, A. J. Sterling, H. D. Pickford, M. L. J. Wong, S. J. Mansfield, D. F. J. Caputo, B. Owen, J. J. Mousseau, F. Duarte, E. A. Anderson, *ACS Catal.* **2019**, *9*, 9568-9574.
[46] J. Nugent, B. R. Shire, D. F. J. Caputo, H. D. Pickford, F. Nightingale, I. T. T. Houlsby, J. J. Mousseau, E. A. Anderson, *Angew. Chem. Int. Ed.* **2020**, *59*, 11866-11870.
[47] H. D. Pickford, J. Nugent, B. Owen, J. J. Mousseau, R. C. Smith, E. A. Anderson, *J. Am. Chem. Soc.* **2021**, *143*, 9729-9736.
[48] J. H. Kim, A. Ruffoni, Y. S. S. Al-Faiyz, N. S. Sheikh, D. Leonori, *Angew. Chem. Int. Ed.* **2020**, *59*, 8225-8231.
[49] S. Shin, S. Lee, W. Choi, N. Kim, S. Hong, *Angew. Chem. Int. Ed.* **2021**.
[50] J. Kanazawa, K. Maeda, M. Uchiyama, *J. Am. Chem. Soc.* **2017**, *139*, 17791-17794.
[51] M. Kondo, J. Kanazawa, T. Ichikawa, T. Shimokawa, Y. Nagashima, K. Miyamoto, M. Uchiyama, *Angew. Chem. Int. Ed.* **2020**, *59*, 1970-1974.
[52] X. Zhang, R. T. Smith, C. Le, S. J. McCarver, B. T. Shireman, N. I. Carruthers, D. W. C. MacMillan, *Nature* **2020**, *580*, 220-226.

[53] K. B. Wiberg, N. McMurdie, *J. Am. Chem. Soc.* **2002**, *116*, 11990-11998.
[54] S. Yu, A. Noble, R. B. Bedford, V. K. Aggarwal, *J. Am. Chem. Soc.* **2019**, *141*, 20325-20334.
[55] D. Lasanyi, G. L. Tolnai, *Org. Lett.* **2019**, *21*, 10057-10062.
[56] S. Livesley, A. J. Sterling, C. M. Robertson, W. R. F. Goundry, J. A. Morris, F. Duarte, C. Aissa, *Angew. Chem. Int. Ed.* **2022**, *61*, e202111291.
[57] R. Pellicciari, M. Raimondo, M. Marinozzi, B. Natalini, G. Costantino, C. Thomsen, *J. Med. Chem.* **1996**, *39*, 2874-2876.
[58] I. Langmuir, *J. Am. Chem. Soc.* **1919**, *41*, 1543-1559.
[59] H. G. Grimm, *Zeitschrift für Elektrochemie und angewandte physikalische Chemie* **1925**, *31*, 474-480.
[60] H. Erlenmeyer, M. Leo, *Helv. Chim. Acta* **1933**, *16*, 1381-1389.
[61] H. L. Friedman, *Influence of Isosteric Replacements Upon Biological Activity*, The National Academies Press., Washington, DC, **1950**.
[62] C. W. Thornber, *Chem. Soc. Rev.* **1979**, *8*, 563-580.
[63] A. Burger, *Prog. Drug. Res.* **1991**, *37*, 287-371.
[64] P. Imming, C. Sinning, A. Meyer, *Nature Reviews Drug Discovery* **2006**, *5*, 821-834.
[65] F. Lovering, J. Bikker, C. Humblet, *J. Med. Chem.* **2009**, *52*, 6752-6756.
[66] T. J. Ritchie, S. J. F. Macdonald, *Drug Discov. Today* **2009**, *14*, 1011-1020.
[67] J. L. Bolton, T. Dunlap, *Chem. Res. Toxicol.* **2017**, *30*, 13-37.
[68] M. A. M. Subbaiah, N. A. Meanwell, *J. Med. Chem.* **2021**, *64*, 14046-14128.
[69] C. Ballatore, D. M. Huryn, A. B. Smith, 3rd, *ChemMedChem* **2013**, *8*, 385-395.
[70] J. A. Bull, R. A. Croft, O. A. Davis, R. Doran, K. F. Morgan, *Chem. Rev.* **2016**, *116*, 12150-12233.
[71] P. K. Mykhailiuk, *Org. Biomol. Chem.* **2019**, *17*, 2839-2849.
[72] M. A. M. Subbaiah, N. A. Meanwell, *J. Med. Chem.* **2021**, *64*, 14046-14128.
[73] A. F. Stepan, C. Subramanyam, I. V. Efremov, J. K. Dutra, T. J. O'Sullivan, K. J. DiRico, W. S. McDonald, A. Won, P. H. Dorff, C. E. Nolan, S. L. Becker, L. R. Pustilnik, D. R. Riddell, G. W. Kauffman, B. L. Kormos, L. Zhang, Y. Lu, S. H. Capetta, M. E. Green, K. Karki, E. Sibley, K. P. Atchison, A. J. Hallgren, C. E. Oborski, A. E. Robshaw, B. Sneed, C. J. O'Donnell, *J. Med. Chem.* **2012**, *55*, 3414-3424.
[74] Y. L. Goh, Y. T. Cui, V. Pendharkar, V. A. Adsool, *ACS Med. Chem. Lett.* **2017**, *8*, 516-520.
[75] B. A. Chalmers, H. Xing, S. Houston, C. Clark, S. Ghassabian, A. Kuo, B. Cao, A. Reitsma, C.-E. P. Murray, J. E. Stok, G. M. Boyle, C. J. Pierce, S. W. Littler, D. A. Winkler, P. V. Bernhardt, C. Pasay, J. J. De Voss, J. McCarthy, P. G. Parsons, G. H. Walter, M. T. Smith, H. M. Cooper, S. K. Nilsson, J. Tsanaktsidis, G. P. Savage, C. M. Williams, *Angew. Chem. Int. Ed.* **2016**, *55*, 3580-3585.
[76] J. Altman, E. Babad, J. Itzchaki, D. Ginsburg, *Tetrahedron* **1966**, *S*, 279-&.
[77] D. Nied, R. Koppe, W. Klopper, H. Schnockel, F. Breher, *J. Am. Chem. Soc.* **2010**, *132*, 10264-10265.

[78] D. Nied, P. Ona-Burgos, W. Klopper, F. Breher, *Organometallics* **2011**, *30*, 1419-1428.
[79] A. M. Dilmaç, E. Spuling, A. de Meijere, S. Bräse, *Angew. Chem. Int. Ed.* **2017**, *56*, 5684-5718.
[80] F. Schneider, K. Samarin, S. Zanella, T. Gaich, *Science* **2020**, *367*, 676-681.
[81] K. B. Wiberg, G. J. Burgmaier, *J. Am. Chem. Soc.* **1972**, *94*, 7396-7401.
[82] P. G. Gassman, A. Topp, J. W. Keller, *Tetrahedron Lett.* **1969**, *10*, 1093-1095.
[83] P. E. Eaton, G. H. Temme, *J. Am. Chem. Soc.* **2002**, *95*, 7508-7510.
[84] F. H. Walker, K. B. Wiberg, J. Michl, *J. Am. Chem. Soc.* **1982**, *104*, 2056-2057.
[85] J. S. Fuchs, G. , *Chem. Ber.* **1992**, *125*, 2517- 2522.
[86] K. B. Wiberg, F. H. Walker, *J. Am. Chem. Soc.* **1982**, *104*, 5239-5240.
[87] P. G. Gassman, G. S. Proehl, *J. Am. Chem. Soc.* **1980**, *102*, 6862-6863.
[88] R. W. Weber, J. M. Cook, *Can. J. Chem.* **1978**, *56*, 189-192.
[89] S. Cristol, J. W. Firth, *J. Org. Chem.* **1961**, *26*, 280-280.
[90] V. Ripenko, D. Vysochyn, I. Klymov, S. Zhersh, P. K. Mykhailiuk, *J. Org. Chem.* **2021**, *86*, 14061-14068.
[91] K. Mlinaric-Majerski, Z. Majerski, *J. Am. Chem. Soc.* **2002**, *102*, 1418-1419.
[92] V. Vinkovic, Z. Majerski, *J. Am. Chem. Soc.* **1982**, *104*, 4027-4029.
[93] K. Mlinaric-Majerski, Z. Majerski, B. Rakvin, Z. Veksli, *J. Org. Chem.* **1989**, *54*, 545-548.
[94] Z. Majerski, K. Mlinaric-Majerski, *J. Org. Chem.* **1986**, *51*, 3219-3221.
[95] A. Watanabe, K. Koyamada, K. Miyamoto, J. Kanazawa, M. Uchiyama, *Org. Process. Res. Dev.* **2020**, *24*, 1328-1334.
[96] E. Della, J. Tsanaktsidis, *Aust. J. Chem.* **1986**, *39*, 2061-2066.
[97] O. G. Kulinkovich, Y. Y. Kozyrkov, A. V. Bekish, E. A. Matiushenkov, I. L. Lysenko, *Synthesis* **2005**, 1713-1717.
[98] K. M. Lynch, W. P. Dailey, *J. Org. Chem.* **1995**, *60*, 4666-4668.
[99] E. W. Della, D. K. Taylor, *J. Org. Chem.* **1994**, *59*, 2986-2996.
[100] K. R. Mondanaro, W. P. Dailey, *Organic Syntheses* **1998**, *75*.
[101] X. Ma, Y. Han, D. J. Bennett, *Org. Lett.* **2020**.
[102] B. Shire, University of Oxford **2022**.
[103] M. Baumann, K. Donnelly, *ChemComm* **2021**.
[104] J. R. H. Pinchman, Chad Daniel; Bunker, Kevin Duane; Huang, Peter Qinhua, *Vol. WO2018039232* (Ed.: W. I. P. Organization), Kalyra Pharmaceuticals, Inc., United States, **2018**.
[105] C. Zarate, M. Ardolino, G. J. Morriello, K. M. Logan, W. P. Kaplan, L. Torres, D. Li, M. Chen, H. Li, J. Su, P. Fuller, M. L. Maddess, Z. J. Song, *Org. Proc. Res. Dev.* **2020**.
[106] Y. Liang, X. Zhang, D. W. C. MacMillan, *Nature* **2018**, *559*, 83-88.
[107] S. Grimme, *Chem. Phys.* **2003**, *118*, 9095-9102.
[108] S. Shaik, D. Danovich, W. Wu, P. C. Hiberty, *Nat. Chem.* **2009**, *1*, 443-449.
[109] R. F. W. Bader, *Atoms in Molecules: A Quantum Theory Vol. 22*, Clarendon Press, **1994**.
[110] T. Lu, F. Chen, *J. Comput. Chem.* **2012**, *33*, 580-592.

[111] K. B. Wiberg, R. F. W. Bader, C. D. H. Lau, *J. Am. Chem. Soc.* **1987**, *109*, 985-1001.
[112] P. Geerlings, F. De Proft, W. Langenaeker, *Chem. Rev.* **2003**, *103*, 1793-1873.
[113] K. B. Wiberg, *Angew. Chem. Int. Ed.* **1986**, *25*, 312-322.
[114] P. R. Rablen, *Chem. Eur. J.* **2020**, *2*, 347-360.
[115] A. J. Sterling, University of Oxford (Oxford), **2021**.
[116] S. E. Wheeler, K. N. Houk, P. v. R. Schleyer, W. D. Allen, *J. Am. Chem. Soc.* **2009**, *131*, 2547-2560.
[117] M. Newcomb, in *Encyclopedia of Radicals in Chemistry, Biology and Materials*, **2012**.
[118] D. Griller, K. U. Ingold, *Acc. Chem. Res.* **1980**, *13*, 317-323.
[119] R. M. Bar, S. Kirschner, M. Nieger, S. Brase, *Chem. Eur. J.* **2018**, *24*, 1373-1382.
[120] K. Tokunaga, M. Sato, K. Kuwata, C. Miura, H. Fuchida, N. Matsunaga, S. Koyanagi, S. Ohdo, N. Shindo, A. Ojida, *J. Am. Chem. Soc.* **2020**, *142*, 18522-18531.
[121] P. Rabe, J. Kamps, K. D. Sutherlin, J. D. S. Linyard, P. Aller, C. C. Pham, H. Makita, I. Clifton, M. A. McDonough, T. M. Leissing, D. Shutin, P. A. Lang, A. Butryn, J. Brem, S. Gul, F. D. Fuller, I. S. Kim, M. H. Cheah, T. Fransson, A. Bhowmick, I. D. Young, L. O'Riordan, A. S. Brewster, I. Pettinati, M. Doyle, Y. Joti, S. Owada, K. Tono, A. Batyuk, M. S. Hunter, R. Alonso-Mori, U. Bergmann, R. L. Owen, N. K. Sauter, T. D. W. Claridge, C. V. Robinson, V. K. Yachandra, J. Yano, J. F. Kern, A. M. Orville, C. J. Schofield, *Sci. Adv.* **2021**, *7*.
[122] H.-J. Böhm, A. Flohr, M. Stahl, *Drug Discovery Today: Technologies* **2004**, *1*, 217-224.
[123] B. Kuhn, W. Guba, J. Hert, D. Banner, C. Bissantz, S. Ceccarelli, W. Haap, M. Körner, A. Kuglstatter, C. Lerner, P. Mattei, W. Neidhart, E. Pinard, M. G. Rudolph, T. Schulz-Gasch, T. Woltering, M. Stahl, *J. Med. Chem.* **2016**, *59*, 4087-4102.
[124] L. L. Winneroski, J. A. Erickson, S. J. Green, J. E. Lopez, S. L. Stout, W. J. Porter, D. E. Timm, J. E. Audia, M. Barberis, J. P. Beck, L. N. Boggs, A. R. Borders, R. D. Boyer, R. A. Brier, E. J. Hembre, J. Hendle, P. Garcia-Losada, J. M. Minguez, B. M. Mathes, P. C. May, S. A. Monk, Z. Rankovic, Y. Shi, B. M. Watson, Z. Yang, D. J. Mergott, *Bioorg. Med. Chem.* **2020**, *28*, 115194.
[125] V. V. Levterov, Y. Panasyuk, V. O. Pivnytska, P. K. Mykhailiuk, *Angew. Chem. Int. Ed.* **2020**, *59*, 7161-7167.
[126] A. Denisenko, P Garbuz, N. M. Voloshchuk, Y. Holota, P. K. Mykhailiuk, *ChemRxiv* **2022**.
[127] R. Kleinmans, T. Pinkert, S. Dutta, T. O. Paulisch, H. Keum, C. G. Daniliuc, F. Glorius, *Nature* **2022**, *605*, 477-482.
[128] S. Agasti, F. Beltran, E. Pye, N. Kaltsoyannis, G. Crisenza, D. Procter, *ChemRxiv* **2022**.
[129] R. Guo, Y.-C. Chang, L. Herter, C. Salome, S. E. Braley, T. C. Fessard, M. K. Brown, *J. Am. Chem. Soc.* **2022**, *144*, 7988-7994.

[130] K. Dhake, K. J. Woelk, J. Becica, A. Un, S. E. Jenny, D. C. Leitch, *Angew. Chem. Int. Ed.* **2022**, *61*, e202204719.
[131] O. O. Grygorenko, P. Babenko, D. M. Volochnyuk, O. Raievskyi, I. V. Komarov, *RSC Adv.* **2016**, *6*, 17595-17605.
[132] P. C. Fong, D. S. Boss, T. A. Yap, A. Tutt, P. Wu, M. Mergui-Roelvink, P. Mortimer, H. Swaisland, A. Lau, M. J. O'Connor, A. Ashworth, J. Carmichael, S. B. Kaye, J. H. M. Schellens, J. S. de Bono, *N. Engl. J. Med.* **2009**, *361*, 123-134.
[133] K. Kuk, J. L. Taylor-Cousar, *Ther. Adv. Respir. Dis.* **2015**, *9*, 313-326.
[134] T. G. Kantor, *Pharmacotherapy: The Journal of Human Pharmacology and Drug Therapy* **1986**, *6*, 93-102.
[135] J. A. Plumb, P. W. Finn, R. J. Williams, M. J. Bandara, M. R. Romero, C. J. Watkins, N. B. La Thangue, R. Brown, *Mol. Cancer Ther.* **2003**, *2*, 721-728.
[136] K. Boutet, I. Frachon, Y. Jobic, C. Gut-Gobert, C. Leroyer, D. Carlhant-Kowalski, O. Sitbon, G. Simonneau, M. Humbert, *Eur. Resp. J.* **2009**, *33*, 684-688.
[137] T. W. G. Peter G. M. Wuts, in *Greene's Protective Groups in Organic Synthesis*, John Wiley & Sons, Inc., **2006**.
[138] A. Krasovskiy, V. Malakhov, A. Gavryushin, P. Knochel, *Angew. Chem. Int. Ed.* **2006**, *45*, 6040-6044.
[139] R. D. Rieke, *Science* **1989**, *246*, 1260-1264.
[140] R. D. Rieke, S. E. Bales, P. M. Hudnall, T. P. Burns, G. S. Poindexter, *Org. Synth.* **1979**, *59*.
[141] R. D. Rieke, T.-C. Wu, L. I. Rieke, *Org. Synth.* **1995**, *72*.
[142] T. C. Wu, H. Xiong, R. D. Rieke, *J. Org. Chem.* **1990**, *55*, 5045-5051.
[143] J. E. Fleckenstein, K. Koszinowski, *Organometallics* **2011**, *30*, 5018-5026.
[144] E. M. Hanada, T. K. S. Tagawa, M. Kawada, S. A. Blum, *J. Am. Chem. Soc.* **2022**, *144*, 12081-12091.
[145] W.-H. Deng, F. Ye, X.-F. Bai, L. Li, T. Song, Y.-L. Wei, L.-W. Xu, *RSC Adv.* **2014**, *4*, 479-483.
[146] J. X. Zhao, Y. X. Chang, C. He, B. J. Burke, M. R. Collins, M. Del Bel, J. Elleraas, G. M. Gallego, T. P. Montgomery, J. J. Mousseau, S. K. Nair, M. A. Perry, J. E. Spangler, J. C. Vantourout, P. S. Baran, *Proc. Natl. Acad. Sci. U.S.A.* **2021**, *118*.
[147] V. Sansanwal, H. G. Krishnamurty, *Synth. Commun.* **1995**, *25*, 1901-1906.
[148] T. A. Young, J. J. Silcock, A. J. Sterling, F. Duarte, *Angew. Chem. Int. Ed.* **2021**, *60*, 4266-4274.
[149] S. Riniker, G. A. Landrum, *J. Chem. Inf. Model* **2015**, *55*, 2562-2574.
[150] F. Neese, *Wiley Interdiscip. Rev. Comput. Mol. Sci.* **2011**, *2*, 73-78.
[151] F. Neese, *Wiley Interdiscip. Rev. Comput. Mol. Sci.* **2017**, *8*.
[152] M. Zollinger, F. Lozac'h, E. Hurh, C. Emotte, H. Bauly, P. Swart, *Cancer Chemother. Pharmacol.* **2014**, *74*, 63-75.
[153] C. B. Burness, *Drugs* **2015**, *75*, 1559-1566.
[154] S. Cuisiat, N. Bourdiol, V. Lacharme, A. Newman-Tancredi, F. Colpaert, B. Vacher, *J. Med. Chem.* **2007**, *50*, 865-876.

[155] J. B. Bussel, G. Cheng, M. N. Saleh, B. Psaila, L. Kovaleva, B. Meddeb, J. Kloczko, H. Hassani, B. Mayer, N. L. Stone, M. Arning, D. Provan, J. M. Jenkins, *N. Engl. J. Med.* **2007**, *357*, 2237-2247.
[156] T. M. Edislav Leksic, Irena Antonac, Mastelic Samardzic *Vol. WO2010114943A1*, **2010**.
[157] J. Shi, Q.-L. Xu, Y.-Q. Ni, L. Li, F. Pan, *Org. Lett.* **2022**, *24*, 4609-4614.
[158] B. Whitaker, University of Oxford **2022**.
[159] L. Itzhaki, E. Altus, H. Basch, S. Hoz, *Angew. Chem. Int. Ed.* **2005**, *44*, 7432-7435.
[160] P. Kaszynski, J. Michl, *J. Am. Chem. Soc.* **1988**, *110*, 5225-5226.
[161] D. F. J. Caputo, C. Arroniz, A. B. Dürr, J. J. Mousseau, A. F. Stepan, S. J. Mansfield, E. A. Anderson, *Chem. Sci.* **2018**, *9*, 5295-5300.
[162] R. M. Bär, G. Heinrich, M. Nieger, O. Fuhr, S. Bräse, *Beilstein J. Org. Chem.* **2019**, *15*, 1172-1180.
[163] S. M. Royalty, J. F. Burns, J. J. Scicinski, G. E. Jagdmann Jr., R. J. Foglesong, K. R. Griffin, T. Dyakonov, D. Middlemiss, *Peptidase inhibitors*, WO2006012395A3**, 2006**.
[164] Y. Y. Kozyrkov, O. G. Kulinkovich, *Synlett* **2002**, 0443-0446.
[165] J. S. Fuchs, G. , *Chem. Ber.* **1992**, *125*, 2517- 2522.
[166] D. J. Jones, E. M. O'Leary, T. P. O'Sullivan, *Beilstein J. Org. Chem.* **2019**, *15*, 801-810.
[167] K. Ikeya, S. Okamoto, A. Sudo, *Results in Chemistry* **2021**, *3*, 100167.
[168] R. M. Risi, S. D. Burke, *Org. Lett.* **2012**, *14*, 2572-2575.
[169] O. Mammoliti et al., *J. Med. Chem*. **2019**, *64*, 14557-14586.
[170] Y. Yamamoto, *Adv. Synth. Catal.* **2010**, *352*, 478-492.
[171] B. Hu, J. Cai, J. Chen, M. Cao, P. Wang, X. Zong, R. Zhang, M. Ji, *J. Chem. Res.* **2014**, *38*, 18-20.
[172] S. Pan, X. Wu, J. Jiang, W. Gao, Y. Wan, D. Cheng, D. Han, J. Liu, N. P. Englund, Y. Wang, S. Peukert, K. Miller-Moslin, J. Yuan, R. Guo, M. Matsumoto, A. Vattay, Y. Jiang, J. Tsao, F. Sun, A. C. Pferdekamper, S. Dodd, T. Tuntland, W. Maniara, J. F. Kelleher, 3rd, Y. M. Yao, M. Warmuth, J. Williams, M. Dorsch, *ACS Med. Chem. Lett.* **2010**, *1*, 130-134.
[173] F.-E. Chen, J.-L. Yuan, H.-F. Dai, Y.-Y. Kuang, Y. Chu, *Synthesis* **2003**, 2155-2160.
[174] F. Neese, F. Wennmohs, A. Hansen, U. Becker, *Chem. Phys.* **2009**, *356*, 98-109.
[175] G. L. Stoychev, A. A. Auer, F. Neese, *J. Chem. Theory Comput.* **2017**, *13*, 554-562.
[176] K. Eichkorn, F. Weigend, O. Treutler, R. Ahlrichs, *Theor. Chim. Acta* **1997**, *97*, 119-124.
[177] F. Weigend, *Phys. Chem. Chem. Phys.* **2006**, *8*, 1057-1065.
[178] F. Weigend, *Phys. Chem. Chem. Phys.* **2002**, *4*, 4285-4291.
[179] S. Grimme, *Chem. Eur. J.* **2012**, *18*, 9955-9964.
[180] T. Young, *github.com/duartegroup/autodE* **2020**.
[181] S. Grimme, J. Antony, S. Ehrlich, H. Krieg, *J. Chem. Phys.* **2010**, *132*, 154104.

[182] S. Grimme, S. Ehrlich, L. Goerigk, *J. Comput. Chem.* **2011**, *32*, 1456-1465.
[183] D. G. Liakos, F. Neese, *J. Chem. Theory Comput.* **2015**, *11*, 4054-4063.
[184] D. G. Liakos, M. Sparta, M. K. Kesharwani, J. M. Martin, F. Neese, *J. Chem. Theory Comput.* **2015**, *11*, 1525-1539.
[185] C. Bannwarth, S. Ehlert, S. Grimme, *J. Chem. Theory Comput.* **2019**, *15*, 1652-1671.
[186] C. Adamo, V. Barone, *Chem. Phys.* **1999**, *110*, 6158-6170.
[187] F. Jensen, *Introduction to Computational Chemistry: Second Edition*, JW, **2011**.
[188] P. de Silva, C. Corminboeuf, *J. Chem. Theory Comput.* **2014**, *10*, 3745-3756.